Unraveling the host specificity within *Streptococcus dysgalactiae* subsp. *dysgalactiae*

CINTHIA ARMELLE BEZERRA ALVES BARROCO

Master in Applied Microbiology

DOCTORATE IN BIOLOGY

NOVA University of Lisbon
March, 2022

Unraveling the host specificity within
Streptococcus dysgalactiae subsp. *dysgalactiae*

CINTHIA ARMELLE BEZERRA ALVES BARROCO

Master in Applied Microbiology, Faculty of Science at the University of Lisbon

Adviser:	Doutora Maria Alexandra Núncio de Carvalho Ramos Fernandes Assistant Professor, NOVA School of Science and Technology
Co-advisers:	Doutora Rosario Mato Labajos Invited Assistant Professor, NOVA School of Science and Technology

Examination Committee:

Chair:	Doutor Pedro Miguel Ribeiro Viana Baptista Full Professor, NOVA School of Science and Technology, NOVA University of Lisbon
Rapporteurs:	Doutora Luísa Maria Sobreira Vieira Peixe Associate Professor with Aggregation, Faculty of Pharmacy of the University of Porto Doutor Mário Nuno Ramos d'Almeida Ramirez Associate Professor with Aggregation, Faculty of Medicine of the University of Lisbon
Adviser:	Doutora Maria Alexandra Núncio de Carvalho Ramos Fernandes Assistant Professor, NOVA School of Science and Technology, NOVA University of Lisbon
Member:	Doutor Pedro Miguel Ribeiro Viana Baptista Full Professor, NOVA School of Science and Technology, NOVA University of Lisbon Doutora Isabel Maria Godinho de Sá Nogueira Full Professor, NOVA School of Science and Technology, NOVA University of Lisbon

DOCTORATE IN BIOLOGY

NOVA University of Lisbon
March, 2022

Unraveling the host specificity within *Streptococcus dysgalactiae* subsp. *dysgalactiae*

Acknowledgement's

Carvalho, Ana Botelho, Carolina Martini, Marcos Correia, and Mariana Severo for their technical support, helpful suggestions, and friendship during my stay in Rio de Janeiro.

I would also like to thank Professor Rogério Tenreiro, and Dr. Lélia Chambel, Faculty of Sciences, University of Lisbon (FC/UL), for letting me use their facilities and giving me support in the BioNumerics software and analysis system.

From the Faculty of Veterinary Medicine, I am grateful to Dr. Ricardo Bexiga and Dr. Manuela Oliveira for their collaboration and Dr. Teresa Semedo-Lemsaddek for providing the required resources and scientific knowledge at the beginning of my journey.

Very special thanks to my friends Rita Drago, Isa Pires, Ricardo Oliveira, Osvaldo Macedo and Soraia Rosa for their unending support and encouragement. Thank you for listening to me, for always being there. Thanks for being part of my life.

Finally, I would like to express my gratitude to my family for all the support that contributed to this work's accomplishment. I love you all.

Thank you all!

Abstract

Streptococcus dysgalactiae subsp. *dysgalactiae* (SDSD) has been considered a strict animal pathogen. Nevertheless, human infections have been reported, suggesting a niche expansion for this subspecies. Previous studies reported the presence of *Streptococcus pyogenes* phage-encoded virulence genes associated with an invasive phenotype in humans among bovine SDSD. However, it is not evident if the carriage of these genes is shared by different SDSD strains, suggesting a subspecies-specific feature. Thus, this study addressed three main objectives: **i)** to characterize SDSD isolates from dairy herds in Portugal, collected between 2011 and 2013 (n= 37) and between 2002 and 2003 (n= 18); **ii)** to compare the genomic profiles of the pyogenic streptococci genomes available at NCBI, aiming to track the temporal evolution of the bovine SDSD isolates; **iii)** to assess the potential for biofilm formation and eradication, and to evaluate the pathogenic potential of bovine SDSD using *in vivo* and *in vitro* models of infection.

Phylogenetic analyses of the core genome of 106 strains showed that *Streptococcus dysgalactiae* subsp. *equisimilis* (SDSE, human) and SDSD (bovine) strains are grouped into different clusters. More importantly, reveals that human and fish SDSD, as well as non-human SDSE isolates, are closely related. Features of the accessory genome provide further support for the phylogenetic relationships observed, suggesting a signature of host adaptation and host-specific SDSD population in bovines.

Comparative analysis showed that bovine SDSD isolates carrying genes of *S. pyogenes* prophages are maintained over time. Bovine SDSD show the ability to form biofilms *in vitro*, and *in vivo* using a murine foreign-body model. This study reports for the first-time conventional antibiotics' resistance associated with biofilm formation by SDSD strains. Additionally, this study provides useful information to assist the development of nanoparticle-based strategies for the treatment of biofilm-related infections triggered by photoirradiation in the visible. Bovine SDSD isolates interact *in vitro* and internalize human cell lines and were able to cause invasive infections in zebrafish. Proteomic analysis showed that the interaction between human keratinocytes cells and bovine SDSD isolate affects the host cell's metabolic pathways, disruption of the mitochondrial membrane potential, and consequently cell death.

In summary, although the data suggested that these SDSD isolates may have different host preferences, it is possible to conclude that bovine SDSD can infect other hosts than their original one, the cow, and can cause localized systemic infections under appropriate conditions.

Keywords: *Streptococcus dysgalactiae* subsp. *dysgalactiae*; Biofilm; Phylogenetic relationships, Accessory genome; Virulence; Pathogenicity potential

Resumo

Streptococcus dysgalactiae subsp. *dysgalactiae* (SDSD) tem sido considerado um agente patogénico estritamente animal. No entanto, têm sido relatadas infeções causadas por SDSD em seres humanos, sugerindo uma expansão de nicho para esta subespécie. Em SDSD bovino foi confirmado a presença de genes de virulência de bacteriófagos de *Streptococcus pyogenes,* conhecidos por estarem associados a doenças invasivas em humanos. No entanto, não é evidente se a presença destes genes é uma característica específica desta subespécie. Assim, este estudo abordou três objetivos principais: **i)** Caracterizar isolados bovinos de SDSD, recolhidos em Portugal entre 2011-2013 (n=37) e entre 2002-2003 (n=18) e estabelecer uma análise comparativa entre ambos; **ii)** comparar perfis genómicos de estreptococos piogénicos disponíveis no NCBI para estudar a evolução temporal dos isolados de SDSD bovinos; **iii)** avaliar o potencial de formação de biofilmes, e o potencial patogénico de SDSD bovino usando modelos de infeção *in vivo* e *in vitro*.

As análises filogenéticas do genoma central de 106 *S. dysgalactiae* mostraram que as estirpes de *Streptococcus dysgalactiae* subsp. *equisimilis* (SDSE, humano) e SDSD (bovino) são agrupadas em diferentes *clusters* e, revela que SDSD isolados de humano e peixe, bem como SDSE de animais (não humanos) estão intimamente relacionados. Características do genoma acessório forneceram suporte adicional para as relações filogenéticas observadas. Adicionalmente, a análise comparativa mostrou que os isolados de SDSD bovino têm superantigénios que são mantidos temporalmente. Foi igualmente demonstrado que SDSD (bovino) é capaz formar biofilmes *in vitro* e *in vivo* utilizando o rato como modelo animal. Este estudo mostra, pela primeira vez, a associação entre a formação de biofilmes por SDSD bovinos e a resistência aos antibióticos, tendo permitido o desenvolvimento de estratégias baseadas na utilização de nanopartículas como agentes hipertérmicos para potenciar a ação dos antibióticos convencionais, no tratamento de infeções associadas aos biofilmes bacterianos. Foi igualmente demonstrado que isolados de SDSD bovino são capazes de interagir e internalizar células humanas *in vitro,* e causam infeções em modelos de peixe-zebra. A análise proteómica mostrou que, a interação entre queratinócitos humanos e SDSD de bovinos, afeta várias vias metabólicas da célula hospedeira, levando à disrupção do potencial da membrana mitocondrial e induzindo a morte celular.

Em conclusão, embora os dados deste trabalho sugiram que SDSD possam ter hospedeiros preferenciais, é possível concluir que SDSD de bovino pode infetar outros hospedeiros além do original, e causar infeções sistémicas em condições apropriadas.

Palavras-chave: *Streptococcus dysgalactiae* subsp. *dysgalactiae*; Biofilme; Relações filogenéticas, Genoma acessório; Virulência; Potencial de patogenicidade.

Table of Contents

Table Index

Abbreviations

A549	Human adenocarcinoma of the alveolar basal epithelia cell line
Abi	abortive infection systems
HEPES	4-(2-hydroxyethyl)-1-piperazineethanesulfonic acid
ATCC	American type culture collection
ANI	Average nucleotide identity
bp	Base pair
BLAST	Basic local alignment search tool
CFSE	Carboxy fluorescein succinimidyl ester
CAT	Catalase
CIP	Ciprofloxacin
CLSI	Clinical and laboratory standards institute
CRISPR	Clustered regularly interspaced short palindromic repeats
CFU	Colony forming units
cDNA	Complementary deoxyribonucleic acid
CLSM	Confocal laser scanning microscopy
CRA	Congo Red Agar
cMLSB	Constitutive resistance to macrolides, lincosamides and streptogramins B
MLSB	Co-resistance to macrolides, lincosamides and streptogramins B
dNTP	Deoxynucleotide triphosphate
DNase	Deoxyribonuclease
DNA	Deoxyribonucleic acid
DMEM	Dulbecco's Modified Eagle's Medium supplemented with 10% (v/v) Foetal Bovine Serum
DLS	Dynamic light scattering
ICP-AES	Elemental composition by inductively coupled plasma atomic emission spectroscopy
EDTA	Ethylenediamine tetraacetic acid
eDNA	Extracellular DNA
EPS	Extracellular polymeric substance matrix
FCT	Fibronectin-binding, collagen-binding, T antigen
AuNPs	Gold nanoparticles
AuAgNPs	Gold-silver alloy nanoparticles
HGT	Horizontal gene transfer
h	Hours
HEKn	Human primary dermal keratinocytes
iMLSB	Inducible resistance to macrolides, lincosamides and streptogramins B
ICE	Integrative and conjugative elements
ICEs	Integrative conjugative elements
LPO	Lipid peroxidation
MDA	Malondialdehyde
Mb	Megabase pair
mRNA	Messenger ribonucleic acid
Detroit 562	Metastatic pharynx carcinoma cell line
MBEC	Minimal biofilm eradication concentration
MIC	Minimum inhibitory concentration

MGE	Mobile genetic elements
MEGA	Molecular evolutionary genetics analysis
MDR	Multidrug-resistant
MLSA	Multilocus sequence analysis
MLST	Multilocus sequence typing
NPs	nanoparticles
NCBI	National center for biotechnology information
NIR	Near-infrared radiation
NAD	Nicotine adenine dinucleotide
NA	Not applicable
nd	Not determined
SLS	Operon encoding streptolysin S
OD	Optical density
PBS	Phosphate-buffered saline
PTS	Phosphotransferase system
PCR	Polymerase chain reaction
BTEC	Primary bronchial/tracheal epithelial cell line
PFGE	Pulsed-field gel electrophoresis
ROS	Reactive oxide species
RT-qPCR	Real-time quantitative PCR
RM	Restriction-modification systems
RT-PCR	Reverse transcriptase PCR
RNase	Ribonuclease
RNA	Ribonucleic acid
rRNA	Ribosomal ribonucleic acid
SEM	Scanning electron microscopy
AgNPs	Silver nanoparticles
SDSD	*Streptococcus dysgalactiae* subsp. *dysgalactiae*
SD	*Streptococcus dysgalactiae*
SDSE	*Streptococcus dysgalactiae* subsp. *equisimilis*
SAgs	Superantigens genes
SOD	Superoxide dismutase
PEG-SH	Thiolated polyethylene glycol
THB	Todd Hewitt broth supplemented with 0.5% (w/v) yeast extract
THA	Todd-Hewitt supplemented with 1.5% (w/v) agar
Tris	Tris(hydroxymethyl)aminomethane
TBE	Tris-borate EDTA buffer
TE	Tris-EDTA buffer
TSB	Trypticase soy broth
TSB-0.5YE	Trypticase soy broth supplemented with 0.5% (w/v) yeast extract
UV-VIS	Ultraviolet-visible spectroscopy
VLI	Visible light irradiation

Gene abbreviations

atoB	Acetyl CoA acetyl-transferase
brpA-like	Biofilm regulatory proteins A homolog
cps	Capsule polysaccharide synthesis
emm	M-protein
erm	Erythromycin ribosome methylation
fbsA	Fibronectin-binding protein FbsA
gki	Glucose kinase
gki	Glucose kinase
gtr	Glutamine transport protein
lin	Lincosamide inactivation nucleotidylation
lmb	Laminin-binding protein Lmb
mef	Macrolide efflux
murL	Glutamate racemase
mutS	DNA mismatch repair protein
recP	Transketolase
sagA	Streptolysin S precursor
scpA/B	C5A peptidase precursor
sdn	Streptodornase
sfb	Streptococcal fibronectin-binding protein I
smeZ	Streptococcal mitogenic exotoxin Z
spd1	Streptococcal phage DNase
spe	Superantigens
spegg	*S. dysgalactiae* subsp. *equisimilis* pyrogenic exotoxin G
ssa	Streptococcal superantigen
tdk	Thymidine kinase
tet	Tetracycline resistance protein
xpt	Xanthine phosphoribosyl transferase
znuA	Homolog of *adcA* gene involved in the processes of adhesion and invasion

List of publications

This thesis is based on eight articles:

Alves-Barroco, C., Brito, P.H., Santos-Sanches, I. and Fernandes, A.R. (2022). Phylogenetic analysis and accessory genome diversity reveal insight into the evolutionary history of *Streptococcus dysgalactiae. Frontiers in Microbiology* 13, 952110 doi: org/10.3389/fmicb.2022.952110.

Alves-Barroco, C., Botelho, A.M.N, Américo, M.A, Fracalanzza, S,E., de Matos, A.P.A., Guimaraes, M.A., Ferreira-Carvalho, B.T, Figueiredo, AMS, Fernandes, A.R. Assessing in vivo and in vitro biofilm development by Streptococcus dysgalactiae subsp. dysgalactiae using a murine model of catheter-associated biofilm and human keratinocyte cell. *Frontiers in Cellular and Infection Microbiology* 12, 874694. (2022). doi: org/10.3389/fcimb.2022.874694.

Alves-Barroco, C., Rivas-García, L., Fernandes, A. R., and Baptista, P. V. (2022). Light triggered enhancement of antibiotic efficacy in biofilm elimination mediated by gold-silver alloy nanoparticles. *Frontiers in microbiology*, 13, 841124. doi: 10.3389/fmicb.2022.841124. 1.

Alves-Barroco, C., Caço, J., Roma-Rodrigues, C., Fernandes, A. R., Bexiga, R., Oliveira, M., Chambel, L., Tenreiro, R., Mato, R., and Santos-Sanches, I. (2021). New insights on *Streptococcus dysgalactiae* subsp. *dysgalactiae* isolates. *Frontiers in microbiology*, 12, 686413. doi: org/10.3389/fmicb.2021.686413.

Alves-Barroco, C., Paquete-Ferreira, J., Santos-Silva, T., and Fernandes, A. R. (2020). Singularities of pyogenic streptococcal biofilms - from formation to health implication. *Frontiers in microbiology*, 11, 584947. doi: org/10.3389/fmicb.2020.584947.

Alves-Barroco, C., Rivas-García, L., Fernandes, A. R., and Baptista, P. V. (2020). Tackling multidrug resistance in streptococci - from novel biotherapeutic strategies to nanomedicines. *Frontiers in microbiology*, 11, 579916. doi: org/10.3389/fmicb.2020.579916.

Alves-Barroco, C., Roma-Rodrigues, C., Balasubramanian, N., Guimarães, M. A., Ferreira-Carvalho, B. T., Muthukumaran, J., Nunes, D., Fortunato, E., Martins, R., Santos-Silva, T., Figueiredo, A., Fernandes, A. R., and Santos-Sanches, I. (2019). Biofilm development and computational screening for new putative inhibitors of a homolog of the regulatory protein BrpA in *Streptococcus dysgalactiae* subsp. *dysgalactiae*. *International journal of medical microbiology*, IJMM, 309(3-4), 169–181. doi: org/10.1016/j.ijmm.2019.02.001.

Alves-Barroco, C., Roma-Rodrigues, C., Raposo, L. R., Brás, C., Diniz, M., Caço, J., Costa, P. M., Santos-Sanches, I., and Fernandes, A. R. (2018). *Streptococcus dysgalactiae* subsp. *dysgalactiae* isolated from milk of the bovine udder as emerging pathogens: *In vitro* and *in vivo* infection of human cells and zebrafish as biological models. *MicrobiologyOpen*, *8* (1), e00623. doi: org/10.1002/mbo3.623.

This PhD Thesis is organized in nine chapters.

Chapter 1 provides a general introduction, it is focused a brief description of the genus and taxonomy of *Streptococcus dysgalactiae*, clinical relevance and host range of the species, horizontal gene transfer, biofilm formation and emergent strategies to fight biofilm infection.

Chapter 2 is entitled "New Insights on *Streptococcus dysgalactiae* subsp. *dysgalactiae* Isolates", which is included in the manuscript (DOI org/10.3389/fmicb.2021.686413). In this chapter, SDSD isolates collected in two different periods (2002–03, partially studied, and 2011–13) were characterized and compared to obtain new information about molecular virulence profiles, antibiotypes, and population structure. We also investigated the Clustered Regularly Interspaced Short Palindromic Repeats (CRISPR)/ CRISPR-associated proteins (Cas) systems in SDSD strains to gain insights into their defense systems and impact on horizontal gene transfer.

Chapter 3 is entitled "Phylogenetic analysis and accessory genome diversity reveal insight into the evolutionary history of *Streptococcus dysgalactiae*." which is included in the manuscript (DOI org/10.3389/fmicb.2022.952110). This chapter gives a background about the phylogenetic relationship of *Streptococcus dysgalactiae* based on the core genome, features of the accessory genome, diversity of prophages regions, and resistome. The phylogenetic structure within *Streptococcus dysgalactiae* is then used to understand the molecular characteristics associated with ability to infect a specific host. The purpose is to provide a core genome-based phylogenetic perspective and present a comparative analysis of the accessory genes that influences the pathogenicity of the strains.

Chapter 4 is entitled "*Streptococcus dysgalactiae* subsp. *dysgalactiae* isolated from milk of the bovine udder as emerging pathogens: *In vitro* and *in vivo* infection of human cells and zebrafish as biological models" which is included in the manuscript (DOI org/10.1002/mbo3.623). This chapter provides information on the ability of bovine SDSD

isolates to cause invasive infections, zebrafish morbidity and mortality and to adhere and internalize into human cells.

Chapter 5 is entitled "Infection of human keratinocytes by bovine *Streptococcus dysgalactiae* subsp. *dysgalactiae:* mechanisms of action". This chapter provides insight into mechanisms involved in bovine SDSD isolate and human keratinocytes cells interactions.

Chapter 6 is entitled "Biofilm development and computational screening for new putative inhibitors of a homolog of the regulatory protein BrpA in *Streptococcus dysgalactiae* subsp. *dysgalactiae*" which is included in the manuscript (DOI org/10.1016/j.ijmm.2019.02.001). This chapter was focused on the evaluation of the biofilm production capability of SDSD isolates in different matrices, the role of BrpA in biofilm production and the identification of putative inhibitors of biofilm formation.

Chapter 7 is entitled "Assessing in vivo and in vitro biofilm development by *Streptococcus dysgalactiae* subsp. *dysgalactiae* using a murine model of catheter-associated biofilm and human keratinocyte cell" which is included in the manuscript (DOI org/10.3389/fcimb.2022.874694). In this chapter the ability of bovine SDSD isolates to form biofilms *in vivo* was evaluated using a foreign-body animal model. Finally, the expression profile of genes associated with virulence, including development and modulation of biofilm formation, was analyzed both *in vivo* and *in vitro.*

Chapter 8 is entitled "Light triggered enhancement of antibiotic efficacy in biofilm elimination mediated by gold-silver alloy nanoparticles". which is included in the manuscript (DOI org/10.3389/fmicb.2022.841124). This chapter provides useful information to assist the development of nanoparticle-based strategies for the active treatment infections associated with biofilms produced by bovine SDSD.

Finally, Chapter 9 provides the final conclusions and an outlook for future research.

Chapter 1 - General Introduction

Part of the literature review presented in this chapter has been published, whole or in part, elsewhere.

Alves-Barroco, C., Paquete-Ferreira, J., Santos-Silva, T., and Fernandes, A. R. (2020). Singularities of Pyogenic Streptococcal Biofilms - From Formation to Health Implication. *Frontiers in microbiology*, 11, 584947.

Alves-Barroco, C., Rivas-García, L., Fernandes, A. R., and Baptista, P. V. (2020). Tackling Multidrug Resistance in Streptococci - From Novel Biotherapeutic Strategies to Nanomedicines. *Frontiers in microbiology*, 11, 579916.

1.1. General features of the genus *Streptococcus* spp.

Streptococcus spp. are often carried as part of the normal microbiota of animals and humans; most species can be regarded as commensal. They are usually found on mucosal surfaces in the oral cavity, upper respiratory and gastrointestinal tract, and under appropriate conditions, can cause localized and systemic infections (Hardie and Whiley, 1997). Streptococci are gram-positive cocci measuring between 0.5 and 2 μm in diameter and forming pairs or short chains. The cells are non-motile and non-spore-forming. Most species are facultative anaerobic, but some strains are capnophiles requiring CO_2-enriched growth conditions, and other strains can use carbohydrates producing lactic acid. The optimum temperature for growth is usually 37 C, but maximum and minimum temperatures may vary among species (Hardie and Whiley, 1997).

Streptococci are divided into groups based on the *16S rRNA* gene sequence homology: "Pyogenic," "Sanguis," "Bovis," "Mutans," "Mitis," "Anginosus," and "Salivarius" (Whiley and Hardie, 2009). Later, the "Downei" group was created to accommodate *S. downei* and *S. cricetid*. However, some relationships between the groups are not fully understood, suggesting the influence of horizontal gene transfer (HGT) during the early diversification of these clusters (Richards *et al.*, 2014). A description of S*treptococcus* species with clinical and veterinary relevance is presented in Table 1.1.

Routinely, the classification schemes used to identify streptococcal species include: (i) hemolytic patterns on agar blood plates, namely, β-hemolysis, which corresponds to the total lysis of erythrocytes, α-hemolysis which corresponds to the incomplete lysis, and γ-hemolysis, which is the absence of lysis; and (ii) Lancefield serologic groups (agglutination tests), based on a specific carbohydrate "group" antigen, which is an integrated part of the cell wall. In this method, the strains are designated by an upper-case letter of the alphabet (Lancefield, 1933). Additionally, biochemical tests such as the API 20 Strep (BioMérieux, Marcy l'Etoile, France) and BD Phoenix system (BD Diagnostics, Sparks, MD) are performed to identify clinically significant isolates of streptococci at the species and group levels (Brigante *et al.*, 2006); however, some strains may not be identified by these biochemical tests. In addition to the phenotypic and molecular techniques are used to complement the identification (e.g. 16S–23S rRNA interspacer region analysis, sequencing of the manganese-dependent superoxide dismutase gene (*sodA*), and inner features of 16S rRNA gene analysis) (Lal *et al.*, 2011; Kosecka-Strojek *et al.*, 2020; Alves-Barroco *et al.*, 2021).

Table 1.1. Main *Streptococcus* species of clinical and veterinary importance

Group	Species	Lancefield group	Main Host	Clinical manifestations	Ref.
Anginosus	*S. anginosus*	A, C, F, G	Human	Bacteremia	Simone *et al.*, 2012; Junckerstorff *et al.*, 2014; Noguchi *et al.*, 2015
	S. intermedius	A, C, F, G	Dogs	Bacteremia and abscesses with active periodontal	Tran *et al.*, 2008
Bovis	*S. bovis*	D	Bovine	Endocarditis, bacteremia, meningitis, septicemia, disease with a potential role in colon carcinogenesis	John P. Dekker, 2016
Mitis	*S. pneumoniae*	Viridans	Human	Otitis media, pneumonia, meningitis, septicemia, pleural empyema, septic arthritis, acute conjunctivitis	Henriques-Normark and Tuomanen, 2013
	S. mitis	Viridans	Human	Throat infection, bacteremia, endocarditis	Shelburne *et al.*, 2014; Basaranoglu *et al.*, 2019
	S. oralis	Viridans	Human		
Mutans	*S. mutans*	Viridans	Human	Dental caries, bacteremia, endocarditis, septicemia	Kojima *et al.*, 2012
	S. sabrinus	Viridans	Human		Berluttil *et al.*, 2010
Pyogenic	*S. pyogenes*	A	Human	Pharyngitis, pyoderma, erysipelas, bacteremia, septicemia, necrotizing fasciitis, meningitis, pneumonia, septic arthritis, streptococcal toxic shock syndrome, scarlet fever, rheumatic	Isaacs and Dobson, 2016
	S. agalactiae	B	Human and Bovine	Human: septicemia, pneumonia, meningitis, cellulitis, tract infection, puerperal sepsis, chorioamnionitis, endometirosis, cystitis, pyelonephritis, bacteremia, bovine mastitis	Rajagopal, 2009; Zadoks and Fitzpatrick, 2009
	S. dysgalactiae subsp. *dysgalactiae*	C	Animal and Human	Bovine mastitis, bacteremia	Koh *et al.*, 2009; Park *et al.*, 2012; Rato *et al.*, 2013b; Jordal *et al.*, 2015
	S. dysgalactiae subsp. *equisimilis*	C, G	Animal and Human	Pharyngitis, bacteremia, septicemia, septic arthritis, endocarditis, meningitis	Brandt and Spellerberg, 2009
Salivarius	*S. salivarius*	K	Human	bacteremia, meningitis	Shewmaker *et al.*, 2010
Sangui	*S. sanguinis*	Viridans	Human	Bacteremia, endocarditis, septicemia, meningitis.	Zhu *et al.*, 2018
	S. gordonii	Viridans	Human	Bacteremia, endocarditis	Krantz *et al.*, 2017

1.2. Brief description of the taxonomy of *Streptococcus dysgalactiae*

S. dysgalactiae includes two subspecies: *Streptococcus dysgalactiae* subsp. *dysgalactiae* (SDSD), and *Streptococcus dysgalactiae* subsp. *equisimilis* (SDSE). In previous studies, phylogenetic analyses have revealed that the species *S. dysgalactiae*, *S. pyogenes*, and *S. canis* are closely related. They form a separate phylogenetic branch of the pyogenic streptococci (Jensen and Kilian, 2012). While *S. canis* and SDSE include several infections similar to those caused by *S. pyogenes*, SDSD, on the other hand, has been regarded as a restricted animal pathogen and as one of the most commonly isolated bovine pathogen (Lundberg *et al.*, 2014; Abdelsalam *et al.*, 2015).

The taxonomic status of *Streptococcus dysgalactiae* remains controversial despite years of debate and reclassifications. The β-hemolytic isolate from a human host was initially called *S. equisimilis*, while the designation *S. dysgalactiae* was given to α-hemolytic bovine isolates. Neither species was included in the Approved Lists of Bacterial names (Skerman *et al.*, 1980). Years later, DNA–DNA hybridization studies demonstrated that *S. dysgalactiae* and *S. equisimilis* belonged to a single specie (Vieira *et al.*, 1998) for which the name "*Streptococcus dysgalactiae*" was proposed. Vandamme and coworkers divided *S. dysgalactiae* isolates into two clusters based on whole-cell-derived polypeptide patterns by SDS-PAGE, chemotaxonomic and phenotypic examination (Vandamme *et al.*, 1996). Cluster I, which included animal strains of Lancefield C and L, was called *Streptococcus dysgalactiae* subsp. *dysgalactiae*, whereas cluster II, which included human strains of Lancefield C and G, the producer of streptokinase activity on human plasminogen, was designated *Streptococcus dysgalactiae* subsp. *equisimilis* (Vandamme *et al.*, 1996). Despite the evidence from phenotypic similarity and DNA–DNA hybridization experiments, several authors differentiate *S. dysgalactiae* subspecies as separate species and subdivide strains according to their pathogenicity and habitat (Efstratiou, 1997, 1994).

To provide more insights into the differentiation of *Streptococcus canis*, *S. dysgalactiae*, *Streptococcus equi* and *Streptococcus pyogenes*, the phylogenetic reconstruction based on the multilocus sequence analysis (MLSA) (methionine aminopeptidase (*map*), pyruvate formate lyase (*pfl*), inorganic pyrophosphatase (*ppac*), RNA polymerase beta subunit (*rpoB*), pyruvate kinase, (*pyk*), superoxide dismutase (*sodA*) and elongation factor Tu (*tuf*)) and on the *16S rRNA* gene sequence was reexamined (Jensen and Kilian, 2012). According to these analysis, *S. dysgalactiae* includes two separate clusters corresponding to the two subspecies, namely

"*dysgalactiae*" and "*equisimilis*". These studies also showed that SDSD and SDSE are further segregated into two subclusters. The clustering of SDSD isolates is in agreement with their hemolytic activity, and while the subcluster I harbored the alpha-hemolytic strains, subcluster II harbored beta-hemolytic strains (Jensen and Kilian, 2012).

1.3. Clinical relevance of the *Streptococcus dysgalactiae*

SDSE was primarily regarded as a human commensal organism but is now recognized as an increasingly important human pathogen, which causes a spectrum of diseases in humans similar to that of *S. pyogenes*, including cellulitis, peritonitis, septic arthritis, pneumonia, endocarditis, acute pharyngitis, bacteraemia, and toxic shock syndrome (Brandt and Spellerberg 2009). SDSE has also been identified in infectious diseases from several animal hosts, such as horses, dogs, and pigs. In horses, SDSE is part of the mucosal surfaces and skin microbiota, although it has been isolated from infections of the reproductive system and respiratory tract (Brandt and Spellerberg 2009). In pigs, SDSE can cause arthritis, endocarditis, septicemia, and meningitis, which overlaps with the diseases caused in humans. Some studies suggest SDSE potential for zoonotic infections; thus, people who work directly with infected pigs or other animals are at increased risk (Pinho *et al.*, 2016; Oh *et al.*, 2020). Usually, SDSE isolates from animals can be distinguished from human SDSE by phenotypic and genotypic characteristics. Interestingly, a MLSA study concluded that animal SDSE isolates were more closely related to the bovine SDSD than human SDSE (Pinho *et al.*, 2016).

A substantial increase in human infections associated with SDSE has been reported since the late 1970s. Some studies revealed that the overlap in the infection spectrum between *S. pyogenes* and SDSE is correlated with some virulence determinants shared between the two species, including the M-like-protein (*emm*-like gene).

Indeed, the M protein is recognized as one of the most important *S. pyogenes* virulence factors. Several studies demonstrated that this protein was able to mediate adhesion to the animal cells and the invasion of host epithelial cells (Alves-Barroco *et al.*, 2020a). Pyogenic group streptococcus is known to express adhesins with different binding properties and affinities, giving rise to a great variety of protein-protein interactions; in some specific strains, the fibronectin-binding proteins have a high affinity for soluble fibronectin, whereas in other strains they required the immobilized fibronectin for binding. Several fibronectin-binding proteins have been described in SDSE, including FnbA, FnbB, FnB, and GfbA (group G fibronectin-binding protein).

These proteins facilitate streptococcal adherence to human skin fibroblasts, contributing to the development of biofilms and persistence of infection (Collin and Olsén, 2003; Brandt and Spellerberg, 2009).

GfbA, homologues to SfbI (also fibronectin-binding proteins) of *S. pyogenes*, is present in 36% in SDSE isolates tested, mediating adherence and invasion of SDSE to human cells (Alves-Barroco *et al.*, 2020a). *S. pyogenes* SfbI takes part in the adhesion to different surfaces and was found to bind to host collagen, facilitating bacterial aggregation, colonization, and evasion of the host immune system (Dinkla *et al.*, 2003). In the adhesion process, SfbI are covered by fibronectin (Fn) allowing the biding of 5β1 integrin receptors (Rohde and Cleary 2016). Besides binding to cellular integrin receptors, SfbI recruit collagen to the bacterial surface, allowing that *S. pyogenes* form aggregates that adhere to collagen matrices (Rohde and Cleary 2016). Studies showed that SfbI triggered the aggregation of caveolae structures defining large invaginations. These caveosomes do not fuse with lysosomes, thus escaping this way the lysosomal degradation of host cells (Rohde *et al.*, 2003).

GfbA bounds to fibronectin resulting in the interaction with 5β1integrins, consequently rearrangements of host cell cytoskeleton with formation of membrane ruffles (Rohde and Cleary 2016). GfbA expressing streptococci follow the classic endocytic pathway with formation of phagolysosomes, differing from SfbI invasion of *S. pyogenes* (Rohde *et al.*, 2011). Sequence of GfbA revealed a proline rich repeat region (PRR) in the middle of the molecule, and a fibronectin-binding repeat region (FnBR) in the C-terminal has high amino acid identity to the SfbI, however, the N-terminal region, specifically the aromatic domain is significantly different (Rohde and Cleary 2016). Intracellular *Streptococccus gordonii* that express GfbA without the aromatic domain failed to fuse with lysosomes and can be released from caveosomes (Rohde *et al.*, 2011).

SDSD has been considered an exclusively animal pathogen and is commonly associated with clinical and subclinical bovine mastitis that induces serious economic consequences by affecting milk production (Zadoks *et al.*, 2011; Abdelsalam *et al.*, 2013; Cervinkova *et al.*, 2013; Rato *et al.*, 2013a). Bovine mastitis, a multifactorial disease that results from a persistent bacterial infection of the mammary glands, leads to an inflammatory response causing visible abnormal milk (e.g., color, fibrin clots), triggering economic losses worldwide (more than $1.1 billion in India, $2 billion in the United States and $371 million in the United Kingdom) (Zadoks and Fitzpatrick, 2009; De Vliegher *et al.*, 2012; Kurjogi and Kaliwal, 2014; Gomes *et al.*, 2016; Mushtaq *et al.*, 2018).

In addition to SDSD, the most prevalent species of the pyogenic group in bovine mastitis are *S. agalactiae* and *S. uberis* (Klaas and Zadoks 2018; Rosini and Margarit 2015; Pang *et al.*, 2017; Rato *et al.*, 2013; Kaczorek, *et al.*, 2017; Tomazi *et al.*, 2018).

SDSD is also the most common cause of infectious arthritis in lambs (Rutherford *et al.*, 2015). In Norway, outbreaks of infection in sheep associated with SDSD isolates have been a growing concern (Smistad *et al.*, 2021). The reservoirs and transmission mode of SDSD remain unknown, although it has been suggested that the vagina, milk, and possibly other secretions of the ewes can act as a reservoir (Smistad *et al.*, 2021). SDSD was found in less than 4% of vaginal swabs from ewes, navels, and in the oral cavity of lambs during outbreaks of infectious arthritis. Outbreaks of arthritis associated with SDSD also occur during indoor housing, which suggests that the floor can be a reservoir of these subspecies and may affect the transmission mode (Rutherford *et al.*, 2015; Smistad *et al.*, 2021). Some studies have suggested that SDSD infection may be acquired from ewes with mastitis (Lacasta *et al.*, 2008). In 2018, SDSD caused septicemia and encephalitis in vampire bats (*Desmodus rotundus*). Overall, the symptoms observed in bats were common to those associated with SDSD in other hosts (bovine, lambs, sheep) (Mioni *et al.*, 2018), suggesting an expansion of the niche of these subspecies.

In recent years, the association of SDSD with human infections, such as, upper limb cellulitis in a woman in contact with raw fish (Koh *et al.*, 2009), prosthetic joint infection after knee arthroplasty (Park *et al.*, 2012), endocarditis (Jordal *et al.*, 2015), cellulitis and bacteremia (Chennapragada *et al.*, 2018) and a case of septic shock in 45-year-old who presented initially with features of upper limb cellulitis has been reported (Nathan *et al.*, 2021). However, these cases are rare, and these subspecies' role in human pathogenesis remains unclear. The presence of human *S. pyogenes* phage-encoded virulence genes was previously reported, namely superantigen genes *speK, speC, speL* and *speM,* phage DNase1 and streptodornase genes *spd1* and *sdn* respectively, located on mobile genetic elements (MGE) among bovine SDSD isolates (Rato *et al.*, 2010, 2011). Generally, genes encoded by MGE are preponderant for host invasion and infection (Ribet and Cossart, 2015; Schmidt and Hensel, 2004), suggesting that these *S. pyogenes* genes could play an important role in the zoonosis of SDSD isolates. There is no doubt that the presence of *S. pyogenes* phage-carried virulence genes among SDSD isolates highlights the important role in the pathogenesis of this species. However, it is largely unknown the adaptation of SDSD within humans and bovines.

1.4.   Horizontal gene transfer and its implication in pathogenesis

Several events in microbial pathogenesis, such as adherence, invasion of host cells, toxin production, host immune system evasion, and dissemination in the host, have been studied for many host-pathogen interactions (McNeilly and McMillan, 2014; McShan *et al.*, 2016). In most cases, the virulence factors associated with pathogenicity are encoded by MGE; among them, bacteriophages, plasmids, integrons, integrative and conjugative elements (ICEs) are self-transmissible elements that are widespread in bacteria. In addition to the genes involved in their mobility, regulation, or maintenance, they carry other determinants, namely virulence factors (e.g., toxins, adhesins, DNase) and antibiotic resistance factors (Pletz *et al.*, 2006; Haenni *et al.*, 2010). Thus, many MGEs act as shuttles for determinants of virulence and resistance that can modulate host-pathogen interactions and extend the host range

The development of high-throughput sequencing tools has resulted in a better understanding of HGT. Within the pyogenic group, particularly in *S. pyogenes, S. agalactiae,* and SDSE, the sequence analysis of the genomes revealed the existence of products associated with the transfer of genes (e.g., such as site-specific recombinases, prophage regions, and transposases), suggesting that the analysed genomes can acquire virulence factors through HGT (Banks *et al.*, 2003; Haenni *et al.*, 2010). Closely related strains harbor similar horizontally genetic elements, including adhesins, and antibiotic resistance genes (Panchaud *et al.*, 2009). Since all *S. pyogenes* prophage regions encode virulence determinants, the prophage-induced diversity among the isolates might explain why epidemiologically similar strains can cause such a wide range of clinical symptoms (Banks *et al.*, 2003).

Although the exact mechanism of the evolution of pathogenicity by HGT is not completely understood, it is clear that virulence and antibiotic resistance determinants encoded by MGE are not limited to human bacteria isolates (Kalia and Bessen, 2004; Beres and Musser, 2007; Davies *et al.*, 2007; Brochet *et al.*, 2008). The exchange of lysogenic phages among *S. pyogenes* and other human and animal species, particularly SDSE, *S. equi* subsp. *equi* and *S. equi* subsp. *zooepidemicus* has been previously reported (Davies *et al.*, 2007; Holden *et al.*, 2009).

Horizontal transfer of genes by bacteriophages

The bacteriophages are typically grouped according to their life cycle: lytic phages and lysogenic or temperate phages. The life cycle of lytic phages begins by

infection of host cells, followed by replication, assembly of the phages, and lysis of the host cell with the release of new viral particles. These phages can change the host cell population by eliminating susceptible cells. In comparison, the lysogenic bacteriophages can integrate their DNA into the host genetic material by site-specific recombination, being passed to daughter cells. These phages are common in *S. pyogenes* (McShan *et al.*, 2016). In 1968 was reported for the first time the transduction in *S. pyogenes* could transduce streptomycin resistance. Of this group of phages, phage A25 showed a greater frequency of transduction of the resistance (McShan *et al.*, 2016).

Several studies reported the role of transduction in the dissemination of virulence and resistance genes among related streptococcal species. The number and diversity of prophage regions among *S. pyogenes* and SDSE genomes show the importance of phages in promoting genetic diversity in these species (Watanabe *et al.*, 2013). There is a large range of virulence-associated *S. pyogenes* genes that are carried by these prophages elements, e.g., Superantigens (*speA, speC, speG, speH, speI, speJ, speK, speL*); DNases (spd1) and phospholipase A2 (*sla*) (Proft and Fraser, 2016). Studies suggested that the expression of phage-encoded virulence determinants is not autonomous, and may be linked to the genetic background (Venturini *et al.*, 2013) or physiological state (Anbalagan and Chaussee, 2013). For example, the expression of SpeC and Spd1 is increased when bateria cells are co-cultured with human cells (Broudy *et al.*, 2001, 2002). Similar results were observed for toxins SpeK and Sla when co-cultured with human cells (Banks *et al.*, 2003). The genetic background of the strains seems to be behind the acquisition of prophages, resulting in the increased pathogenic potential of the host strain (Venturini *et al.*, 2013).

Despite the benefits of HGT, due to the vast diversity of bacteriophages in the environment, the bacteria are under constant phage attack (Maciejewska *et al.*, 2018; Ghosh *et al.*, 2019). To survive, bacteria have conceived several strategies that involve innate and adaptive immune responses and interfere with the infection process (Barrangou and Marraffini, 2014; Hille *et al.*, 2018). The bacteriophage resistome can be divided into broad categories: i) adsorption resistance mechanisms; ii) restriction-modification systems; iii) clustered regularly interspaced short palindromic repeat (CRISPR)/CRISPR-associated (Cas) systems, and iv) abortive infection systems (Bhaya *et al.*, 2011; Nozawa *et al.*, 2011; Lopez-Sanchez *et al.*, 2012; Johnston *et al.*, 2013; Harms *et al.*, 2018). The CRISPR, together with a group of Cas and Cse (CRISPR Cascade complex) proteins constitutes part of the adaptive immune system in prokaryotic cells,

conferring resistance to MGEs, including **bacteriophages** (Lopez-Sanchez *et al.*, 2012). CRISPR-Cas systems function by uptake and integration of foreign genetic element sequences into the CRISPR array, which constitutes a genomic archive of iterative vaccination events (Bhaya *et al.*, 2011; Sorek *et al.*, 2013; Barrangou and Marraffini, 2014). Consequently, CRISPR spacers can be investigated to reconstruct the interplay between viruses and bacteria, and data can provide insights into host-phage interactions within a niche. Given their diversity and rapid evolution, CRISPR sequences have been proposed as a discrimination tool for typing closely related isolates (Grissa *et al.*, 2007).

1.5.   Resistance to antimicrobial drugs

In general, bacterial drug resistance can be divided into intrinsic and acquired resistance (Reygaert, 2018). Intrinsic resistance is a naturally occurring phenomenon that prevents antimicrobial activity and is common to most strains of a given specie, which may be constitutive or induced. One example of intrinsic resistance is mediated by activation of efflux transporters (Fernandez *et al.*, 2010). Acquired resistance might be due to chromosomal point mutations or by the acquisition of mobile resistance genes, in which resistant strains emerge from previously sensitive bacterial populations, usually after exposure to the antimicrobial agent (e.g., antibiotic pressure) (Baptista *et al.*, 2018; Enault *et al.*, 2017).

Several antibiotic resistance mechanisms among pyogenic streptococci have been reported. Table 1.2 summarizes the main antibiotics used for the treatment of pyogenic streptococcal infections and their respective resistance mechanisms.

Table 1.2. Main mechanisms of antibiotic resistance in pyogenic streptococci.

Mechanism	Target antibiotics	Examples	Location	Reference
Enzyme inactivation	Aminoglycosides	Aminoglycoside-modifying enzymes (AMEs) - APH(3')-IIIa; ANT(6)-Ia; AAC(6')-APH(2″)	Chromosome and MGE, e.g., Tn4001, Tn5405 and Tn3706 (Tn4001 derivative)	Cattoir 2016; Doumith *et al.*, 2017; Galimand *et al.*, 1999; Kristich *et al.*, 2014; Prudhomme *et al.*, 2002
	Chloramphenicol	Chloramphenicol O-acetyltransferase (CAT) enzyme encoded by genetic determinants *cat*(pC194); *cat*(pC221); *cat*(pSCS7); *cat*S, and *cat*Q	Plasmid and conjugative transposon Tn1545 and Tn5253-like	Del Grosso *et al.*, 2011; Mingoia *et al.*, 2015; Schwarz *et al.*, 2004; Woodford 2005
	Lincosamide	LinB/A catalyze adenylylation of antibiotics	MGE	Osei Sekyere and Mensah 2019; Rato *et al.*, 2013
Preventing drug acess to target	Tetracycline	Efflux pumps Tet(K)	Chromosomal insertion element	Emaneini *et al.*, 2014; Nguyen *et al.*, 2014; Rato 2013
	Quinolones	Efflux pumps PmrA	Chromosome	Martinez-Garriga *et al.*, 2007
	Macrolides	Efflux pumps Mef and Msr	MGE such as Tn917 and bacteriophage Φm46.1.	Brenciani *et al.*, 2004, 2007; Del Grosso; Di Luca *et al.*, 2010; Hadjirin *et al.*, 2014; Rato *et al.*, 2013
	Tetracycline	Tet(M), Tet(O), Tet(Q), Tet(S), Tet(T), Tet(W) ribosomal protection proteins dissociate tetracycline from ribosome	MGE (Tn916 and Tn3701) and bacteriophages Φ m46.1	2007; Cunha *et al.*, 2015; Nguyen *et al.*, 2014; Nikaido 2009; Silva *et al.*, 2015
Target modification	Quinolones and Fluoroquinolones	Point mutations primarily in quinolone resistance-determining regions (QRDRs), of *par*C and *gyr*A genes	Chromosome. Evidence for horizontal transfer of QRDR between streptococci has been reported.	Balsalobre *et al.*, 2003; Hooper and Jacoby 2016; Orscheln *et al.*, 2005; Pham *et al.*, 2019
	Tetracycline;Aminoglycosides	Modification in rRNA	Chromosomal mutation	Nguyen *et al.*, 2014
	Macrolides	Modification of 23S rRNA and/or ribosomal proteins L4 and L22 determinants	Chromosomal mutation	Jalava *et al.*, 2004; Malbruny *et al.*, 2002
	β-lactam	Modification of penicillin-binding proteins 1A [PBP1A], PBP2B, and PBP2X	Chromosomal mutation	Vannice *et al.*, 2019; Fuursted *et al.*, 2016; Kimura *et al.*, 2013; Moroi *et al.*, 2019; Musser *et al.*, 2020; Pillai *et al.*, 2009;
	Macrolides-Lincosamide-Streptogramin B	Modification by methylation of rRNA (*erm*-class genes)	The *erm*(B) and *erm*(TR) genes are found in the chromosome of streptococci and conjugative transposons	Cattoir 2016; Brenciani *et al.*, 2007, 2011

The acquisition of MGEs is recognized as a key point in the emergence of multidrug-resistant (MDR) strains (Lehtinen *et al.*, 2019). Among streptococci, many resistance determinants can be encoded in the same mobile genetic element; for example, genes encoding resistance to tetracycline (e.g., *tet*M, *tet*O) are frequently acquired by

MGEs, which also harbor erythromycin resistance determinants (e.g., *erm*B, *erm*TR/*mef*A) (Brenciani *et al.*, 2004, 2007, 2011; Cattoir 2016; Emaneini *et al.*, 2014). There is a significant association between *tet*M and *erm*B that has been identified among the strains of pyogenic streptococci, and can be co-transferred among *S. agalactiae* and S*. pyogenes* strains (Brenciani *et al.*, 2007; Emaneini *et al.*, 2014). There is also evidence of the linkage between *tet*O and *erm*TR/*mef*A genes (Giovanetti *et al.*, 2003) and the lysogenic transfer of these genes carried by Φ m46.1 among *S. pyogenes* (Di Luca *et al.*, 2010) that contribute to the MDR phenotype.

It was suggested that the emergence of *S. agalactiae* clones able to cause human infections in the 1960s was associated with the acquisition of tetracycline resistance determinants (in particular the *tetM* gene) (Cunha *et al.*, 2015). This report has suggested that a few *S. agalactiae* clones, originally adapted to the bovine host, acquired *tetM* genes via conjugative transposons of the Tn916 family, which were then selected by the widespread use of tetracycline in human medicine during the 1950s. The clones were fixed and rapidly spread throughout the world. Thus, tetracycline resistance mediated by the *tetM* gene can be considered a marker of success among human-adapted *S. agalactiae* lineages (Cunha *et al.*, 2015). High ratios of tetracycline resistance, ranging from 70 to 95%, are usually observed in human *S. agalactiae* strains in different countries, among which *tetM* is harbored by up to 90% (Sharmila *et al.*, 2011). In turn, bovine *S. agalactiae* strains are usually resistant to tetracycline, among which *tetM* can be found in only 2–20% (Dogan *et al.*, 2005; Gao *et al.*, 2012). Interestingly, among the *S. agalactiae* resistant strains*, tetM* is found with the *ermB* gene in the same conjugative transposon, such as those of the Tn916 family conveying resistance to both antibiotics (Ciric *et al.*, 2011; Cunha *et al.*, 2015). Tetracycline is no longer indicated for the treatment of bovine mastitis-associated streptococci in Portugal, as research regarding the molecular epidemiology and evaluation of antimicrobial drug resistance patterns of *S. agalactiae*, SDSD, and *S. uberis* collected from bovine subclinical mastitis between 2002/2003 in Portugal revealed high levels of resistant isolates (64.8 to 100%) (Rato *et al.*, 2013). All the tetracycline-resistant isolates carried at least one of the *tet* genes (*tetM*, *tetO*, *tetK* and *tetS*) (Rato *et al.*, 2013).

More recently, Horiuk and coworkers analyzed the resistance to antimicrobials among bovine mastitis pathogens. Their results showed resistance to penicillin, aminoglycosides, and macrolides (Horiuk *et al.*, 2019). In addition, the indiscriminate administration of antibiotics in dairy cows for the promotion of growth and treatment

provides substantial residues of antibiotics that are released through the milk and have significant impact on human health (Sachi *et al.* 2019), emphasizing the need of alternative approaches to effectively treat bovine mastitis.

MDR SDSD strains with differential sensitivity to antibiotics (e.g., cloxacillin, penicillin, oxacillin, clindamycin, vancomycin, third-generation cephalosporin, gentamicin) were found within these human infections, only dying after complex antibiotic combinations (Koh *et al.*, 2009; Park *et al.*, 2012; Jordal *et al.*, 2015; Chennapragada *et al.*, 2018).

1.6. Biofilm formation

In nature, bacteria can exist in the planktonic form, where cells live freely in solution, or in a biofilm or sessile form, where they grow attached to a biotic or abiotic surface (Alves-Barroco *et al.*, 2020a; Jamal *et al.*, 2018). Biofilm formation is part of a defense mechanism that bacteria adapt to achieve a favorable environment, keep nutrients and increase the chances of survival; thus, the ability of bacteria cells to colonize a habitat is frequently dependent on the biofilm formation (Alves-Barroco *et al.*, 2020a; Chen and Wen, 2011; Young *et al.*, 2016; Del Pozo, 2018; Jamal *et al.*, 2018; Khatoon *et al.*, 2018). Bacterial biofilms are ubiquitous in the environment and can be found on almost any hydrated non-shedding surface, including rivers, stagnant pools, man-made and biological materials (Garnett and Matthews, 2012). Some characteristics of the human body, such as shear forces caused by teeth, blood pressure, or the innate immune system, trigger bacterial cells to adopt the biofilm phenotype, as they resemble some of the stimuli that induce biofilm formation in challenging environments (Jefferson, 2004; Gupta *et al.*, 2016).

The biofilm consists of a complex community of genetically similar and/or distinct cells encased in a self-produced extracellular polymeric substance matrix (EPS), accounting for 80% of the structure. The EPS contains a mixture of alginates, extracellular teichoic acid (TA), proteins, poly-N-acetyl glucosamine, lipids, phospholipids, polysaccharides, and extracellular DNA (eDNA) (Alves-Barroco *et al.*, 2020a). About 97% of the EPS is composed of water, which is a solvent dictating viscosity and mobility (Sutherland, 2001; Lu and Collins, 2007; Flemming and Wingender, 2010; Kumar *et al.*, 2017; Jamal *et al.*, 2018). The EPS composition is a crucial biofilm property as it provides cohesion and a three-dimensional architecture. Overall, the nature of the biofilm matrix

depends on the microbial cells, their physiological status, the nutrients available, and the physical conditions (Alves-Barroco *et al.*, 2020a).

Several reports indicate that the extracellular matrix of pyogenic streptococcal biofilms is rich in proteins (Alves-Barroco *et al.*, 2019; Genteluci *et al.*, 2015; Young *et al.*, 2016). A role for eDNA was also demonstrated by reducing biofilms formed by SDSE isolates after treatment with DNase I (Genteluci *et al.*, 2015). The addition of a carbohydrate oxidant, such as sodium metaperiodate, to the biofilm of SDSE, indicated the presence of an exopolysaccharide. Doern and coworkers examined *S. pyogenes* strains from different clinical sources and demonstrated the requirement for protein and eDNA in the biofilm matrix and only a passive role for carbohydrates (Doern *et al.*, 2009). This is interesting and in contrast to SDSE biofilms for which several polysaccharides have been shown to be required (Genteluci *et al.*, 2015).

Biofilm growth of streptococci has been investigated, but insights into the genetic origin of biofilm formation are limited. Although most pyogenic streptococci are able to form biofilms, there is substantial heterogeneity among strains in the strength of adherence to different surfaces. In streptococci biofilms, as in those of most bacterial genera, gradients of nutrients, waste, and signaling molecules are formed, allowing groups of cells to adapt to different environments within the same biofilm and grow at different rates (Genteluci *et al.*, 2015; Rosini and Margarit, 2015; Young *et al.*, 2016).

Overall, biofilm formation is a complex multi-step process that interplay between adhesive and disruptive forces. The formation of a biofilm is typically described in three stages (1) initiation, where attachment occurs (which can be reversible or irreversible), (2) maturation, with development of microcolonies, and (3) dispersion, when some members of the community are released from the biofilm and assume the planktonic phenotype (Alves-Barroco *et al.*, 2020a). Table 1.3 summarizes the main virulence factors associated with biofilm formation among streptococci.

Table 1.3. Streptococci virulence factors involved in biofilm formation in pyogenic streptococci.

Protein	Function and/or substrate	Species	Reference(s)
Adhesion protein – AdcA	Cell adhesion; Zinc ion transport - Contributes to the infection process	*S. pyogenes*, SDSE, SDSD, *S. pneumoniae, S. canis, S. agalactiae*	Cao *et al.*, 2018; Moulin *et al.* 2016
Collagen-like protein 1 (*scl-1*)	Promotes adhesion and biofilm formation, decreases bacterial killing by neutrophil extracellular traps	*S. pyogenes, S. agalactiae, S. pneumoniae, and S. equi.*	Döhrmann *et al.*, 2014; Lukomski etal., 2017; Oliver-Kozup 2011
Collagen-like protein SclB (*sclB*)		S. *pyogenes, S. uberis*, SDSE, SDSD*, S. agalactiae, S. pneumoniae, and S. equi.*	Lukomski etal., 2017; Rato *et al.*, 2011
FnbA, FnbB	Fibronectin-binding proteins	SDSD; SDSE	Alves-Barroco *et al.*, 2018; O'Neill *et al.*, 2009
GfbA	Fibronectin-binding proteins	SDSE	Lindgren *et al.*, 1994; Oppegaard *et al.*, 2018
Glyceraldehyde-3-phosphate dehydrogenase (*plr*)	Plasmin and Fn-binding protein	*S. pyogenes*, SDSE, SDSD, *S. suis, S. agalactiae, S. uberis*	Rato *et al.*, 2011; Reinoso 2017
Laminin-binding protein (*lmb*)	Laminin-binding surface proteins	*S. pyogenes*, SDSE, SDSD, *S. pneumoniae, S. canis, S. agalactiae*	Al Safadi *et al.*, 2010; Rato *et al.*, 2011
Lipoteichoic acid (LTA)	Adherence to epithelial cells of host Biofilm formation	*S. pyogenes, S. uberis*, SDSE, SDSD*, S. agalactiae, S. pneumoniae, and S. equi, S. gordonii*	Courtney *et al.*, 2009; Lima *et al.*, 2019; Rato *et al.*, 2011; Shiraishi *et al.*, 2016
M protein (emm)	Adherence to epithelial cells of host; Plasminogen, fibronectin and Fibrinogen-binding proteins; Ig-binding proteins Biofilm formation	*S. pyogenes*, SDSE, *S. canis*	Courtney *et al.*, 2009; Frost *et al.*, 2018; McNeilly *et al.*, 2014; Rato *et al.*, 2011
M-like protein (*emm-like*)			
R28	Promotes adhesion to host cells via direct binding to integrins	*S. pyogenes*, SDSE, SDSD	Eraso et aal., 2020; Rato *et al.*, 2011; Weckel *et al.*, 2018
DNases	Degradation of NETs that are produced by the host's immune system cells (like neutrophils)	*S. pyogenes, S. agalactiae*, SDSD, SDSE	Rato *et al.*, 2010, 2011; Genteluci *et al.*, 2015; Remmington and Turner, 2018
Biofilm regulatory proteins A (BrpA)	Biofilm formation, autolysis, and cell division	*S. pyogenes, S. agalactiae, S. mutans*, SDSD, SDSE	Alves-Barroco *et al.*, 2018; Bitoun *et al.*, 2012, 2014; Patras *et al.*, 2018

1.6.1.   Biofilms and antimicrobial resistance

Biofilms protect microorganisms from nutrient scarcity, mechanical forces, host's immune system and from antimicrobial agents' action. Several *in vitro* studies demonstrated that a bacterial biofilm could become 10 to 1000 times more resistant to the effects of antimicrobials than their planktonic counterparts (Alves-Barroco *et al.*,

2020b). Therefore, biofilm formation should be considered a core resistance mechanism since it increases treatment failure and promotes persistent infection.

Even though the resistance associated with streptococci biofilms is not entirely understood, several mechanisms have been proposed to support increased resistance to antimicrobials. These mechanisms result from the biofilms' multicellular nature, which leads to an additive and/or synergistic effect among the biofilm community's protection (Rosini and Margarit 2015; Young *et al.*, 2016).

The composition of the EPS matrix likely influences the resistance against different antimicrobial classes. For certain compounds, it is known that the EPS matrix represents a primary physical and/or chemical diffusion barrier that prevents the entrance of polar and charged antibiotics, but studies showed that the biofilm matrix does not form an impermeable barrier to the diffusion of antimicrobials, and other mechanisms may contribute to promote biofilm cell survival (Trappetti *et al.*, 2011, Alves-Barroco *et al.*, 2020b).

Previous studies show that a biofilm-specific phenotype is stimulated within a particular subpopulation, resulting in the differential expression of mechanisms against the antimicrobials (Genteluci *et al.*, 2015; Konto-Ghiorghi *et al.*, 2009), in other words, the heterogeneous growth of cells within the biofilm and the activation of stress response genes may contribute to the resistance phenotype. During biofilm development, a gradient is established, in which the outer layers are metabolically active and aerobic, while the more inner layers are anaerobic with a reduced growth rate. This slow growth has been observed in streptococci biofilms that are frequently accompanied by a significant increase in antibiotic resistance (Bjarnsholt *et al.*, 2013; Macià *et al.*, 2014). Several antibiotics, such as aminoglycosides, β-lactams, and fluoroquinolones, do not seem to be active in anaerobic conditions, affecting only the outermost layers of the biofilm (Borriello *et al.*, 2004). Cell-wall active antibiotics, namely β-lactams and glycopeptides, have minimal activity against bacteria that are not replicating and are metabolically inactive posing several problems in the clinical context (Del Pozo 2018).

1.6.2. Clinical relevance of pyogenic biofilm

According to the National Institute of Health, biofilms account for up to 80% of the total bacterial infections in humans, including endocarditis, periodontitis, sinusitis, meningitis, osteomyelitis, and chronic wounds and prosthesis and implantable devices related infections (Khatoon *et al.*, 2018). In many of these cases, infection arises from

implantable medical devices, such as catheters, implants, and implantable electronic devices (Khatoon *et al.* 2018; Pelling *et al.*, 2019; Narayana and Srihari 2019 Garnett and Matthews, 2012; Garnett *et al.*, 2012) that become contaminated with biofilms of staphylococci or streptococci (Kokare *et al.*, 2009; Marks *et al.*, 2014b; Rosini and Margarit, 2015; Gomes *et al.*, 2016; Young *et al.*, 2016; Castilho *et al.*, 2017; Stewart and Bjarnsholt 2020). In veterinary settings, the production of biofilms can significantly affect the effectiveness of the treatment of bovine mastitis. Besides increased resistance to different antibiotics, the biofilm promotes mammary tissue adherence and colonization (Wallis *et al.*, 2018).

It is known that biofilms play an important role in streptococci pathogenesis. These can cause opportunistic infections that give rise to localized and systemic infections under appropriate conditions, with considerable implications on public health and the veterinary industry (Pires *et al.*, 2005; Rato *et al.*, 2013; Barnett *et al.*, 2015; Peters, 2017). *S. pyogenes* biofilm was first detected in the skin (Akiyama *et al.*, 2003) and other infection sites (Lembke *et al.*, 2006; Swidsinski *et al.*, 2007).

The biofilm phenotype can be correlated with asymptomatic carrier persons, recurrent infections, systemic dissemination of the infection, and antibiotic failure (Fiedler 2013, Fiedler 2015). In addition, biofilms can promote horizontal spread of resistance determinants (Savage *et al.*, 2013). The increasing recognition of the impact of pyogenic infections, namely when adopting the biofilm phenotype, recurrent infections, uncontrolled contagion, therapeutic failure and morbidity, has motivated scientists to find new solutions for this old problem.

1.7.   Emergent strategies to fight biofilm infection

To tackle the growing MDR concerns, a plethora of alternative compounds, strategies and platforms has been proposed as an alternative to conventional antimicrobials. Some of these alternatives are mere concepts whose promising *in vitro* efficacy has been the focus of attention. Many of these novel solutions have been proposed to be used alone against MDR bacteria, but many others have been proposed to be used in combinatory strategies with traditional antibacterial drugs to enhance efficacy, circumvent the onset of mechanisms of resistance.

Among these new innovative strategies alternative to conventional antibiotics, are included bacteriocins, bacteriophage, and phage lysins, and metal nanoparticles (Alves-Barroco *et al.*, 2020b). Nanomaterials have recently gained great interest due to

the variety of applications in biomedicine (McNamara and Tofail, 2017). Nanomaterials comprise a range of constructs, materials, and functional systems of particles whose size Is between 1 and 100 nm. The use of nanoparticles as antibiotic therapy has relied on these nanostructures acting as carrier of drugs, either via their integration or incorporation into the nano formulations, or adsorbed to the surface so as to improve biodistribution and pharmacokinetics, e.g., solubility, controlled drug liberation and therapeutic effectivity (Gao *et al.*, 2018). Furthermore, nanoparticles could be designed to enhance solubility, control the release of drug, and increase clearance from the organism, thus improving the therapeutic window of the cargo drug. Also, some synergistic strategies may be used, such as photothermal ablation of cells, where combination to the "traditional" chemotherapeutic may lead to an increase of efficacy.

Silver Nanoparticles (AgNPs)

Traditionally, Silver (Ag) has been employed as antimicrobial, namely silver sulfadiazine and silver nitrate (Lansdown, 2006), which relied on the release of Ag+ that triggers a range of processes resulting in hampered bacterial growth. Silver nanoparticles has allowed improved release of silver ions and, thus, enhance the bactericide action (Dakal *et al.*, 2016).

Although the biocidal action of AgNPs has been attributed mainly to the Ag+ release, the actual mechanism is not yet completely elucidated. Crucial to their effect is the fact that AgNPs tend to accumulate at the membrane where they progressively aggregate, allowing silver ions to interact with different functional groups, such as sulfate or phosphate, and disturb the function of the bacterial membrane, promoting its rupture and liberate the cytoplasmatic content (Le Ouay and Stellacci, 2015). Other studies have suggested that Ag+ is able to interact and inactivate some biological structures and affect the bacteria' respiratory process, namely inhibiting the respiratory chain (Costa *et al.*, 2010). However, perhaps the most widely accepted hypothesis is the production of reactive oxygen species (ROS), like superoxide or hydrogen peroxide, which interact with the lipids, proteins or DNA, promoting alteration in the normal functions, triggering lysis and cell death (Quinteros *et al.*, 2016).

Furthermore, the synergistic effect with other conventional antibiotics makes possible the application of AgNPs as an alternative tool to tackle MDR strains. In fact, AgNPs and conventional antibiotics exert their biocidal action via different mechanisms and, therefore, their combination would prevent the development of added resistance.

For example, clindamycin has already been combined with AgNPs resulting in lower MICs in a synergistic effect and rifampicin coupled to AgNPs increased the antibiotic effect against methicillin resistant bacteria (Khan *et al.*, 2019).

Gold Nanoparticles (AuNPs)

Gold nanoparticles have also been employed in different fields of biomedical research due to their ease of synthesis, biocompatibility, and low toxicity to higher eukaryotes. They are easier to functionalize with different biological moieties like DNA, mRNA, peptides, etc. than their silver counterparts. Moreover, AuNPs present remarkable optical and photoelectric properties that have demonstrated high potential toward the development of new therapy tools (Amendoeira *et al.*, 2019).

AuNPs have been reported to exhibit antimicrobial activity against a wide range of bacteria and fungus (Tao, 2018). Several mechanisms of action have been highlighted as the basis of their antimicrobial properties, namely: AuNPs may bind to the membrane of bacteria, modify the membrane's potential, decrease intracellular ATP levels, disturb intracellular trafficking, aggregate together with proteins and disturb the assembly of tRNA to the ribosome (Cui *et al.*, 2012). Perhaps, the main aspect related to antimicrobial efficacy relates to nanoparticle dispersion and the AuNPs' surface roughness that could interact with the bacteria membrane (Lima *et al.*, 2013).AuNPs have also been proposed as drug carriers, conveyors of gene therapy and photothermal therapy (Li *et al.*, 2019).

The use of AuNPs as drug delivery systems for traditional antibiotics has made possible to administrate drugs more effectively and uniformly distributed toward the target tissue, improving the efficacy and biocompatibility of antibiotic conjugated AuNPs. The surface of AuNPs may be easily functionalized with small ligands harboring carboxylic acid, hydroxyl, or amine functional groups that can then be used to conjugate antimicrobials (Lee *et al.*, 2017). The assembled nano formulations improves solubility of non-water-soluble drugs and allows for controlled and localized release of the antibiotic, for example with an external stimulus (Canaparo *et al.*, 2019).

When AuNPs are irradiated by light with an appropriate wavelength, they tend to convert the received energy into heat, thus resulting in a hyperthermal effect capable to induce damage to the membrane structure (Amendoeira *et al.*, 2019; Kirui *et al.*, 2019). The antimicrobial effect using photothermally active nanomaterials may become an interesting tool against antibiotic resistance. For example, near-infrared (NIR) radiation is useful to promote hyperthermy based on AuNPs, effective against *S. aureus* and *E.*

coli after 10 min of irradiation at 808 nm (Alhmoud *et al.*, 2017). NIR photothermy using AuNPs has been also used as an efficient technique to eliminate a broader range of microorganism with improved antibiofilm activity. In fact this approach was demonstrated effective at damaging the cell wall of streptococci, such as *S. mutans*, *S. sobrinus*, *S. oralis* and *S. salivarius* (Castillo-Martínez *et al.*, 2015).

The combination of these two metals, silver, and gold, in alloy nanoparticles has also been proposed as suitable nanoagent against microbes. In fact, such approach combines the improved stability and ease of functionalization provided by gold, with the higher antimicrobial activity of silver, while avoiding some problems associated with the aggregation and toxicity to the host (Dos Santos *et al.*, 2012). Gold-silver alloy nanoparticles have shown their potential to eradicate biofilm and reduce the MICs against Gram-positive and Gram-negative bacteria, which could then be used to circumvent drug resistance (Ramasamy *et al.*, 2016). Kyaw and coworkers showed that submitting triangular AuNPs coated by silver to laser irradiation, induced a change of shape to spherical and increased the antibacterial activity (Kyaw *et al.*, 2017).

Despite the progress achieved to date, most alternative approaches are of narrow spectrum unlike the broad-spectrum of conventional antibiotics. However, the combined action of one of these alternative approaches with traditional antibiotics may increase the success rate of therapeutics once that most new strategies attenuate bacterial pathogenesis allowing bacteria to be eliminated by antibiotics and action of the immune system. Moreover, combination therapies may decrease the selective pressure for resistance to antibiotics, and consequently to reduce the rate of emergence of resistance.

1.8.   Thesis aims

Given what we have learn so far, there is plenty of room for advancing our knowledge on bovine SDSD temporal evolution at the level of genotype and phenotype providing a deep information on their mechanisms of action and virulence potential. By increasing our knowledge on their pathogenic potential using *in vivo* and *in vitro* models of infection, their virulence and antibiotic resistance factors, their capability to form biofilms and drugs/treatment strategies for surpassing this MDR mechanisms, we could contribute for the decrease of bovine mastitis in Portugal and elsewhere and to reveal novel treatment strategies towards their eradication.

Considering this, the specific aims of this thesis were:

(i)   To assess epidemiologically clusters defined by molecular typing tools to compare bovine mastitis SDSD isolates collected during two different periods (2002-03 and 2011-13) and to identify putative prevalent and time-persistent clones. This temporal evolution will allow to search for virulence determinants, including genes associated with streptococcal infections, particular adhesion, invasion, biofilm formation, and evasion of the host immune system and to assess resistance profiles to several classes of antimicrobial drugs and evaluate the mechanisms involved in the resistance phenotypes.

(ii)   To observe the ability of bovine *S. dysgalactiae* subsp. *dysgalactiae* to form biofilms on abiotic surfaces (polystyrene, glass), evaluate biofilm nature and structure, and assess the ability of different compounds to eradicate the biofilms produced. To assess the capability of SDSD to form biofilms *in vivo* and investigate new treatment strategies for SDSD biofilms eradication.

(iii)   To characterize the different bacterial strains' ability to adhere to and invade human and other animals' cells, and to assess quantitative bacterial proliferation in zebrafish. To explore further the infection mechanisms of bovine SDSD in human cells by proteomic analysis to investigate the colonization factors that promote pathogen adhesion and invasion to human cells.

(iv)   To analyze whole-genome sequences of *S. dysgalactiae* subsp. *dysgalactiae* and *S. dysgalactiae* subsp. *equisimilis* from different hosts (including genomes of *S. dysgalactiae* isolated from human, dog, horse, pig, and fish available from NCBI) to retrieve their phylogenetic structure and accessory genes that influence the pathogenicity of SDSD isolates, and to understand if *S. dysgalactiae* subsp. *dysgalactiae*, *S. dysgalactiae* subsp. *equisimilis* and *S. pyogenes* share mobile genetic elements (e.g., prophages regions) and establish their influence on the pathogenicity potential of bovine isolates.

Chapter 2 - New Insights on *Streptococcus dysgalactiae* subsp. *dysgalactiae* Isolates

Alves-Barroco, C., Caço, J., Roma-Rodrigues, C., Fernandes, A. R., Bexiga, R., Oliveira, M., Chambel, L., Tenreiro, R., Mato, R., and Santos-Sanches, I.

Abstract

This study aimed to characterize the bovine SDSD isolates collected in 2011–13 and compare them with SDSD isolates collected in 2002–03 and pyogenic streptococcus genomes available at the National Center for Biotechnology Information (NCBI) database, including human SDSD and SDSE strains to track temporal shifts on bovine SDSD genotypes. The very close genetic relationships between humans SDSD and SDSE were evident from the analysis of housekeeping genes, while bovine SDSD isolates seem more divergent. The results showed that all bovine SDSD harbor Clustered Regularly Interspaced Short Palindromic Repeats (CRISPR)/Cas IIA system. The widespread presence of this system among bovine SDSD isolates, high conservation of repeat sequences, and the polymorphism observed in spacer can be considered indicators of the system activity. Overall, comparative analysis shows that bovine SDSD isolates carry *speK, speC, speL, speM, spd1*, and *sdn* virulence genes of *S. pyogenes* prophages. Our data suggest that these genes are maintained over time and seem to be exclusively a property of bovine SDSD strains. Although the bovine SDSD genomes characterized in the present study were not sequenced, the data set, including the high homology of superantigen (SAgs) genes between bovine SDSD and *S. pyogenes* strains, may indicate that events of horizontal genetic transfer occurred before habitat separation. All bovine SDSD isolates were negative for genes of operon encoding streptolysin S, except for *sagA* gene, while the presence of this operon was detected in all SDSE and human SDSD strains. The data set of this study suggests that the separation between the subspecies "*dysgalactiae*" and "*equisimilis*" should be reconsidered. However, a study including the most comprehensive collection of strains from different environments would be required for definitive conclusions regarding the two taxa.

2.1. Introduction

Streptococcus dysgalactiae includes two subspecies: SDSD and SDSE (Jensen and Kilian, 2012). While SDSE has been recognized as an increasingly important human pathogen, SDSD has been considered a strictly animal pathogen and is commonly associated with bovine mastitis (Zadoks *et al.*, 2011; Rato *et al.*, 2013). In the last years, although rare, human diseases by this subspecies have been reported (Koh *et al.*, 2009; Park *et al.*, 2012; Jordal *et al.*, 2015; Chennapragada *et al.*, 2018), and it is urgent to understand the role of this subspecies in human pathogenesis. Recently, we have reported bovine SDSD isolates' ability to adhere to and internalize different human cell lines, including keratinocytes (Roma-Rodrigues *et al.*, 2016; Alves-Barroco *et al.*, 2018).

SDSD and SDSE, together with *S. agalactiae, S. canis,* and *S. pyogenes*, are the major pathogens of the pyogenic group. Previous studies reveal that these species are closely related. Phylogenetic analysis involving the *Streptococcus* core genome within the pyogenic clade displayed consensus. Though the issue is not entirely clear-cut, the most likely scenario is that the species tree has *S. dysgalactiae* and *S. pyogenes* as sister species and, together with *S. canis*, establishes a very closely related branch. These data suggest that they have recently descended from a common ancestor (Suzuki *et al.*, 2011; Jensen and Kilian, 2012; Lefébure *et al.*, 2012). The divergence among species has been mainly associated with MGEs (Lefébure *et al.*, 2012). Indeed, about a quarter of streptococci's genome consists of exogenous and mobile DNA, e.g., transposons, prophage, and plasmid. Thus, HGT is considered the primary mechanism for generating diversity in this genus (Baiano and Barnes, 2009; Haenni *et al.*, 2010; De la Casa-Esperón, 2012; Richards *et al.*, 2012; Wong and Yuen, 2012; Rohde and Cleary, 2016). Overall, the MGEs are self-transmissible elements that are omnipresent in bacteria, harboring genes responsible for their maintenance, regulation, and mobility and genes encoding antimicrobial resistance, as well as other determinants, such as genes that encode virulence factors (Grohmann *et al.*, 2003; McNeilly and McMillan, 2014).

Thus, many MGEs serve as shuttles for genes that are beneficial to bacteria during their proliferation in a host environment. Although several mechanisms can mediate genetic transfer in pyogenic streptococci, the transduction might be particularly relevant since bacteriophages have been detected in a considerable proportion (McShan and Nguyen, 2016). In *S. pyogenes* and SDSE, more than 20% of the accessory genomes consist of prophage DNA, highlighting the critical role of transduction in the evolution of these bacteria (Lier *et al.*, 2015; Yamada *et al.*, 2019).

The presence of phage-carrying *S. pyogenes* virulence genes among SDSD isolates from bovine mastitis was previously reported, namely, the superantigen genes (*speK*, *speC*, *speL*, and *speM*), the phage DNase (*spd*1), and determinants of antibiotic resistance located on MGEs (Rato *et al.*, 2011; Abdelsalam *et al.*, 2015). It was hypothesized that these virulence genes might contribute to the increased pathogenic potential; thus, SDSD should not be ignored as a potential human pathogen.

Despite the benefits of HGT, due to the vast diversity of the bacteriophages in the environment, the bacteria are under constant phage attack. To survive, the bacteria have devised various strategies that involve innate and adaptive immunity and interfere with the infection process (Barrangou and Marraffini, 2014). Among all of these strategies, the Clustered Regularly Interspaced Short Palindromic Repeats (CRISPR)/Cas system is the one that provides the bacteria with the ability to "memorize" a piece of the invaders' genetic material (Bhaya *et al.*, 2011; Bondy-Denomy *et al.*, 2013; Rath *et al.*, 2015; Makarova *et al.*, 2015; Makarova *et al.*, 2018) by acquiring foreign nucleic acid fragments called spacers. Together with host Cas proteins, the spacers behave as an adaptive immune system in bacteria and archaea. Besides, the sequential order of the spacers in the array provides chronological information about the bacteria's exposure to foreign nucleic acids (Lier *et al.*, 2015), providing insights into host–phage interactions within a specific niche. These data show indicators of the evolution of the bacteria that carry them (Lier *et al.*, 2015).

To date, studies on the presence of *S. pyogenes* phages among SDSD isolates are scarce. For example, it is unclear whether these phages (and other MGEs) contribute to more pathogenic SDSD phenotypes. The CRISPR/Cas system in the SDSD and its impact on HGT are examples of how little is known, so far, about this microorganism.

In the present study, bovines SDSD isolates collected in two different periods (2002–03, partially studied, and 2011–13) were characterized and compared to obtain new information about molecular virulence profiles, antibiotypes, and population structure. We also investigated the CRISPR/Cas systems in SDSD strains to gain insights into defense systems and their impact on HGT. Additionally, pyogenic streptococcus genomes available at National Center for Biotechnology Information (NCBI) database, including human SDSD and SDSE strains, were included in this study to characterize CRISPR/Cas system, prophage regions, giving further insights on horizontal acquisitions of genetic elements, particularly associated with resistance traits or virulence to track temporal shifts of SDSD genotypes.

2.2. Materials and Methods

2.2.1. Bacterial Isolates

Out of a total of 194 Gram-positive cocci, 37 SDSD were isolated and included in this study (collection II). The isolates were collected from 2011 to 2013, from 250 animals with mastitis of 12 dairy farms located in Portugal. The presumptive identification of the SDSD isolates was performed by traditional phenotypic tests such as colony morphology, type of hemolysis, Lancefield serologic groups using the SLIDEX Strepto Plus (Biomérieux, Marcy-l'Étoile, France), and absence of catalase. For a comparative analysis, 18 strains of bovine SDSD (collection I), partially characterized (Rato *et al.*, 2010, 2011, 2013) and collected between 2002 and 2003 from 248 animals with mastitis on eight farms located in Portugal, were included in the study.

2.2.2. Genomic DNA extraction

Genomic DNA was obtained according to (Seppalla *et al.*, 1998) with few modifications. Briefly, bacterial cells were grown in 4 mL of Todd-Hewitt broth (BBL, Cockeysville) supplemented with 1% (w/v) of yeast extract (Oxoid, Basingstoke, United Kingdom) at 37 °C for 16–18 h. The culture was centrifuged at 11,269 g for 3 min and the pellet resuspended in 500 µl of 10 mM Tris HCl (pH 8.5). Cell lysis was obtained by incubating (2 h at 37 °C) the bacterial suspension with 40 µL of lysozyme (0.8 mg/mL final concentration) and 11 µL of mutanolysin (110 U/mL or 0.5 mg/mL final concentration). The lysate was centrifuged at 13,552 g f or 10 min at 4 °C. The DNA was extracted once with 1 mL phenol:chloroform (1:1). The water phase was then collected, and the DNA precipitated by overnight incubation at 20 °C using 2 volumes of cold ethanol (P.A.) containing 0.3 M sodium acetate (pH 5.2). The pellets were washed with 70% (v/v) ethanol and dried in an oven at 50 °C for 20 min. The DNA was dissolved in 50 µL of milli-Q water and stored at 20 °C.

2.2.3. Identification by 16S rRNA sequence

The identification of the SDSD isolates was confirmed by 16S rRNA gene sequencing analysis. Amplification and sequencing were performed with the same primers (Takahashi *et al.*, 1997). The sequencing of PCR products was carried out by STAB-Vida (Lisbon, Portugal). The sequences were analyzed and aligned using CLC Main Workbench 20.1 alignment program editor (QIAGEN, Venlo, Netherlands) and

then compared with sequences from the NCBI database using the Basic Local Alignment Search Tool (BLAST). Subsequently, the nucleotide sequences were subjected to phylogenetic analysis using MEGA X (Kumar *et al.*, 2018).

2.2.4. Pulsed-Field Gel Electrophoresis

The agarose plugs containing the genomic DNA from streptococcal strains were prepared as previously described (Rato *et al.*, 2008). All pulsed-field gel electrophoresis (PFGE) patterns were analyzed visually and by computer-assisted cluster analysis using BioNumerics v. 6.6 (Applied Maths, Sint-Martens-Latem, Belgium). Levels of similarity were calculated using Dice coefficient, and unweighted pair group method with arithmetic mean (UPGMA) was used for clustering to produce band-based dendrograms (1.5% and no optimization). Groups of patterns with similarity of 100% were considered indistinguishable and were assigned to the same subtype of PFGE type.

2.2.5. Phylogenetic analysis

For the phylogenetic analysis of bovine SDSD isolates, the Multilocus Sequence Analysis (MLSA) scheme was performed according to the method previously described for SDSE based on sequences of seven housekeeping genes (McMillan *et al.*, 2010). Seven housekeeping genes, namely, glucose kinase *gki*, glutamine transport protein *gtr*, glutamate racemase *murI*, DNA mismatch repair protein *mutS*, transketolase *recP*, xanthine phosphoribosyl transferase *xpt*, and acetoacetyl-coathioloase *atoB*, were amplified; and all amplified DNA fragments were sequenced. The sequences were edited, aligned, and subjected to phylogenetic analysis using CLC Bio Main Workbench 20.1 alignment program editor (QIAGEN, Venlo, Netherlands). Housekeeping gene sequences were trimmed, concatenated, and subjected to phylogenetic analysis. For concatenated housekeeping alleles, phylogenetic relationships were inferred using the minimum evolution method, and the distances were computed using the maximum composite likelihood method.

For the phylogenetic analysis, bovine SDSD isolates representatives of collection I and II (a total of 15 strains) were selected based on their different resistance, virulence, and PFGE profiles. Additionally, the sequences of SDSD strains ($n = 12$), SDSE strains ($n = 15$), *S. pyogenes* strains ($n = 11$), and *S. canis* strains ($n = 3$) (Supplementary Table S1 in Appendix I), available in the NCBI Nucleotide database, were included in this study for comparison.

2.2.6.   Virulence gene screening

The following genetic determinants of *S. pyogenes* (i.e., *speA, speB, speC, speF, speG, speH, speK, speL, speM, spegg, smeZ, spd1,* and *sdn*) were screened in bovine SDSD isolates by PCR. Additionally, we investigated the presence of operon encoding streptolysin S (SLS), namely, *sagA, sagB, sagE,* and *sagI* genes. For each 25 μl PCR mixture were added 100 ng of bacterial DNA, 1x reaction buffer for NZYTaq DNA polymerase, 2.5 mM of $MgCl_2$, 0.4 mM of dNTPs NZYMix, 1 U of NZYTaq DNA polymerase (NZYTech, Lisbon, Portugal), and 1 μM of each primer (Thermo Fisher Scientific, Waltham, MA, United States).

Negative results were confirmed in at least three independent assays. VSD13 and VSD7 were used as positive control. Primer sequences and amplicon expected size PCR conditions for amplifying all the genetic determinants are listed in Supplementary Table S2 (Appendix I). Screening of virulence genes and comparative analysis *in silico* among SDSD (from bovine, human, and fish strains), SDSE, *S. canis*, and *S. pyogenes* sequences (Supplementary Table S1, Appendix I) were performed using the CLC Bio Main Workbench. Alignment of *speC, speK, speL, speM,* and *spd1* sequence of bovine SDSD against the GenBank database using BLAST was performed to trace homolog genes among streptococcal species.

2.2.7.   Antimicrobial resistance patterns

All SDSD strains were tested for antimicrobial resistance by disk diffusion method (Oxoid Ltd., Basingstoke, United Kingdom), and the determination of minimum inhibitory concentration (MIC) follows the guidelines from the Clinical and Laboratory Standards Institute (CLSI) for antimicrobial susceptibility tests for bacteria isolated from animals (CLSI M31-A3, 2008). The following antimicrobials were selected for testing, based on several criteria: (a) licensing for mastitis treatment in cattle, amoxicillin–clavulanic acid 30 μg (AMC), gentamicin 10 μg (CN), penicillin 10 units (P), pirlimycin 2 μg (PRL), and streptomycin 10 μg (S); and (b) use in human medicine, chloramphenicol 30 μg (CHL), erythromycin 15 μg (ERY), tetracycline 30 μg (TET), and vancomycin 30 μg (VA). According to the CLSI guidelines (CLSI M31-A3, 2008). The antimicrobial manufacturers' instructions were followed when CLSI guidelines were not available. The reference strain *Staphylococcus aureus* ATCC 29213 was used for quality control for both methods.

2.2.8. Macrolide resistance phenotypes

All the isolates were tested for resistance only to macrolides (M phenotype) or to macrolides, lincosamides, and streptogramin-B (MLSB phenotype). The MLSB resistance, inducible (iMLSB) or constitutive (cMLSB), was checked by a double-disk test with erythromycin and pirlimycin disks. Resistance only to lincosamides (L phenotype) and to lincosamides and streptogramin-A (LSA phenotype) was described previously (Malbruny *et al.*, 2004; Rato *et al.*, 2013).

2.2.9. Antimicrobial resistance gene detection

All the isolates with M or MLSB phenotypes (Pires *et al.*, 2005) were screened to detect *ermA*, *ermB*, and *mefA* macrolide resistance genes. Genes *tetM*, *tetT*, *tetW*, *tetL*, *tetQ* *tetO*, *tetK*, and *tetS* were screened among all tetracycline-resistant strains (Pires *et al.*, 2005). All strains were tested for the presence of *linB* gene (lincosamide resistance) (Bozdogan *et al.*, 1999). Primer sequences and amplicon expected sizes are listed in Supplementary Table S2 (Appendix I). Negative results were confirmed in at least three independent assays. VSD13 and VSD19 strains were used as positive control.

2.2.10. CRISPR array sequencing and CRISPR-associated (Cas) gene screening

This study used the genome sequence of an SDSE strain ATCC 12394 (GenBank accession number: NC_017567) to design specific primers to amplify the CRISPR array and *cas* genes (Supplementary Table S2 in Appendix I). PCRs were performed in a thermocycler (Biometra, Göttingen, Germany) in a final volume of 25 µl containing 100 ng of bacterial DNA, 1x PCR buffer, 2.5 mM of $MgCl_2$, 0.4 mM of dNTPs, 1 U of Taq polymerase (NZYTech, Lisbon, Portugal), and 1 µM of each primer (NZYTech, Lisbon, Portugal). PCR conditions consisted of an initial denaturation cycle (95 °C for 5 min), followed by 35 cycles of denaturation (95 °C for 30 s), annealing (52 °C for 30 s), and extension (72 °C for 80 s). A final extension at 72 °C for 7 min was also performed. Milli-Q water was used as a negative control in each PCR. The PCR products of CRISPR array regions were purified using the Wizard PCR Preps DNA Purification System (Promega, Madison, WI, United States). Sequencing was performed by STAB-Vida (Lisbon, Portugal) using specific primers (CRISPR Sdys For and CRISPR Sdys Rev; Supplementary Table S2 in Appendix I). The obtained DNA sequences were analyzed and edited using the software CLC Bio Main Workbench. For each CRISPR

array sequence, the spacers, repeats, and flanking regions were determined using CRISPRfinder and CRISPRtionary. All experiments were carried out in triplicate (Grissa *et al.*, 2007).

The similarity of the spacers, repeats, and flanking regions was analyzed using software currently available for CRISPR miner to infer a large-scale microbe–phage infection network. The spacers from each strain were selected and used to BLAST (blastn with parameters settings: *e*-value < 0.01, and up to three mismatches allowed) against both bacteria and archaea virus genomes of an integrated database from the NCBI viral Genome Resource. Matches with a query cover above 90% with 100% identity were considered.

2.2.11. Prophage identification

Prophinder (Lima-Mendez *et al.*, 2008) was used to screen for prophage-specifying regions among the genome of SDSD, SDSE, *S. canis*, and *S. pyogenes* strains. Prophage sequences were annotated using RAST (Aziz *et al.*, 2008). Intact prophages were manually analyzed to confirm the presence of genes indispensable to produce functional phages: left attachment site (attL); lysogeny; DNA replication; transcriptional regulation; head; tail; lysis modules; and right attachment site (attR).

2.2.12. Statistical analysis

GraphPad Prism version 7.0 was used for statistical analysis. Data analysis was performed using the chi-square method. Statistical significance was considered when $p < 0.05$.

2.3.   Results

2.3.1.   Bacterial Isolates and Identification

The SDSD isolates' identification was confirmed using 16S rRNA gene sequencing. Out of 194 Gram-positive cocci, 37 isolates (19%) were identified as *S. dysgalactiae* species. Sequence analysis of the rRNA 16S from bovine SDSD isolates showed between 99.2% and 100% nucleotide identity to SDSD ATCC 2795, SDSD NCTC4670, SDSD NCTC13731, and SDSD NCTC4669 strains deposited in the NCBI Nucleotide database.

2.3.2.   Pulsed-Field Gel Electrophoresis Profiles

The 55 SDSD isolates from subclinical mastitis isolated in Portugal during 2002–03 (collection I) and 2011–13 (collection II) were resolved into 45 PFGE types. Epidemiologically groups or clusters (at 70% similarity) revealed two major clonal groups, including close to 90% of all bovine isolates. The macro-restriction profiles are listed in Table 2.1. Two or more strains share six PFGE patterns, and 31 PFGE patterns were of single isolates. Results demonstrated that there are no distinct groups among isolates of collection I and collection II.

Table 2.1. Characterization of bovine SDSD isolates from collection I (VSD1 to VSD11 and VSD13 to VSD19) (2002–2003) and from collection II (VSD20 to VSD55) (2011–2013).

Strain	Farm	PFGE Type	Virulence genotype	Resistance genotype	Resistance phenotype
VSD1	F	A-1	*sagA, speC, speK, spd1*		TET
VSD2	F	J-1	*sagA*		TET
VSD3	J	L-1	*sagA*	*ermA/TR, tetM*	cMLSB + TET
VSD4	E	M-1	*sagA,speC, speK, spd1*	*linB, tetM*	L + TET
VSD5	E	F-1	*sagA, sdn*	*tetM*	TET
VSD6	I	D-1	*sagA, speK, speL*	*tetM*	TET
VSD7	D	G-1	*sagA,speM, sdn*	*tetO*	TET
VSD8	G	C-1	*sagA,sdn*		TET
VSD9	B	N-1	*sagA*	*ermB, tetO*	cMLSB + TET
VSD10	G	C-1	*sagA,sdn*		TET
VSD11	F	B-1	*sagA,speC, speK, spd1*	*linB, tetO*	L + TET
VSD13	G	I-1	*sagA,speC, speK, speL, speM, spd1*	*ermB, tetO*	cMLSB + TET
VSD14	F	C-2	*sagA,*	*ermB, tetO*	cMLSB + TET
VSD15	J	D-1	*sagA,speK, speL*	*tetM*	TET
VSD16	B	A-2	*sagA, speC, speK, spd1*		TET
VSD17	C	E-1	*sagA*		TET
VSD18	I	D-1	*sagA,speK, speL*	*tetM*	TET
VSD19	E	M-1	*sagA, speC, speK, spd1*	*linB, tetM*	L + TET
VSD20	S	O-1	*sagA, speL*	*ermB, tetO*	cMLSB + TET
VSD21	Q	P-1	*sagA, speL, speM*	*ermB, tetM, tetO*	cMLSB + TET
VSD22	Q	Q-1	*sagA, speM*	*tetM, tetO*	TET
VSD23	V	R-1	*sagA, speM, sdn*	*tetM, teto, tetK*	TET
VSD24	S	S-1	*sagA, speC, speK, spd1*		
VSD25	N	T-1	*sagA, sdn*	*tetM, tetK*	TET
VSD26	N	V-1	*sagA, speK*	*tetM, tetO*	TET
VSD27	M	X-1	*sagA*	*tetM, tetO*	TET
VSD28	X	Z-1	*sagA, sdn*	*tetO, tetK*	TET
VSD29	M	K-1	*sagA, speM*	*tetM, tetO*	TET
VSD30	T	Y-1	*sagA, speL, speM*	*tetM*	TET
VSD31	M	W-1	*sagA*	*tetM, tetO*	TET
VSD32	O	AA-1	*sagA, speK, sdn*	*tetO*	TET
VSD33	O	AA-1	*sagA, speK, sdn*	*tetO*	TET
VSD34	P	AB-1	*sagA, speM*	*tetM, tetO, tetK*	TET
VSD35	N	Z-1	*sagA, speL, speM, sdn*	*tetO, tetK*	TET
VSD36	M	W-1	*sagA, speL, speM*	*tetM, tetO*	TET
VSD37	O	AC-1	*sagA, speK, sdn*	*tetO*	
VSD38	U	W-1	*sagA*	*tetM, tetO*	TET
VSD39	U	AD-1	*sagA*	*tetM, tetO*	TET
VSD40	R	AE-1	*sagA, sdn*	*tetO, tetK*	TET
VSD41	M	W-1	*sagA*	*tetM, tetO*	TET
VSD42	M	W-1	*sagA*	*tetM, tetO*	TET
VSD43	M	AF-1	*sagA, speK, sdn*	*tetM, tetO*	TET
VSD44	S	AG-1	*sagA, speC, speK, spd1*	*tetO*	TET
VSD45	U	AH-1	*sagA*	*tetM*	TET
VSD46	U	AI-1	*sagA*	*tetM*	TET
VSD47	M	AJ-1	*sagA, speC, speK, spd1*	*tetM, tetO*	TET
VSD48	M	AJ-1	*sagA, speC, speK, spd1*	*tetM, tetO*	TET
VSD49	M	AL-1	*sagA, speC, spd1 speK*	*tetM, tetO*	TET
VSD50	R	V-1	*sagA, speL, speK*	*tetM, tetO*	TET
VSD51	M	AM-1	*sagA, speL, speM*	*tetM, tetO*	TET
VSD52	O	AN-1	*sagA*		TET
VSD53	U	AI-1	*sagA*	*tetM, tetO*	TET
VSD54	R	V-1	*sagA, speL, speK*	*tetM, tetO*	TET
VSD55	R	AO-1	*sagA, speM, sdn*	*tetM, tetO*	TET
VSD56	X	AP-1	*sagA, speM, sdn*		

2.3.3. Phylogenetic analysis

Alignment of concatenated sequences of seven housekeeping genes (*gki, gtr, murI, mutS, recP, xpt*, and *atoB*) was created using the standard parameters of ClustalW. Then a minimum evolution tree was obtained from sequences from bovine SDSD isolates (determined in this study) and sequences of a selection of SDSD, SDSE, *S. pyogenes*, and *S. canis* strains (Figure 2.1). The number of accessions of *gki, gtr, murI, mutS, recP, xpt*, and *atoB* genes are present in the Appendix II.
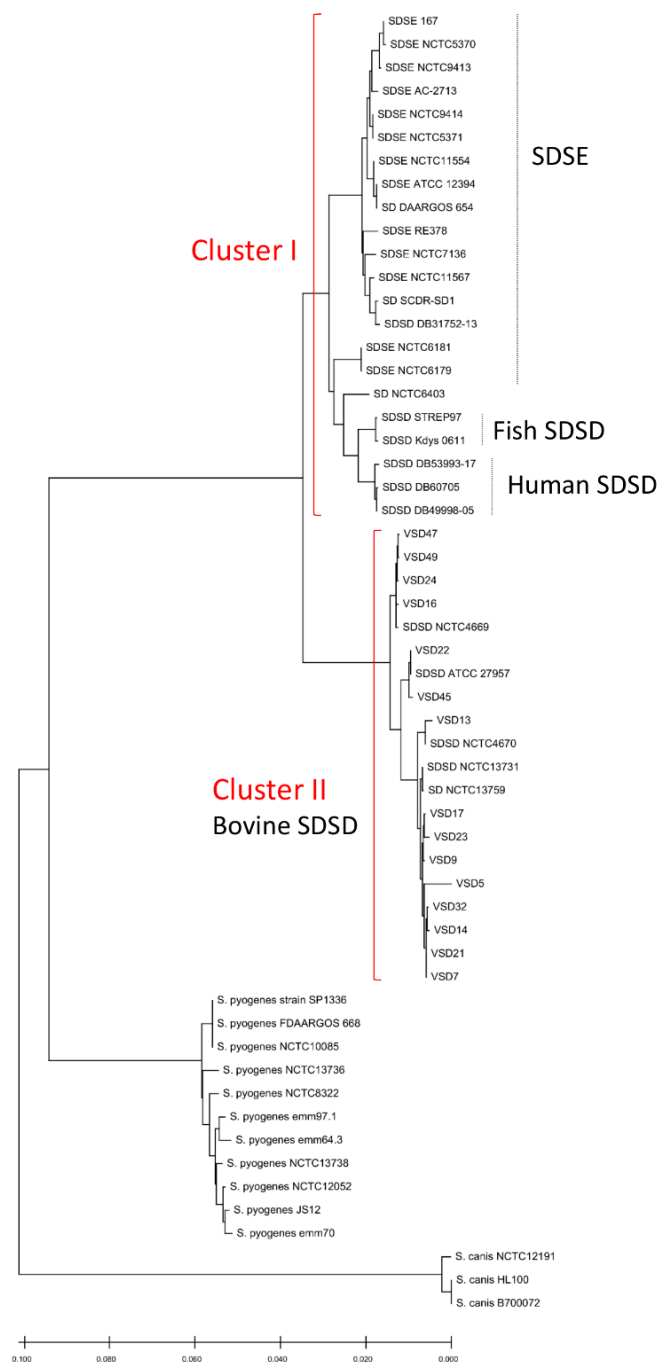
Figure 2.1. Phylogenetic analysis based on concatenated sequences of seven housekeeping genes (*gki, gtr, murI, mutS, recP, xpt*, and *atoB*) showing the position of the 15 bovine SDSD isolates and sequences of strains available in the National Center for Biotechnology Information (NCBI) database, including SDSD strains (n = 12), SDSE strains (n = 15), *S. pyogenes* strains (n = 11), *S. canis* strains (n = 3). VSD, Vet *S. dysgalactiae* subsp. *dysgalactiae*. Bovine SDSD isolates: ATCC27957; NCTC13731; NCTC4669; NCTC4670 and VSDs. Human SDSD strains: DB49998-05; DB60705-15, and DB53993-17. Fish SDSD strain: SDSDKdys0611. SDSE, *S. dysgalactiae* subsp. *equisimilis*. The phylogenetic relationships were inferred using the minimum evolution method, and phylogenetic distances were estimated using the maximum composite likelihood method using the MEGA (Kumar *et al.*, 2018). The tree is drawn to scale, with branch lengths in the same units as those of the evolutionary distances used to infer the phylogenetic tree.

S. canis and *S. pyogenes* constitute monophyletic clusters. The *S. dysgalactiae* cluster was divided into two groups: cluster 1—human and fish SDSD strains, and SDSE; cluster 2—bovine SDSD isolates. Data show that human SDSD strains are closer to SDSE than bovine SDSD isolates. Interestingly, this phylogenetic relationship between SDSD and SDSE obtained by MLSA does not reflect the relationship based on the 16S rRNA sequences (Figure 2.1 and Supplementary Figure S1 in Appendix I).

2.3.4. Virulence gene screening

All the 37 bovine SDSD isolates (collection II), screened by PCR, carry at least one of the following superantigen genes (*speC*, *speK*, *speL*, and *speM*), DNase (*spd1*), streptodornase (*sdn*), or SLS (*sagA*).

None of the strains carry *speA*, *speB*, *speF*, *speG*, *spegg* and *speH* SAgs genes; *smeZ* mitogenic exotoxin gene; and *sagB*, *sagE*, and *sagI* genes.

The results showed that the SAgs genes were unevenly distributed among all the 37 bovine SDSD isolates (Table 2.1). The screening revealed the following distribution: *speC*, 20%; *speK*, 40%; *speL*, 20%; *speM*, 23.6%; *spd1*, 20%; and *sdn*, 27.2% positive isolates. Transcriptional analysis showed that all virulence genes were transcribed in all SDSD isolates that carried them.

Similar virulence gene patterns were found among bovine SDSD from collection I (Rato *et al.*, 2010, 2011) and II. No relationships were found between virulence profiles and the farm or macro-restriction patterns (see Table 2.1).

The comparison of the distribution of virulence genes between SDSD isolates from collection I and II is shown in Figure 2.2. Chi-square statistical analysis revealed that each independent virulence gene proportion was not statistically different between collections.
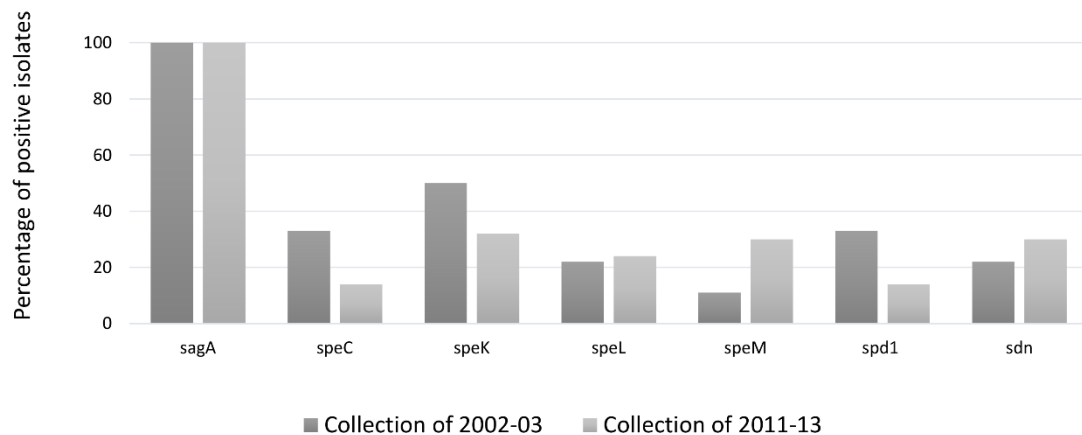
Figure 2.2. Distribution (%) of *S. pyogenes* virulence gene among SDSD isolates.
speC, speK, speL, speM: encode superantigens; *spd1*: DNase and *sdn*: streptodornase (DNase).

The comparison of the homologous sequences of bovine SDSD SAgs genes with *S. pyogenes* pyrogenic exotoxin gene from the NCBI databases, showed high identity: >98% identity for *speC*; >97% for *speK*; >98% for *speM*; and >97% for *speL*. In addition, a high identity was also found for DNases *spd1* (>98%).

For a comparative analysis, the presence of virulence genes in the genomes of the streptococci listed in Supplementary Table S1 (Appendix I) was analyzed. None of the *speB, speC, speF, speG, speH, speK, speL, speM,* and *smeZ* virulence genes were detected among human SDSD or SDSE strains. Streptodornase (*sdn*) was found among the human SDSE strains (3/15), *S. pyogenes* strains (2/15), bovine SDSD isolates (5/20), but it was not detected in human SDSD or *S. canis* strains. The *spegg* gene was found in SDSE, *S. pyogenes*, and human SDSD, but not in bovine SDSD; and the *smeZ* was found only among *S. pyogenes* strains (Supplementary Figure S2 in Appendix I). The nucleotide sequences of *spegg* gene in human and fish SDSD strains revealed >99% identity with its homolog in *S. pyogenes* from the NCBI database.

In addition, all the bovine SDSD isolates from collection I and the genomes listed in Supplementary Table S1 (Appendix I) were tracked for the presence of the SLS operon. The comparative analysis showed that of the nine genes that are part of the SLS operon, the bovine SDSD isolates only had *sagA* gene (Table 2.1), while the SDSE, human and fish SDSD, *S. pyogenes*, and *S. canis* strains harbored the complete operon (Figures 2.3 A-B and Supplementary Figure S2 in Appendix I). Figure 2.3C shows the amino acid sequence of SagA protein of the bovine SDSD isolates deduced through *in*

silico analysis, compared with SDSE, SDSD, *S. canis*, and *S. pyogenes* sequences. The alignment of SagA peptide demonstrated that the leader-peptide region is highly conserved, while the pro-peptide region is more variable. In this last region, the bovine SDSD isolates present a deletion of two cysteine residues.
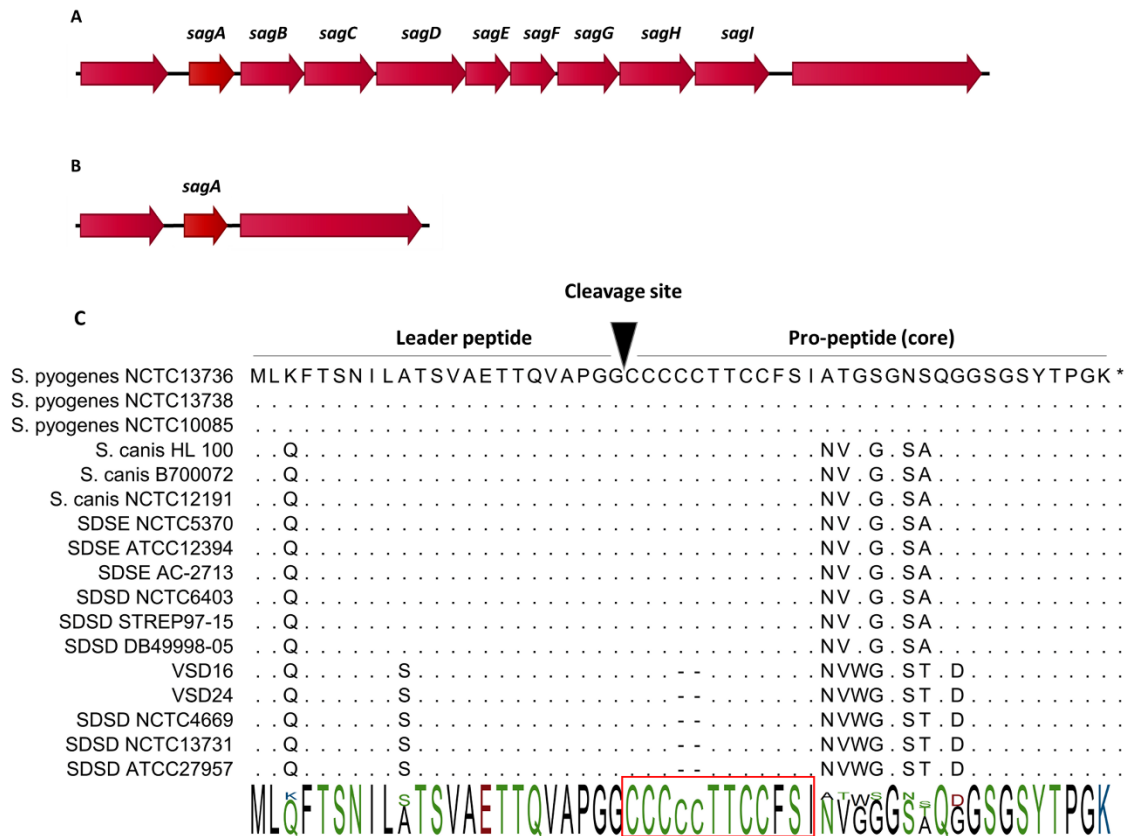
Figure 2.3. Gene cluster organization of streptolysin S (SLS) operon and precursor peptide sequences of SLS cytolysins (SagA). (A) Organization of the SLS operon in SDSE, SDSD, *S. pyogenes*, and *S. canis*. The operon encoding SLS includes the prepropeptide structural gene (*sagA*), followed by eight genes responsible for the conversion of SagA into SLS (*sagBCD*), transport across the membrane (*sagFGHI*), and accountable for leader cleavage (*sagE*). (B) Organization of the genomic region flanking *sagA* in bovine SDSD isolates. (C) Alignment of SagA peptide, the precursor of SLS. SLS core region possesses a highly conserved N-terminus, while the C-terminus is more variable. The putative leader peptide cleavage site is shown. Red rectangle, minimal core region required for hemolytic activity of SLS in *S. pyogenes*. STAB-Vida performed sequencing of sagA. Deduced amino acid sequences from this bovine allele were compared with sequences from the National Center for Biotechnology Information (NCBI) database and were analyzed with the CLC-bio Main Workbench sequence alignment tool (QIAGEN, Netherlands).

2.3.5. Antimicrobial resistance patterns

Among the 37 bovine isolates from collection II, the highest antimicrobial resistance patterns were observed for tetracycline (90%), followed by streptomycin (69%) and gentamicin (60%). None of the streptococcal isolates tested showed resistance to amoxicillin/clavulanic acid, cefazolin, cefoperazone, chloramphenicol, penicillin,

rifaximin, and vancomycin (Table 2.1 and Figure 2.4). Two isolates resistant to pirlimycin and erythromycin presented the cMLSB phenotype (Table 2.1), while the phenotype M (erythromycin-resistant only) was not detected. The two strains showed the cMLS$_B$ phenotype (constitutive MLSB). Strains of the cMLSB phenotype harbored *ermB* gene, while *ermA* and *mefA* (macrolide resistance genes) were not detected (Table 2.1). The resistance to tetracycline was associated with *tetM*, *tetK*, and *tetO* (*tetS, tetT, tetW, tetL,* and *tetQ* negative). Figure 2.4 compares the resistance phenotypes distribution and genotypes among the 55 bovine SDSD isolates from collection I (Rato *et al.*, 2013) and collection II. Chi-square statistical analysis revealed that each independent resistance phenotype proportion was not statistically different between collections. However, statistically significant differences were observed between *tetM*, *tetK*, and *tetO*.
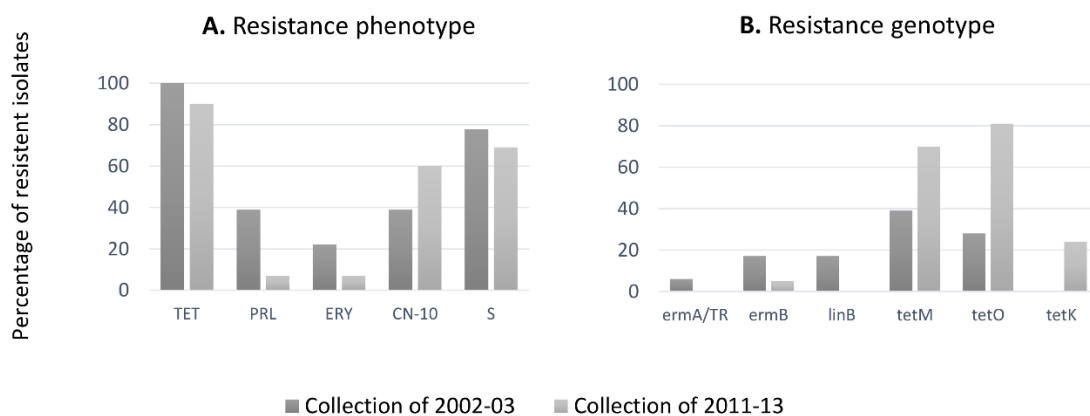
Figure 2.4. (A) Percentages of antimicrobial resistance among bovine SDSD isolates from the present study against erythromycin (ERY), gentamicin (CN), pirlimycin (PRL), streptomycin (S), and tetracycline (TET). Resistance was not observed against amoxicillin–clavulanic acid (AMC), cefazolin (KZ), chloramphenicol (CHL), penicillin (P), rifaximin (RAX), and vancomycin (VA). (B) Distribution resistance genotypes among bovine SDSD: *ermA* and *ermB*: macrolide resistance genes; *linB*: lincosamide resistance gene; *tetK, tetM*, and *tetO*: resistance to tetracycline genes.

2.3.6. CRISPR system analysis and prophage identification

SDSD isolates from collection I of 2002–03 (N = 18) and collection II of 2011–13 (N = 37) were analyzed by sequencing the CRISPR loci. Overall, the analysis of CRISPR array discloses a high intrinsic diversity among bovine SDSD understudy, demonstrating the distinguish groups among isolates from both collections (Figure 2.5).

STRAIN	COLECTION	VIRULENCE GENES	RESISTANCE GENES	FARM	PFGE TYPE
VSD22	II	speM	tetM, tetO	Q	Q-1
VSD14	I	-	ermB, tetO	F	C-2
VSD21	II	speL, speM	ermB, tetM, tetO	Q	P-1
VSD3	I	-	ermA/TR, tetM	J	L-1
VSD17	I	-	-	C	E-1
VSD45	II	-	tetM, tetO	M	W-1
VSD41	II	-	tetM, tetO	M	W-1
VSD36	II	speL, speM	tetM, tetO	M	W-1
VSD42	II	-	tetM, tetO	M	W-1
VSD31	II	-	tetM, tetO	M	W-1
VSD27	II	-	tetM, tetO	M	X-1
VSD38	II	-	tetM, tetO	U	W-1
VSD50	II	speL, speK	tetM, tetO	R	V-1
VSD23	II	speM, sdn	tetM, teto, tetK	V	R-1
VSD52	II	-	-	O	AN-1
VSD39	II	-	tetM, tetO	U	AD-1
VSD46	II	-	tetM	U	AI-1
VSD30	II	speL, speM	tetM	T	Y-1
VSD20	II	speL	ermB, tetO	S	O-1
VSD32	II	speK, sdn	tetO	O	AA-1
VSD1	I	speC, speK, spd1	-	F	A-1
VSD2	I	-	-	F	J-1
VSD26	II	speK	tetM, tetO	N	V-1
VSD18	I	speK, speL	tetM	I	D-1
VSD7	I	speM, sdn	tetO	D	G-1
VSD34	II	speM	tetM, tetO, tetK	P	AB-1
VSD28	II	sdn	tetO, tetK	X	Z-1
VSD25	II	sdn	tetM, tetK	N	T-1
VSD6	I	speK, speL	tetM	I	D-1
VSD16	I	speC, speK, spd1	tetM	B	A-2
NCTC4669		speC, speK, spd1	tetM	n.d.	n.d.
VSD24	II	speC, speK, spd1	-	S	S-1
VSD49	II	speC, speK, spd1	tetM, tetO	M	AL-1
VSD47	II	speC, speK, spd1	tetM, tetO	M	AJ-1
VSD48	II	speC, speK, spd1	tetM, tetO	M	AJ-1
VSD19	I	speC, speK, spd1	linB, tetM	E	M-1
VSD44	II	speC, speK, spd1	tetO	S	AG-1
VSD8	I	sdn	-	G	C-1
VSD10	I	sdn	-	G	C-1

Figure 2.5. Dendrogram based on spacer CRISPR IIA cluster of SDSD isolates of mastitis in cattle collected in 2002 - 2003, 2011, 2013) (VSD1 to VSD19 - collection I) and 2011–2013 (VSD20 to VSD56 - collection II). *Streptococcus pyogenes* phages encode genes *speC*, *speK*, *speL*, *speM*, *spd1*, and *sdn*. The dendrogram was obtained by means of Dice coefficient and the agglomerative clustering of the unweighted pair group method with arithmetic mean (UPGMA).

Among the 55 bovine SDSD isolates analyzed for the CRISPR array, 49 were PCR positive (but only 41 strains were CRISPR spacer positive), and four were PCR negative. For two strains, the amplified product showed high homology (>99%) with ISSdy transposase (ORF A, GenBank accession: VDZ39966.1 and ORF B, GenBank accession: VDZ39965.1).

A high degree of direct repeat (DR) sequence (5'GTTTTAGAGCTGTGCTGTTTCGAATGGTTCCAAAAC'3) conservation was observed among bovine SDSD isolates. The DR showed sequence similarity to typical

repeat sequences of other streptococci species, such as *S. agalactiae* with 100% of identity (Lier *et al.*, 2015), *Streptococcus thermophilus* with an average identity of about 85% (Hu *et al.*, 2020), and *S. pyogenes* with >95% of identity (Nozawa *et al.*, 2011).

A total of 158 spacers were identified among the 41 CRISPR spacer positive strains, of which 80 (50%) were found to be unique. The number of spacers in each CRISPR array was eight on average, ranging from a maximum of 26 to a minimum of 2. Most strains (39 of 41) shared at least one spacer. Only VSD4 and VSD13 did not share spacers; these strains harbored six and three unique spacers, respectively. The SDSD VSD5, VSD9, VSD11, VSD29, VSD33, VSD37, and VSD40 isolates were CRISPR spacer negative.

Three major groups were observed based on the common spacer sequences or absence of spacers (Figure 2.5). Some old spacers were detected in bovine SDSD that harbored the same combinations of SAgs. For example, the 41, 42, 62, 63, 64, 65, 66, 118, 119, 120, and 121 spacers were detected among isolates from collection I (VSD16 and VSD19) and collection II (VSD24, VSD47, VSD48, and VSD49) harboring *speC*, *speK*, and *spd1* genes (Figure 2.5). Some of these spacers were also detected in SDSD NCTC4669 (isolated in 1935).

About 72% (114/158) spacers matched with sequences present in the genome of *S. pyogenes*, *S. agalactiae*, *S. canis*, and *S. dysgalactiae* with a similarity >95. A BLAST was carried out to determine if the spacers had an origin in bacteriophage. Sequences above 95% of identity, in both query coverage and percent identity, were considered. Of the 158-spacer sequence, 29 (18.4%) showed high identity (bit scores 50) with prophage regions. These regions correspond to phage isolated from *S. pyogenes* and phages belonging to others species, namely, *S. agalactiae* str. ILRI005; *Listeria* phage B054; *Flavobacterium* phage 11b; *Streptococcus* phage SpSL1; *Synechococcus* phage S-CAM7; *Bacillus* virus IEBH; and *Bacillus* virus 250 (Table 2.2). About 28% of the sequence spacers of SDSD were not identified in the NCBI database.

Table 2.2. Identification and nucleotide sequence of the bacteriophage spacers in a CRISPR array of SDSD.

Spacer	Sequence	Bacteriophage	SDSD strain
sp4	ATAAATTTTTGTTGTAGCGAGTCTTACCGT	Streptococcus phage phi3396	NCTC4669
sp6	ATTGAGAATAGAGCGATATAAACAGGAGAA	Temperate phage phiNIH1.1	NCTC4669, VSD16
sp7	TTAGGCGCCAGCGTTAAAGAGGTGTTTGCT	Streptococcus phage 315.6	NCTC4669
sp11	TTGTTTTTGGACTTGCGGTTAATCATAAAA	Streptococcus phage 315.2	NCTC4669, VSD16
sp14	AGTGTTACTTGAACCAACACCCCATCTAAG	Streptococcus phage 315.6 or S. phage P9	NCTC4669, VSD16
sp15	AGTGTTACTTGAACCAACACCCCATCTAAG	Streptococcus phage P9	NCTC4669
sp17	TTAGGCGCCAGCGTTAAAGAGGTGTTTGCT	Streptococcus phage P9	NCTC4669, VSD24
sp25	TAGCGACAATTTAATAATAGCTTCGATTTT	Streptococcus phage 315.5	VSD1, VSD2, VSD32, VSD46, VSD55
sp30	TCATGCACCTCAATGTCCTTACGCATCTCC	Streptococcus phage phi3396	VSD1, VSD2
sp35	AGCATTTCTGCAAACTCTGCCATGTATTGA	Streptococcus phage 315.1	VSD10, VSD8
sp36	CAAAGCCCCTCAAAATGCAACACAGTAATG	Streptococcus phage 315.3	VSD10, VSD8
sp49	AGCCTAGCAAGCATAAGTAATCGCTAATGG	Streptococcus phage 315.1	VSD14, VSD22, VSD45
sp50	CCTTTTGCACGGCTTCGCCCATAGCGATTT	Streptococcus phage 315.2	VSD14, VSD21, VSD22, VSD45
sp52	TATATCATCTCCTAGTGATAAACCTGCCAG	Streptococcus phage 315.3	VSD14, VSD21, VSD22, VSD3
sp53	AGAACGTATTGACGGTATCGTTAAAGTAAC	Bacillus virus IEBH or Bacillus virus 250	VSD14, VSD22, VSD3
sp55	AACCATTGCGTAGTCATAATCATCAAGCAT	Streptococcus phage 315.5	VSD14, VSD3
sp58	TTAAAGGCAGATACGTTCTGATATGGGGCT	Listeria phage B054	VSD14, VSD21, VSD22, VSD27, VSD31, VSD36, VSD38, VSD41
sp81	GTTGATTGATCAACAGTTGGTTGAGACAAA	Streptococcus phage 315.5 or S. phage phi3396	VSD19, VSD47, VSD48, VSD49
sp88	ACTAACCACAAGCAAGGTTGCGACCCTTGT	Temperate phage phiNIH1.1 or S. phage 315.2	VSD20, VSD30, VSD32, VSD39, VSD46, VSD53, VSD55
sp103	TTTCCCTATGATAAACCTTTAATAAAGTGT	Temperate phage phiNIH1.1 or S. phage 315.4	VSD25
sp104	AAAACTACAAACGCTTGCTGATAAAACCAA	Streptococcus phage phi3396	VSD25
sp105	TAATAAGCATTTTGATTTAGCTATTGTTG	Flavobacterium phage 11b or S. phage SpSL1	VSD25, VSD35
sp106	CCATTAGCAATAGCAGGATTA	Synechococcus phage S-CAM7	VSD25
sp116	AGAATAGAGAAAAAGAGATATTTTTTGAT	Temperate phage phiNIH1.1 or S.s phage 315.1	VSD32
sp138	TCAACCACATCTTTATAAGACATCTCAAGC	Streptococcus phage 315.3	VSD45
sp139	AGCCTCGCAAGCATAAGTAATCGCTAATGG	Streptococcus phage 315.5	VSD45
sp140	GCTTGGGACGTTGGATTGTTGATTTTTATT	Streptococcus phage 315.4	VSD45
sp149	AGATTTGCCTTCATCAGCGATGTTTTTGTT	Streptococcus phage 315.5	VSD47, VSD48, VSD49, VSD16
sp158	AAAATTTATTGATGGCGAATCGGTGCCAGA	Streptococcus phage 315.3	VSD49, VSD16

Due to the similarity of some spacers between contemporary bovine SDSD isolates and SDSD NCTC4669 (isolated in 1935, the oldest documented with sequenced genome) (Chanter *et al.*, 1997), we analyze the sequences adjacent to a CRISPR array of this oldest strain. The genetic map of this region consisted of only four *cas* genes (*cas9*, *cas1*, *cas2*, and *csn2*), corresponding to the CRISPR type IIA system. Additionally, the ISSdys transposase gene was found in type IIA system.

The genes associated with the type IIA CRISPR system were searched among the 55 bovine SDSD isolates (collection I and II). All bovine SDSD isolates were PCR positive to *cas9*, *cas1*, *cas2*, and *csn2* genes. Additionally, two of the 55 strains were PCR positive for ISSdys transposase.

To elucidate the relationship between the prophages and CRISPR systems among SDSD strains, we analyzed CRISPR array, CRISPR-associated (Cas) proteins, and prophage structure using complete genome sequences of SDSD. For a comparative analysis, the complete genome of SDSE, *S. canis*, and *S. pyogenes* was also analyzed. The CRISPR/Cas loci of the SDSD and SDSE strains analyzed were classified as type I-C and/or type II-A (Table 2.3). SDSD and SDSE genomes showed a high number of spacers when compared with *S. pyogenes*. While CRISPR arrays of *S. pyogenes* have between 0 and 10 spacers, SDSD and SDSE can have more than 40 spacers (Table 2.3). No CRISPR system was observed in 15% and 42% of the SDSE and *S. pyogenes* genomes, respectively, while in all SDSD strains, CRISPR/Cas system is present.

The total number of prophage regions obtained through *in silico* analysis was 228 in 42 genomes, with an average of 5.45 prophages per genome (Table 2.3). *S. pyogenes* had the highest number of complete prophages per genome, i.e., 2.1, followed by SDSD with two complete prophages per genome. SDSE and *S. canis* had 1.15 and 1 complete prophages per genome.

Table 2.3. Identification of CRISPR/Cas systems and prophage regions

Strain	CRISPR system ǀ n° spacer	Prophage regions*
S. canis B700072	type IIA ǀ 18	0ǀ4
S. canis NCTC12191	type IC ǀ 8; type IIA ǀ 2	2ǀ3
S. canis HL100	type IC ǀ 12; type IIA ǀ 21	1ǀ4
S. pyogenes emm64.3	No detected	1ǀ3
S. pyogenes emm70	No detected	1ǀ3
S. pyogenes emm97.1	No detected	1ǀ1
S. pyogenes FDAARGOS668	type IC ǀ 7; type IIA ǀ 3	2ǀ4
S. pyogenes JS12	type IIA ǀ 3	1ǀ2
S. pyogenes NCTC10085	type IC ǀ 4; type IIA ǀ 3	2ǀ2
S. pyogenes NCTC12052	type IIA ǀ 3	3ǀ7
S. pyogenes NCTC12696	type IIA ǀ 0	3ǀ6
S. pyogenes NCTC13736	No detected	4ǀ5
S. pyogenes NCTC13738	No detected	3ǀ5
S. pyogenes NCTC8322	type IC ǀ 7; type IIA ǀ 10	3ǀ4
S. pyogenes SP1336	type IC ǀ 6; type IIA ǀ 0	2ǀ4
SDSD ATCC27957	type IC ǀ 3	2ǀ6
SDSD DB3175213	type IC ǀ 33; type IIA ǀ 11	0ǀ5
SDSD DB4999805	type IIA ǀ 28	0ǀ4
SDSD DB5399317	type IC ǀ 3	0ǀ2
SDSD DB6070515	type IIA ǀ 42	3ǀ8
SDSD Kdys0611	type IIA ǀ 22	1ǀ12
SDSD NCTC13731	type IC ǀ 3	2ǀ8
SDSD NCTC13759	type IC ǀ 3	2ǀ8
SDSD NCTC4669	type IC ǀ 14; type IIA ǀ 22	3ǀ13
SDSD NCTC4670	type IIAA ǀ 4	2ǀ11
SDSD STREP97-15	type IIA ǀ 7	3ǀ21
SDSE NCTC11554	type IC ǀ 13; type IIA ǀ 34	1ǀ5
SDSE NCTC5370	No detected	1ǀ4
SDSE NCTC5371	type IIA ǀ 42	1ǀ5
SDSE NCTC6179	type IC ǀ 3; type IIA ǀ 9	2ǀ4
SDSE NCTC6181	type IC ǀ 3; type IIA ǀ 9	2ǀ6
SDSE NCTC7136	type IC ǀ 25; type IIA ǀ 15	3ǀ4
SDSE NCTC9413	type IIA ǀ 11	1ǀ5
SDSE NCTC9414	type IIA ǀ 42	1ǀ6
SDSE 167	No detected	1ǀ4
SDSE AC2713	type IC ǀ 15; type IIA ǀ 20	1ǀ8
SDSE ATCC 12394	type IC ǀ 30; type IIA ǀ 26	0ǀ4
SDSE FDAARGOS 654	type IC ǀ 12; type IIA ǀ 19	1ǀ5
SDSE GGS 124	type IIA ǀ 19	1ǀ4
SDSE NCTC6403	type IIA ǀ 9	1ǀ2
SDSE RE378	type IC ǀ 14; type IIA ǀ 8	0ǀ5
SDSE SCDRSD1	type IC ǀ 15; type IIA ǀ 20	0ǀ3

*complete prophagesǀ total of putative prophage regions. **Bovine SDSD isolates**: ATCC27957, NCTC13731; NCTC4669; NCTC4670. **Human SDSD strains**: DB49998-05; DB60705-15, and DB53993-17. **Fish SDSD strain**: SDSD Kdys0611 and SDSD STREP97-15. **SDSE:** *S. dysgalactiae* subsp. *equisimilis.*

2.4. Discussion

In the present study, the MLSA was performed according to the method previously described (McMillan *et al.*, 2010). In a previous study, the phylogeny of *S. canis, S. dysgalactiae, Streptococcus equi*, and *S. pyogenes* species based on MLSA (*map, pfl, ppaC, pyk, rpoB, sodA*, and *tuf* genes) was reconstructed according to this analysis; S. dysgalactiae includes two separate clusters corresponding to the "*dysgalactiae*" and "*equisimilis*" subspecies (Jensen and Kilian, 2012). Surprisingly, our results show the separation of bovine SDSD from human SDSD strains in different clusters, the latter being closer to the SDSE (Figure 2.1).

In this study, we searched for the presence of different *S. pyogenes* virulence genes (encoded by MGE or either chromosomal) among bovine SDSD isolates, namely, genes encoding DNases, SAgs, and SLS.

Some of the SAgs genes are phage- and transposon-associated among *S. pyogenes* strains (Proft and Fraser, 2016). Previous studies have related some of these genes to an increase in the pathogenic potential of SDSD isolates (Rato *et al.*, 2010, 2011). Our results show that the SAgs genes (*speC, speK, speL*, and *speM*) and *spd1* are unevenly distributed among bovine SDSD isolates (from collection I and collection II) but not among human and fish SDSD strains (Table 2.1 and Supplementary Figure S2 in Appendix I).

The *speC* and *spd1* (initially identified in the M1 phage) genes were always detected together, and it was also found to be associated with *speK* (initially identified in the M3 phage) among bovine SDSD isolates, indicating the probable poly-lysogeny, as described for *S. pyogenes* (Giovanetti *et al.*, 2015).

Alignment of *speC, speK, speL, speM*, and *spd1* sequence of bovine SDSD against the GenBank database, using BLAST, revealed a nucleotide identity of 97% to >99% with the homologous *S. pyogenes* virulence. Although the genomes of the bovine SDSD isolates from collection I and II had not been sequenced, the high identity of SAgs and the presence of these genes in prophage regions among *S. pyogenes* could indicate that similar phages (or even the same) are shared among the bovine SDSD and *S. pyogenes*. The high identity of the SAgs and the different habitats of SDSD (animals) and *S. pyogenes* (human pathogen) may suggest that the HGT events occurred before habitat separation.

We analyzed the presence of virulence genes among streptococcal genomes (Supplementary Figure S2 in Appendix I). We found the superantigen G gene

(*spegg*) in SDSE, *S. pyogenes*, and human SDSD, but not in bovine SDSD. The presence of *spegg* has been documented in fish SDSD strains (Abdelsalam *et al.*, 2010); however, to our knowledge, the presence of this gene has not been reported so far among human SDSD strains. Nucleotide sequences from the human and fish SDSD strains revealed >99% identity with the homologous *spegg* of *S. pyogenes* from the NCBI database. To date, there is no evidence of HGT of the *spegg*; so its absence may mean the loss of this in bovine SDSD isolates common ancestor.

SDSD (*α*-hemolytic) and SDSE (β-hemolytic) have been distinguished based on their hemolytic properties on blood agar in routine laboratory practice. The hemolytic activity is mainly attributed to SLS production among the pyogenic group of streptococci. In this study, the results showed the loss of *sag*B-I genes among bovine SDSD isolates. At the same time, the presence of the SLS operon was observed in human and fish SDSD, SDSE, *S. pyogenes*, and *S. canis* (β-hemolytic strains). Our data are the first to suggest that hemolytic differences between human SDSD strains (β-hemolytic) and bovine SDSD isolates (*α*-hemolytic) may be related to the loss of SagB-I and mutation of *sag*A gene observed in bovine SDSD isolates (Figure 2.3). Likely, the exact incidence of SDSD human infections on a global basis can be underestimated, mainly because of the failure to distinguish SDSD from SDSE strains in clinical laboratories.

Even though SDSD remains susceptible to most prescribed antibiotics, a significant number of treatment failures have been reported (Trieu-Cuot *et al.*, 1993; Arthur *et al.*, 1995; González Pedraza Avilés and Ortiz Zaragoza, 2000; Schwarz *et al.*, 2004; Woodford, 2005; Pletz *et al.*, 2006; Kimura *et al.*, 2013; Cattoir, 2016; Doumith *et al.*, 2017; Lai *et al.*, 2017). Although tetracycline is not indicated for bovine mastitis-associated streptococci treatment in Portugal nowadays, high resistance to this class of antibiotics has been observed among bovine SDSD isolates. We observed a significant increase in the frequency of *tetM*, *tetK*, and *tetO* tetracycline resistance genes among bovine SDSD of collection II compared with bovine strains of the collection I. This frequency is likely associated with the fact that tetracycline has been extensively used to treat infections in bovine for many decades; tetracycline resistance determinants are linked to other resistance genes. For example, tetracycline resistance genes can be acquired via MGEs (e.g., plasmids and/or transposons), which also harbored erythromycin resistance genes (Brenciani *et al.*, 2007, 2010; Emaneini *et al.*, 2014; Santoro *et al.*, 2014; Cattoir, 2016), contributing to a multiresistant phenotype. In our SDSD isolates, we identified the presence

of *ermB*/ *tetO*/ *tetK* and *ermB*/ *tetO* macrolide/tetracycline resistance genes, suggesting a possible horizontal gene co-transference of these genes.

Since the sequential order of the spacers in the CRISPR array provides chronological information about the bacteria's exposure to foreign nucleic acids (Lier *et al.*, 2015), providing insights into host–phage interactions within a specific niche, herein, we investigated the occurrence of CRISPR/Cas systems and CRISPR spacer content in bovine SDSD isolates to gain insight into the population diversity and the impact of this system on HGT.

Our results showed that all bovine SDSD strains characterized in the present study carried the CRISPR/Cas IIA system. In addition, we also observed a high degree of polymorphism in the CRISPR spacers providing a high ability to discriminate between strains. About 18.4% of spacers match known prophages with over 96% identity indicating a cross-species exchange of genetic material. The most frequent bacteriophages are listed in Table 2.2. Some studies have suggested that some common phages act as spacer donors (Le Rhun *et al.*, 2019; Hu *et al.*, 2020); thus, different spacers in different strains but identified as the same phage may be correlated with phage's evolution (Sorek *et al.*, 2013; Landsberger *et al.*, 2018; Watson *et al.*, 2018). About 28% of the sequence spacers of SDSD were not identified in the database, probably because of the rapid evolution of phage sequences, and sequences of new phages are not available.

The widespread presence of this CRISPR/Cas system among SDSD bovine strains, the high conservation of repeated sequences, and the polymorphism observed among the CRISPR IIA array spacers of these strains may lead us to consider them as indicators of the activity of the system (Figure 2.5).

To elucidate the relationship between the prophages and CRISPR systems among SDSD strains, we analyzed CRISPR array, CRISPR-associated (Cas) proteins, and prophage structure using complete genome sequences of SDSD. For a comparative analysis, complete genome of SDSE, *S. canis*, and *S. pyogenes* were also analyzed.

We observed that the CRISPR II-A system had increased the number of spacers relative to CRISPR I-C. Indeed, CRISPR II-A locus is the most widespread type among streptococci strains and has the most significant number of spacers. Several studies concluded that type II-A CRISPR might be the primary phage prevention or elimination system in the streptococcus genome (Serbanescu *et al.*, 2015; Yamada *et al.*, 2019; Hu *et al.*, 2020).

The genomes of SDSD and SDSE show a high number of spacers compared with those of *S. pyogenes* (Table 2.3). Some studies have speculated on the loss of the CRISPR array and/or the CRISPR/Cas locus in some clinical isolates. In this regard, it was proposed that the lack of CRISPR/Cas could indicate an adaptation to acquire new virulence genes. It has also been hypothesized that the low number of spacers acquired by *S. pyogenes* could be a strategy to acquire virulence genes and thus increase its pathogenic capacity (Le Rhun *et al.*, 2019). Among our SDSD strains, there was no statistically significant difference in the total number of prophages in the strains with type IC and type IIA systems. A more significant number of prophage regions would be expected in the absence of the CRISPR/Cas system; however, we observe SDSD strains with an active CRISPR/Cas system harboring several prophage regions per genome.

2.5.   Conclusion

The results showed a significant increase in the frequencies of the *tetM*, *tetO*, and *tetK* genes over time, although tetracycline is not indicated for bovine mastitis-associated streptococcus treatment in Portugal nowadays. Our data suggest that carriage of *S. pyogenes* prophage virulence genes (*speC*, *speK*, *speL*, *speM*, and *spd1*) is maintained over time and seems to be a property of bovine SDSD, but not of human and fish SDSD and SDSE strains. The high homology of SAgs genes between bovine SDSD and *S. pyogenes* strains may suggest that the HGT events occurred before habitat separation.

This study documented for the first time the widespread presence of the CRISPR/Cas IIA system among bovine SDSD isolates, and the polymorphism observed in spacer content can be considered indicators of the system activity. However, no correlation was observed between the number of spacers CRISPR IIA and the number of prophages in the SDSD genomes. Further studies are necessary to understand better the CRISPR/Cas systems among SDSD strains, such as other CRISPR systems, and its impact on the evolution of SDSD virulence. Our data are the first to suggest that hemolytic differences between human SDSD strains (β-hemolytic) and bovine SDSD isolates (α-hemolytic) may be related to the loss of SagB-I and mutation of *sagA* gene observed in bovine SDSD isolates. The SagA alignment reveals higher homology between human and fish SDSD and SDSE strains when compared with the bovine SDSD isolates. The close genetic relationship between non-bovine SDSD and SDSE was also

clear from phylogenetic analysis based on MLSA, while bovine SDSD isolates seem more divergent.

The data set of this study suggests that the separation between the subspecies "*dysgalactiae*" and "*equisimilis*" should be reconsidered. However, a study including the most comprehensive collection of strains from different environments would be required for definitive conclusions regarding the two taxa.

Author Contributions

IS-S, CA-B, and RM contributed to the idea or design of the research. RB and MO collaborated with the collection of bovine mastitis samples. CA-B contributed to the experimental work, analysis of sequences and complete genomes. JC and CA-B contributed to the research of virulence genes. LC and RT contributed with the support in the BioNumerics software and assistance in the analysis. CA-B wrote down the first draft and the subsequent revisions of the manuscript. RM and ARF performed the revision of the final manuscript. The author of this thesis opted for reproduction of the resulting scientific paper, thus apologizing for any repeated content in different contexts of the document.

Funding

Chapter 3 - Phylogenetic analysis and accessory genome diversity reveal insight into the evolutionary history of *Streptococcus dysgalactiae*

Abstract

In this work, we provide a phylogenomic analysis based on the single-copy core genome of 106 isolates from both subspecies and different infected hosts (animal and human hosts). The accessory genome of this species was also analyzed for screening of genes that could be specifically involved with adaptation to different hosts. Additionally, we searched putatively adaptive traits among prophage regions to infer the importance of transduction in adapting the SD to different hosts.

Core genome phylogenetic relationships segregate all human SDSE in a single cluster separated from animal SD isolates. The subgroup of bovine SDSD evolved from this later clade and harbors a specialized accessory genome characterized by the presence of specific virulence determinants (e.g., *cspZ*) and carbohydrate metabolic functions (e.g., fructose operon).

Together, our results indicate a host-specific SD and that the existence of an SDSD group that causes human-animal cluster infections may be due to opportunistic infections, and that the exact incidence of SDSD human infections may be underestimated due to failures in identification based on the hemolytic patterns. Yet, more detailed research into the isolation of human SD is needed to assess whether it is a carrier phenomenon or whether the species can be permanently integrated into the human microbiome, making it ready to cause opportunistic infections.

3.1. Introduction

The taxonomic status of subspecies Streptococcus dysgalactiae remains controversial despite years of debate and reclassifications. Based on whole-cell-derived polypeptide patterns, chemotaxonomic and phenotypic examination, Vandamme and co-workers proposed criteria for the classification of Streptococcus dysgalactiae subspecies, in which subspecies *dysgalactiae* includes isolates from the host animal, while the subspecies *equisimilis* includes isolates from the human host (Vandamme *et al.*, 1996). Posteriorly, Vieira and co-workers classified the two subspecies based on hemolytic patterns, SDSD and SDSE, including α-hemolytic and β-hemolytic isolates, respectively (Vieira *et al.*, 1998).

SDSE, initially regarded as human commensal bacteria (Suzuki *et al.*, 2011), is now recognized to be an important human pathogen, causing several infections, including bacteremia, cellulitis, endocarditis, peritonitis, septicemia, pneumonia, pharyngitis, and toxic shock syndrome, similar to those caused by *S. pyogenes* (Brandt and Spellerberg, 2009; Hagiya *et al.*, 2012; Bruun *et al.*, 2013; Fuursted *et al.*, 2016). Additionally, β-hemolytic isolates from animal hosts have been frequently identified as SDSE (Acke *et al.*, 2015; Pinho *et al.*, 2016; Oh *et al.*, 2018; Oh *et al.*, 2020; Porcellato *et al.*, 2022).

SDSD has been considered a strictly animal and is commonly associated with bovine mastitis (Rato *et al.*, 2013) and infectious arthritis in sheep (Smistad *et al.*, 2021) and septicemia in vampire bats (Mioni *et al.*, 2018). SDSD has been considered an important pathogen in aquaculture systems worldwide (Hawke *et al.*, 2021; Maekawa *et al.*, 2020). Phylogenetic studies based on the *sodA* gene revealed that isolated from human blood cultures are closely related to SDSD from the fish host suggesting that SDSD represents an important potential causative agent of zoonoses (Koh *et al.*, 2009; Koh *et al.*, 2020).

Recently, we have reported that bovine SDSD can adhere to and internalize human cells, including human epidermal keratinocyte cells (Alves-Barroco *et al.*, 2018), suggesting that bovine SDSD may cause skin/soft tissue infections, and this might be an important mechanism in the pathogenesis of human cellulitis. In fact, human cellulitis by SDSD, although still rare, has been reported (Chennapragada *et al.*, 2018; Koh *et al.*, 2009; Nathan *et al.*, 2021).

Differences in the adaptation of SDSD to humans and bovines are still unknown. It is critical to understand further the pathogenic potential of the most clinically

significant strains and their epidemiology. Previous studies have reported the presence of S. pyogenes phage-carried virulence genes among SDSD strains from bovine mastitis, such as the streptococcal pyrogenic exotoxin genes and DNases extracellular (Rato *et al.*, 2011; Abdelsalam *et al.*, 2013; Alves-barroco *et al.*, 2021). It was suggested that the presence of these S. pyogenes virulence genes in SDSD contributes to the increased virulence potential of this subspecies (Rato *et al.*, 2011).

In routine laboratory practice, SDSD and SDSE have been distinguished based on their hemolytic properties on blood agar. However, failures in identification were shown based on hemolytic patterns since SDSD can also produce β-hemolysis (Jensen and Kilian, 2012).

The purpose of this study was to analyze whole-genome sequences of SD from the National Center for Biotechnology Information that included the previously described SDSD and SDSE and four new bovine SDSD strains to understand the molecular characteristics associated with the ability to infect different hosts. More specifically, our purpose is to reexamine the phylogenetic relationship among SD strains from different hosts (human and non-human) using the single-copy core genome and present comparative analyses of accessory genes that influence the adaptation to different hosts.

3.2.   Materials and Methods

To understand the complete genomic repertoire, we analyzed 102 different SD genomes from National Center for Biotechnology Information (all genome assemblies presented were downloaded on January 2021) (Supplementary Table S1, Appendix III). Four alpha-hemolytic SDSD bovine strains previously studied (Rato *et al.*, 2010, Chapter 2) from Portugal were included in the study. The classification at the subspecies level and source presented in Table S1, Appendix III follow information from databases and previous publications.

3.2.1.   Genomic DNA Extraction, sequencing, assembly, and annotation.

Genomic DNA was extracted according to Section 2.2.1 of Chapter 2. Each gDNA was quantified in a Nanodrop Spectrophotometer (ThermoFisher Scientific, USA) (VSD9 - 29.6 ng/µL; VSD16 - 41.2 ng/µL; VSD22 - 33.0 ng/µL; VSD43 - 34.8 ng/µL). The integrity samples were confirmed by gel electrophoresis (1% (w/v) agarose), and images were captured using the Gel Doc XR system and Quantity One 1-D analysis software

(Bio-Rad, USA). The samples fulfilled all conditions and therefore proceeded for library construction and sequencing. The generated DNA fragments (DNA libraries) were sequenced with the Illumina Novaseq platform, using 150bp paired-end sequencing reads at STAB VIDA, Caparica, Portugal. The quality of the produced data was determined by Phred quality score at each cycle (position in read). The plot containing the average quality at each cycle was created with FastQC tool (Andrews, 2010).

Sequencing reads were quality trimmed using the CLC Genomic Workbench 20.1 (Qiagen, Denmark), with default parameters for the removal of low-quality sequences. Preprocessed reads were de novo assembled with the CLC Genomic Workbench, using the default settings and a minimum contig length setting of 500 bp. The complete genome sequence data have been submitted to the NCBI and have been deposited at DDBJ/ENA/GenBank under accessions: JAJSPH000000000 (SDSDVSD9), JAJSPI000000000 (SDSDVSD16), JAJSPJ000000000 (SDSDVSD22), JAJSPK000000000 (SDSDVSD45).

Genome sequences were annotated using the Rapid Annotation using Subsystem Technology (RAST) server (Aziz *et al.*, 2008). The RASTtk pipeline applies Prodigal and Glimmer3 prokaryote gene prediction tools. Annotates protein-encoding genes hypothetical proteins with k-mers and performs a basic gene overlap removal. RAST bases its genome identifiers on NCBI taxonomy IDs. The RAST annotation scheme was performed using the RASTtk pipeline. Additionally, we selected the option to automatically resolve the automatic annotation (such as gene candidates overlapping RNAs or genes embedded inside other genes).

3.2.2. Pangenome analysis of *S. dysgalactiae* genomes

The Spine software (v0.2.3) (Ozer *et al.*, 2014) was used to identify *S. dysgalactiae* conserved core genome sequences (genomic sequences present in 100% of the strains) using SDSE NCTC6403 as the reference genome sequence. Alignments with at least 85% sequence identity among *S. dysgalactiae* strains were considered homologous. For a comparative analysis, the core genome using four strains of *S. pyogenes* used as outgroups was also estimated (Supplementary Table S1, Appendix III). Only alignments with at least 70% sequence identity were considered homologous.

Core genome phylogenetic analysis. Nucleotide sequences of single-copy protein-encoding genes were identified and selected, creating alignment blocks using CLC Genomic Workbench. Subsequently, the phylogenetic tree was inferred using

maximum-likelihood in IQ-TREE v2.0.3 (Nguyen *et al.*, 2015). Modelfinder (Kalyaanamoorthy *et al.*, 2017) was used to determine the best model and branch support was estimated using fast bootstrap approximation with NNI optimization and 1000 replicates (Hoang *et al.*, 2018). For each pair of core *S. dysgalactiae* genomes in the alignment, the average nucleotide identity (ANI) was performed using CLC Genomic Workbench. clustering of the pairwise comparison of ANI results was constructed using Euclidian distances.

Accessory genome prediction and characterization. The AGEnt was used for identifying accessory genomic elements (AGEs) in only *S. dysgalactiae* genomes by using an in-silico subtractive hybridization approach against a core genome generated using the Spine algorithm and the default threshold for alignments of 85% sequence identity over at least 100 bp. Annotation of the core and accessory genome was performed using the RAST (Rapid Annotations using Subsystems Technology) (Aziz *et al.*, 2008).

The CCMetagen analysis tool was used to determine the probable origin of the accessory genome of S. dysgalactiae strains (Marcelino *et al.*, 2020). Alignment of accessory genes against the GenBank database using BLAST was performed to trace homolog genes. For comparative analysis of the accessory genome of *S. dysgalactiae* infecting different hosts, genes present in only single or less than 5% genomes (for each group of isolates from different hosts) were not considered due to their higher probability of being false positives.

CLC Genomics Workbench was used to analyze predicted proteins and find suitable structures for M-like proteins. BLAST against M-like protein structure sequence database was carried out by the Find and Model Structure. BLAST hits with an identity to the query sequence lower than 40 % are removed since they most likely would result in inaccurate models. Protein Data Bank (PDB) structures with a resolution lower than 4 Å were removed since they cannot be expected to represent a trustworthy atomistic model. A template quality score is calculated for the available structures found for the query sequence. The score's purpose is to consider both their quality and their homology to the query sequence.

Prophage Identification. PHASTER software (Arndt *et al.*, 2016) was used to screen for prophage-specifying DNA regions within the genomes of available Streptococcus dysgalactiae. Based on the completeness and potential viability of

identified prophages, these were identified as "intact," "questionable," or "incomplete" prophages. Intact prophages were manually analyzed to confirm the presence of all genes required to produce a functional phage particle, including genes encoding left attachment site (attL); lysogeny; DNA replication; transcriptional regulation; head; tail; lysis modules; right attachment site (attR) (Canchaya *et al.*, 2003). The intact prophage sequences were extracted and used as query in BLAST searches against the NCBInr database to screen for the presence of similar prophages in all available genomes. Since several of the SD genomes analyzed are contigs, some regions of prophages may have split into different contigs, only complete sequences of intact prophages were analyzed. For this analysis, only overlap and identity greater than 60% and 80%, respectively, were considered.

3.3. Results

3.3.1 Characterization of four new genomes of bovine SDSD

This study provides new complete genome sequences for four SDSD isolates, Vet *Streptococcus dysgalactiae* (VSD) isolated from bovine mastitis in a Portuguese dairy herd (Table S1, Appendix III). For comparative purposes, we provide the same information for representative SDSD genomes available at NCBI that are associated with infections of different hosts (human, fish, and bovine). The overview of the general characteristics of the new SDSD genomes is shown in Table 3.1. The whole-genome size of the VSDs isolates had an average of 2.05 MB with an average G+C content of 39.6%. On average there are 2,123 coding sequences (CDSs), representing 95.6%, 91%, 93.5%, and 93.6% of the entire genome of VSD9, VSD16, VSD23, and VSD45, respectively. Of the protein-coding genes, 83% of the CDSs were successfully assigned to a functional category of cluster of Orthologous Groups (COG), and approximately 16% of the chromosomal products are hypothetical proteins. The results obtained for the new genomes are similar across all SDSD genomes analysed (Table 3.1). Yet, some interesting genome features tend to differentiate the strains depending on the infected host. Namely, strains that infect bovine host tend to have more genes associated with carbohydrate metabolism, fatty acids, lipids and isoprenoids, and respiration than strains that infect humans and fish, but a lower number of genes associated with virulence and defense systems, iron acquisition, metabolism, and membrane transport (Figure S1, Appendix III).

Table 3.1. Overview of the general characteristics SDSD genomes

Subsystem Feature Counts	Bovine (10)	Fish (2)	Human (3)
Amino Acids and Derivatives	100 ± 3.2	98 ± 1	98 ± 3
Carbohydrates *	158 ± 6.7	132 ± 3.5	133 ± 4.0
Cell Division and Cell Cycle	4 ± 0.0	4 ± 0.0	4 ± 0.0
Cell Wall and Capsule	41 ± 1.6	42 ± 1	39.3 ± 1
Cofactors. Vitamins. Prosthetic Groups. Pigments	71 ± 0.8	71 ± 1	72 ± 3
DNA Metabolism	55 ± 4.0	57 ± 3	55 ± 6
Fatty Acids. Lipids. and Isoprenoids *	57 ± 0.0	41 ± 4	38.3 ± 3
Iron acquisition and metabolism*	20 ± 3.6	25 ± 1	27.3 ± 4
Membrane Transport*	22 ± 0.6	26 ± 2	26 ± 1
Metabolism of Aromatic Compounds	2 ± 0.0	2,5 ± 1	2.3 ± 0.0
Miscellaneous	10 ± 0.0	10,5 ± 1	11 ± 1
Nucleosides and Nucleotides	81 ± 1.9	79 ± 3	82.6 ± 5
Prophages	21 ± 7.3	30 ± 11	14.3 ± 6
Protein Metabolism	107 ± 6.1	112,5 ± 1	109 ± 6
Regulation and Cell signaling	17 ± 0.6	17 ± 1	17.3 ± 0.0
Respiration*	26 ± 3.5	20 ± 1	19.6 ± 1
RNA Metabolism	32 ± 2.0	30,5 ± 1	30.6 ± 0.0
Stress Response	16 ± 0.4	15,5 ± 1	16 ± 0.0
Virulence. Disease and Defense *	33 ± 3.7	40.5 ± 5.5	42.3 ± 3

*Mean and standard deviation of the values observed in the different SDSD genomes listed in table S1. Bovine isolates: VSD9, VSD16, VSD22, VSD45, NCTC4669, NCTC4670, NCTC4671, NCTC13731, FDAARGOS1157 and ATCC27957. Fish isolates: Kdys0611 and STREP9715. Human isolates: DB4999805, DB6070515 and DB5399317.

3.3.2 Pangenome diversity and phylogenetic analysis of *S. dysgalactiae*

The *S. dysgalactiae* pangenome was inferred from a dataset of 106 whole-genome sequences. In total, it comprises 6,745,861bp, that includes 6632 and 1134 (1,542,420 bp) protein-coding sequences identified as accessory and core genome, respectively. The functional distribution of system categories between the accessory and core genome of *S. dysgalactiae* is shown in Figure 3.1. The highest percentage of genes associated with the accessory genome was attributed to the category of prophages and transposable elements, followed by DNA metabolism, Virulence and defense, Regulation, and Cell signaling. As expected, genes belonging to Division and Cell cycle categories and Dormancy and Sporulation were entirely attributed to the core genome.

The phylogenetic relationships between SDSD and SDSE strains were inferred based on the single-copy core genome of these 106 *S. dysgalactiae* genome sequences (Figure 3.2). This tree was rooted on the largest branch as the closest outgroup species, *S. pyogenes* was too distant to provide a robust root inference (Figure S2, Appendix III).

The phylogenetic analysis with *S. pyogenes* was inferred following the same methodology and produced a dataset of 431 single-copy core protein-coding sequences shared by the 106 *S. dysgalactiae* and four *S. pyogenes* isolates (Figure S2, Appendix III). Both analyses segregated all human SDSE in a single cluster separated from all other animal SD. The animal SDSE strains are more closely related to SDSD strains (Figure 3.2A and 3.2B, Figure S2, Appendix III).
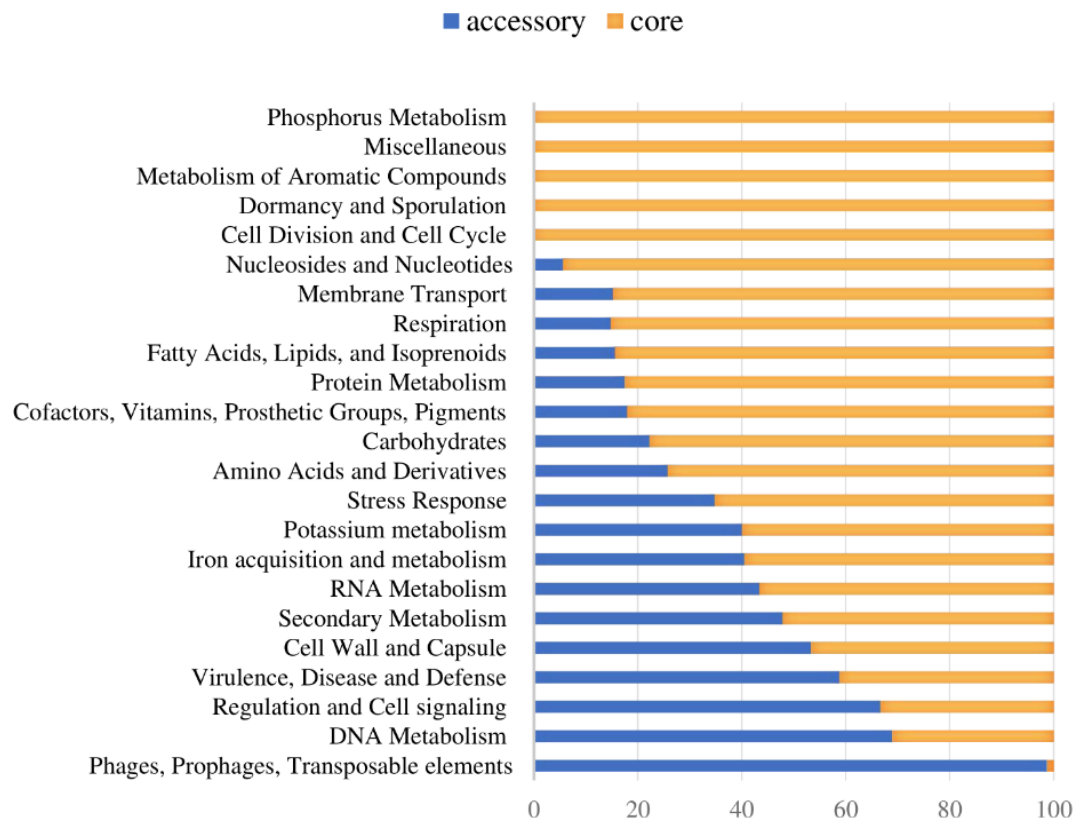
Figure 3.1. Distribution of core and accessory genes in different functional categories investigated *S. dysgalactiae* genomes.
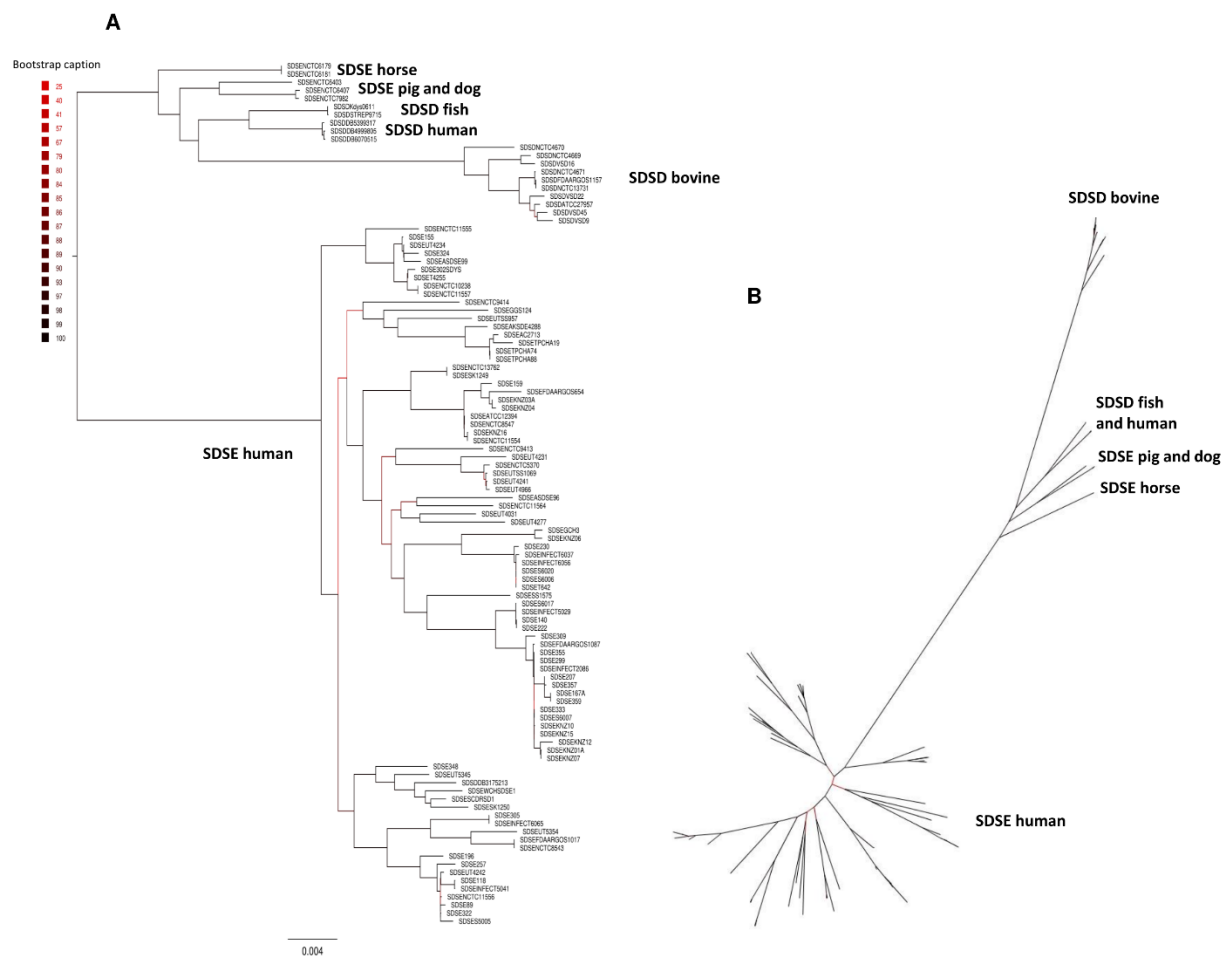
Figure 3.2. Phylogenetic analysis of the S. dysgalactiae single-copy core genome. Phylogenetic analysis of the *S. dysgalactiae* single-copy core genome. (A) The tree was rooted on the largest branch as the closest outgroup species (B) Phylogenetic unroote tree relationships. The evolutionary history was inferred using the Maximum Likelihood analysis of the alignment of 1134 single-copy core protein-coding sequences shared by 106 *S. dysgalactiae* strains. Bootstrap support values were calculated from 1000 replicates. A phylogenetic tree was generated using IQ-TREE v2.0.3.

To quantify the genomic similarities among isolates, we generated a dendrogram and a heatmap with the ANI values of all *S. dysgalactiae* using the core genome dataset (Figure 3.3). All within-group and among group comparisons are above 96%, indicating the high similarity of these genomes. Similar to the phylogenetic analysis, ANI values segregate *S. dysgalactiae* genomes into two main groups: cluster I, comprising the humans SDSE, and cluster II comprising the animal SDSE and the SDSD isolates. Interestingly, the latter can be further subdivided based on the host isolates. All SDSD bovine strains are segregated into a single group within cluster II, while the

second subcluster is subdivided into two groups separating humans and fish SDSD isolates and horse, dog, and pig SDSE isolates. The ANI analyses reinforce that bovine SDSD comprises a very homogenous group separated from the remaining strains.
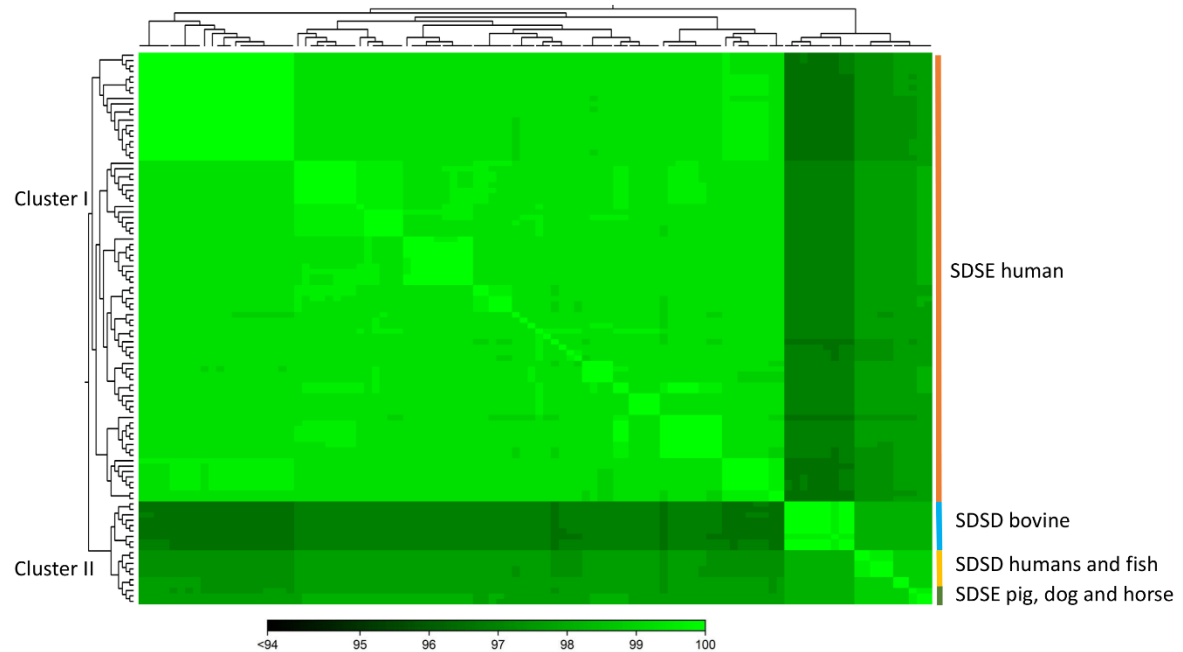
Figure 3.3. Heatmap chart generated from distances calculated based on the ANI values of *S. dysgalactiae* core genome. The colors in the heatmap represent pairwise ANI values, with a gradient from dark green (low identity) to light green (high identity). The dendrogram directly reflects the degree of identity between genomes increasing in similarity from dark to green. Heatmap and dendrogram of ANI values were performed using the CLC Genomic Workbench.

3.3.3 Accessory genome characterization

The software CCMetagen was used to investigate the possible origin of accessory genes by screening with the NCBI database (Figure 3.4). CCMetagen results suggest that 38% of the accessory genes of *S. dysgalactiae* are only found in this species. These are putative orphan genes (or errors). About 14% of the accessory genome is shared with *S. pyogenes*, 18% is shared with other species of the genus *Streptococcus*, and approximately 20% of the genes are shared with other bacteria. Interestingly, *S. dysgalactiae* has been found to share genes with phylogenetically distant bacteria, such as the Enterobacteriaceae.
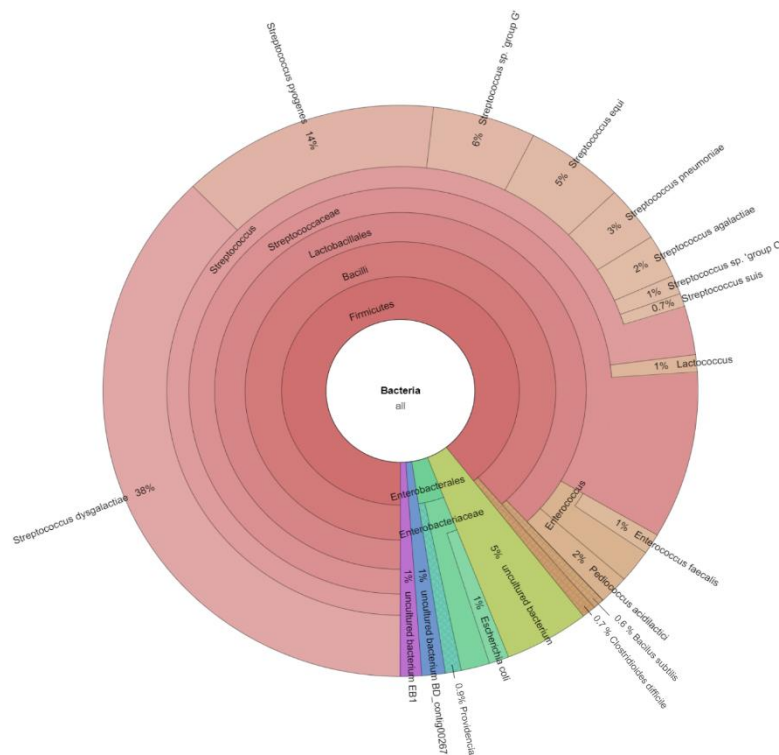
Figure 3.4. Metagenomics analysis of the accessory genome of *S. dysgalactiae*. CCMetagen graph shows the percentage of accessory genes shared with other bacteria. The alignment of accessory genes against the GenBank database using BLAST was performed to trace homolog genes using CCMetagen analysis tool. The figure and legend were automatically generated based on the nomenclature deposited in the NCBI.

To investigate genes/operons that may be related to host adaptation, we compared the *S. dysgalactiae* accessory genome from different hosts. Thus, virulence genes, carbohydrate metabolism profiles, and antimicrobial and metal resistance determinants of each *S. dysgalactiae* accessory genome were analyzed (Table S2, Appendix III). Our results reveal that, although most accessory genes of *S. dysgalactiae* are widely distributed among isolates from different hosts, some genes seem to be associated with distinct clusters (Figure 3.5, Table S2, Appendix III). Some of these genes/operons were found to be unique for bovine SDSD isolates, e. g., fructose and sorbitol metabolism operons and genes encoding M-like proteins. Additionally, several genes were shared between all SDSD isolates and SDSE from host animals (non-humans), e. g., genes encoding heme efflux system ATPase (*hrtA* and *hrtB* genes) and *vpr* gene.
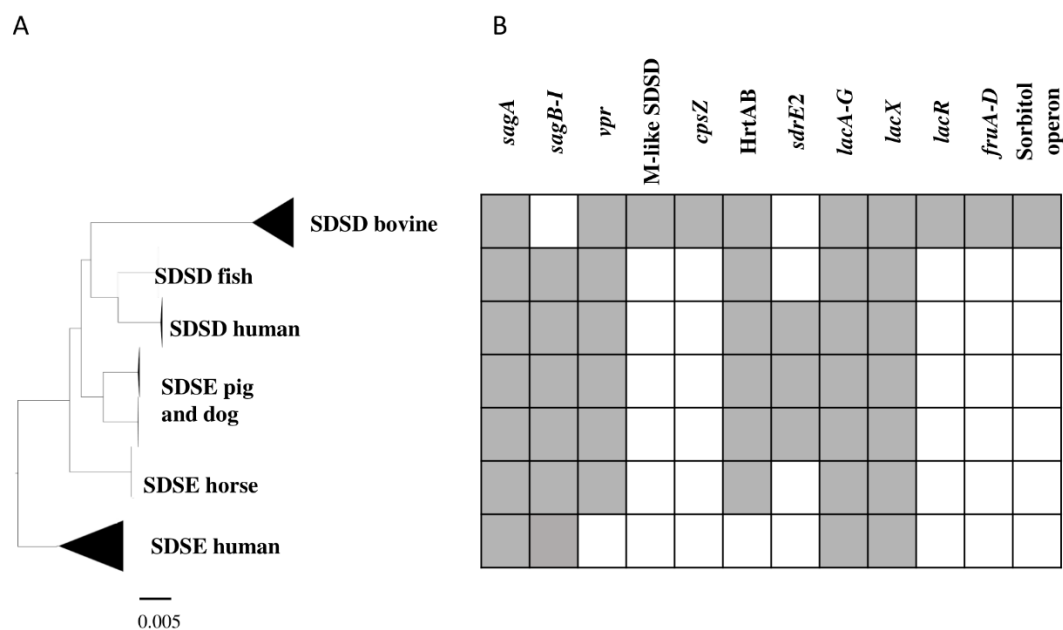
Figure 3.5. Virulence and carbohydrate metabolism profiles of the 106 *S. dysgalactiae* isolates. (A) Phylogenetic analysis of the *S. dysgalactiae* single-copy core genome. (B) Graphic representation of the presence (gray) and absence (white) of the identified relevant genes clusters in the *S. dysgalactiae* genomes in this study. *sagA* to *sagI* – Streptolysin (SLS) operon; *vpr* gene - C5a peptidase; M protein-like (SDSD); *cpsZ* gene - Emm-like cell surface protein; *sdRE2* - adhesin; HrtAB - Heme efflux system; *lacA* to *G, lacX and lacR* genes - lactose metabolization operon; *fruA* to *D* - fructose metabolism operon; Sorbitol operon - Sorbitol/glucitol metabolism operon. The complete set of data is shown in supplementary Table S2, Appendix III.

Regarding antibiotic and metal resistance profiles, no differences were observed between groups (Table S2, Appendix III). Interestingly, genes coding for β-lactamases and VanZ were identified in the *S. dysgalactiae* genome. We compared the sequences coding for β-lactamases enzymes (CDS: WP226316797.1 and WP226316205.1) and glycopeptide resistance functional domain and glycopeptide resistance (*vanZ* gene, CDS: WP003049062.1) sequences from the NCBI database using the BLAST Tool. Our analyses reveal that these genes are highly conserved among strains belonging to the pyogenic group of *Streptococcus*, with an identity greater than 70%.

Nine-genes associated with the operon for lactose metabolism (*lacABCDEFGX*) were found in both subspecies; however, the *lacR* gene (lactose phosphotransferase system repressor) was only found among bovine SDSD strains. The *lacR* gene was just downstream of the nitrogen regulatory protein P-II and fructose metabolism operon, found exclusively in bovine SDSD isolates. BLAST analysis revealed that the operons for

lactose and fructose metabolism of bovine SDSD shared a high identity (> 98%) with the homologous region present in *S. agalactiae* NCTC8184. The operon for Sorbitol/glucitol metabolism was also found exclusive in bovine SDSD genomes.

The *cspZ* gene (Emm-like cell surface protein, CDS: VDZ39525.1) was found exclusively in bovine SDSD isolates. This gene shares greater than 70% identity between bovine SDSD and *Streptococcus equi.* Among the bovine SDSD genomes, the *mga* gene and an open reading frame (ORF) previously identified as homologous to *S. pyogenes* M proteins (Porcellato *et al.*, 2021) were observed upstream of the *cspZ* gene. The *mga* gene of bovine SDSD shares approximately 70% identity with *S. pyogenes,* but the ORF is about 40% identical to the *S. pyogenes* sequence. To confirm this homology, we performed a structured-based alignment of the predicted amino acid sequences against the PDB database. Our results corroborate the M protein identification for five SDSD genomes in our dataset (Table 3.2). Sequences from VSD22, VSD45, and NCTC4670 SDSD isolates produced significant results against chain M of 2XNX PDB structure that corresponds to bc1 fragment of streptococcal M1 protein, while sequences from FDAARGOS1157 and NCTC4671 strains had significant results against chains B and D, respectively of 2OTO structure PDB matching the N-terminal fragment M1 protein (Table 3.2, Figure S3, Appendix III). The alignments performed with VSD9, VSD16, and NCTC4669, did not retrieved any significant result in the PDB database but their ORF contains conserved peptide signal homologous to the one present in M protein of the *S. pyogenes* (Figure S4, Appendix III). A second homolog (DemA, CDS: CAB65411.1) of the M and M-like protein was found restricted to bovine SDSD genomes.

Table 3.2. Characterization of the M-like protein region among SDSD bovine strains.

Isolates	PDB structures	Chain	E-value	% Match identity	Resolution (Å)
SDSDVSD22	2XNX	M	2.82E-8	63.64	3.30
SDSDVSD45	2XNX	M	2.91E-8	63.64	3.30
SDSDNCTC4670	2XNX	M	2.93E-8	63.64	3.30
SDSDNCTC4671	2OTO	D	7.26E-7	53.03	3.04
SDSDFDAARGOS1157	2OTO	B	6.87E-7	53.03	3.04

1) E-value measures the quality of the match from the BLAST search; **2)** % Match identity is the identity between the query sequence and the BLAST hit in the matched region; **3)** Resolution of crystal structure.

In SDSD and animals SDSE isolates (pig, dog, and horse host), the *vpr* gene was found to share an identity greater than 95%. BLASTP alignment of predicted protein

indicates that *vpr* encodes peptidase S8 family domain in Streptococcal C5a peptidases, protease, and adhesin/invasin. The LP$_X$TG-motif cell wall anchor domain was also identified. This C5a peptidase is flanked by the *fhs1* and *cls* genes encoding formate-tetrahydrofolate ligase and cardiolipin synthetase, respectively, shared an identity greater than 95% among *S. dysgalactiae* isolates (Figure 3.6). Results also show that the *scp* gene found among human SDSE isolates (CDS: VTT04007.1) was found to share >90% identity (overlap of about 40%) with the *vpr* gene (Figure 3.6). BLASTp alignment of predicted protein SCP indicates the presence only of the LP$_X$TG-motif cell wall anchor domain, suggesting that this gene may have been disrupted by mobile genetic elements in the human SDSE lineage (Figure 3.6).
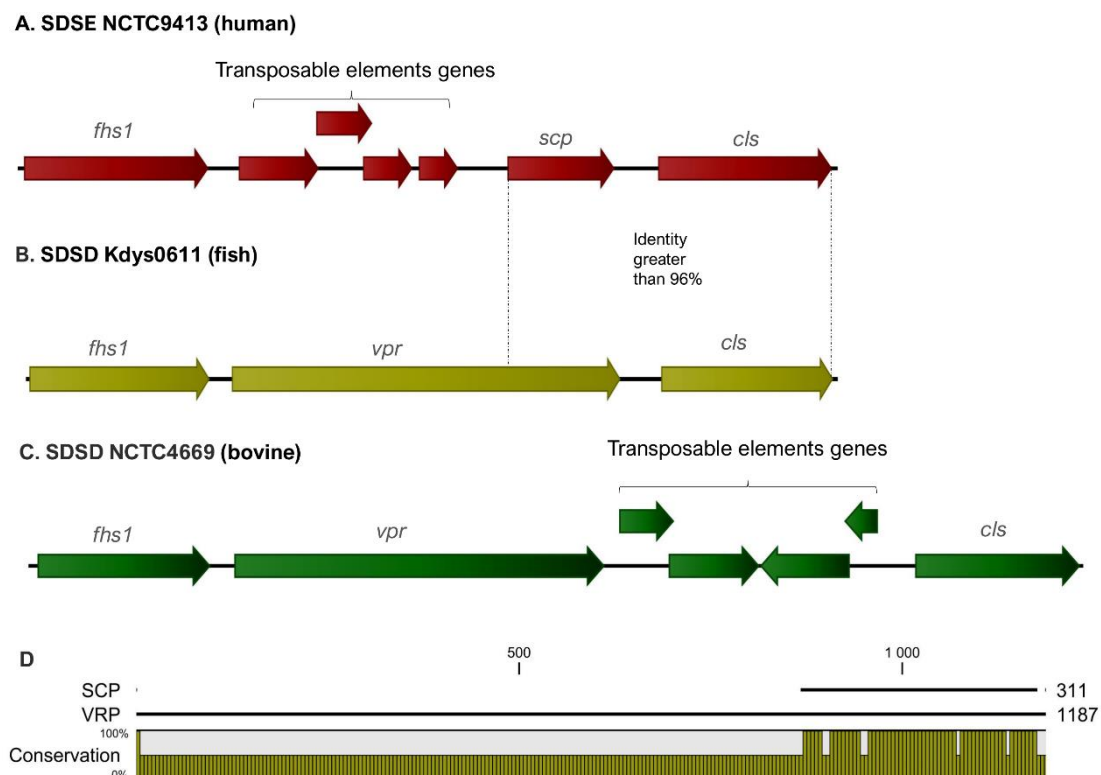
Figure 3.6. (A), (B) and (C) Graphical representation of organization of the region flanking gene that code for the C5a peptidase. The *fhs1* and *cls* genes encoding formate-tetrahydrofolate ligase and cardiolipin synthetase, respectively, shared an identity greater than 95% among *S. dysgalactiae* strains. The gene identified as *vpr* (C5a peptidase precursor ScpZ) in strain SDSENCTC4669 (CDS: VDZ40442.1) is shared among all SDSD non-human SDSE strains, while *scp* gene (C5a peptidase) of the SDSENCTC9413 strain (CDS: VTT04007.1) is shared among all human SDSE strains. (D) BLASTp alignment of predicted proteins VPR and SCP suggest that *scp* is a fragment of the *vpr* gene and reveals that the region coding for the C5a peptidase is absent from the *scp* gene.

The adhesin *sdrE_2* gene (CDS VTT00995.1) shared an identity greater than 85% among animals SDSE and humans SDSD isolates. This adhesin belongs to MSCRAMM (acronym for "microbial surface components recognizing adhesive matrix molecules") family SdrC/SdrD. Features of this protein family include a YSIRK-type signal peptide at the N-terminus and a variable-length C-terminal region of Ser-Asp (SD) repeats followed by an LPXTG-motif. The *sdrE_2* gene was found in genomic regions with insertion sequences, commonly associated with signals of horizontal gene transfer, and flanked by homologous regions among S. *dysgalactiae* isolates. The structure of the genomic regions flanking the *sdrE_2* gene is shown in Figure S5, Appendix III.

Streptococcus dysgalactiae prophages regions

Prophage regions were found on all genomes analyzed. No differences were found in the number of prophage regions among the different groups of isolates, except for the fish SDSD isolates. The fish SDSD Kdys0611 and SDSD STREP9715 isolates were found with the highest number of regions of prophages per genome, with 12 and 23 regions, respectively. Overall, 72 of the prophage regions were considered intact, 68 were considered questionable, and 310 prophage regions were considered incomplete. Since several of the SD genomes analyzed are contigs, some regions of prophages may have split into different contigs, only complete sequences of intact prophages were analyzed.

The regions of S. *dysgalactiae* prophages intact ranged from 19.4Kb to 87.7Kb, with 24 and 112 protein-coding regions, respectively. Based on the identity of coding regions within intact prophages, PHASTER indicates that the most prevalent intact prophages corresponded to prophages initially identified in S. *pyogenes*, such as Strept_315; Strept_phi3396; Strept_phiNJ2; Strept_T12; Strept_P9, and Strept_A25.

In order to identify the prophage intact and screening similar prophage regions, a blast against the NCBI database sequences was also performed. The result of sequence similarity analysis showed that approximately 69% (50/72) of the intact prophages are unknown. About 30% (22/72) of the prophage regions found in the genomes studied in the present study showed overlap greater than 60% and nucleotide identity greater than or equal to 80% with known phage genomes (Table 3.3). Most intact prophages are shared between genomes of the pyogenic streptococcus group. A total of 3 and 7 prophages were found only among SDSD and SDSE, respectively; 8 prophages are

shared only by *S. dysgalactiae* genomes; 42 prophages are shared by the *S. dysgalactiae* and *S. pyogenes* genomes. *S. dysgalactiae* prophage regions were also found to share high identity with *S. agalactiae*, *S. canis*, *S. pyogenes*, *S. equi* subsp. *equi*, *S. parauberis*, *Lactococcus garvieae* prophage regions (Table 3.3).

Table 3.3. Prophage genome identification using BLASTn at NCBI

Genome	Phage (ID. PHASTER)	Blast NCBI	Host
SDSD ATCC 27957	Strept_315.3B	S. phage Javan119	SDSD
SDSD DB6070515	Strept_phiNJ2	S. phage Javan88	SDSD, SDSE, *S. canis*, *S. pyogenes*
		S. phage Javan91	
SDSD NCTC13731	Strept_315.4	S. phage Javan157	SDSD, SDSE, *S. pyogenes*
SDSD STREP9715	Strept_phiNJ2	S. phage Javan91 or	SDSD, SDSE, S. canis, *S. pyogenes*
		S. phage Javan88	
SDSE 167A	Strept_phi3396	S. phage Javan133	SDSE, SDSD
SDSE ASDSE99	Strept_315.3	S. phage Javan117	SDSE
SDSE GGS124	Strept_315.3	S. phage Javan144	SDSE, *S. pyogenes*
SDSE KNZ15	Strept_phi3396	S. phage Javan137	SDSD, SDSE, *S. canis*, *S. pyogenes*
SDSE KNZ16	Strept_phi3396	S. phage Javan143	SDSD, SDSE, *S. canis*, *S. pyogenes*
SDSE NCTC10238	Strept_T12	S. phage Javan128	SDSD, SDSE
	Lister_2389	S. phage Javan274	SDSD, SDSE
SDSE NCTC11555	Strept_315.5	S. phage Javan510	SDSD, SDSE, *S. pyogenes*
SDSE NCTC11564	Strept_A25	Siphoviridae phage	SDSE
	Strept_315.4	S. phage Javan470	*S. pyogenes*
SDSE NCTC13762	Strept_T12	S. phage Javan471	SDSE, *S. pyogenes*
	Strept_phi3396	S. phage Javan117	SDSD, SDSE
SDSE NCTC9414	Strept_315.6	S. phage Javan135	SDSD, SDSE, *S. canis*, *S. pyogenes*, *S. equi* subsp. *equi*
SDSE S6020	Strept_315.3	S. phage Javan150	SDSE, *S. pyogenes*
SDSE UT4234	Strept_315.4	S. phage Javan88	SDSD, SDSE, *S. canis*, *S. pyogenes*, *S. equi* subsp. *equi*
SDSE UT5345	Strept_315.5	S. phage Javan166	SDSE, *S. pyogenes*

Phage Resistome Analysis

To better comprehend the phage-host interplay among *S. dysgalactiae*, the screening of Abortive Infection (Abi) and Restriction-Modification (RM) systems and non-specific endonuclease among accessory genomes were performed. The results of this analysis suggest that the phage resistome-associated sequences are widely

distributed throughout *S. dysgalactiae* strains. Table 3.4 summarizes the *S. dysgalactiae* phage resistome.

We identify the AbiE and AbiSD systems among the *S. dysgalactiae* strains. AbiE system is organized in a bicistronic operon, encoding the AbiEi toxin and AbiEii antitoxin, while AbiSD has not been fully understood yet. Alignment of *abiEi, abiEii,* and *abiSD* sequence of *S. dysgalactiae* against the GenBank database using BLAST was performed. The analysis revealed that *abiEi, abiEii* is present in the genome of *S. agalactiae*, *S. suis*, and *S. plurianimarium*, and *abiSD* is present in the genome of bovines SDSD strains. AbiEi and AbiEii proteins of the *S. dysgalactiae* strains share high amino acid identity (>87%) with *S. agalactiae* sequences. The high sequence identity of AbiEi (96%) was observed between VSD22 and SDSD NCTC4670 strain. Interestingly, the bovine SDSD NCTC4670 strain does not harbor the *abiEii* gene (Figure S6, Appendix III).

Several non-specific extracellular nucleases were identified in the accessory genome of *S. dysgalactiae*. While the Spd3 and streptodornase D nucleases seem to have ubiquitous distribution within the *S. dysgalactiae,* it is also present in other species of *Streptococcus*, such as *S. canis, S. equi and S. pyogenes,* the streptodornase B nuclease (*spd1*) was found only in bovine SDSD isolates, associated with the putative prophage found in *S. pyogenes* genomes. The *spd1* gene has been found associated with *speC* gene (streptococcal pyrogenic exotoxin). Studies carried out by our research team showed that *speC* and *spd1* genes are present in bovine SDSD from different geographic regions and years of isolation, namely SDSD from bovine mastitis isolated in Portugal during 2002-03 and 2011-13 (Rato *et al.*, 2013; Alves-barroco *et al.*, 2021). In the present work, we have identified *speC-spd1* genes only in putative prophages of the bovine SDSD NCTC4669 (isolated in 1935, London) and SDSDVSD16 (isolated in 2002, Portugal) with high nucleotide identity (greater than 97%). In bovine SDSD prophages, another streptococcal pyrogenic exotoxin gene (*speK*) downstream of the *speC-spd1* region was identified. While the *speC-spd1* genes were originally identified in the M1 phage (from *S. pyogenes*), *speK* was identified in the M3 phage (from *S. pyogenes*), suggesting poly-lysogeny and stable genetic linkage of the *speC-spd1-speK* genes among bovines SDSD isolates.

Regarding the restriction-modification (RM) systems of the accessory genome of *S. dysgalactiae*, the putative DNA methyltransferase YeeAM and the respective

restriction enzyme (herein referred to as YeeAR) were identified only among bovine SDSD strains. However, an analysis of the NCBI database reveals that these enzymes are present in *S. equinus, S. pseudopneumoniae, S. mitis, S. suis,* and *S. parasuis.* The Hsd RM system was found only in fish SDSD strains and shared with closely related genera such as *Lactococcus* and *Leuconostoc,* whereas the type III RM system was found only in the human SDSD SDSDDB49998-05 strain was also detected in *Enterococcus* and *Lactococcus.* Interestingly, DNA modification methylase (CDS QBX23397.1 of S. phage Javan128) was found in all putative Strep_12 prophages identified in this study.

Table 3.4. Distribution of the Abi and RM systems and non-specific endonuclease of *S. dysgalactiae*

	Proteins	Frequency* (%)	Function/ description	Strains	RefSeq/ BLAST nt	Other Species
Abi	AbiEi	26.08	Interfering with transcription	*S. dysgalactiae*	CCW38134.1	*S. agalactiae, S. suis, S. pluranimalium*
	AbiEii	25.21			CCW38135.2	
	AbiSD	9.56	unknown	Bovine *S. dysgalactiae*	YP_006081091.1	-
RM	YeeAM	8.69	type I	Bovine *S. dysgalactiae*	WP_003049571.1	*S. equinus, S. pseudopneumoniae, S. mitis, S. suis, S.parasuis*
	YeeAR				WP_011527759.1	
	HsdM	0.87	type I	SDSDKdys0611 and SDSDSTREP9715	WP_002265322.1	*Lactococcus lactis* subsp. *lactis, Leuconostoc mesenteroides* subsp. *mesenteroides, Lactococcus raffinolactis*
	HsdR				QGH04647.1	
	Subunit M	1.73	type III	SDSDDB49998-05	WP_016175772.1	*Enterococcus gilvus, Enterococcus faecalis, Lactococcus raffinolactis*
	Subunit R				WP_016175771.1	
Non-specific endonuclease	Spd3	8.69	Streptococcal phage DNase protein	*S. dysgalactiae*	CP_043530.1	*S. pyogenes, S. canis, S. equi*
	Streptodornase B	11.3	Mitogenic factor phage DNase protein	Bovine *S. dysgalactiae*	YP_008243972.1	*S. pyogenes*
	Streptodornase D	100	Streptococcal phage DNase protein	*S. dysgalactiae*	WP_012766664.1	*S. pyogenes, S. equi*

3.4. Discussion

This study provided an analysis of genomic features of SD associated with specific hosts. The phylogenetic relationship of SD strains showed that human and animal isolates are segregated into two clearly distinct groups. Supporting our results, ANI pairwise comparison of the core genome grouping SD isolates into two main clusters: cluster I harbor only human SDSE isolates, while cluster II harbors SDSD and animal SDSE isolates (Figure 3.3), corroborating the groups detected by phylogenetic analysis.

Our phylogenetic relationship analysis and the ANI values of the comparison of isolates revealed that human and fish SDSD are closely related. These results corroborate the phylogenetic relationships based on the *sodA* gene sequences (Koh *et al.*, 2020). Koh and co-workers' findings suggest that the source of infection in humans by SDSD was suspected to be the fish.

Additionally, Koh and co-workers reveal that the human SDSD isolates were isolated from blood cultures of human patients with a similar clinical presentation: DB6070515 (isolated in 2015) from a patient with breast cancer; DB5399317 (isolated in 2017) from a breast cancer patient, and DB4999805 (isolated in 2005) from a patient that had a partial mastectomy. This patient developed septicemia after a cut on her hand while cleaning fish (Koh *et al.*, 2020). Apparently, the compromised immune system of those patients' favored infections associated with SDSD isolates. Yet, more detailed research into the isolation of human SD is needed to assess whether it is a carrier phenomenon or whether the species can be permanently integrated into the human microbiome, making it ready to cause opportunistic infections.

Currently, the taxonomic status of subspecies SD remains controversial despite years of debate and reclassifications. In routine human and veterinary clinical laboratories SDSD and SDSE have been distinguished based on their hemolytic properties on blood agar (Jensen and Kilian, 2012). Among the pyogenic group of streptococci, the hemolytic activity is mainly attributed to streptolysin S (SLS) production. The operon encoding SLS includes the prepropeptide structural gene (*sagA*), followed by genes responsible for converting SagA into SLS, transport and leader cleavage (*sagBCDEFGHI*). Datta and co-works reported that all genes of the *sag* operon are required for the expression of functional Streptolysin S (Datta *et al.*, 2005).

Furthermore, previous studies revealed that mutations in the core region of *sagA* cause to loss of β-hemolytic activity (Molloy *et al.*, 2015).

We previously reported that differences in hemolytic patterns between human SDSD and SDSE (β-hemolytic) and bovine SDSD isolates (α-hemolytic) may be related to the loss of *sagB-I* genes observed in bovine SDSD isolates (Alves-Barroco *et al.*, 2021). According to the present study's analysis, the Streptolysin S operon is present in the animal cluster but absent in the bovine isolates.

Together, the data suggest that hemolytic profiles are not a good indicator for the taxonomic classification of subspecies SD. Thus, the failure to distinguish SDSD from SDSE in routine laboratory tests underestimates the exact incidence of SDSD human infections.

To determine the robustness of the phylogenetic relationships observed with the core genome, we analyzed the genome accessory to identify differences among isolates of the different hosts. Interestingly, our results on the presence/absence of some genes of the accessory genome also provide further support for phylogenetic relationships based on the core genome. We found virulence genes, e.g., *hrtA* and *hrtB* encoding heme efflux system ATPase, *vpr* gene encoding C5a peptidase that is shared by SDSD and animal SDSE isolates but is absent in all human SDSE isolates.

Among human SDSE, the *scpG* gene, encoding C5a peptidase, was found with a high degree of identity with the protein from *S. agalactiae* and *S. pyogenes* (Brandt and Spellerberg, 2009). In the present work, we find that the *vrp* gene contained a functional domain encoding a C5a peptidase not previously described in *S. dysgalactiae*. The *scp* gene that showed an overlap of about 40% with the homologous *vpr* gene is shared by only human SDSE isolates. Transposable elements were found upstream of *scp* gene, suggesting that this gene may have been disrupted by mobile genetic elements in the human SDSE lineage.

S. dysgalactiae harbor a great repertoire of adhesins that interact with the extracellular matrix of animal cells, including SfbI, GfbA, FbaA, FbaB, FBP54, and M-like proteins (Alves-Barroco *et al.*, 2020). Here, we found several adhesins ubiquitously and randomly distributed among *S. dysgalactiae* isolates, except the *sdrE_2* gene that was found only in animals SDSE and humans SDSD isolates.

Since carbohydrate metabolism may be associated with adaptation to different niches, we search for the presence of the lactose, fructose, and sorbitol/glucitol metabolism operons in the accessory genome of *S. dysgalactiae*. While the operons for fructose and sorbitol/glucitol metabolism were restricted to bovine SDSD, the operon for lactose metabolism was widely distributed among *S. dysgalactiae*; however, the *lacR* gene (lactose system repressor) was restricted to bovine SDSD isolates. These data suggest that the operons for fructose and sorbitol/glucitol metabolism may be specific biomarkers for the bovine host. Like *S. agalactiae*, *S. dysgalactiae* also harbors two Lac operons. In *S. agalactiae*, Lac.1 was suggested to be a virulence system and specific for human isolates, while Lac.2 regulate lactose metabolism in bovine isolates (Richards *et al.*, 2011). These results also revealed that the operon for fructose metabolism is present in bovine isolates samples but absent among human isolates. This study suggests a unique fructose metabolism for the bovine *S. agalactiae* isolates, facilitating survival in organs or extramammary tissues (e.g., bovine rumen). Richard and co-workers' findings suggest the transfer of the operons for fructose and lactose between species causing bovine mastitis. This exchange of genetic material may have provided adaptation to the bovine environment (Richards *et al.*, 2011).

Overall, no differences in antibiotic resistance profiles were observed between groups. *S. dysgalactiae* has been recognized as non-β-lactamase-producing (Bonofiglio *et al.*, 2018); however, the presence of coding regions for β-lactamase enzymes among *S. uberis* and SDSD genomes recovered from dairy cows in the Canadian was identified (Vélez *et al.*, 2017). Here, we identified the presence of a genetic determinant for widely distributed β-lactamases among *S. dysgalactiae* of human and animal origins (Supplementary Table S5). However, further studies are needed to assess the potential of these β-lactamases, target antibiotics, and the potential of SD as a reservoir of resistance genes. Although some streptococci strains have been identified as resistant to glycopeptides (Park *et al.*, 2014; Srinivasan *et al.*, 2014; Lai *et al.*, 2017), the mechanisms of resistance to glycopeptides in *Streptococcus* are unclear. The teicoplanin resistance gene (vanZ) was widely distributed among the *S. dysgalactiae* genomes in the present study. The protein encoded by *vanZ* of the *S. dysgalactiae* shares about 57% similarity with *E. faecium* VanZ, indicating the likely origin of the gene.

Our analysis reassesses previous taxonomic identifications and recovers an evolutionary history suggest that is not compatible with the current taxonomy based on the proposal by Vieira *et al.*, 1998. The phylogenetic relationship showed that human and animal isolates are segregated into two clearly distinct groups. ANI values and characteristics of the accessory genome reinforce the classification based on the phylogeny of the core genome. Thus, we suggest that all isolates in cluster I of Figure 3.2 should be classified as SDSD, regardless of the hemolytic pattern. However, a more conclusive analysis requires a more sample size of SD isolates sampled from different animal hosts.

Different prophage regions were observed in the *S. dysgalactiae* genomes. Despite the different origins of isolates, most prophages are related. The *S. dysgalactiae* prophage regions display considerable similarity with *S. pyogenes* sequences (about 61%, 51/83), suggesting phage HGT involving these species.

Studies reported the presence of *S. pyogenes* phage-carried virulence genes among bovine SDSD isolates, genes that were not found among SDSE isolates (Rato *et al.*, 2011; Alves-barroco *et al.*, 2021). Though SDSD and SDSE share homologous regions of prophages, the presence of non-essential genes differentially distributed and different regions of integration of the prophages indicates that HGT events between *S. pyogenes* and both subspecies occurred independently.

Although we did not formally analysed, the presence of current gene flow between *S. pyogenes* and SDSD, the results indicated the possibility of gene flow between both. If SDSD isolates can cause zoonotic disease, it seems likely that they occasionally have shared the same niche favoring the transfer of prophages. A second hypothesis is that the exchange of bacteriophages may have occurred before the ecological niche divergence between the two species, as previously suggested (Alves-Barroco *et al.*, 2021). However, the direction of evolution and gene flow between SDSD and *S. pyogenes* remains to be clarified.

Overall, the data suggest that although bacteriophage resistome-associated systems are widely distributed throughout *S. dysgalactiae*. However, greater diversity of systems is found in SD isolated from animal sources.

Restriction-modification (RM) system was found to share a high identity with species belonging to another bacterial genus, such as *Lactococcus lactis subsp. lactis*, *Lactococcus raffinolactis*, *Enterococcus gilvus* and *Enterococcus*. RM systems are

considered the most ubiquitous bacteriophage resist mechanism, and therefore the easiest for phages (Labrie *et al.*, 2010), including the phage-encoded methylases. Here, DNA modification methylase was found in all putative Strep_12 prophages. Besides that, when RM systems fail, the bacteriophages will be replicated and modified by the bacteria cell, becoming resistant to restriction.

In the abortive infection (Abi) system, the resistance results in the death of the phage and the bacteria; therefore, they are 'altruistic' cell death systems, protecting the bacterial population. The Abi mechanisms arrest bacteriophage development in different stages, e.g., phage transcription or genome replication (Labrie *et al.*, 2010). Here, we identify the AbiE and AbiSD systems. AbiE is organized in a bicistronic operon, encoding the antitoxin (AbiEi) and toxin (AbiEii). While AbiE is widely distributed throughout *S. dysgalactiae*, AbiSD is restricted to SDSD bovines. Most toxin-antitoxin (TA) systems encode two components, a toxic protein that generally targets essential cellular processes and an antitoxin (Labrie *et al.*, 2010).

Alignment of the *abiEi* and *abiEii* sequence of *S. dysgalactiae* against the GenBank database revealed > 87% identity with the *S. agalactiae* homologous. In *S. agalactiae*, AbiE system functions as a Type IV TA system. AbiEii induces bacteriostasis, while AbiEi can to neutral the AbiEii expression. Furthermore, it was observed that AbiEi negatively autoregulates abiE operon expression; thus, AbiEi is an antitoxin and a transcriptional repressor (Dy *et al.*, 2014). Interestingly, the bovine SDSD NCTC4670 strain does not harbor the *abiEii* gene but has the *abiEi* gene, and it likely regulates the expression of other genes besides the AbiE operon.

Here we did not observe a correlation between the number of prophages regions and resistome systems in the genomes of *S. dysgalactiae*, suggesting that no mechanism of resistance to bacteriophages is completely efficient. Furthermore, bacteriophage genomes are flexible, with fast evolution in response to bacterial resistance systems.

3.5.   Conclusion

The phylogenetic relationship based on the core genome suggests that *S. dysgalactiae* strains do not cluster by subspecies as it was suggested by Vieira *et al.*, 1998. The phylogenetic analysis and ANI pairwise comparison showed that human and animal isolates are segregated into two clearly distinct groups, supporting the classification proposed by Vandamme *et al.*, 1996. According to the proposal of

Vandamme and co-workers, all SD isolates from the animal source must be classified as SDSD. Thus, the existence of an SDSD group that causes human-animal cluster infections may be due to opportunistic infections, and the exact incidence of SDSD human infections may be underestimated due to failures in identification based on the hemolytic patterns. Yet, more detailed research into the isolation of human SD is needed to assess whether it is a carrier phenomenon or whether the species can be permanently integrated into the human microbiome, making it ready to cause opportunistic infections. The number and diversity of prophage regions in the *S. dysgalactiae* genome enforce the premise that horizontal transfer influences the genomic features, being able to contribute to genetic repertoire and adaptation to changing environments. Features of the accessory genome provide further support for the phylogenetic relationships observed, suggesting a signature of host adaptation and host-specific SDSD population in bovines.

Author Contributions

CA-B, PHB and ARF contributed to the idea or design of the research. CA-B performed the genomic DNA extraction, assembly, annotation of the VSD genomes, phylogenetic analysis and pangenome diversity of the *S. dysgalactiae*, and manuscript writing. All authors performed the revision of the final manuscript.

Funding

Chapter 4 - *Streptococcus dysgalactiae* subsp. *dysgalactiae* isolated from milk of the bovine udder as emerging pathogens: *In vitro* and *in vivo* infection of human cells and zebrafish as biological models

Alves-Barroco, C., Roma-Rodrigues, C., Raposo, L. R., Brás, C., Diniz, M., Caço, J., Costa, P. M., Santos-Sanches, I., and Fernandes, A. R.

Abstract

In this work, the *in vitro* and *in vivo* potential of bovine SDSD to internalize/adhere human cells of the respiratory track and zebrafish as biological models was evaluated. The results showed that, *in vitro*, bovine SDSD strains could interact and internalize human respiratory cell lines and that, *in vivo*, SDSD are able to cause invasive infections producing zebrafish morbidity and mortality. The infectious potential of these isolates showed to be isolate-specific and appeared to be independent of the presence or absence of *S. pyogenes* phage-encoded virulence genes. Although the infection ability of the bovine SDSD strains was not as strong as the human pathogenic *S. pyogenes* in the zebrafish model, results suggested that these SDSD isolates are able to interact with human cells and infect zebrafish, a vertebrate infectious model, emerging as pathogens with zoonotic capability.

4.1. Introduction

In the last years, the association of SDSD with human infections such as upper limb cellulitis in a woman in contact with raw fish (Koh *et al.*, 2009), prosthetic joint infection after knee arthroplasty (Park *et al.*, 2012), and infective endocarditis (Jordal, Glambek, Oppegaard, and Kittang, 2015) has been reported. However, these cases seem to be rare and the role of this subspecies in human pathogenesis remains unclear. It was previously reported the presence of human *S. pyogenes* phage virulence genes among bovine SDSD isolates (Rato *et al.*, 2010; Rato *et al.*, 2011). Generally, genes encoded by MGE are preponderant for host invasion and infection (Ribet and Cossart, 2015; Schmidt and Hensel, 2004), suggesting that these *S. pyogenes* genes could play an important role in zoonosis of bovine SDSD. Recently, we have reported for the first time the ability of milk udder SDSD isolates containing phage encoded *S. pyogenes* genes to adhere and internalize primary human keratinocytes (Roma-Rodrigues *et al.*, 2016).

As previously reported, zebrafish, *Danio rerio*, show great potential in providing novel information about the pathogenic mechanisms and host responses associated with human streptococcal infections and several zebrafish infection models for the most relevant streptococcal species, the human-specific *S. pneumoniae*, *S. pyogenes*, *S. iniae* and *S. agalactiae* have been described (Borst, Patterson, Lanka, Suyemoto, and Maddox, 2013; Miller and Neely, 2005; Novoa and Figueras, 2012; Patterson *et al.*, 2012; Phelps, Runft, and Neely, 2009; Saralahti and Ramet, 2015; Wu, Zhang, Lu, and Lu, 2010).

Adult zebrafish have well-developed innate and adaptive immune systems resembling the human, since the latter system evolved prior to the evolutionary divergence between fishes and other vertebrates (Novoa and Figueras, 2012; Saralahti and Ramet, 2015). Together, the characteristics of this animal model accentuate the importance in the study of human diseases, thus helping in the study of the zoonotic potential of animal pathogens (Borst *et al.*, 2013; Miller and Neely, 2005; Neely, 2017; Novoa and Figueras, 2012; Patterson *et al.*, 2012; Phelps *et al.*, 2009; Saralahti and Ramet, 2015; Torraca and Mostowy, 2017; Wu *et al.*, 2010; Yoshida, Frickel, and Mostowy, 2017).

The main objective of this work was to further elucidate the zoonotic potential of bovine SDSD isolates containing phage encoded *S. pyogenes* genes collected in two different time periods, 2002–03 (SDSD VSD5, VSD9, and VSD13) (Rato *et*

al., 2010, 2011, 2013) and 2011–13 (VSD21, VSD23, and VSD24) to adhere and internalize human respiratory tract cell lines (Detroit 562: pharynx cell carcinoma line, BTEC: primary bronchial/tracheal epithelial cells and A549: lung adenocarcinoma cell line), a preferential niche of colonization/infection of *S. pyogenes*, and to analyze the pathogenicity of those isolates using wild-type zebrafish as the vertebrate animal model.

4.2. Materials and Methods

4.2.1. Ethical statement

The study design followed the international (Directive 2010/63/EU of the European parliament, on the protection of animals used for scientific purposes) and national (Decreto-Lei nº 113/2013) welfare regulations and guidelines (ARRIVE). The animal assays were previously approved by the Portuguese "Direção Geral de Alimentação e Veterinária (DGAV)" (authorization document 0421/000/000/2013). In addition, two authors have a level C FELASA certification (Federation of European Laboratory Animal Science Associations).

4.2.2. SDSD collection

SDSD isolates were collected in two different time periods, 2002–03 (SDSD VSD5, VSD9, and VSD13) (Rato *et al.*, 2010, 2011, 2013) and 2011–13 (VSD21, VSD23, and VSD24) were studied.

4.2.3. Adhesins genes screening (PCR) and expression analyze by RT-PCR

Genomic DNA was obtained according to Section 2.2.1 of Chapter 2. SDSD isolates were screened for the presence and expression of genes encoding proteins involved in the adhesion or the internalization process in SDSE, namely *fbpA* (Fibronectin-binding protein A) and *znuA* (homolog of *adcA* gene of the *S. pyogenes* involved in the processes of adhesion and invasion). The *fbpA,* and *znuA* presence and expression were analyzed using total DNA and cDNA, respectively, as a template. For RNA extraction, SDSD isolates were grown in Todd-Hewitt broth (Oxoid Limited, Basingstoke, England) supplemented with 0.5% (w/v) of yeast extract (BD, Franklin Lakes) at 37 °C until the mid-exponential phase was reached (OD$_{600}$ of 0.5–0.6). RNA was extracted using NucleoSpin RNAII kit (Macherey-Nagel, Dueren, Germany) according to the manufacturer's instructions, followed by the addition of 2 U/µl of DNase I (Applied Biosystems/Ambion). RNA was quantified in a Nanodrop

Spectrophotometer (ThermoFisher Scientific, USA) and integrity was confirmed by gel electrophoresis (1% (w/v) agarose), and images were captured using the Gel Doc XR system and Quantity One 1-D analysis software (Bio-Rad, USA). The cDNA first-strand was synthesized from 100 ng of total RNA using SuperScript first strand synthesis system (Invitrogen, Germany) according to manufacturer's instructions.

Primer sequences and amplicons expected sizes are listed in Table S2 (Appendix I). For each 25 µl PCR reaction mixture, 100 ng of cDNA, 1X reaction buffer for NZYTaq DNA polymerase, 2.5 mmol/L $MgCl_2$, 0.4 mmol/L dNTPs NZYMix, 1U NZYTaq DNA polymerase (NZYTech, Lisbon, Portugal) and 1 µmol/L of each primer (ThermoFisher Scientific, Waltham, United States of America) were added. 16S rRNA gene was used as an endogenous control. PCR conditions of amplification consisted of an initial denaturation cycle (95 °C for 5 min) followed by 35 cycles of denaturation (95 °C for 30 s), annealing (48 °C for *fbpA* or 54 °C for *znuA*, for 30 s), and extension (72 °C for 45 s). A final extension at 72 °C for 7 min was performed. Ultrapure water was used as a negative control in each PCR reaction. 16S rRNA gene was used as an endogenous control. The PCR products were analyzed by gel electrophoresis (1% (w/v) agarose). The NZYDNA Ladder III (NZYTech, Portugal) was used to estimate DNA fragment size. For *znuA* and *fbpA*, genes, primers were designed using to the available genomic information from SDSE strains in GenBank and two strains of SDSE COI289 and HSM53 were used as positive controls for PCR.

4.2.4. Determination of minimal inhibitory concentration

Mueller-Hinton agar (MHA) with 5% sheep blood Broth was supplemented with different concentrations of Gentamicin and TETracycline (0.5 µg/ml; 1 µg/ml; 2 µg/ml; 4 µg/ml; 8 µg/ml and 16 µg/ml, 64 µg/ml; 125 µg/ml and 250 µg/ml). Higher concentrations of Erythromycin antibiotic were used (8 µg/ml; 16 µg/ml; 32 µg/ml; 63 µg/ml; 125 µg/ml; 250 µg/ml; 500 µg/ml; 1000 µg/ml). Direct colony suspension, equivalent to a 0.5 McFarland standard, using colonies from an overnight (18- to 20-hour) sheep blood agar plate and incubated at 37 °C, 5% CO_2, 20–24 hours. *Staphylococcus aureus* ATCC 29213 was used for quality control of determination of minimal inhibitory concentration methods. Results were interpreted according to CLSI (M31-A3).

4.2.5. Human cell lines and culture conditions

Human cell lines used in the *in vitro* studies included preferred niches of colonization/infection of *S. pyogenes* from the respiratory track: Detroit 562 (ATCC® CCL138™), a cell line derived from the metastatic site of pharynx carcinoma, primary Bronchial/Tracheal Epithelial Cells (BTEC) (ATCC® PCS300010™), and A549 (ATCC® CCL185™), a cell line derived from a human adenocarcinoma of the alveolar basal epithelial cells. All cell lines were purchased from the American Type Culture Collection (ATCC) (www.atcc.org) and cultured according to the manufacturer's specifications. Detroit 562 cultures were maintained in Dulbecco's modified eagle medium (DMEM, ThermoFisher Scientific) supplemented with 10% (v/v) Fetal Bovine serum (ThermoFisher Scientific), and a mixture of 100 U/ml penicillin and 100 µg/ml streptomycin (ThermoFisher Scientific). BTEC were maintained in Airway Epithelial Cell Basal medium (ATCC) supplemented with Bronchial epithelial cell growth kit (ATCC), 33 µmol/l Phenol Red (Sigma) and a mixture of 100 U/ml penicillin and 100 µg/ml streptomycin (ThermoFisher Scientific). For bacterial internalization and adherence assays, human cells were seeded in a 96-well culture plate (Sigma-Aldrich Co. LLC, St. Louis, United States of America) at a density of 3×10^4 cells/well and incubated for 24 hours at 37 C, 5% (v/v) CO_2 and 99% (v/v) relative humidity.

4.2.6. Bacterial internalization and adherence assays

The internalization and adhesion of each streptococcal isolate was performed as previously described (Roma-Rodrigues *et al.*, 2016) with some modifications. Bacterial isolates were cultivated in 20 ml Todd Hewitt broth supplemented with 0.5% (w/v) yeast extract (THB) in 100 ml Erlenmeyer flask and grown at 37 °C until a standardized optical density at 600 nm (OD_{600}) of 0.3–0.4 ($5 \times 10^7 – 1 \times 10^8$ cells/ml) was reached. For each isolate, an aliquot of 1 ml of cell suspension was collected and cells were washed three times in fresh THB and finally resuspended in DMEM. Human cells cultured as described previously (Roma-Rodrigues *et al.*, 2016). In a 96-well cell culture plate were then washed three times with phosphate buffer saline (PBS) and each bacterial suspension added on top of the human cell monolayer (multiplicity of infection of 1:100). Bacterial suspensions were simultaneously serial diluted and plated on Todd-Hewitt supplemented with 1.5% (w/v) agar (THA) to confirm the initial number of bacteria added to each well (CFU/ml). The 96-well cell culture plate was then incubated for 2 hours at 37 °C, 5% (v/v) CO_2, and 99% (v/v) relative humidity. A549 cells were also

alternatively grown at 4 °C for 2 hours. After the incubation period, the supernatant in each well was removed, cells were washed three times with PBS (to remove all extracellular nonadherent bacteria) and used for assessing the number of CFU/ml. Washed cells were then detached and collected from each well through the addition of TrypLE Express Enzyme (ThermoFisher Scientific). After treatment with 0.1% (v/v) Triton X-100 (Sigma-Aldrich Co. LLC, St. Louis, United States of America) in PBS to assure lysis of eukaryotic cells, internalized and adherent bacteria were serial diluted and plated on THA to determine CFU/ml [(Adh + int)$_{value}$]. The exact same procedure was performed in human cell free wells in order to obtain procedural negative control values [(Adh + Int)$_{ctrl}$]. The number of total bacteria (final CFU/ml) was estimated using the sum of CFUs counted for the human infected cells (Adh + Int)$_{value}$ and the CFUs of supernatants. *In vitro* assays were performed using at least three biological replicates and two technical replicates per assay.

Percentage of adherent and internalized Streptococci was calculated with the Equation **(4.1)**.

$$\% \ Adhered \ and \ Internalized \ Streptococci = \frac{(Adh+Int)value - (Adh+Int)ctrl}{\Delta f} \ x \ 100 \qquad (\mathbf{4.1})$$

(Adh + Int) value: average CFUs counted for the human infected cells (adhered and internalized); (Adh + Int) ctrl: average CFUs obtained in wells without human cells; Δ*f*: Total CFUs ((Adh+Int) value + average CFUs of supernatants) - number of initial CFUs.

4.2.7. Fluorescence microscopy

For fluorescence microscopy analysis, pelleted bacteria were resuspended in THB supplemented with Hoechst 33258 (LifeTechnologies) to a final concentration of 2 μg/mL, incubated at 37 °C for 45 min, washed with PBS and resuspended in DMEM. A549 cells grown in 24-well plates were washed 3 times with PBS and bacterial cells placed over the human cells. After 2 h and 4 h of incubation at 37 °C or at 4 °C, 5 % (v/v) CO_2 and 99 % (v/v) relative humidity, cells were fixed with 2 % (w/v) paraformaldehyde for 20 min. at RT, permeabilized with 0.1 % (v/v) Triton X-100 for 5 min and stained with AlexaFluor 488 Phalloidin (LifeTechnologies) according to the manufacturer's instructions. Samples were observed in a Ti-U Eclipse inverted microscope (Nikon, Tokyo, Japan) with DAPI and FITC fluorescence filter cubes (Nikon)

(excitation filter of 340-380 nm and barrier filter at 435-485 nm for DAPI fluorescence filter cube and excitation filter of 465-495 nm and barrier filter at 515-555 nm for FITC fluorescence filter cube). Images were acquired using NIS Elements Basic software (Nikon).

4.2.8. *In vivo* assays

For the *in vivo* analysis, SDSD isolates VSD9, VSD13, VSD21, VSD23, and VSD24 were used. *S. pyogenes* GAP58 was used as a positive control. The *in vivo* animal model used was *Danio rerio* (zebrafish), wild-type, obtained from national suppliers (Aquaplante, Lisbon, Portugal) and housed at the FCT/UNL fish facilities following the acclimation and experimental conditions described previously (Diniz *et al.*, 2015). SDSD isolates were grown at 37 °C until reach a standardized optical density at 600 nm (OD$_{600}$) of 0.3–0.4 in TSB-0.5YE. For each isolate, an aliquot of 1 ml of cell suspension was collected and washed three times with fresh TSB-0.5YE. A 10 µl of the suspension (1x10^7 bacteria (per isolate)) was injected intraperitoneally in a group of 10 wild-type zebrafish using a Nanofill micro-syringe (World Precision Instruments, USA). Control groups were injected with 10 µl of TSB-0.5YE growth medium. Zebrafish groups were then maintained separately in aquaria at a constant temperature of 28 °C, using a heated water bath circulator (Haake D1, Haake Messtecknik GmbH Co., Karlsruhe, Germany), without being fed during the 15 days of experiment. Three zebrafish per group were used for histological analysis and were processed while alive (see below). The remaining seven zebrafish per group were used for CFUs assessment after death. To accomplished that, the caudal peduncle (a slice of muscle) and the intraperitoneal region (viscera) were separated, homogenized in PBS (500 µl), and platted (20 µl) in Columbia Blood Agar Base containing 5% sheep blood (Oxoid, Basingstoke, United Kingdom) supplemented with the specific antibiotics. The antibiotics used for supplementation of the medium were selected based on the resistance of the strains in analysis, SDSD VSD13 and VSD21 were grown in medium supplemented with erythromycin (50 µg/ml) (Sigma-Aldrich Missouri, EUA), SDSD VSD9, VSD21, VSD24 and *S. pyogenes* GAP58 were grown in medium supplemented with tetracycline (10 µg/ml) (Sigma-Aldrich), SDSD VSD24 was grown in medium supplemented with gentamicin (2 µg/ml) (Sigma-Aldrich). Fifteen days after injection, the remaining zebrafish were euthanized and processed as described previously (Diniz *et al.*, 2015). The relative CFUs load of each organ was categorized as follows: **0**, no colonies; **1**, 1 to 50 colonies; **2**, 51 to 200 colonies; **3**, 201 to

500 colonies; **4**, 500–700 colonies, **5**, >701 colonies. Four independent experiments were performed for each group of zebrafish (a total of 40 animals per group).

4.2.9. Histological analysis

Whole-animals were fixed by complete immersion in Davidson's solution (formol acetic acid-alcohol) for 36 h (assisted by injection of the fixative intraperitoneally), washed, dehydrated in a graded series of ethanol, infiltrated with xylenes and embedded in paraplast. Sections (5–7 μm thick) were produced longitudinally along the entire body plan to permit a full histopathological screening, with emphasis on the abdominal cavity. Sections were obtained using a Jung RM 2035 microtome (Leica Microsystems). Following deparaffination and rehydration, sections were stained with Hematoxylin (Harris') and counterstained with Alcoholic Eosin Y (HandE), dehydrated, cleared with xylenes, and mounted with DPX medium. Observations were made with a DMLB model microscope equipped with a DFC 480 digital camera (LeicaMicrosystems) (Costa, 2018).

4.2.10. Identification of the isolates recovered from Zebrafish

The identification of the SDSD and *S. pyogenes* strains was performed by traditional phenotypic tests based on hemolysis in blood agar plates, Lancefield serologic groups using the SLIDEX Strepto Plus (Biomérieux, France) as previously described (Rato *et al.*, 2010, 2011, 2013). PCR amplification of the *brpA-like* gene was performed as complementary method for identification of the SDSD isolates. Genomic DNA was obtained according to Section 2.2.1 of Chapter 2. The genome sequence of SDSE strain of Lancefield's group A antigen AC-2713 (Genebank accession number NC_019042) was used to design specific primers (Supplementary Table S2, Appendix I). The PCR reactions were performed in a thermocycler (Biometra, Göttingen, Germany) in a final volume of 25 μL containing: 1 μL of bacterial genomic DNA (0.01 μg), PCR buffer, 2.5 mM of $MgCl_2$, 0.4 mM dNTPs, 1U Taq polymerase (NZYTech, Lisbon, Portugal) and 1 μM of each primer (Invitrogen). The PCR conditions consisted of an initial denaturation cycle (95 °C for 5 min) followed by 35 cycles of denaturation (95 °C for 30 s), annealing (42 °C for 30 s), and extension (72 °C for 80 s). A final extension at 72 °C for 7 min was also performed. Milli-Q water was used as a negative control in each PCR reaction. The PCR products were analyzed by electrophoresis on 1% (w/v) agarose gel mixed with 5 μL (5 μg/100 mL) of Green Safe Premium (NZYTech). The PCR product

(5 µL) was mixed with NzyDNA loading dye (1 µL, NZYTech) and loaded into the agarose slot (Sigma-Aldrich Missouri, USA). TAE buffer (Tris-Acetate-EDTA, pH 8.0) was used as a running buffer. DNA was visualized by UV light and photographed with a digital capture system (BioRad, California, USA). The 100 bp molecular weight marker Ladder III (NZYTech) was used to estimate DNA fragment size.

The resulting *brpA-like* amplicon, with 1.27 kb, is only amplified in *Streptococcus dysgalactiae*. The *S. pyogenes* isolates was confirmed by sequencing of 16S rRNA as described previously (Takahashi *et al.*, 1997).

4.2.11. Statistical analysis

GraphPad Prism version 7.0 was used for statistical analysis. Data analyses of *in vitro* assays were performed using Student's *t* test method. Survival curves of Zebrafish infection assay were analyzed by statistical multiple comparisons performed using Holm-Sidak method. Statistical significance was considered when $p < .05$.

4.3.   Results and Discussion

4.3.1.   Adhesins screening

The SDSD strains were tested for the presence of Adhesins (*fbpA* and *znuA*) by PCR. *S. pyogenes* GAP58, GAP90, and GAP447 isolates and SDSE isolates HSM53 and COI289 were use as controls. *fbpA* gene was detected in all the SDSD isolates and SDSE control positive strains while the *znuA* gene was observed only in the SDSE strains (Table 4.1). Analysis of the *fbpA* sequences gene revealed 94%–96% homology between the sequences of the SDSD and SDSE strains. The transcriptional analysis showed that all expected virulence genes studied were expressed in the respective SDSD isolates carrying them.

Table 4.1. Characterization of the bovine SDSD isolates collected and for control SDSE isolates HSME53 and COI289 and control *Streptococcus pyogenes* GAP58, GAP90, and GAP447 isolates

Isolate code	Host	Samples Origin	Clinical	*S. pyogenes* virulence genes	Adhesin genes	Ref.
VSD5	Bovine	Milk from udder	Subclinical mastitis	*sdn sagA*	*fbpA*	(Rato *et al.*, 2013, Rato *et al.*, 2011, Rato *et al.*, 2010)
VSD9	Bovine	Milk from udder	Subclinical mastitis	*sagA*	*fbpA*	
VSD13	Bovine	Milk from udder	Subclinical mastitis	*speC speK speL speM spd1 sagA*	*fbpA*	
VSD21	Bovine	Milk from udder	Clinical mastitis	*sdn sagA*	*fbpA*	This study Chapter 2
VSD23	Bovine	Milk from udder	Clinical mastitis	*sagA*	*fbpA*	
VSD24	Bovine	Milk from udder	Clinical mastitis	*speC speK spd1 sagA*	*fbpA*	
HSM53	Human (adult)	Blood	Invasive infection	-	*fbpA znuA*	(Rato *et al.*, 2013, Rato *et al.*, 2011, Rato *et al.*, 2010)
COI289	Human (adult)	Pharyng	Non-Invasive infection	-	*fbpA znuA*	
GAP58	Human (adult)	Blood	Invasive infection	*speA speB speF speJ smeZ sagA*	n.d.	(Diniz *et al.*, 2015)
GAP90	Human (child)	Blood	Invasive infection	*speC speK speL speM spd1*	n.d.	
GAP447	Human (adult)	Pharingytis	colonization	*speC speK speL speM spd1*	n.d.	

[a]VSD5, VSD9, and VSD13 were collected in 2002–03 and VSD21, VSD23, VSD24 were collected in 2011–13. [b] *speC, speK, speL, speM* (superantigens); *spd1*- DNase; *sdn*-streptodornase (DNase); *fbpA*-Fibronectin-binding protein A *znuA*, high-affinity zinc uptake system protein precursor).

Antimicrobial resistance was assessed using standard international methodologies and breakpoints (Clinical and Laboratory Standards Institute) established for beta-hemolytic streptococci. Accordingly, the analysis of the minimum inhibitory concentrations (MICs) of Erytromicin by serial dilutions revealed that both strains were resistant to high concentrations of erythromycin (Table 4.2). The VSD21 isolate displayed a MIC between 250 µg/ml and 500 µg/ml and VSD13 growth was not inhibited by any of the erythromycin concentrations tested (MIC > 1000 µg/ml). TET resistance phenotype was observed for VSD5, VSD9, VSD21 VSD23, and GAP58 isolates (resistant to more than 16 µg/ml) (Table 4.2). GEN resistance phenotype was observed for the three isolates VSD21, VSD23, and VSD24 by disk diffusion method (diameter of

inhibition < 11 mm), however, the minimum inhibitory concentration observed was 4 µg/ml for the VSD24 isolate and 2 µg/ml for the VSD21 and VSD23 isolates (Table 4.2).

Table 4.2. Resistance profiles and antibiotic minimal inhibitory concentration

	Resistance phenotype	Minimum inhibitory concentration (µg/mL)		
	(by disc difusion)	TET	GEN	ERY
VSD5	TET	64	2	nd
VSD9	TET	16	2	nd
VSD13	TET + cMLS$_B$	16	2	> 1000
VSD21	TET+ GEN + cMLS$_B$	16	2	250 - 500
VSD23	TET+ GEN	16	2	nd
VSD24	GEN	4	4	nd
GAP58	TET	16	2	nd

In order to further validate our previous results observed in human keratinocytes (Roma-Rodrigues *et al.*, 2016), the *in vitro* interaction/internalization of SDSD isolates in three human cell lines from the respiratory track (a common a niche of colonization/infection of Streptococcus in humans) and the *in vivo* infection potential in zebrafish of the bovine SDSD isolates was analyzed and correlated with the presence of different virulence factors from human pathogens *S. pyogenes* and SDSE strains in the different SDSD isolates genomes (Table 4.1) that could be transferred horizontally within *Streptococcus* species (Rato *et al.*, 2010, 2011).

4.3.2. *In vitro* assays

The interaction of bovine SDSD VSD5, VSD9, VSD13, VSD21, VSD23, and VSD24 was analyzed in human cells derived from a preferred niche of colonization/infection of *S. pyogenes* - the airway system (including pharynx (Detroit 562, pharynx carcinoma), bronchia and trachea (BTEC, primary bronchial/tracheal epithelial cells) and lung (A549, adenocarcinoma human alveolar basal epithelial cells). In the same way invasive human isolates of *S. pyogenes* GAP58 and GAP90 and a colonization human isolate of *S. pyogenes* GAP447 (Table 4.1) were also analyzed in these cells.

Overall, the *in vitro* results suggested that SDSD strains from bovine mastitis isolated in Portugal from both collections can adhere and internalize Detroit 562, A549, and BTEC human cell lines (Figure 4.1).
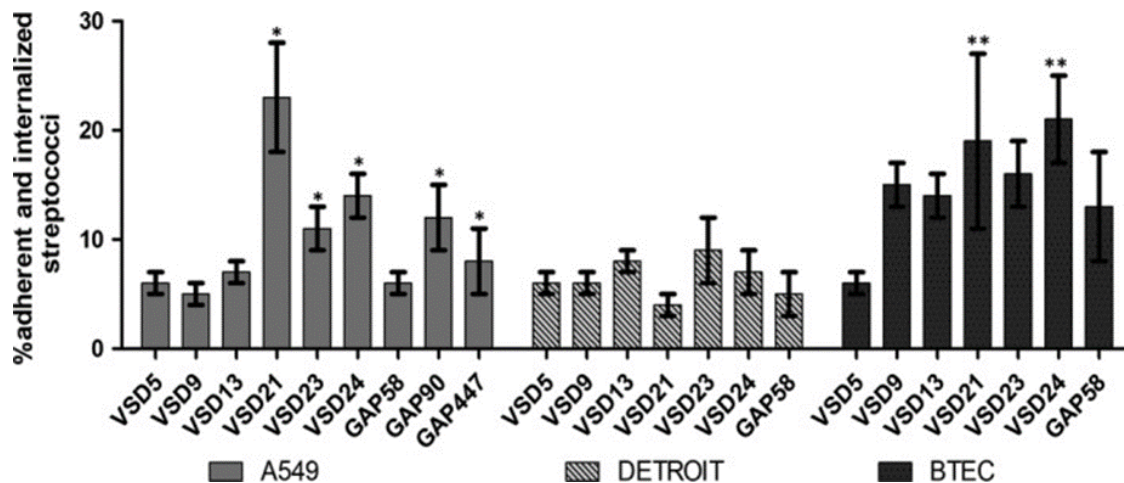
Figure 4.1. Infection potential of bovine SDSD isolates in human airway stem cell lines. Percentage of adherent and internalized VSD5, VSD9, VSD13 VSD21, VSD23, VSD24 and *S. pyogenes* GAP58, GAP90, and GAP447 isolates after the incubation for 2 hours in Detroit 562, A549, and BTEC human cell lines. Represented values are the average value with SEM. *p-value < .005 for results obtained for A549 cells infection of VSD21, VSD23, VSD24 relative to GAP58. **p-value < .05 for results obtained for BTEC infection of VSD5 and VSD24 relative to GAP58.

Previously we have reported that compared to SDSD VSD5, SDSD VSD13 had a higher adherence and internalization potential in human primary keratinocytes (Roma-Rodrigues *et al.*, 2016). This was also observed with airway human cell lines, particularly in primary BTEC (Figure 4.1). Interestingly, except for SDSD VSD21 in Detroit 562 cell line, SDSD isolates from the 2011–13 collection have a higher ability to interact with human airway cells compared to the *S. pyogenes* invasive isolate GAP58 and SDSD isolates from the 2002–03 collection (Figure 4.1). Comparing the results in *S. pyogenes* controls, GAP90 and GAP447 isolates had a significantly higher potential to adhere and colonize A549 cells than *S. pyogenes* GAP58 (Figure 4.1).

Fluorescence microscopy images of A549 cells infected with bovine SDSD VSD9 and SDSD VSD21, as examples, are presented in Figure S1 (Appendix IV). It is possible to observe bacteria co-localized with A549 cells. Bacterial cells seem to be surrounded by actin, which suggests that active transport phenomena may be involved. Indeed, incubation for 2 h of A549 cells with SDSD VSD9 and VSD21 at 4 C showed a marked decrease in the MOI (for VSD9).

No significant correlation between the number of *S. pyogenes* genes and SDSE adhesins present in the genome of the bovine isolates and the capability of the SDSD isolates to interact with human cells was observed (Figure 4.1 and Table 4.1).

The results indicate that there is no correlation between the expression of the analyzed *S. pyogenes* virulence genes or the *fbpA* and *znuA* adhesin genes in the SDSD

isolates and the ability to interact with the airway system human cell lines, suggesting that other mechanisms may be responsible for this ability of SDSD isolates to adhere to and internalize into human cells.

Adherence and invasion of SDSD isolates in epithelial cells has previously documented to occur in mammary cell lines and fish epithelial cell lines cultured *in vitro* (Calvinho, Almeida, and Oliver, 1998; Calvinho and Oliver, 1998). According to Calvinho and Oliver (1998), the involvement of host kinases, intact microfilaments and de novo eukaryotic protein synthesis are required for the internalization process: a process that appeared to occur by a receptor mediated endocytosis mechanism (Calvinho and Oliver, 1998).

4.3.3. Zebrafish infection assays

Since our bovine SDSD isolates (VSD9, VSD13, VSD21, VSD23, and VSD24 (Table 5.1) can infect *in vitro* human cells from the respiratory tract, we questioned if these isolates could infect and trigger an immune system response in other organisms beside the bovine host. For that purpose, the SDSD isolates were inoculated into the well described vertebrate model for the study of infectious diseases, zebrafish (Novoa and Figueras, 2012; Saralahti and Ramet, 2015; Miller and Neely, 2005; Borst *et al.*, 2013; Patterson *et al.*, 2012; Wu *et al.*, 2010; Phelps *et al.*, 2009).

All SDSD isolates were injected intraperitoneally in adult zebrafish. From the total 134 injected zebrafish, 33 zebrafish were injected with sterile TSB, 8 with GAP58 strain, and 93 with the selected SDSD isolates.

The *S. pyogenes* GAP58 (Table 4.1) was used as a positive control since it is an invasive human isolate. Zebrafish injected in the same conditions with TSB medium were used as negative controls. After injection, all isolates (VSD9, VSD13, VSD21, VSD23, VSD24, and GAP58) induced an increased zebrafish mortality compared to the negative control (Figure 4.2). The human isolate *S. pyogenes* GAP58 resulted in an increased mortality compared to SDSD isolates, with 100% mortality after one day postinjection (Figure 4.2). After 5 days of injection with the SDSD isolates, more than 50% of zebrafish had died (Figure 4.3). Zebrafish injected with *S. pyogenes* GAP58 showed the highest mortality, followed by VSD23, VSD13, and VSD21. VSD24 and VSD9 isolates showed the lowest mortality (Figure 4.2). Interestingly, the results of *in vivo* assays agree with the *in vitro* assays with VSD13 (from the first collection) and the SDSD

isolates from the second collection with a higher effect (adherence and internalization and mortality) (Figures 4.1 and 4.2).

Survival of Zebrafish
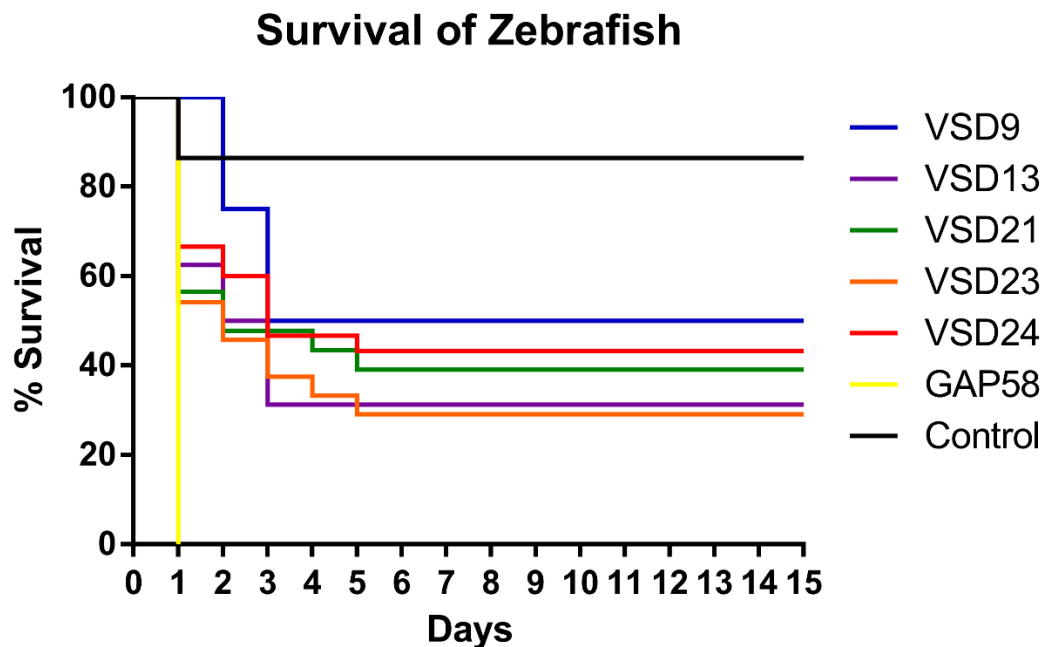
Figure 4.2. Percentage of survival of zebrafish infected with SDSD VSD9 (blue line), VSD13 (purple line), VSD21 (green line), VSD23 (orange line), VSD24 (red line), *S. pyogenes* GAP58 (yellow line), and with growth medium TSB-0.5YE (negative control) (black line). Results are the mean of at least four independent experiments with more than 10 zebrafish in each group and are significantly different with a *p-value* < .001.

Among the zebrafish that died in the first 5 days after bacterial inoculation, focal infection (Figure 4.3B–D) and systemic infection (Figure 4.3E-G) with organ necrosis (data not showed) were observed. For instance, zebrafish infection with VSD13 resulted in both focal and systemic infection (Figure 4.3B, 4.3G1, and 4.3G2, respectively). The remaining inoculated zebrafish that survived until the end of the experiment (15 days) presented no signs of infection (30% with SDSD VSD13 and VSD23, 40% with SDSD VSD21 and 50% with SDSD VSD24 and VSD9).
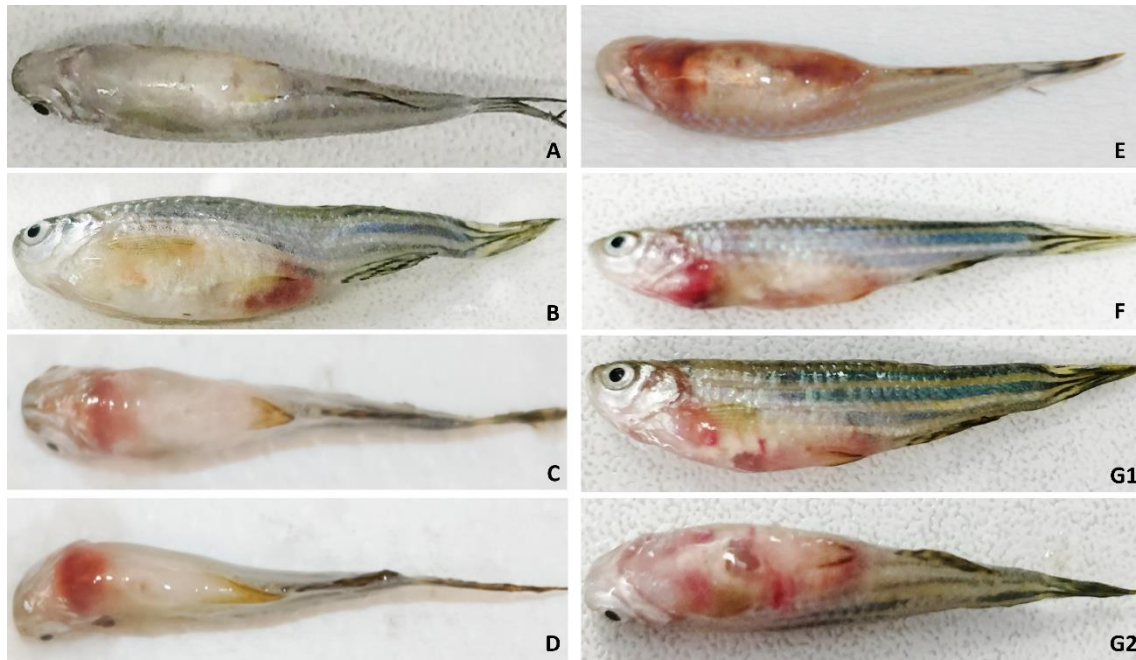
Figure 4.3. Images of injected zebrafish with (A) no sign of infection/disease (control zebrafish that died 24 hours after inoculation), (B-D) Focal infection (zebrafish injected with SDSD VSD13, VSD24, and VSD21 isolates, respectively), and (E), (F) and (G1; G2) Gross pathology (zebrafish injected intraperitoneally with SDSD VSD21, VSD9, and VSD13, respectively). Photos: Cinthia Alves Barroco.

The animals that died during the experience or the ones that were euthanized in the end, were recovered, dissected to allow the analysis of the intraperitoneal region (fish viscera) and caudal peduncle (fish muscle) and the number of CFUs assessed. To accomplished this, the homogenates were plated on Columbia Blood Agar Base with 5% Sheep Blood and supplemented with selective antibiotics based on the isolates antibiotic resistance (Table 5.2; SDSD VSD13 and VSD21 supplemented with erythromycin (50 µg/ml), SDSD VSD9, VSD21, VSD23, and *S. pyogenes* GAP58 supplemented with tetracycline (10 µg/ml), and SDSD VSD24 was grown in medium supplemented with gentamicin (2 µg/ml)) to assess the number of CFUs. The confirmation of the presence of SDSD isolates and GAP58 isolate recovered from homogenates of muscles and viscera was performed by phenotypic tests, based on hemolysis in blood agar plates and Lancefield groups. PCR amplification of the *brpA-like* gene was performed as complementary method for identification of the SDSD isolates. *brpA-like* gene was detected among isolates recovered from muscles and viscera of the death zebrafish injected with SDSD strains. The species identification of *S. pyogenes* isolates was confirmed by sequencing of 16S rRNA.

As observed in Figure 4.4A the bacterial load recovered from the muscles was lower than the bacterial load recovered from the viscera. Interestingly, TET-resistant,

GEN-resistant and ERY-resistant mixed cultures (α and β hemolytic) were recovered from both viscera and muscle of zebrafish that died during the experiment (Figure 5.4B and 5.4C). The microbiological analysis also allowed to detect the presence of α-hemolytic SDSD isolates in the viscera (33%) and muscles (5.9%) of the injected zebrafish that were euthanized after 15 days, suggesting a possible colonization ability of the bovine SDSD isolates in these fish.
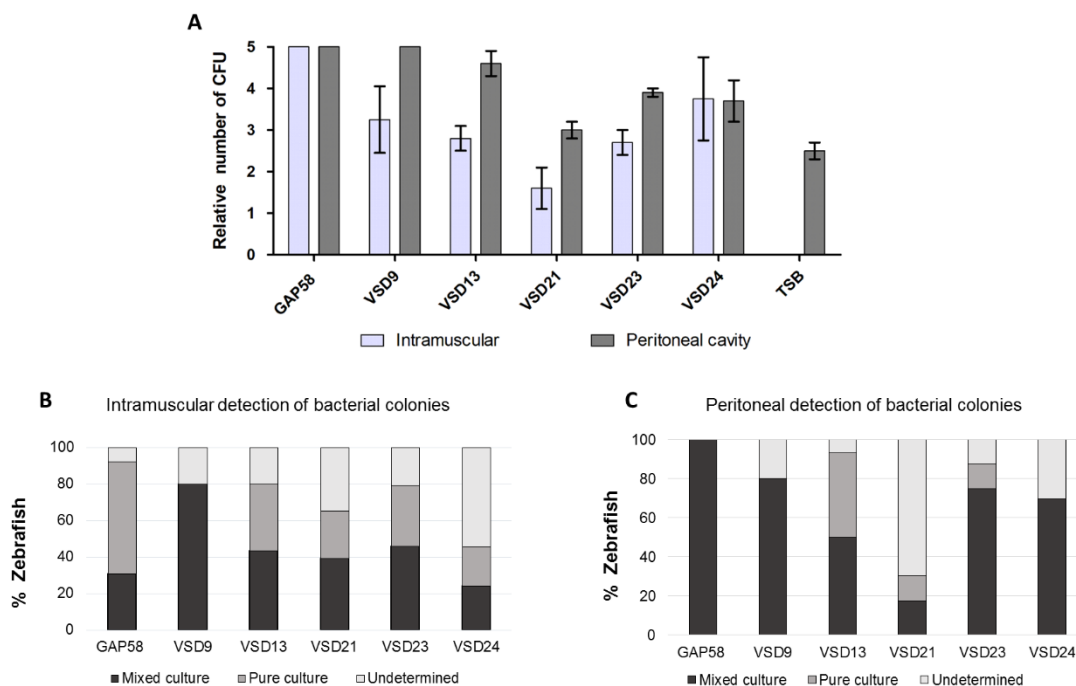
Figure 4.4. (A) Relative number of CFUs in intramuscular and peritoneal region of zebrafish inoculated with SDSD isolates (VSD13, VSD9, VSD21, VSD23, and VSD24) or *S. pyogenes* GAP58. For control purposes, zebrafish were inoculated with 10 µl of TSB-0.5YE. The relative CFUs in both anatomic regions were scored as follows: 0, no colonies; 1: 1 to 50 colonies; 2: 51 to 200 colonies; 3: 201 to 500 colonies; 4: > 500 colonies. (B) Percentage of zebrafish that died before 15 days of experiment with mixed and pure colonies in the intramuscular region. (C) Percentage of zebrafish that died before 15 days of experiment with mixed and pure colonies in the peritoneal region. Pure culture: containing colonies of the respective SDSD isolate. Mixed culture: contains colonies from more than one type of bacteria.

The presence of mixed cultures in the muscle suggests that a systemic infection might have occurred, and animal death permitted the spread of other bacteria to this tissue. This can be explained by the presence of and β-hemolytic gut bacteria such as *Pseudomonas aeruginosa*, a commensal organism that can cause opportunistic infections in zebrafish (Cantas, Sorby, Alestrom, and Sorum, 2012).
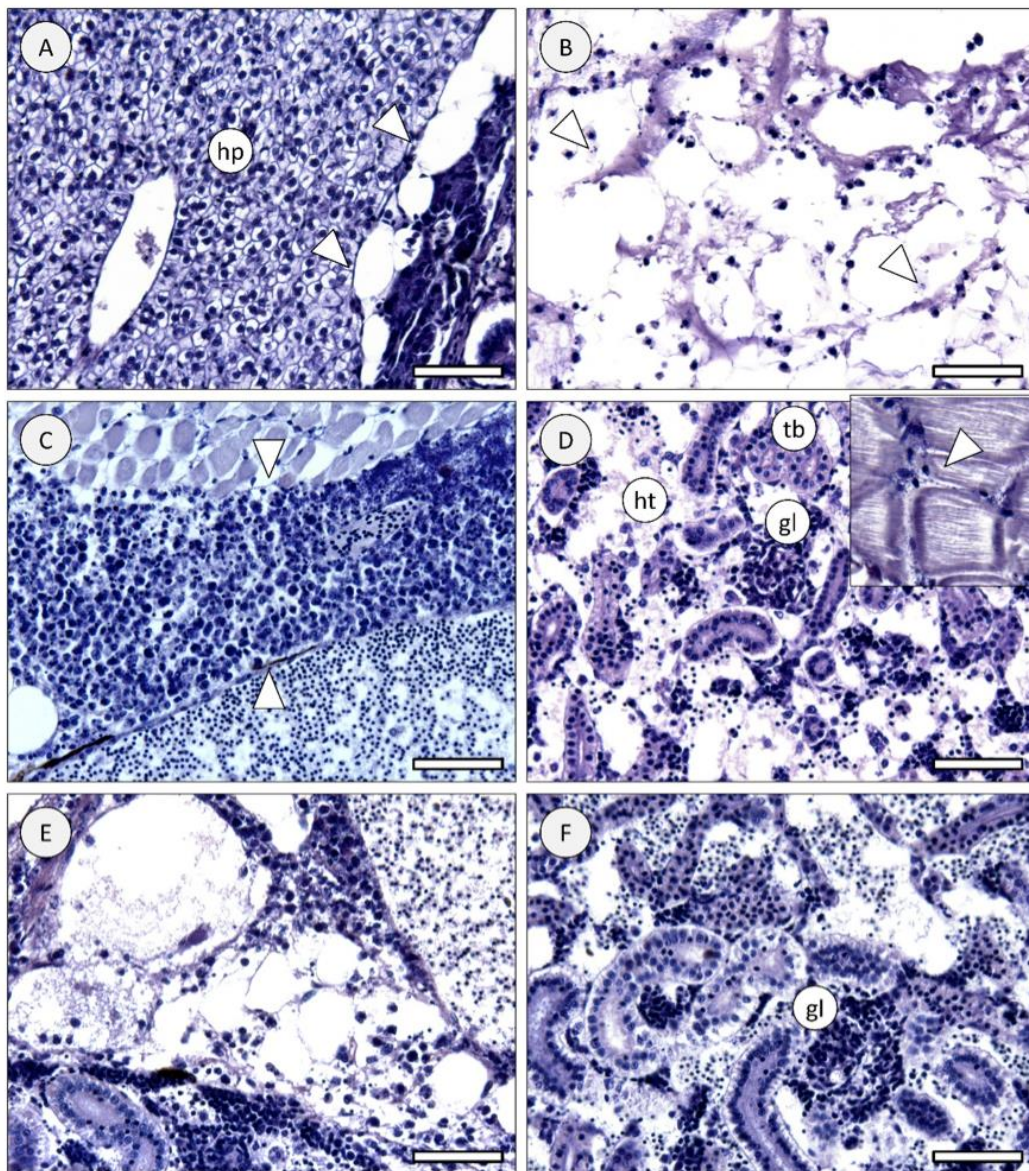
Figure 4.5. Zebrafish histology (Davidson, HandE). (A) Exemplificative section across the abdominal cavity of a control animal, highlighting hepatic tissue (hp) and interorgan adipose tissue (arrowheads), both devoid of any signs of infection or other pathological features. (B) Section of an animal inoculated with the GAP58 strain, exhibiting severe infection in the interorgan adipose tissue, leading to tissue liquefaction. Cocci can be seen in small clumps of chains, most of which inside the remnants of macrophages (arrowheads). Note that most of the adipose material has been washed-off during sample processing, leading to potential under evaluation of infection. (C) Massive exudate holding defense cells and bacteria (between arrowheads) in the abdomen of a fish inoculated with the VSD23 strain. The alteration is formed between skeletal muscle and major visceral blood vessel. (D) Severely infected body (trunk) kidney of a zebrafish injected with VSD24 strain. The hematopoietic tissue (ht) shows liquefying necrosis, cocci and macrophage aggregates. Kidney tubules (tb) were obviously less affected, but glomeruli (gl) were severely infected as well. *Inset*: Cocci between fascicles of skeletal muscle, with leukocytes infiltrating adjacently. (E) Section across the abdominal cavity of a fish inoculated with the VSD21 strain, showing severe infection in the interorgan adipose tissue and adjacent kidney. (f) Section of a zebrafish treated with the same strain as previous, revealing acute kidney infection affecting hematopoietic tissue and glomeruli, similarly to panel D. Scale bars: 50 μm.

The histological evidence suggested that the tested isolates of bacteria can infect wild-type strains of the zebrafish model and elicit acute and potentially lethal infection, despite the lack of significant evidence for dissemination via blood stream. The effects are consistent between isolates, with the possibility that VSD21 causes the most adverse consequences. The immune system of fish was activated in all cases, with emphasis of massive inflammatory response. Even though the maturation and recruitment of B-cells in zebrafish remains elusive, the severity of infection in kidney, where B-cells are mostly produced in this organism (Trede *et al.*, 2004), likely hindered the deployment of adaptive immune response. The dissemination of infection was piecemeal in the abdominal cavity, from the interorgan space to the surface of visceral organs. However, the kidney was the most rapidly and most severely affected organ in all cases. This led to seemingly little compromised hepatic function under the present circumstances of assessment, where other main organs exhibited early failure due to infection, with emphasis on kidney, leading to death. Most of immunity-related studies with the zebrafish model involving infection has been performed on larval organisms. The current results are accordant with recent studies with the adult model to address *Mycobacterium* inoculation and development of novel vaccines (Oksanen *et al.*, 2013) with respect to efficiency as a model but the present work revealed that bovine SDSD infects primarily B-cell forming tissue, thus hindering adaptive immune responses.

Our results show the ability of bovine SDSD isolates to cause infections in zebrafish. This agrees with previous reports had already shown that SDSD isolates can cause disease in fish (Abdelsalam *et al.*, 2013). These observations may indicate that bovine SDSD strains may have a broader spectrum of hosts than anticipated.

4.4. Conclusion

Bovines SDSD isolates were found to adhere to and internalize into several human cells and to interact *in vivo* with the wild-type, adult, zebrafish model (i.e., with uncompromised immunity), this capability seems to be isolate-specific and independent of the *S. pyogenes* virulence gene content and the tested adhesins *fbpA* and *znuA*. The findings show that the zebrafish is suitable model to study bacterial pathogens, as it can activate the innate immune system and suffer adverse effects, albeit with differences between strains, which make it an appealing model to study virulence and inflammation. Altogether, the results obtained with the bovine SDSD isolates studied

confirm that this subspecies interact with human culture cells *in vitro* and *in vivo* can infect the zebrafish model with immune system response. Although the data suggest that these SDSD isolates may have different host preferences, is possible to conclude that SDSD strains are able to infect other hosts than their original one, the cow, and may have a potential zoonotic capability.

Author Contributions

IS-S and ARF contributed to the idea or design of the research. CA-B contributed to the all-experimental work, performed the statistical analysis and manuscript writing. CR-R and LR contributed to maintenance of human cell lines. CA-B and JC contributed to the virulence genes screening. MD and CA-B contributed to *in vivo* assays. PMC and CA-B contributed to histological analysis. The author of this thesis opted for reproduction of the resulting scientific paper, thus apologizing for any repeated content in different contexts of the document.

Funding

Chapter 5 - Infection of human keratinocytes by bovine *Streptococcus dysgalactiae* subsp. *dysgalactiae:* mechanisms of action

Alves-Barroco, C., Brás, C., Roma-Rodrigues, C., Costa, M., Fortunato, E., Diniz, M., Alves de Matos, A.P., Baptista, P.V., and Fernandes, A.R.

Abstract

Keratinocytes have a major role in host defense, providing a physical and immunological barrier against pathogenic bacteria. Bovine SDSD isolates were found to adhere and internalize to human keratinocytes (HEK), but the mechanism is unclear. This study investigated the infection mechanisms of bovine SDSD VSD13 isolate in HEK. An invasive human isolate *S. pyogenes* GAP58 collected from a patient's blood was also studied for comparative analysis. The adherence and internalization of bovine SDSD in HEK was analyzed by confocal laser scanning microscopy (CLSM), Transmission electron microscopy (TEM), and scanning electron microscopy (SEM). The results suggested that the internalization process for SDSD isolate (VSD13) begins with changes in the plasma membrane by cytoskeletal rearrangement, providing the internalization of VSD13 into HEK endocytic vesicles. Further assessment of the internalization mechanism using specific inhibitors for different endocytic pathways, indicated that bovine SDSD isolates, and *S. pyogenes* strain activate different uptake pathways, namely macropinocytosis and clathrin-mediated endocytosis, respectively.

Proteomic analysis allowed us to postulate that the interaction of bovine SDSD VSD13 with HEK triggers similar responses as the *S. pyogenes* invasive strain, namely, by interfering in HEK metabolism (glycolysis) and proliferation, stress response and protein folding.

Moreover, when we incubated HEK with supernatants from bacterial growth mitochondrial membrane potential alterations and the induction of reactive oxygen species (ROS) were observed. In summary, the present study provides for the first-time insight into mechanisms involved in bovine SDSD and HEK interactions, opening an avenue for further investigations towards the complete understanding of the molecular mechanisms of infection of bovine SDSD.

5.1.   Introduction

SDSD is considered an animal pathogen and the main cause of bovine mastitis (Alves-Barroco *et al.*, 2021). Despite the high impact of SDSD in dairy production, little is known about the uptake and infection mechanisms of SDSD in mammary epithelial cells. The knowledge about mechanisms of uptake of SDSD mounts back to the late 90's, when Calvinho *et al.* studied early host-pathogen interactions of SDSD strains isolated from subclinical and clinical cases of mastitis with mammary epithelial cell line MAC-T cells. Results suggested that adherence and internalization of SDSD to MAC-T was an active process that occur via cell surface proteins, possibly mediated by protein tyrosine kinases. Moreover, pre-treatment of MAC-T cells with cytochalasin, fungal metabolites that bind to filamentous (F)-actin and inhibit its polymerization and elongation, inhibited SDSD adherence and internalization (Calvinho and Oliver, 1998a). Further treatment of MAC-T cells with monodansyl cadaverine, a transglutaminase inhibitor usually used to analyze the effect of receptor-mediated endocytosis (Davies *et al.*, 1984), suggested that SDSD uptake by MAC-T cells occur via a receptor-mediated endocytosis mechanism (Calvinho and Oliver, 1998a).

In the last years, the association of SDSD with human infections such as upper limb cellulitis in a woman in contact with raw fish (Koh *et al.*, 2009), lower limb cellulitis (Chennapragada *et al.*, 2018), and a case of septic shock in 45-year-old who presented initially with features of upper limb cellulitis has been reported (Nathan *et al.*, 2021).

Cellulitis is a common bacterial epidermis infection, and the estimated mortality is 0.5%. Cellulitis-related *Streptococcus pyogenes* cause keratinocyte death (Regnier *et al.*, 2016). Keratinocytes are present in the four layers of the epidermis and constitute the first defense line against microbial infection (Wickersham *et al.*, 2017). Keratinocytes are recognized as an important constituent of the immune system. They can act as pro-inflammatory signal transducers. The expression of pro-inflammatory signals can be induced by various stimuli, including microbial virulence factors and lesions (Jiang *et al.*, 2020).

We previously reported for the first time that bovine SDSD isolates are capable to adhere and internalize human keratinocytes cells (HEK) (Roma-Rodrigues *et al.*, 2016) and niches of colonization/infection of *S. pyogenes* from the respiratory track: Detroit 562, BTEC, and A549 (Chapter 4). Notably, the adherence and internalization rates of bovine SDSD isolates in HEK are higher than those of human *S. pyogenes* and SDSD DB49998-05 (GCS-Si) isolates (Roma-Rodrigues *et al.* 2016). The ability of bovine SDSD

isolates to be internalized keratinocytes cells may contribute to persistent infections and lead to deeper tissue infections.

The entry of bacteria into mammal cells involves the utilization of host cell functions to trigger cytoskeletal rearrangement and bacterial uptake (Rohde and Cleary, 2016). Therefore, to understand bacterial internalization, the role of components and functions of the host cell need to be delineated. This study investigated the mechanism involved in the adherence and internalization of bovine SDSD into HEK and proteomic analysis was used to further explore the infection mechanisms of bovine SDSD into HEK.

5.2. Materials and Methods

5.2.1. Bacterial isolates

The previously characterized bovine VSD13 isolate (Rato *et al.*, 2013; Roma-Rodrigues *et al.*, 2015) was used to investigate the modulation of the inflammatory response in human keratinocytes cells. *S. pyogenes* GAP58 was used as human infection control (Pires *et al.*, 2012; Roma-Rodrigues *et al.*, 2015).

5.2.2. Human cell lines and culture conditions

Human primary dermal keratinocytes (HEK, ATCC-PCS-200-010) were purchased in ATCC (Manassas, VA, USA) and maintained according to manufacturer's instructions in keratinocyte growth media (ATCC PCS-200-040). Cells were maintained and incubated at 37 ℃, 5% (v/v) CO_2 and 99% (v/v) relative humidity. For infection assays, cells were seeded in a 96-well culture plate at a density of 3 x 10^4 cells/well and incubated for 24 h at 37 ℃, 5 % (v/v) CO_2, and 99 % (v/v) relative humidity. For confocal microscopy analysis, 1 x 10^5 cells were placed over a Polylysine treated microscope slide and incubated for 24 h at 37 ℃, 5 % (v/v) CO_2 and 99 % (v/v) humidity.

5.2.3. Adherence and internalization of the bovine SDSD to HEK cells

Confocal laser scanning microscopy

The CLSM experiments were performed as previously described (Roma-Rodrigues *et al.*, 2015). Briefly, 1 x 10^5 HEK were seeded in polylisine treated microscope slides, washed three times with phosphate buffer saline (PBS) and incubated with bacterial cells previously treated for 45 min with 0.2 mg/mL Hoechst 33258 (ThermoFisher Scientific, Waltham, MA, USA). Untreated HEK incubated with Hoechst 33258 were used as control samples. After 0 h, 2 h, 4 h and 6 h of incubation (at 37 ℃, 5%

(v/v) CO_2 and 99% (v/v) relative humidity), cells were incubated with 2% (w/v) paraformaldehyde (Sigma Aldrich, St Louis, MO, USA), followed by 0.1% (v/v) Triton X-100 (Sigma Aldrich) and stained with AlexaFluor 488 Phalloidin (ThermoFisher Scientific). Cells were visualized in a CLSM (Carl Zeiss, LSM 700) and data analyzed with the respective software (ZEN Black, 2011).

Scanning electron microscopy (SEM)

The adhesion assays were based on our previously described protocol (Roma-Rodrigues *et al.*, 2016), with minor modifications. Briefly, bacteria were grown at 37ºC in Todd Hewitt broth (THB) supplemented with 0.5% (w/v) yeast extract until the middle of the exponential phase. The infection was started by adding 10^6 bacterial cells resuspended in Dulbecco's Modified Eagle's Medium (DMEM) supplemented with 10% (v/v) Foetal Bovine Serum (FBS) to 10^4 HEK. After 2 h of incubation (37 ºC, 5% (v/v) CO_2 and 99% (v/v) relative humidity), cell monolayers were washed with Phosphate Buffer saline (PBS) to remove unbound bacteria and then fixed with 2% glutaraldehyde solution in PBS for 2 h at room temperature. Cells were then washed three times with PBS, post-fixed with osmium tetroxide for 1 h at 4 ºC, processed as previously described (García-Pérez *et al.*, 2003) and observed by SEM (JEOL JSM-5400).

Transmission electron microscopy (TEM)

The internalization and adhesion bovine SDSD assay were performed as previously described (Roma-Rodrigues *et al.*, 2016). After 2h of infection, HEK were washed four times with PBS to remove SDSD cells adhered and not internalized. Cells were fixed with 2% glutaraldehyde solution in 0.1 M PBS for 2 h (at room temperature), washed three times with PBS and post-fixed with osmium tetroxide for 1 h (at 4 ºC). The osmium tetroxide was removed with PBS, and then cells were processed following previously described protocols (Rodrigo *et al.*, 2021). The final sections obtained were analyzed using TEM (JEOL 100-SX model) operated at 80 kV.

5.2.4. Inhibition of *Streptococcus* internalization into human keratinocytes

To understand the mechanisms involved in SDSD VSD13 internalization (a comparison with *S. pyogenes* GAP58 strain was also performed), HEK cells were treated with different combinations of four endocytic pathways inhibitors, namely, Chlorpromazine hydrochloride (30 µM) (Sigma, MW 355.3), Filipin III (5 µM) (Sigma, MW 654.8), Amiloride (12,5 µM) (Sigma, MW 266.1) and Wortmannin (0,3 µM) (Sigma, W1628). The concentrations of the four endocytic inhibitors used were based on previous

studies (Pooja *et al.*, 2015; Sousa De Almeida *et al.*, 2021). In Figure 5.1 we show the endocytic pathways of mammalian cells and the respective target of each inhibitor (red cross).
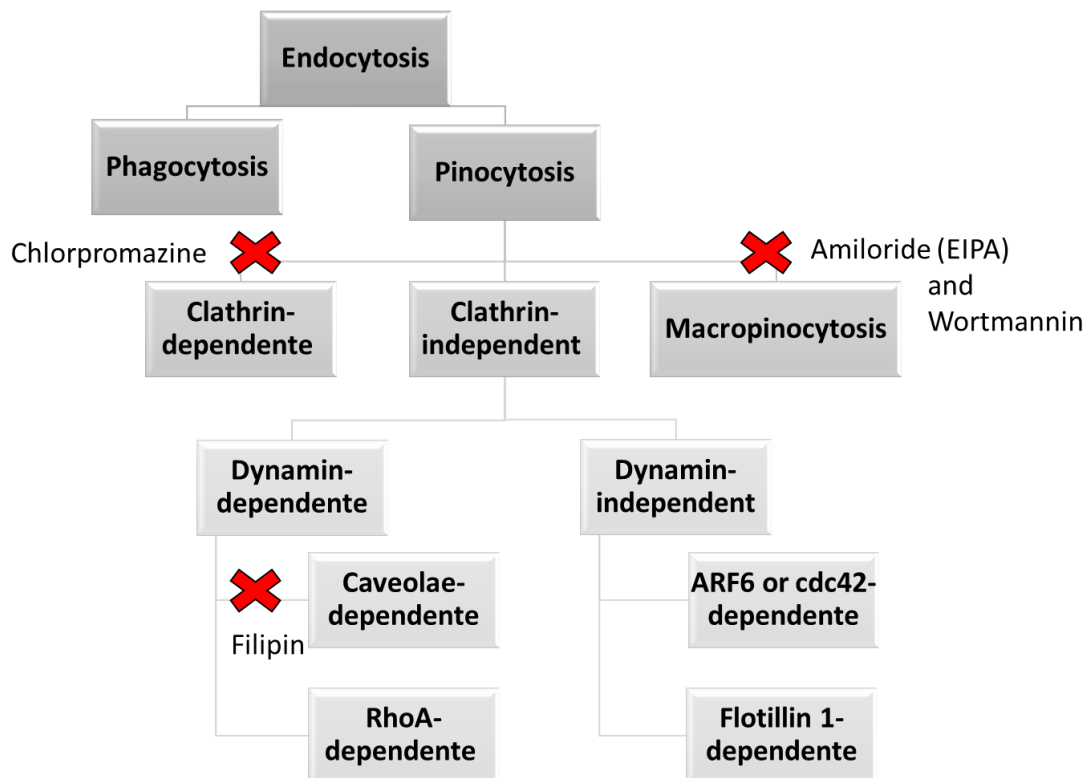
Figure 5.1. Classification of the endocytic mechanisms in mammalian cells (Miaczynska and Stenmark, 2008). The red symbol corresponds to the pathways inhibited by the respective endocytosis inhibitors (Koivusalo *et al.*, 2010; Dutta and Donaldson, 2012; Lin *et al.*, 2018; Sousa De Almeida *et al.*, 2021).

The internalization assays were based on our previously described protocols (Roma-Rodrigues *et al.*, 2015) with minor modifications. Briefly, 1 x 10^5 HEK were seeded in a 96-well culture plate at a density of 3 x 10^4 cells/well. Media in each well was discarded, and cells were washed with PBS. Where detailed in the text, HEK cells were pre-treated for 2 h (37 C, 5% CO_2 and 99% (v/v) relative humidity) in the absence or presence of inhibitors, under the following conditions: i) Ctrl; ii) Chlorpromazine; iii) Filipin; iv) Chlorpromazine + Filipin; v) Amiloride; vi) Wortmannin and vii) Amiloride + Wortmannin. GAP58 and SDSD VSD13 isolates were grown at 37 °C in THB until the middle of the exponential phase. The infection was started by adding 10^6 bacterial cells in DMEM to 10^4 Pre-treated HEK cells in the presence or absence of inhibitors (control). After 4 hours of incubation (37 °C, 5% (v/v) CO_2, and 99% (v/v) relative humidity), cell monolayers were washed with PBS to remove unbound bacteria. To obtain the number of internalized bacteria, infected HEK cell monolayers were incubated for 30 minutes

with DMEM or DMEM supplemented with gentamicin 50 µg/mL + lysozyme 20 µg/mL, respectively. HEK were detached from the wells, disrupted with Triton X-100 0.01% (v/v) (Sigma), and the bacterial CFUs were calculated using standard plate counting techniques (Sieuwerts *et al.*, 2008). The absence of inhibitors (Control) was set as 100% of bacteria internalization.

HEK viability was determined using 3-(4,5-dimethylthiazol-2-yl)-5-(3-carboxymethoxyphenyl)-2-(4-sulfophenyl)-2Htetrazolium, inner salt - MTS assay as previously described (Fernandes *et al.*, 2017). HEK were seeded in 96-well plates and grown for 24 h prior to incubation for 6 h in fresh diluted medium with i) filipin; ii) chlorpromazine; iii) chlorpromazine + filipin; iv) amiloride; v) wortmannin and vi) amiloride + wortmannin (37 °C in a 99% humidified atmosphere of 5% (v/v) CO_2). After the incubation period, the culture medium was removed from each well, cells were washed with PBS, and medium containing 10% of MTS reagent was added. The 96 well plate was incubated for 60 min at 37 °C in a 99% humidified atmosphere of 5% v/v) CO_2, and the absorbance was measured directly in a microplate reader at 490 nm (Infinite M200, Tecan, Switzerland). The following equation was applied to calculate the cell viability (%) = 100 x (mean Abs of treatment group /mean Abs of control group, without treatment).

5.2.5. Protein Sample preparation

For proteomic analysis, HEK were seeded in T25 flasks at a density of 4 x 10^5 cells/flask in 5 mL keratinocyte growth media. After 24 h incubation, the medium was replaced by fresh medium containing approximately 2 x 10^7 cells/mL of GAP58 or VSD13 strains. Untreated cells, incubated only with fresh medium, were used for control purposes. After 2 h incubation (37 °C, 5% (v/v) CO_2, 99% (v/v) humidity), medium was removed, cells were washed three times with PBS and detached with a cell scraper in 1 mL cold PBS. After centrifugation at 750 g for 5 min, pelleted cells were solubilized in 30 µL lysis buffer (150 mM NaCl (Sigma Aldrich), 50 mM Tris-HCl pH 8.0 (VWR, Radnor, PA, USA); 5 mM Ethylenediamine tetraacetic acid (EDTA) (VWR), 1x phosphatase inhibitors (PhosSTOP EASYPack, Roche, Basel, Switzerland), 1x protease inhibitors (Complete Protease Inhibitor Cocktail, Roche), 2% (v/v) NP-40 (ThermoFisher Scientific), 0.1% (w/v) Dithiothreitol (DTT) (Amresco, Dallas, TX, USA) and 1 mM Phenylmethylsulfonyl fluoride (PMSF) (Sigma Aldrich)). To promote a complete disruption of the cells, samples were incubated at -80 °C and then submitted to the

following sonication conditions: 1) 10 pulses at 60% intensity for 5 times, 2) 20 pulses at 70% intensity for 10 times, 3) 20 pulses at 80% intensity for 20 times, 4) 20 pulses at 100% intensity for 5 times. Cell debris were removed by centrifugation at 5,000 g for 5min and total protein suspension was treated with 2-D Clean-up Kit (GE Healthcare, Chicago, Il, USA) according to the manufacturer's instructions.

5.2.6. Two-dimensional gel electrophoresis

The pellets obtained after protein sample preparation were solubilized in 125 µL rehydration buffer solution containing 7 M urea (VWR), 2 M thiourea (Merck, Kenilworth, NJ, USA), 4 % (w/v) CHAPS (GE Healthcare), 1x protease inhibitors (Protease inhibitor cocktail, Roche), 1x phosphatase inhibitors (PhosSTOP, Roche), 0.5% (v/v) IPG electrolytes 3-10NL (GE Healthcare), 0.5 % (v/v) Destreak rehydration solution (GE Healthcare), 0.5 % (w/v) DTT (Amresco), 1 mM PMSF (Sigma Aldrich) and traces of bromophenol blue (Merck). Samples were incubated at room temperature, centrifuged at 12 000 g for 15 min, supernatant was transferred to a clean tube and proteins were quantified using Pierce™ 660nm Protein Assay Kit (ThermoFisher Scientific) according to the user's manual. Isoelectric focusing (IEF) was performed using Immobiline Drystrips (IPG strips) with 7 cm long and a non-linear pH gradient 3 - 10 (GE Healthcare) in an EttanIPGphor focusing unit (GE Healthcare). Afterwards, IPG strips were incubated for 15 min with equilibration buffer (50 mM Tris-HCl pH 8.8, 2% (w/v) SDS (GE Healthcare), 6M urea, 30% (v/v) glycerol (VWR) and traces of bromophenol blue) supplemented with 1% (w/v) DTT, followed by another 15 min incubation with equilibration buffer supplemented with 2.5% (w/v) iodoacetamide and then placed in the top of a 10% SDS-polyacrylamide gel. After SDS-PAGE in Tris-Glycine buffer, proteins in 2-DE gels were stained with PhastGel Blue R-350 (GE Healthcare) according to manufacturer's instructions. 2-DE gel images were analyzed with Melanie 7.0 software (GeneBio, Geneva, Switzerland) using a semi-automatic matching analysis. Briefly, controls were matched against the infected human HEK, and each protein spot match was manually checked. To evaluate the fold change, the values corresponding to the percentage of volume of each protein spot were extracted from the software, normalize with the protein quantity used for the IEF and lastly, the normalized values of the samples were divided by the normalized controls. Spots presenting fold changes superior to 1.5 and lower than 0.7 were selected for identification (Sequeira *et al.*, 2021).

5.2.7. MALDI-TOF characterization and in situ analysis

A total of 71 spots were excised from 2D electrophoresis gels for identification by the Mass Spectrometry Unit (UniMS, ITQB/iBET, Oeiras, Portugal) by peptide mass fingerprint. For the protein identification in infected HEK, data was submitted into MASCOT software (Matrix Science©, USA) against two taxonomic restrictions: *Homo sapiens* and *Streptococcus dysgalactiae*, separately, and possible proteins for each spot were displayed by their best match. To distinguish to which species each spot of 2-DE belongs to, a post-analysis was performed by comparing the percentage of identity (% I) of the best matches for each species. Briefly, protein BLAST® (https://blast.ncbi.nlm.nih.gov/) of every match with a given UniProt Accession number was performed and the percentage of identity was noted. If this value was higher in *H. sapiens* than in *S. dysgalactiae* match, the protein was most likely produced by the human cell than from the streptococci bacteria and vice-versa. Once identified, the spots were selected for a network building analysis using online STRING© software (http://string-db.org) and the biological processes with the higher count in gene set and lower false discovery rate were selected for further evaluation.

5.2.8. Western Blot for β-actin quantification

Protein sample preparation was performed as described in section 5.2.5 and (Oliveira *et al.*, 2019). Pelleted cells solubilized in lysis buffer were incubated for at least 2 h, at 80 °C, and subjected to 5 cycles of 2 min 30 sec of ultrasounds with 30 sec intervals on ice between each cycle. Total extracts were then centrifuged (750 g, 5 min), and the supernatant was transferred to a new clean tube. The total amount of protein of each sample was quantified using Pierce 660 nm protein assay kit (Thermo Scientific) according to the manufacturer instructions, and 10 μg protein total was used for the Western-Blot analysis. Protein extracts were first separated in a Sodium Dodecyl Sulfate polyacrylamide gel electrophoresis (SDS-PAGE) using a 10 % (w/v) polyacrylamide gel with acrylamide: bisacrylamide (Merck Millipore) and then transferred onto a 0.45 μm polyvinylidene difluoride (PVDF) membrane (GE Healthcare). After blocking membrane with 5 % (w/v) low fat milk in TBST (50 mM Tris-HCl, pH 7.5, 150 mM NaCl, 0.1 % (w/v) Tween-20), the blots were of incubated for 1 h with a 1:5.000 dilution of β-actin antibody (A5441, Sigma), washed 3 times for 5 min with TBST, incubated for 1 h with 1:3.000 dilution of anti-IgG mouse HRP-linked antibody (7076, Cell Signalling), washed 3 times for 5 min with TBST and treated with WesternBright ECL (Advansta,

USA) for signal acquisition in a Hyperfilm ECL (GE Healthcare). The percentage of area of each protein band was measured using ImageJ2 software. Normalization of data was a two-step process (first using β-actin intensities in each sample for protein loading normalization and after infected HEK (with VSD13 or GAP58) data was normalized to the control sample (non-infected HEK).

5.2.9. Determination of enzymes activity and lipid peroxidation assay

Protein sample preparation was performed as described in section 5.2.5. Additionally, HEK were also incubated with the bacterial growth supernatants. For obtaining bacterial culture supernatants, bacteria were grown in DMEM at 37 °C until the middle of the exponential phase, centrifuged at 5,000 g for 10 min, and then cell-free conditioned medium was prepared by filtering the supernatant through a 0.22 μm pore-size filter. The resulting supernatants were used for stimulation experiments.

After 2 h incubation at 37 °C, 5 % (v/v) CO_2, 99 % (v/v) humidity, the medium was removed, cells were washed three times with PBS, and detached with a cell scraper in 1 mL cold PBS. After centrifugation at 750 g for 5 min, pelleted cells were solubilized in 30 μL lysis buffer (150 mM NaCl, 50 mM Tris-HCl pH 8.0 and 1x protease inhibitors). To promote a complete disruption of the cells, samples were submitted to the following sonication conditions: 1) 10 pulses at 60 % intensity for 5 times, 2) 20 pulses at 70 % intensity for 10 times, 3) 20 pulses at 80 % intensity for 20 times, 4) 20 pulses at 100 % intensity for 5 times. Proteins were quantified using Pierce™ 660nm Protein Assay Kit according to the user's manual (ThermoFisher Scientific).

The enzymatic assay of catalase (CAT) was carried out according to the procedures described previously (Johansson and Håkan Borg, 1988). Activity from a standard bovine catalase solution of 1523.6 U.mL^{-1} (Sigma-Aldric, Germany) was used as a positive control. Formaldehyde standards were used to produce a calibration curve. Catalase activity was calculated considering that one unit of catalase is defined as the amount that will cause the formation of 1.0 nmol of formaldehyde per minute at 25°C. The reaction is followed by a decrease in absorbance as the peroxide is transformed into oxygen and water. To perform this reaction 100 μl of each sample were added to 2900 μl of hydrogen peroxide (50 nmol/L potassium phosphate buffer (pH 7.0), 12.1 mmol/L H_2O_2) using quartz cuvettes. Peroxide consumption was monitored by reading the absorbance every 15 seconds at 540 nm (BIO-RAD, Banchmark, USA). The results were

divided by the total amount of protein in the sample and expressed as micrograms of total protein (nmol min^{-1} µg^{-1}).

Superoxide dismutase (SOD) activity was determined according to the method previously described (Sun *et al.*, 1988). This assay for SOD activity involves inhibition of nitroblue tetrazolium reduction, with xanthine-xanthine oxidase used as a superoxide generator. SOD activity was determined spectrophotometrically (BIO-RAD, Banchmark, USA) in the supernatant at 560 nm. The adapted assay contained, at 25 °C, 50 mM Potassium Phosphate Buffer (pH 7.8), 3 mM EDTA, 3 mM Xantine solution, 0.75 mM NBT (nitroblue tetrazolium), 100 mU XOD (Xanthine Oxidase Solution) and 1 U/µL SOD (Sigma-Aldric, Germany). Superoxide Dismutase from bovine erythrocytes (Sigma-Aldrich, Germany) was used as the standard and positive control. Enzymatic assay results are given in units of SOD activity per milligram of total protein in the sample (U mg^{-1} total protein), where one unit of SOD is defined as the amount of sample causing % inhibition of NBT reduction. SOD activity was calculated using the equation 5.1:

Equation 5.1:

$$\left(\frac{Abs560/ \min negative\ control - Abs560/ \min sample}{Abs560/min\ negative\ control} \right) x\ 100$$

Lipid peroxidation (LPO) assay was adapted from the thiobarbituric acid reactive substances (TBARS) protocol (Uchiyama and Mihara, 1978). Monobasic sodium phosphate buffer (50 mM) was added to each sample, followed by SDS 8.1%, trichloroacetic acid (20%, pH = 3.5), and thiobarbituric acid (1%). Milli-Q grade ultrapure water was added to each mixture, and microtubes were then put in a vortex for 30 s and incubated in boiling water for 10 min. To stop the reaction, microtubes were placed on ice for 10 minutes. Duplicates of the supernatant of each reaction were put into a 96-well microplate, and absorbance was read at 530 nm. To quantify the lipid peroxides, an eight-point calibration curve (0–0.3 M TBARS) was calculated using malondialdehyde-bis(dimethylacetal) (MDA) standards (Merck Millipore, Portugal). The results were divided by the total amount of protein in the sample and expressed as micrograms of total protein (nmol/mg total protein).

5.2.10. Mitochondrial membrane potential

The mitochondrial transmembrane potential was analyzed using the bis(5,6-dichloro-1,3-diethyl-2-benzimidazole) trimethinecyanine iodide (JC-1) dye (Abnova Corporation, Walnut, CA, USA). The infection assays were based on previously described protocols (Roma-Rodrigues *et al.*, 2015) with few modifications. Bacteria were grown at 37ºC in THB until the middle of the exponential phase. The infection was started by adding 10^6 bacterial cells DMEM to 10^4 HEK. After 2 h of incubation at 37 ºC, 5 % (v/v) CO_2, and 99 % (v/v) relative humidity, cell monolayers were washed with PBS to remove unbound bacteria. HEK cells infected and uninfected were then stained with the JC-1 staining solution for 20 min at 37 ºC in the dark. Image acquisition and analysis was done an Eclipse Ti fluorescence microscope, equipped with a DS-QiMc camera (Nikon Instruments, Amsterdam, Netherlands), based on the ratio between green and red fluorescence.

5.2.11. Statistical analysis

GraphPad Prism version 7.0 was used for statistical analysis. Each assay was done with triplicates in three independent experiments. Data analyses of *in vitro* assays were performed using Student's t-test method. Statistical significance was considered when $p < 0.05$.

5.3. Results and Discussion

5.3.1. Analysis of adherence and internalization in HEK

The capability of bovine SDSD isolates to adhere and invade HEK cells was initially demonstrated by Roma-Rodrigues *et al.*, 2016. To investigate the mechanism involved in the internalization, HEK cells monolayers infected with streptococci isolates were analyzed by CLSM, TEM, and SEM.

CLSM images of HEK cells infected with bovine SDSD VSD13 and *S. pyogenes* GAP58 after 2, 4, and 6 h of incubation are presented in Figure 5.2. Confocal images of the time-course of HEK infection with streptococci suggest that SDSD VSD13 is able to adhere and internalize in these human cells (Figure 5.2). Interestingly, the infection process of the SDSD isolate seems to differ from the infection potential of the human invasive strain *S. pyogenes* GAP58 (Figure 5.2). After 6 h of infection, *S. pyogenes* GAP58 bacterial cells are observed growing inside HEK. On the other end, SDSD VSD13 strain seems to have a peak after 4 h of infection where bacterial cells can be observed growing adherent to HEK, as well as inside them. After 6 h of incubation most bacteria are inside the keratinocyte cell.
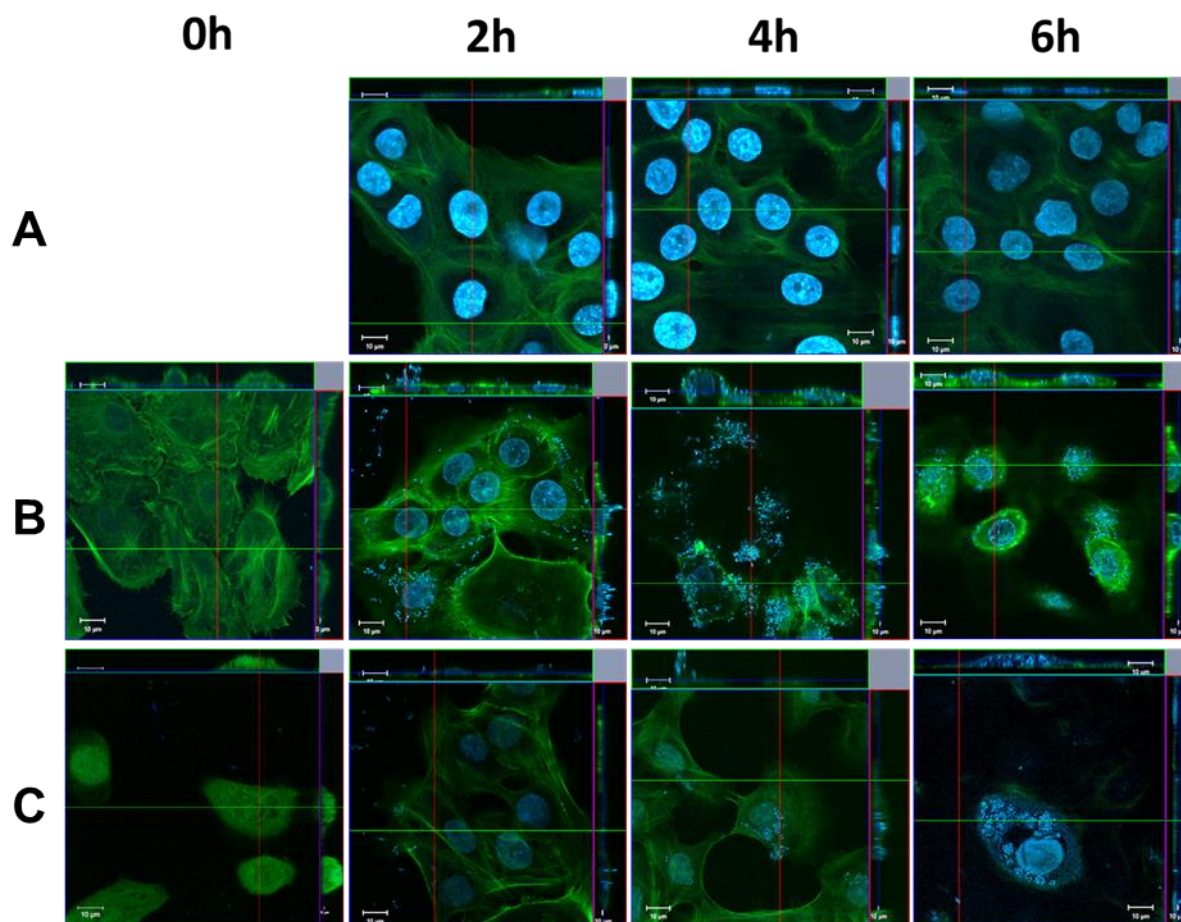
Figure 5.2. Representative CLSM images acquired after 2 h, 4 h and 6 h of incubation of HEK (green, stained with AlexaFluor 488 Phaloidin, LifeTechnologies) with the SDSD VSD13 or *S. pyogenes* GAP58 (blue, stained with Hoechst 33258, LifeTechnologies). A) HEK cells in the absence of bacterial cells; B) HEK cells infected with SDSD VSD13 collected from the milk of bovine udder. C) HEK cells infected with the invasive human isolate *S. pyogenes* GAP58. The centered panel is the X-Y view of the image, corresponding to the blue line in the upper and right panels. The upper panel, with a green outline, is the X-Z cross section of the green line in the centered image. The image at the right, with a red outline, is the Y-Z cross section of the red line in the X-Y view.

SEM micrographs suggested that the internalization process of bovine SDSD VSD13 isolate in HEK initiated with changes in the plasma membrane by cytoskeletal

rearrangement (Figure 5.3). Moreover, by looking at TEM micrographs after 2 h of infection, we can observe the VSD13 isolate in endocytic vesicles (Figure 5.4). However, it is unclear whether SDSD VSD13 isolate survives and replicates within these vesicles, as some morphologic changes in the structure of the SDSD VSD13 cells were observed (Figure 5.4).
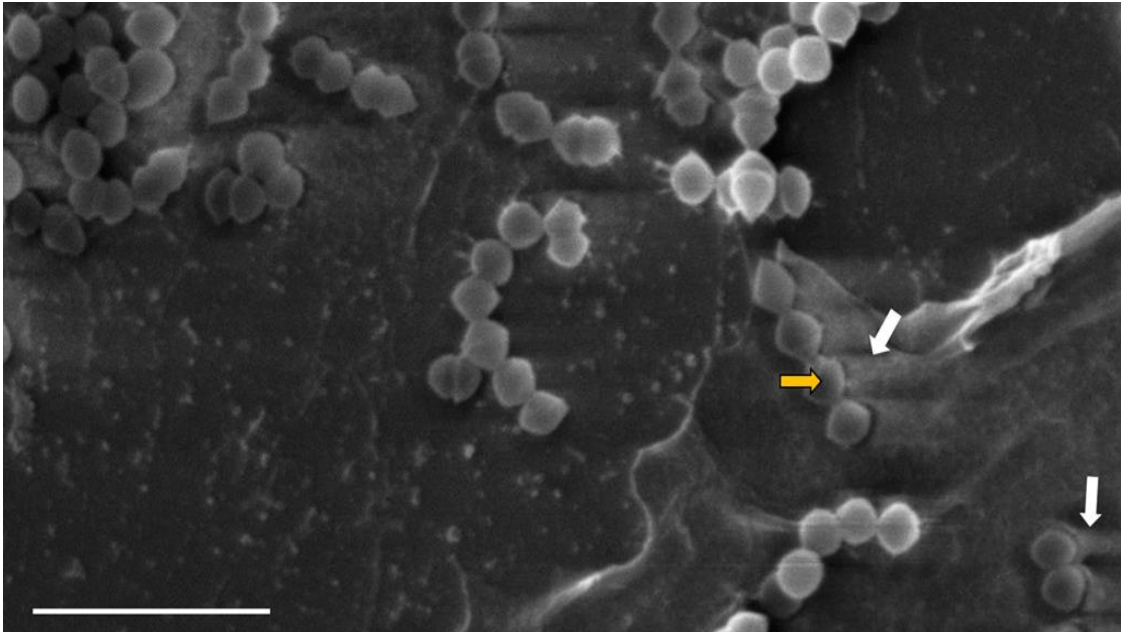
Figure 5.3. SEM micrographs of the interaction of SDSD VSD13 isolate with HEK. Yellow arrows -SDSD VSD13 cells; White arrows - Membrane ruffling surrounding the SDSD VSD13 cells. Scale bar - 4 μm.
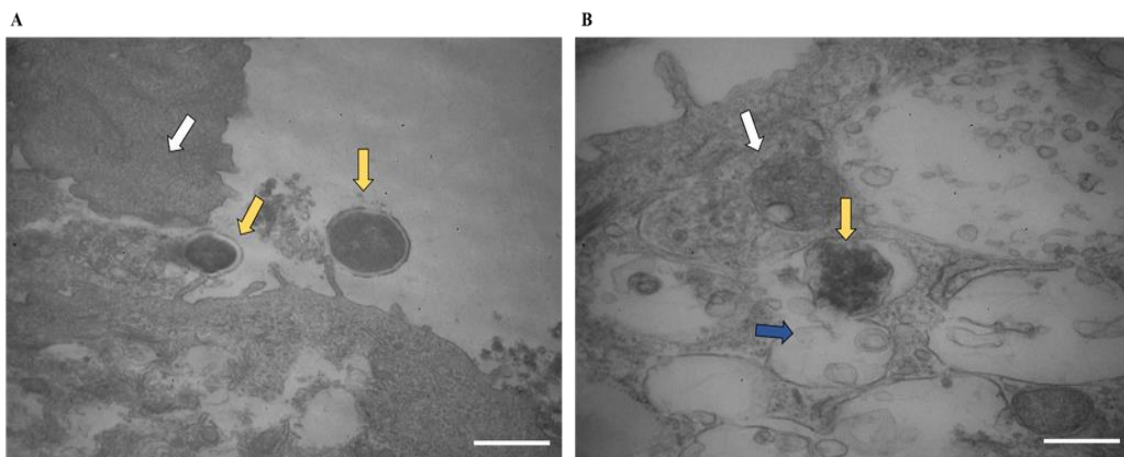
Figure 5.4. TEM micrographs showing the internalization of SDSD VSD13 isolate in HEK. (A) SDSD VSD13 isolate approximating to the apical face of the cell. (B) SDSD VSD13 into HEK´s vesicles. Yellow arrows - SDSD VSD13 cells; white arrows - HEK cells; blue arrow – vesicles; Scale bar – 500 nm.

Together, TEM and SEM data suggest that VSD13 infection of HEK promoted changes that resembles macropinocytosis (Figures 5.3 and 5.4). Macropinocytosis can be defined as a nonselective form of endocytosis. Three main processes have been described in this type of endocytosis: 1. Actin cytoskeleton-driven ruffle formation; 2. closure of the ruffle into a vesicle (macropinosome); 3. Subsequent fusion with components of the endocytic pathway, and formation of the macropino-lysosome, where the enclosed content may be degraded (Canton, 2018). Several pathogenic bacteria exploit the macropinocytosis to invade the host cells and promote your own survival (Swanson and King 2019). Although the mechanism remains unclear, the lysis of macropinosomes by bacteria and viruses contributes to the spread of infections (Chang *et al.*, 2021).

García-Pérez and co-workers observed similar results for the interaction of *Mycobacterium tuberculosis* (MTBC) with human A549 adenocarcinoma cell line (García-Pérez *et al.*, 2003). In this study, the authors showed that MTBC infection of A549 cells induced a reorganization of host cell cytoskeleton (García-Pérez *et al.*, 2003), one of the events that is triggered during macropinocytosis. Their results suggested that the ability to induce this cytoskeletal reorganization depended on bacterial viability since suspensions of non-viable bacteria failed to trigger the process. The cytoskeletal reorganization was also observed by the authors in the presence of bacteria supernatants, suggesting that bacterial secreted products might also promote the membrane ruffling formation (García-Pérez *et al.*, 2003).

5.3.2. Internalization inhibition uptake pathways

To further dissect the process of *S. pyogenes* GAP58 and SDSD VSD13 internalization, the endocytic process in HEK cells was chemically inhibited using chlorpromazine hydrochloride (inhibitor of clathrin-mediated endocytosis), filipin (inhibitor of caveolae-mediated endocytosis), amiloride, and wortmannin (macropinocytosis inhibitors).

The intracellular bacterial CFUs recovered from GAP58 -infected HEK cells were drastically reduced with the increase of chlorpromazine concentration (Figure 5.5A), whereas the VSD13 internalization was inhibited by amiloride and at a higher extent wortmannin (Figure 5.5B).
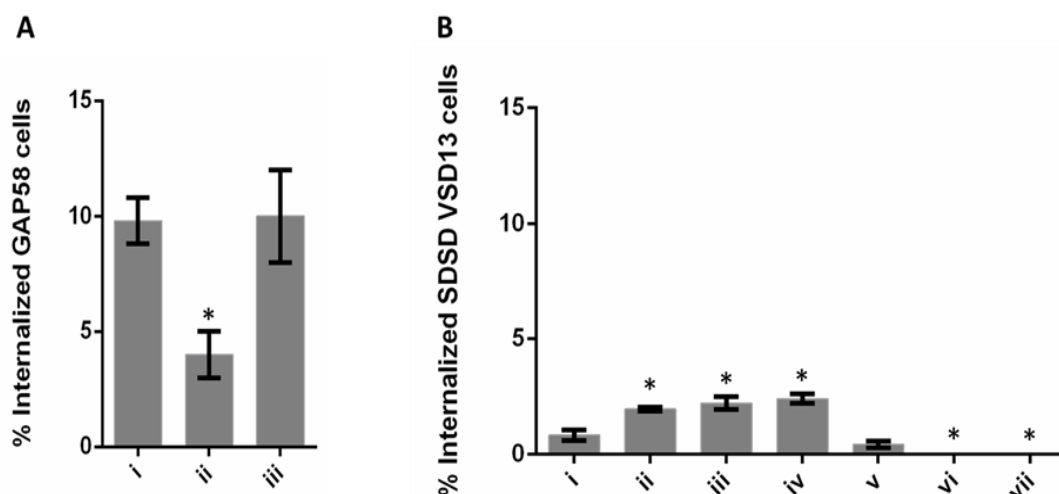
Figure 5.3. Percentage of internalization of **(A)** *S. Pyogenes* GAP58 and **(B)** SDSD VSD13 isolates after the incubation for 4 hours in HEK in the presence or absence of endocytosis inhibitors: i) Ctrl (without any inhibitor); ii) chlorpromazine; iii) filipin; iv) chlorpromazine + filipin; v) amiloride; vi) wortmannin and vii) amiloride + wortmannin. Represented values are the average value with SEM. * value (P) 0.05 was considered statistically significant.

The viability of HEK in the presence of endocytosis inhibitors was also evaluated (Figure S2, Appendix IV). Although the amiloride and wortmannin concentrations used affected the viability of HEK (about 50%), the results showed that the uptake of SDSD VSD13 by HEK was completely inhibited in the presence of wortmannin and in a less extend amiloride. As wortmannin (Phosphoinositide 3-kinases inhibitor) blocks macropinocytosis in human cells (Lin *et al.*, 2018), our data so far points out that SDSD VSD13 internalization into HEK is mediated by macropinocytosis (Figures 5.3 to 5.5).

Interestingly, previous studies have shown that bovine SDSD can adhere and internalize bovine mammary epithelial cells and once internalized, bovine SDSD could survive within the host cell (Almeida and Oliver, 1995; Calvinho and Oliver, 1998a, 1998b; Calvinho *et al.*, 1998). The results of Almeida and Oliver suggested that the internalization of bovine SDSD into mammary epithelial cells was mainly mediated by macropinocytosis since that pre-treatment with cytochalasins B and D caused inhibition of bovine SDSD internalization (Almeida and Oliver, 1995). However, the signaling mechanisms that coordinated these processes were unclear at that time. Several fibronectin-binding proteins that facilitate adherence to human skin cells have also been described in *S. dysgalactiae*, including FnbA, FnbB, FnB, and GfbA (Collin and Olsén, 2003; Brandt and Spellerberg, 2009). GfbA (group G fibronectin-

binding protein) is homologues to SfbI protein of *S. pyogenes*, mediating adherence and invasion of SDSE to human skin fibroblasts (Kline *et al.*, 1996). GfbA bounds to fibronectin resulting in the formation of membrane ruffles and rearrangements of host cell cytoskeleton (Kline *et al.*, 1996). SDSE strains that express GfbA protein follow the classic endocytic pathway, subsequent fusion with lysosomes forming phagolysosomes (Rohde *et al.*, 2011). Although several adhesins have been identified in bovine SDSD genomes (Chapter 3), the exact role of these proteins in mammalian cell infection remains unclear.

Among *S. pyogenes,* two main pathways for invading non-phagocytic cells have been described (Molinari *et al.*, 2000). The SfbI (fibronectin-binding surface) and M1 protein have been implicated in both adherence and invasion processes since fibronectin interactions bound to Sfb1 and M1 protein lead to different internalization pathways (Rohde and Cleary, 2016). Sfb1-Fibronectin complexes promote uptake of *S. pyogenes* via caveolae. The complexes were found to be sufficient for triggering the formation of the invaginations and the aggregation of caveolae. In comparison, M1-Fibronectin complexes foster receptor-mediated endocytosis (Rohde and Cleary, 2016). The M1 protein interacts with several cellular receptors, directly or indirectly. M1 protein-expressing isolates trigger cytoskeletal rearrangements that provide traffic inside the host cell through endosomes and fuse with lysosomes to form phagolysosomes (Rohde and Cleary, 2016).

The data from the present study suggest that *S. pyogenes* GAP58 is internalized in part via a clathrin-dependent pathway since chlorpromazine inhibited 50% of its internalization.

Curiously, the chlorpromazine and filipin treatment showed a significant increase in intracellular viable VSD13 CFUs compared to control (Figure 5.5B). We hypothesize that the inhibition of dynamin and clathrin pathways might trigger an increase in the uptake of SDSD VSD13 in HEK by macropinocytosis. Studies revealed that blocking clathrin-dependent uptake can induce an increase in clathrin-independent endocytosis (Sandvig *et al.*, 2018), which can partly explain our results; however, the mechanism behind this change is not still fully understood. More studies are required to confirm our hypothesis and understand the molecular mechanism responsible for this increased internalization of SDSD VSD13 in HEK (Figure 5.5).

5.3.3. Proteomic analysis of keratinocytes after *in vitro* incubation with bacteria cells: potential biomarkers

The interaction of streptococci bacteria with HEK might induce several intracellular changes in HEK cells to rapidly respond to the invasion of microbial pathogens. To identify possible targets for streptococci infection a comparative proteomic analysis was performed. Seventy-one spots (Figure 5.6) were excised for MALDI-TOF characterization at the UniMS – Mass Spectrometry Unit, ITQB/IBET, Oeiras, Portugal. Species identification for each spot was done by comparing the percentage of identity (%I) between the *Homo sapiens* and the *Streptococcus dysgalactiae* matches for each spot. According to our results, the % suggests that most of the characterized proteins are human based. Subsequently, STRING© database software was used to predict possible protein-protein interactions inside each protein set. The set of protein obtained for HEK infected with the SDSD strain suggests an alteration on processes such as oxidation-reduction, ATP metabolism and biosynthesis (Table 5.1 Figure 5.6). As for *S. pyogenes* infection in HEK, protein-protein interactions are mostly related to oxidation-reduction and ATP metabolism processes (Table 5.1 and Figure 5.6).
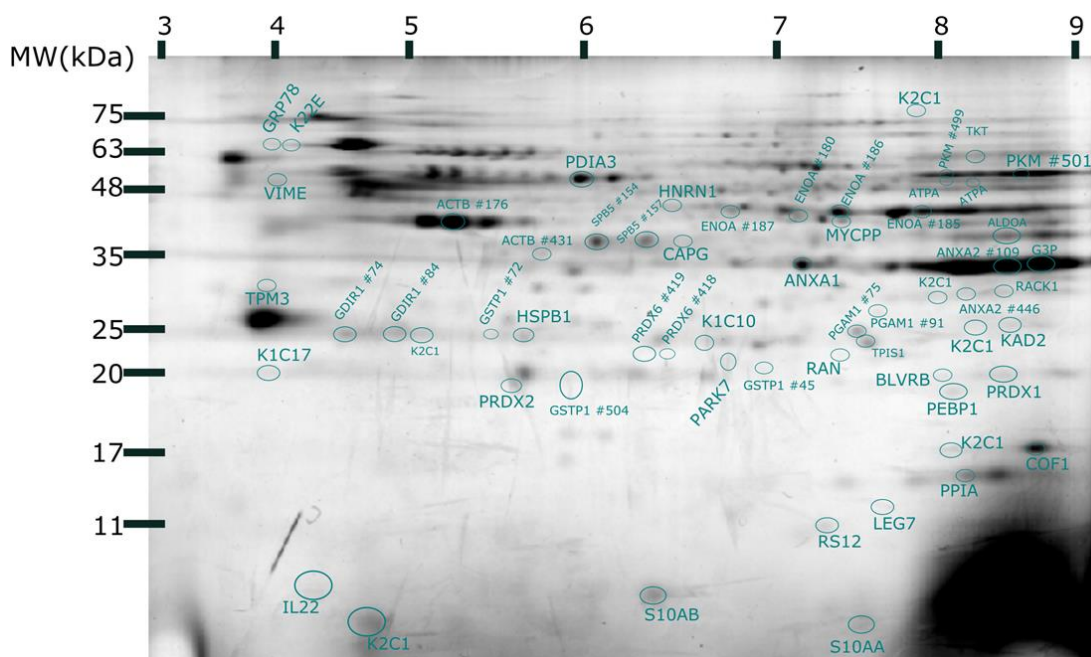
Figure 5.4. Spots with altered regulation in infected human keratinocytes with the SDSD VSD13 strain and the *S. pyogenes* GAP58 strain. Altered regulation of spots/proteins were given by calculating the fold-change of each spot between the controls and the samples: fold values superior to 1,5 and under 0,7 represent proteins up-regulated and down-regulated, respectively. Spots characterized using MALDI-TOF technology by the Mass Spectrometry Unit (UniMS), ITQB/iBET, Oeiras, Portugal.

Data shows that the interaction of *Streptococcus* with HEK induces several changes in the regulation of glycolysis, cell proliferation, protein folding and stress response (Table 5.1). Indeed, proteins such as ALDOA (Fructose-bisphosphate aldolase A, downregulation), PGAM1 (Phosphoglycerate mutase 1, upregulation), PDIA3 (Protein disulfide-isomerase A3, upregulation), GAPDH (Glyceraldehyde-3-phosphate dehydrogenase, downregulation), ENO1 (Alpha-enolase, upregulation), PKM (Pyruvate kinase, upregulation) and TPI1 (Triosephosphate isomerase, upregulation) are differently affected, suggesting that streptococcal infection can activate the glycolytic pathway in human keratinocytes, as previously described in staphylococcal infections (Wickersham *et al.,* 2017). Previous studies described that *S. pyogenes* and *S. aureus* colonization and/or infection of the skin generates localized hypoxia (Lone *et al.*, 2015; Peyssonnaux *et al.*, 2008). Bacterial competition for glucose causes the keratinocyte to rapidly generate energy in response to perceived infection (O'Shaughnessy and Brown, 2015). So, HEK seem primed for the activation of the glycolytic pathway. In clinical environments, the induction of glycolysis has been associated the successful host response to infection (Shalova *et al.*, 2015; O'Neill and Pearce, 2016), So, the stimulation of glycolysis here presented in the presence of SDSD VSD13 appears to be a common response to bacterial infections or stress.

The upregulation of two proteins involved in the production of ATP, AK2 (Adenylate kinase 2, mitochondrial) and ATP5A1 (ATP synthase subunit alpha, mitochondrial), could be related to the nucleotide regulation of P2 receptors in the epidermis to restore its homeostasis (Burrell *et al.*, 2015) upon interaction with SDSD VSD13 isolate.

Peroxiredoxins are a highly conserved family of enzymes that can reduce peroxides, such as H_2O_2, thus playing an important role in cellular redox levels (Hampton *et al.*, 2016; Rhee et a., 2016). Interestingly, it was observed an increased abundance of Peroxiredoxin-6 (PRDX), involved in the oxidative stress response of the cell (Yun *et al.*, 2005; Fisher, 2011), thus revealing that PRDX6 increase might serve as the "first leader" in the combat to the oxidative stress triggered by both *Streptococcus*. This high increase might be related with the secretion of *S. pyogenes* exotoxin SpeC by SDSD VSD13. Indeed, Christ and co-workers described that Streptococcal pyrogenic exotoxin SpeC can induce an increased the expression of nitric oxide (NO) synthase that trigger oxidative stress in cells (Christ *et al.*, 1997).

Our proteomic data showed the downregulation of PRDX2 (in SDSD VSD13 infected HEK) and PRDX1 (in GAP58 infected HEK) (Table 5.1), and these low levels of expression might be linked to a decrease of cell proliferation and activation of apoptosis (Hampton *et al.*, 2016; Hsu, *et al.*, 2011; Yun *et al.*, 2005).

Major modifications also occur in the cytoskeleton structure of the human cell in the presence of the bacteria (Table 5.1). Indeed, an increased abundance of Vimentin (VIM) and Actin cytoplasmatic 1 (ACTB), Keratin type I cytoskeletal 10 (KRT10 in HEK+GAP58) and Keratin type II cytoskeletal 2 (KRT2 in HEK+VSD13), suggesting a rearrangement of the cytoskeleton induced possibly due to bacterial contact and internalization, that agrees with results described above (Figures 5.2-5.5). Moreover, the increased actin expression was confirmed by western blot (Figure 5.7).
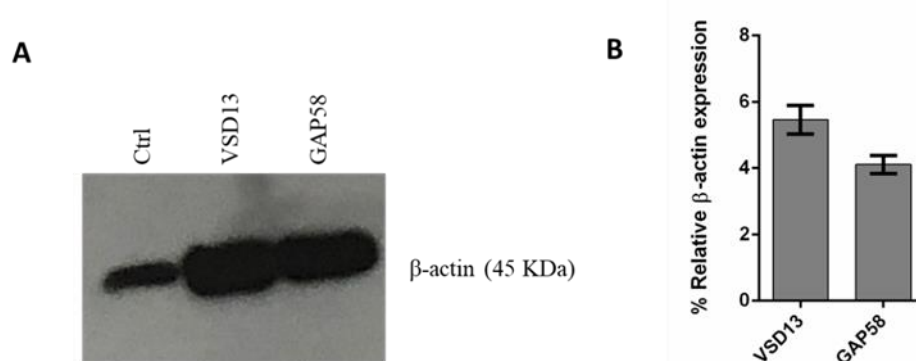
Figure 5.5. Western Blot analysis of β-actin protein. **(A)** Western Blot analysis of β-actin proteins, correspond to 10 µg total protein. **(B)** β-actin relative intensity values. Relative alteration of protein content in HEK after 2h infection with SDSD VSD13 and *S. pyogenes* GAP58 relative to the uninfected HEK (ctrl).

The actin cytoskeleton rearrangement of host cell membranes is often suggested to be a crucial mechanism during pathogen-induced phagocytosis (May and Machesky 2001) facilitating all types of endocytosis processes (Sandvig *et al.*, 2018). These variations in the expression of actin and other cytoskeletal proteins agrees with Figure 5.4 and the internalization of SDSD VSD13 in HEK cells by macropinocytosis and of *S. pyogenes* GAP58 via clathrin-dependent pathways.

Moreover, an increased expression of Annexin 2 (AnxA2) and S100A10 was also observed (Table 5.1). AnxA2 protein functions at the early stages of the endocytic pathway, including in clathrin and caveola-mediated internalization, macropinocytic rocketing, multivesicular endosome biogenesis, and subsequent fusion with lysosomes. In contrast to the role of AnxA2 in endocytosis, intracellular S100A10 participates in the trafficking of several proteins, including AnxA2, to the plasma membrane. S100A10

appears to be required for AnxA2 activities at the cell surface in cultured cells, and S100A10 is undetectable unless AnxA2 is also expressed (Dziduszko and Ozbun 2013). These results agree with the previous data of internalization of GAP58 into HEK cells via a clathrin-mediated processes and in VSD13 via clathrin-independent processes (Figure 5.5) and macropinocytosis (Figure 5.4).

Table 5.1. Principal biological processes involved in the streptococci infection in human keratinocytes. Fold change corresponds to the ration between the percentage of volume of the normalized samples by the normalized controls. Proteins with folds higher than 1.5 were considered up-regulated while folds under 0.7 were considered down-regulated.

Gene name	Protein name	VSD13 / control	GAP58 / control
Protein Folding and Transport			
HSPA5	78 kDa glucose-regulated protein	6.2	1.8
PDIA3	Protein disulfide-isomerase A3	1.5	1.5
RAN	GTP-binding nuclear protein Ran	1.8	2.7
S100A10	Protein S100-A10	1.5	3.7
Oxidative Stress			
HSPB1	Heat shock protein beta-1	0.26	Absent
PARK7	Protein/nucleic acid deglycase DJ-1	0.39	0.5
PPIA	Peptidyl-prolyl cis-trans isomerase A	2.1	0.2
PRDX1	Peroxiredoxin-1	1.2	0.2
PRDX2	Peroxiredoxin-2	0.4	1.1
PRDX6	Peroxiredoxin-6	10.9	13.7
Cytoskeleton structure			
KRT17	Keratin. Type I cytoskeletal 17	0.5	0.4
VIM	Vimentin	5.5	4.0
ACTB	Actin. Cytoplasmic 1	3.8	2.5
KRT10	Keratin. Type I cytoskeletal 10	0.4	1.9
KRT2	Keratin. Type II cytoskeletal 2	4.8	0.7
Energetic Metabolism			
AK2	Adenylate kinase 2, mitochondrial	1.5	Absent
ALDOA	Fructose-bisphosphate aldolase A	0.6	0.2
ATP5A1	ATP synthase subunit alpha, mitochondrial	2.2	0.6
BLVRB	Flavin reductase (NADPH)	2.1	1.4
ENO1	Alpha-enolase	1.6	2.2
		1.7	3.2
GAPDH	Glyceraldehyde-3-phosphate dehydrogenase	0.5	0.2
PGAM1	Phosphoglycerate mutase 1	2.1	2.1
PKM	Pyruvate kinase PKM	1.9	1.9
		3.1	Absent
RPS12	40S ribosomal protein S12	1.5	1.4
TKT	Transketolase	1.3	1.8
TPI1	Triosephosphate isomerase	2.2	1.7

Considering the similar protein expression profiles obtained for HEK infected with SDSD VSD13 and *S. pyogenes* GAP58 (Figure 5.6 and Table 5.1), it seems that both streptococci induce similar responses in this type of human cells.

5.3.4. Oxidative stress biomakers

Considering that the comparative proteomic analysis revealed an up-regulation of oxidative stress (OS) response, we further investigated these results. OS is defined as an imbalance between prooxidants and antioxidants that arises when reactive oxygen species (ROS) production overwhelms the intrinsic antioxidants. OS adversely influences various cell mechanisms, leading to loss of function and cell death (Tejchman *et al.*, 2021). Lipid peroxidation (LPO) is the process where ROS remove electrons from the lipids in the cell membranes. LPO products often react with proteins present in the cell membranes, leading to aldehydes syntheses such as MDA that diffuse through the cell membrane and can cause DNA damage. LPO process can also affect electron transport in the respiratory with diminished ATP production (Tejchman *et al.*, 2021).

It is known that skin cells, like keratinocytes, express several antioxidant enzymes which protect against oxidative stress, including SOD, CAT, and glutathione peroxidase (Black *et al.*, 2009). While the SOD enzyme provides antioxidant defense against reactive superoxide radicals, dismutating them into H_2O_2 and O_2, CAT enzyme catalyzes the conversion of H_2O_2 to water and molecular oxygen. The glutathione peroxidase catalyzes the detoxification of H_2O_2 and lipid peroxides (Black *et al.*, 2009).

Lipid peroxidation and activity of CAT and SOD enzymes in HEK infected with GAP58 or SDSD VSD13, or HEK cells exposed to bacterial culture supernatants were assessed. Statistical significative differences were found between HEK control cells and HEK incubated with VSD13 and GAP58 or supernatants from VSD13 and GAP58 (Figure 5.7).
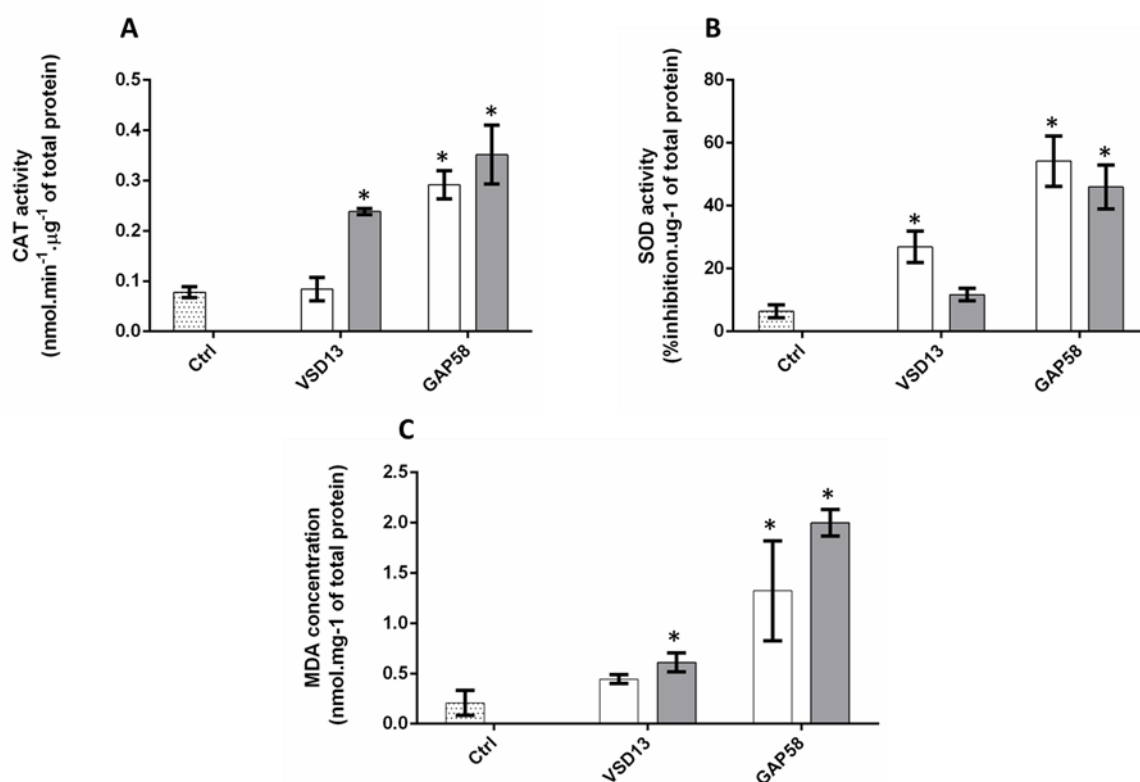
Figure 5.6. Levels of oxidative stress biomarkers (A) CAT, (B) SOD, and (C) lipid peroxidation in HEK cell lines in the absence (ctrl; dotted bars) or after infection (2h) with SDSD VSD13 and GAP58 isolates (white bars) or with bacterial supernatants (grey bars). Lipid peroxides were quantified using malondialdehyde bis (dimethylacetal) standards (MDA). Represented values are the average value with SEM of three independent experiments. * $p < 0.05$, statistically significant difference compared to control cells (HEK in the absence of bacteria or bacterial supernatants).

The results show that VSD13 and GAP58 isolates, or their respective supernatants increased the lipid peroxidation and the activity of SOD and CAT in HEK (Figure 5.8). These results are in line with the proteomic data above described (Table 5.1) and data from others (Black *et al.*, 2009, Regnier *et al.*, 2016). Indeed, Black and coworkers showed an increased oxidative stress in mouse keratinocytes cells following exposure to Paraquat, an herbicide known to induce skin toxicity (Black *et al.*, 2009). Regnier and co-workers showed that *S. pyogenes* could stimulate HEK to develop an innate immune response based on ROS production, that induces HEK necrosis, resulting in the skin lesions observed in cellulitis infections (Regnier *et al.*, 2016).

The oxidative stress response induced in HEK by *S. pyogenes* GAP58 was higher compared to the oxidative stress response induced by SDSD VSD13 (Figure 5.7). Interestingly, the increase in SOD activity in HEK was higher when streptococci were incubated with the human cells compared to their respective supernatants, and this

difference is more evidenced for VSD13 (Figure 5.7, white bars versus grey bars). On the contrary, CAT activity was higher when HEK cells were exposed to streptococci supernatants compared to incubation with bacterial cells, once again more evident for VSD13 (Figure 5.7, grey bars compared to white bars). Since streptococci are also superoxide dismutase producers (Hardie and Whiley, 1997) and the SOD activity assay is not specific to human SOD, we cannot discharge that we might also be measuring some activity of bacterial SOD. On the other hand, streptococci are not catalase producers (Hardie and Whiley, 1997) and thus, increased CAT activity in HEK is due to the presence of VSD13 or GAP58 bacterial supernatants.

Oxidative stresses caused by ROS can induce a depolarization of mitochondrial membrane potential and subsequent impairment of oxidative phosphorylation (Park *et al.*, 2011). Herein, we analyzed the mitochondrial membrane potential of HEK infected with GAP58 and SDSD VSD13 which confirmed the depolarization of mitochondrial membrane potential (Figure 5.8).
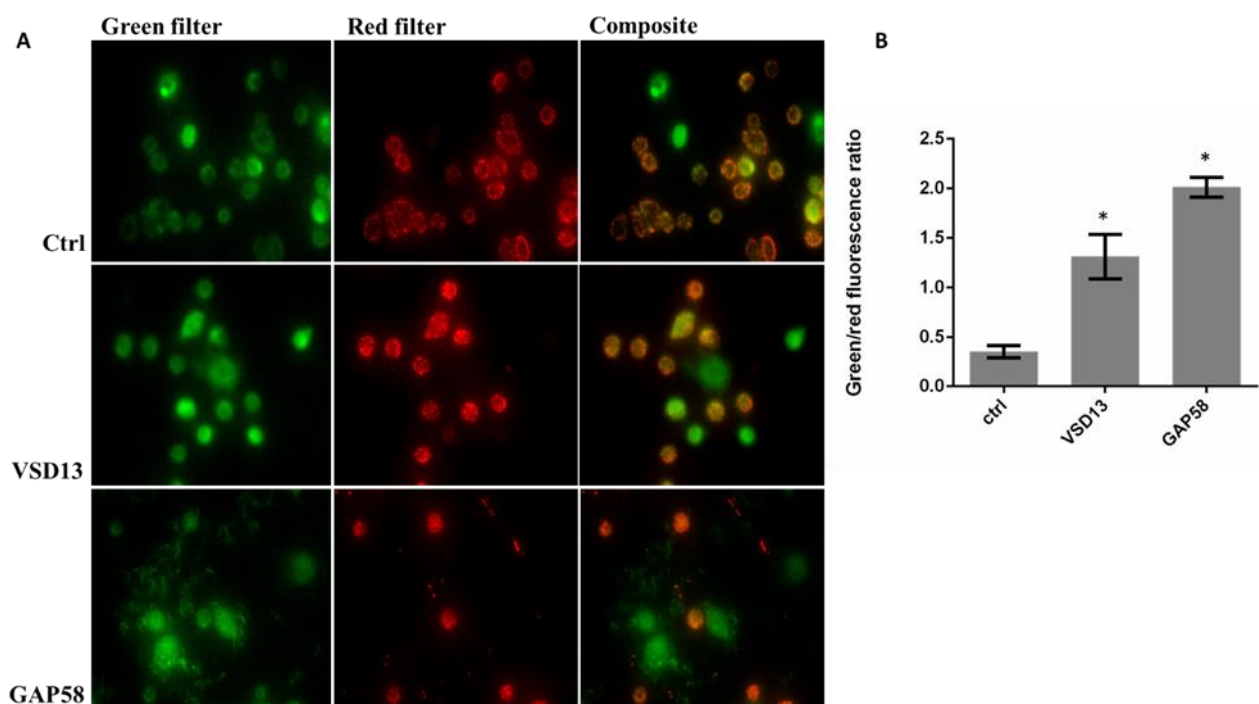
Figure 5.7. Mitochondrial Membrane Potential (A) in HEK exposed during 2 hours to GAP58 or SDSD VSD13 isolates. JC-1, a cationic carbocyanine dye (green) exhibits potential-dependent accumulation in mitochondria where it starts forming aggregates (red), upon depolarization, it remains as monomer showing green fluorescence (Sivandzade *et al.*, 2019). (B) Green/red fluorescence ratio. * $p<0.05$, a statistically significant difference compared to control (HEK not incubated with bacteria).

GAP58 and VSD13 infection enhanced ROS production in HEK and an altered mitochondrial membrane potential (Figures 5.7 and 5.8). These results are also in agreement with an increased apoptosis of HEK (Table 5.1). Interestingly, the number of human cells after 6 h of infection in the presence of VSD13 and particularly GAP58 decreases (Figure 5.2). Similar results were observed when human macrophages were treated with *S. pyogenes* strains (Tsao *et al.*, 2019). Tsao and co-workers observed that streptolysin S played an important role in GAP-induced macrophage death through increasing the mitochondrial ROS generation (Tsao *et al.*, 2019). Streptolysin S possesses cytotoxic effects against a broad spectrum of mammal cells including epithelial cells, macrophages, neutrophils, lymphocytes, and platelets (Molloy *et al.*, 2011). SDSD VSD13 is not Streptolysin S producer, despite harboring the *sagA* gene (prepropeptide structural) (Chapter 2). The mechanisms by which SLS contributes to virulence have been the subject of several investigations. The loss of SagB-I observed in bovine SDSD isolates is associated with loss of β-hemolytic activity (Chapter 2), However, the *sagA* gene has been maintained in the bovine SDSD genome which indicates an additional function to the product of this gene (Chapter 2). Some studies suggest that SLS also functions as a quorum-sensing molecule, and SagA mRNA has been implicated in the regulation of several virulence genes, including M proteins (Datta *et al.*, 2005; Molloy *et al.*, 2011).

5.4.   Conclusion

In summary, we have presented evidence for the internalization and cytotoxicity induction by bovine SDSD in human keratinocytes cells. The findings of TEM and SEM hereby described show that bovine SDSD infection of HEK caused ultrastructural changes resembling those changes following macropinocytosis. We have shown that the isolate SDSD VSD13 induced oxidative stress in keratinocytes with the disruption of the mitochondrial membrane potential, and consequently cell death by apoptosis.

Considering the protein abundance profiles obtained for keratinocytes cells infected with bovine SDSD VSD13 and human S. pyogenes GAP58 strains, similar trends can be observed, suggesting similar responses of the host cell to both bacterial species. The present study results require further investigation for a complete understanding of the molecular mechanisms of infection of bovine SDSD.

Author Contributions

CA-B contributed to adhesion and internalization assays, inhibition of streptococci internalization into human HEK, protein sample preparation, Western Blot for β-actin quantification, Mitochondrial membrane potential analyses, performed the statistical analysis and manuscript writing. CA-B and MD contributed to the determination of enzymes activity and lipid peroxidation assay. CA-B, CR-R, and MC participated in the confocal analysis and the interpretation of the data. CA-B and APAM contributed to analysis of TEM and SEM. CA-B, CR-R and CB participated in the protein sample preparation for proteomic and situ analysis. ARF was involved in the study coordination, and revision of the final version of the manuscript.

Funding

Chapter 6 - Biofilm development and computational screening for new putative inhibitors of a homolog of the regulatory protein BrpA in *Streptococcus dysgalactiae* subsp. *dysgalactiae*

Alves-Barroco, C., Roma-Rodrigues, C., Balasubramanian, N., Guimarães, M. A., Ferreira-Carvalho, B. T., Muthukumaran, J., Nunes, D., Fortunato, E., Martins, R., Santos-Silva, T., Figueiredo, A., Fernandes, A. R., and Santos-Sanches, I.

Abstract

In this work we integrated microbiology, imaging and computational methods to evaluate the biofilm production capability of bovine SDSD isolates; to assess the presence of biofilm regulatory protein BrpA homolog in the biofilm producers; and to predict a structural model of BrpA-like protein and its binding to putative inhibitors. Our results show that SDSD isolates form biofilms on abiotic surface such as glass (hydrophilic) and polystyrene (hydrophobic), with the strongest biofilm formation observed in glass. This ability was mainly associated with a proteinaceous extracellular matrix, confirmed by the dispersion of the biofilms after proteinase K and trypsin treatment. The biofilm formation in bovine SDSD isolates was also confirmed by confocal laser scanning microscopy (CLSM) and scanning electron microscopy (SEM). Under SEM observation, SDSDVSD16 isolate formed cell aggregates during biofilm growth while VSD9 and VSD10 formed smooth and filmy layers. We show that *brpA*-like gene is present and expressed in SDSD biofilm-producing isolates and its expression levels correlated with the biofilm production capability, being more expressed in the late exponential phase of planktonic growth compared to biofilm growth. Fisetin, a known biofilm inhibitor and a putative BrpA binding molecule, dramatically inhibited biofilm formation by the SDSD isolates but did not affect planktonic growth, at the tested concentrations. Homology modeling was used to predict the 3D structure of BrpA-like protein. Using high throughput virtual screening and molecular docking, we selected five ligand molecules with strong binding affinity to the hydrophobic cleft of the protein, making them potential inhibitor candidates of the SDSD BrpA-like protein. These results warrant further investigations for developing novel strategies for SDSD anti-biofilm therapy.

6.1. Introduction

Biofilms are heterogeneous structures composed of bacterial cells surrounded by a matrix and attached to solid surfaces (Olsen, 2015). During biofilm growth, bacteria are transferred from a free-swimming state (planktonic cells) to a multitude of bacterial cells enclosed by a self-produced polysaccharide matrix of hydrated extracellular polymeric substances, attached to biotic or abiotic surfaces (sessile cells) (Flemming and Wingender, 2010). However, in some bacteria, such as *Staphylococcus aureus*, the biofilm matrix can be mostly composed by bacterial surface proteins and extracellular DNA (eDNA) (Toledo-arana *et al.*, 2005). Biofilms can differentiate, to form mushroom- and tower-like structures surrounded by fluid filled channels (Olsen, 2015). Bacterial biofilms are ubiquitous in the environment and can be found on almost any hydrated non-shedding surface including rivers, stagnant pools, man-made and also biological materials (Garnett and Matthews, 2012). As a response to environmental changes such as pH, oxygen, carbon source and/or nutrient availability, cell density, and the presence of a solid surface, bacterial cells in biofilms interact with each other, resulting in the global coordination of their gene expression (Jefferson, 2004; Wen and Burne, 2002). Quorum sensing is the signaling network for cell-to-cell communication that regulates biofilms and other cellular processes (Galante *et al.*, 2015).

Biofilm formation has been implicated in different types of bacterial infections in both humans and animals, making those infections difficult to eradicate with antimicrobials. This is the case, for example, of orthopedic and cardiac implant-associated infections, cystic fibrosis, urinary tract infections, osteoarticular infections and periodontal diseases (Olsen, 2015). Many persistent and chronic bacterial infections are now thought to be linked to biofilm formation, and over 80% of all bacterial infections have been estimated to involve biofilms (Kvist *et al.*, 2008; Reid *et al.*, 2009). Biofilm-associated infections are particularly problematic because bacteria sessile cells tolerate host defense mechanisms, antibiotics, biocides, and hydrodynamic shear forces far better than the corresponding planktonic ones (Dürig *et al.*, 2010; Rosini and Margarit, 2015). Therefore, biofilms are clinically important not only because they form a defensive barrier against other potential pathogens (in case of the host microbiota), but they also generate a break line between minor and debilitating infectious diseases. Indeed, biofilms can promote horizontal spread of resistance determinants (Savage *et al.*, 2013).

Streptococcus can form biofilms on natural or abiotic surfaces such as glass (hydrophilic) or polystyrene (hydrophobic) (Marks *et al.*, 2014a,b; Oliver-Kozup *et al.*, 2011; Silva *et al.*, 2014). Studies in *Streptococcus mutans* showed that several genes are required for biofilm development (Bitoun *et al.*, 2014; Shemesh *et al.*, 2007a). Several studies reported that the expression of genes responsible for biofilm formation is dependent on environmental conditions (Li and Burne, 2001; Shemesh *et al.*, 2007a) and genetically regulated (Lee *et al.*, 2004). In 2007, Shemesh *et al* described in *Streptococcus mutans* the presence of the paralogues *brpA* and *brpB*, encoding the biofilm regulatory proteins A and B (BrpA and BrpB, respectively) which are members of the LytR/CpsA/Psr– LCP family (Shemesh *et al.*, 2007a). The LCP family of proteins, important for the bacterial adaptation in different environments, has been found in the genome of both pathogenic and non-pathogenic bacteria (Chatfield *et al.*, 2005). LCP proteins have an important role in cell-wall biogenesis and structural maintenance, by regulating autolysin. In addition, these proteins have been implicated in biofilm development and bacterial adhesion to host cells (Bitoun *et al.*, 2014; Shemesh *et al.*, 2007b). Considering the importance of biofilm development in a plethora of infectious diseases (Del Pozo, 2018), including bovine mastitis by *Staphylococcus aureus* (Ghinet *et al.*, 2017), and the fact that SDSD is an important mediator of this bovine disease and also capable to infect human cells (Jordal *et al.*, 2015; Koh *et al.*, 2009; Park *et al.*, 2012; Roma-Rodrigues *et al.*, 2015), characterizing biofilm formation by SDSD is a major step to mitigate infection. Thus, the aim of the present study was to evaluate and characterize biofilm production by SDSD isolates and to assess the presence of the *brpA*-like gene. Using *in silico* methods, we predicted the 3D-homology model of the cytoplasmic domain of BrpA homolog protein of SDSD and combined high throughput virtual screening-molecular docking to identify potential inhibitors of this protein.

6.2.   Materials and Methods

6.2.1.   Bacterial collection

A total of 18 alpha hemolytic SDSD isolates from Portuguese animals diagnosed with subclinical and clinical mastitis were used in the present study. An SDSD isolate from Canada (GCS-Mo), associated with bovine cellulitis and Toxic Shock-Like Syndrome, and another from Singapore, (GCS-Si) responsible for an ascending upper limb cellulitis in a woman that was pricked by the fins and scales of a raw fish, were also included in this study (Rato *et al.*, 2011). Additionally, two Portuguese *S.*

dysgalactiae subsp*. equisimilis* (SDSE) COI 289 and HSM 53 isolates, and one *S. pyogenes* GAP58 isolate, were also included in this study for comparative analysis. The SDSE isolates were already identified by our group as weak and strong biofilm producers on glass and polystyrene and hence were used as controls (Genteluci *et al.*, 2015).

6.2.2. Media, bacterial growth and storage condition

Colombia agar supplemented with 5% (v/v) sheep blood (Probiologica, Belas, Portugal) was used for colony isolation. The bacteria were grown in Todd-Hewitt broth (BBL, Cockeysville, Md., USA) supplemented with 1% (w/v) of yeast extract (Oxoid, Basingstoke, United Kingdom) and incubated at 37 °C for 14–16 h. The late exponential phase culture was mixed with 20% (v/v) sterilized glycerol and were kept and maintained at - 80 °C.

6.2.3. Biofilm formation assay on glass

Biofilm production on glass surfaces was carried as previously described (Ferreira *et al.*, 2012; Genteluci *et al.*, 2015). SDSD, SDSE and GAP58 isolates were streaked on a blood agar plate and incubated at 37 °C for 18 h in a 5% (v/v) CO_2 incubator. About 5–10 colonies were transferred to 4 mL of Trypticase Soy Broth (TSB) supplemented with 0.5% (w/v) glucose and incubated overnight at 37 C in a water bath without agitation. Culture growth was followed by measuring the optical density (OD) at 570 nm (OD_{570}). 100 µL of bacterial culture ($OD_{570} = 0.6$) was transferred to a test tube containing 3.9 mL of TSB supplemented with 0.5% (w/v) glucose and incubated in a horizontal position for 20 h at 37 °C. The supernatant was carefully removed and washed with sterile saline solution (0.85% (w/v) NaCl) by manually rotating the tube. The test tubes were incubated in an oven at 65 °C for 1 h or at 45 °C for 3 h for the attachment of biofilm. The biofilm formation capability of each strain was classified by visual inspection as weak (+); moderate (++); and strong (+++). Biofilms were resuspended in 4 mL of saline solution. Then, the OD at 600 nm (OD_{600}) was measured (saline solution as blank) and used to rate biofilm formation: OD_{600} 0.099, no formation; OD_{600} between 0.1–0.299, weak; OD_{600} between 0.3–0.599, moderate; $OD_{600}>0.600$, strong (Ferreira *et al.*, 2012).

6.2.4. Biofilm formation assay on polystyrene

Biofilm production on polystyrene surfaces was carried as previously described (Ferreira *et al.*, 2012). Briefly, 100 μl of bacterial culture (OD_{570} = 0.6) was added to 100 μl of TSB broth supplemented with 0.5% (w/v) glucose in a 96 well plate and mixed by pipetting. A 200 μl of TSB broth supplemented with 0.5% (w/v) of glucose was used as control. The 96 well plate was sealed and incubated for 20 h at 37 °C. The OD_{570} was measured in an ELISA plate reader (Bio Rad, California, USA). The supernatant was carefully removed, and each well was washed twice with sterile saline solution (0.85% w/v) to remove non-adherent bacteria and dried at 65 °C for 1 h. The biofilm was stained with crystal violet 1% (w/v) for 1 min. The wells were washed again gently with sterile distilled water 3 or 4 times (until the control-wells dye was completely removed). The OD_{570} of the stained biofilm was directly measured in the plate reader. Interpretation of biofilm formation was performed according to the criteria previously described (Stepanovi *et al.*, 2007) and the isolates were therefore categorized as follows: non producer: OD OD$_{ctrl}$, (all strains which OD values were below 0.060); weak producer: OD$_{ctrl}$ < OD 2 OD$_{ctrl}$, (all strains which OD values were above 0.060 and below 0.120); moderate producer: 2 OD$_{ctrl}$ < OD 4 OD$_{ctrl}$ (all strains which OD values were above 0.120 and below 0.240). strong producer: OD > 4 OD$_{ctrl}$ (all strains which OD values were above 0.240).

6.2.5. Characterization of biofilm matrix by Congo Red Agar binding assay

A modification of a previously described Congo Red Agar (CRA) binding assay was used to detect extracellular polysaccharides (Rollefson *et al.*, 2011). The strains were grown in Todd Hewitt broth (18 h/37 °C). Cells were harvested by centrifugation (9072 g for 10 min), washed twice with phosphate buffered saline (PBS, containing 137 mM NaCl; 2.7 mM KCl; 10 mM Na_2HPO_4; 2 mM KH_2PO_4, pH 7.4) and the density of the suspension was adjusted to an optical density (OD_{600}) of 0.5. Cells were cultured in Todd Hewitt Agar supplemented with different sugars (glucose, sucrose or lactose), at different concentrations (1, 2 and 5% (w/v)), and 0.08% (v/v) Congo Red (Sigma-Aldrich Missouri, USA). All plates were incubated for 24 h at 37 °C in aerobic atmosphere with 5% (v/v) CO_2. The presence of polysaccharides was indicated by black colonies with a dry crystalline consistency. Weak or non-polysaccharide producing colonies remained red. The darkening of the colonies with the absence of a dry crystalline colonial

morphology indicated an indeterminate result. The *Staphylococcus aureus* ATCC 25923 was used as a positive control.

6.2.6. Enzymatic treatment of the biofilm matrix

Bacteria were grown in a 4 mL of TSB supplemented with 0.5% (w/v) of glucose, incubated overnight at 37 °C in a water bath without agitation. The culture was grown until an OD_{570} of 0.6, and 50 μL was transferred to 2 mL of TSB medium supplemented with 0.5% (w/v) glucose containing: i) pronase or protease (0.75 U/mL), ii) trypsin (55 U/mL), iii) proteinase K (30 U/mL; (Ferreira *et al.*, 2012)), iv) DNase I (280 U/mL) or v) sodium metaperiodate (10 mM). After an incubation for 20 h at 37 °C, the supernatant was removed, and the tube washed with 2 mL of distilled water. The biofilm formation was classified by visual inspection as stated above and quantified by measuring the $OD600$ after resuspension in 2 mL of saline solution (0.85% (w/v) NaCl (Genteluci *et al.*, 2015).

6.2.7. Analysis of the biofilm structure

The structure of the biofilm produced by three bovines SDSD isolates - VSD9, VSD10 and VSD16 - was analyzed by fluorescence microscopy, Confocal laser scanning microscopy (CLSM) and Scanning electron microscopy (SEM). For fluorescence microscopy studies, SDSD isolates were grown over a cover glass as previously described (Roma-Rodrigues *et al.*, 2015). The media containing the non-adherent cells was removed and the biofilms were gently washed (3 times) with PBS and stained with the LIVE/DEAD reagent (0.25 μg/mL propidium iodide (PI) and 20 μM Carboxy fluorescein succinimidyl ester (CFSE) in PBS; Life Technologies, Carlsbad, CA, USA) for 30 min. After 3 washes with PBS, the cover glass was placed in a microscope slide on a drop of ProLong Diamond antifade mountant (LifeTechnologies). Biofilms were imaged using a fluorescence microscope Zeiss Axioplan 2 Imaging Microscope coupled with a Nikon DXM1200 F digital camera (software ZEN Blue edition, 2011). CFSE was used to stain live cells (excitation and fluorescence emission at 492 and 517 nm, respectively); PI was used to stain dead cells (maximal excitation and fluorescence emission at 565 and 617 nm, respectively). A microscope objective of 40 magnification plus ocular lenses of 10x magnification (total magnification of 400) were used. The amplification used for collecting the images is described in the respective Figure caption. For CLSM, biofilms were produced and fixed as described above for fluorescence microscopy. Subsequently,

the cells were treated with Triton X-100 at 0.1% (v/v) (Sigma), washed with PBS and stained with Hoechst 33,258 (0.2 µg/mL, Life Technologies, Carlsbad, CA, USA) for 1 h at 37 C in the dark. Samples were washed 3 times with PBS and the cover glass containing the biofilm was placed on top of a drop of ProLong Diamond antifade mountant (Life Technologies, California, USA) in a microscope slide. To determine the biofilm thickness, 10 different regions per microscope slide were analysed using a fluorescence confocal microscope (CLSM, Carl Zeiss, LSM 700) and the top and bottom layers of the thicker region of the biofilm and the maximum biofilm height measured using the software ZEN Black, 2011. Three measures in each microscopic field were used for analysing the thickness of the biofilm.

SEM procedure followed the protocol described by Pluk *et al.* (2009) with some little modifications. A commercial indium tin oxide (ITO) glasses were gently washed with 70% (v/v) ethanol, followed by sterile water and then placed in a sterile Petri plate with a lid. 100 µL of bacterial culture (OD = 0.6) was added to a 1.9 ml of TSB medium with glucose (0.5%) and added to the ITO glass. The glass plates were incubated for 20 h at 37 C. The media was carefully removed, washed with sterile saline solution (NaCl 0.85%) to remove planktonic cells and dried for 1 h at 37 ºC. The ITO glasses with biofilms were frozen in liquid nitrogen and subsequently dried in a freeze-dryer (TLMCSP-80, Thermoline L + M, Northgate, QLD, Australia) at 30 C under vacuum for 10 min (Crang and Klomparens, 1988; Dykstra and Reuss, 2003). The samples were warmed to room temperature before use. SEM observations were carried out using a Carl Zeiss AURIGA CrossBeam (FIB-SEM) workstation, equipped for EDS and EBSD measurements.

6.2.8. Inhibition of biofilms by fisetin

Fisetin (Sigma-Aldrich Missouri, USA) was used to inhibit biofilm development as previously described (Dürig *et al.*, 2010). Bovines SDSD isolates VSD1, VSD9 and VSD16 were used for these inhibition studies. About 5 colonies were transferred to 4 mL of TSB supplemented with glucose 0.5% (w/v) and incubated overnight at 37 ºC. Culture growth was followed by measuring the OD_{570}. 100 µL of bacterial culture (OD_{570} = 0.6) was transferred to a test tube containing 3.9 mL of TSB supplemented with 0.5% (w/v) glucose and three different concentrations of fisetin - 32 µg/mL, 64 µg/mL and 128 µg/mL. The tubes were incubated in a horizontal position for 20 h at 37 ºC. The supernatant was carefully removed, washed with saline solution

(0.85% (w/v) NaCl) by manually rotating the tube. The tubes were incubated in an oven at 65 °C for 1 h for biofilm attachment. Biofilms were resuspended in 4 mL of saline solution and the OD_{600} measured.

6.2.9. Screening of *brpA*-like gene

Genomic DNA was obtained according to Section 2.2.1 of Chapter 2. Polymerase Chain Reaction amplification of *brpA-like* gene was performed as described in Section 4.2.10 of Chapter 4. **DNA sequencing analysis.** The PCR products of *brpA*-like gene were purified using the Wizard PCR Preps DNA Purification System (Promega, Madison, USA). Sequencing was performed by STAB-Vida (Lisbon, Portugal) using specific primers (Supplementary Table S2, Appendix I). The DNA sequence was analyzed by CLC Genomics Workbench 7.0.4 alignment program.

6.2.10. Expression analysis of the *brpA*-like

Total RNA preparation and cDNA synthesis was performed according to Section 4.2.3 of Chapter 4.

Reverse transcription - PCR (RT-PCR). The *brpA*-like gene expression was analyzed using cDNA as a template and the same primers and conditions described for PCR amplification. 16S RNA gene was used as an endogenous control. The PCR products were analyzed by gel electrophoresis [1% (w/v) agarose]. A molecular weight marker Ladder III (NZYTech) was used to estimate DNA fragment size.

Reverse transcriptase quantitative PCR (RT-qPCR)

The quantitative analysis of *brpA*-like gene expression of the three SDSD isolates - VSD9, VSD10 and VSD16 - was carried out by RT-qPCR. For obtaining total RNA, cells were harvested after 20 h of incubation (biofilm forming conditions); during late exponential phase of planktonic growth (OD_{600} of 1.2–1.4) and in the stationary phase planktonic growth (20 h of incubation). All isolates were grown in TSB supplemented with 0.5% (w/v) and incubated under the same conditions used for analysis of biofilm formation on glass. Extraction of total RNA and cDNA synthesis was performed according to Section 4.2.3 of Chapter 4. The RT-qPCR reaction mixture (20 µL) contained NZY qPCR Green Master Mix (NZYTech, Lisbon, Portugal), 1 µL cDNA, and 0.5 µM of the P2F and P2R primers described in Table 4.1. PCR conditions included an initial denaturation at 95 °C for 10 min, followed by 30 cycles of amplification consisting of denaturation at 95 °C for 15 s, and annealing at 58 °C for 30 s and extension at 60 °C

for 45 s. All primer pairs were checked for primer-dimer formation by using the dissociation curve analysis. The critical Ct was defined as the cycle in which fluorescence becomes detectable above the background fluorescence. The expression levels of *brpA*-like gene were normalized using the 16S rRNA gene of SDSD as an internal standard. There was no significant difference in the expression of the 16S rRNA gene under the various conditions nor in the various samples tested. Each assay was performed with at least three independent RNA samples (and using technical duplicates). Student's *t*-test was used to calculate the significance of the difference between the mean expression of *brpA* gene in biofilm growth compared to planktonic growth (late exponential phase and stationary phase). A p value of <0.05 was considered significant.

6.2.11. Sequence analysis of the BrpA homolog protein

The *brpA*-like gene sequence of SDSD strain VSD9 (NCBI Accession Number: AIZ65938) was translated into the BrpA homolog protein by NCBI ORF Finder (http://www.ncbi.nlm.nih.gov/projects/gorf/orfig.cgi) and subjected to protein sequence analysis (ExPASy Proteomics Server; www.expasy.org/tools) (Gasteiger *et al.*, 2005).The ProtParam web server (Gasteiger *et al.*, 2005) was used to compute the physico-chemical properties such as: i) amino acid composition, ii) molecular weight (MW), iii) isoelectric point (pI), iv) instability index (II), v) aliphatic index (AI) and vi) extinction coefficient (EC). Functional domains present in the protein sequence were identified by Motif search (http://www.genome.jp/tools/motif/). The sub cellular localization of the protein was predicted using PSort server (http://psort.hgc.jp/) (Gardy *et al.*, 2003) and the presence of *N*-terminal signal peptide in the protein sequence were identified through TOPCONS server (http://topcons.cbr.su.se/) (Tsirigos *et al.*, 2015).

6.2.12. Protein structure prediction and identification of putative inhibitors for BrpA homolog

The protein sequence of the BrpA homolog was submitted to Protein BLAST server (http://blast.ncbi.nlm.nih.gov/Blast.cgi?PAGE=Proteins) (Camacho *et al.*, 2009) against Protein Data Bank (http://www.rcsb.org/pdb/home/home.do) (Berman *et al.*, 2000) to identify suitable structural templates. Subsequently, the ModWeb server (https://modbase.compbio.ucsf.edu/modweb/) (Pieper *et al.*, 2011) was used to predict the three-dimensional model of the homolog protein and the structural quality of the *in*

silico generated model was investigated by RamPage (http://mordred.bioc.cam.ac.uk/rapper/rampage.php) server (Lovell *et al.*, 2003) for analysis of the Ramachandran plot. Finally, the DrugDiscovery@TACC web portal (https://drugdiscovery.tacc.utexas.edu/) was used to perform the High Throughput Virtual Screening (HTVS) analysis of BrpA homolog against a Zinc Natural compound database (http://zinc.docking.org/) (Irwin and Shoichet, 2005) using Auto Dock Vina (Trott and Olson, 2010). Based on the literature (Dürig *et al.*, 2010), we used ellagic acid and fisetin molecules as a reference and standard for the comparison of docking results with putative inhibitors. Binding mode, binding orientation, interacting residues and intermolecular interactions were carried out using LigPlus (Laskowski and Swindells, 2011) and figures were prepared using PyMOL (http://pymol.org/) (Rother, 2005).

6.2.13. Statistical analysis

All data were expressed as mean ± SEM from at least three independent experiments. GraphPad Prism version 7.0 was used for statistical analysis. The statistical significance was determined for each data set using the student's *t* test and statistical significance was considered when $p < 0.05$.

6.3.   Results

6.3.1.   Biofilm development assay on glass and polystyrene surfaces

The ability of the 20 SDSD isolates to develop biofilms on glass surfaces was evaluated after 20 h of growth (Figure 6.1A). and compared with SDSE producer and non-producer control strains previously described by us (Genteluci *et al.*, 2015). Portuguese SDSE COI 289 and HSM 53 and *S. pyogenes* GAP58 isolates analysis was also carried out for comparison. All 20 SDSD isolates and the SDSE COI 289 accumulate heavy amounts of biofilms on glass. The *S. pyogenes* GAP58 and SDSE HSM53, were not capable of producing biofilms.

The ability of all the isolates to form biofilms on a polystyrene surface was also evaluated. Among the tested isolates, SDSD VSD2 and VSD6 produced high levels of biofilms; SDSD VSD5, VSD9, VSD15, GCS-SI and GCS-MO were classified as weak producers; and the remaining 13 SDSD isolates were not able to develop biofilm in polystyrene (Figure 6.1B). SDSE HSM53 and COI 289 produced high levels of biofilms,

whereas the *S. pyogenes* GAP58 isolate did not produce biofilm on this surface (Figure 6.1B).

BIOFILM PRODUTION ON GLASS
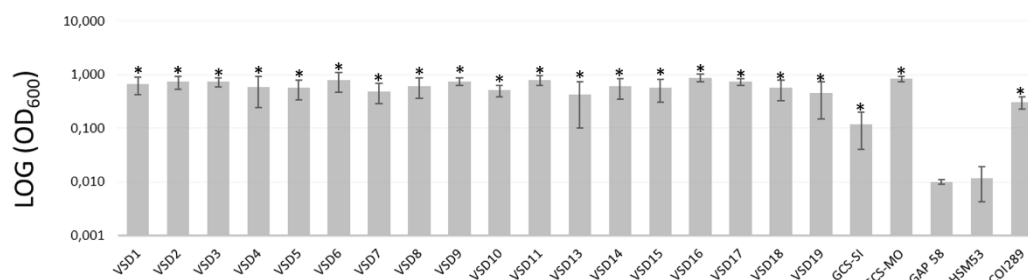
BIOFILM PRODUTION ON POLYSTYRENE
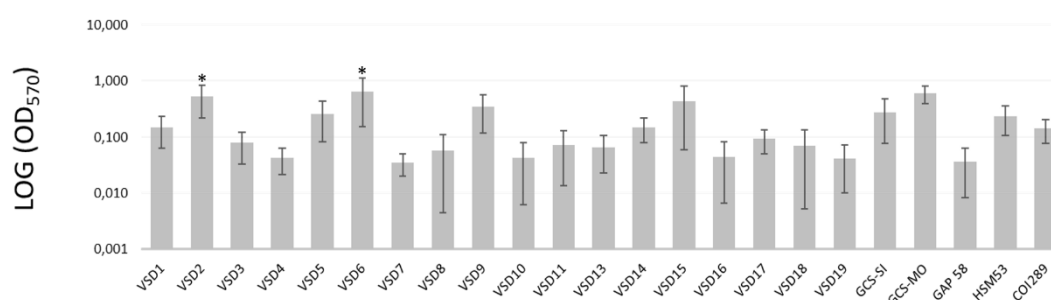
Figure 6.1. Biofilm development on glass (A) and polystyrene (B) surfaces by *Streptococcus dysgalactiae* subsp. *dysgalactiae* (SDSD). VSD1-11 and VSD13-19: SDSD isolates obtained from clinical and subclinical mastitis in cattle. GCS-SI: SDSD isolate associated with an invasive infection of a human host in contact with raw fish. GCS-MO: SDSD associated with bovine cellulitis and toxic shock like syndrome. HSM53: SDSE from human blood. COI289: SDSE from human oropharynx. GAP58: *S. pyogenes* from human blood. Represented values are the mean value with SEM. *p-value < 0.05 for results obtained for VSD strains relative to the SDSE negative control strain (Genteluci *et al.*, 2015).

6.3.2. Characterization of biofilm composition matrix

The biofilm matrix was initially evaluated using CRA Method. After 24 h-incubation, all SDSD isolates were identified as non-producers of extracellular polysaccharide. The biofilm composition was also evaluated by treatment with proteinase K, trypsin, DNase, and sodium metaperiodate. Only proteinase K and trypsin caused a drastic dispersion of the biofilm accumulated, suggesting that the biofilm produced by SDSD isolates on glass surfaces was mainly associated with a proteinaceous extracellular matrix.

6.3.3. SDSD biofilm analysis by fluorescence microscopy, CLSM and SEM

Fluorescence microscopy, CLSM and SEM were used to get further insights into the biofilm structure. SEM has been previously used for studying different biofilm morphologies and structures (Gomes and Mergulhão, 2017; Kostakioti *et al.*, 2013; Parnasa *et al.*, 2016). The results obtained suggest that the biofilms produced by the SDSD isolates VSD9 and VSD10 are different from the biofilm produced by VSD16 isolate (Figures. 6.2, 6.3 and 6.4). Fluorescence microscopy also shows a higher number of dead cells in the biofilm produced by VSD16 (Figure 6.2). Indeed, CLSM results indicate that VSD9 and VSD10 biofilms could cover 90% of the glass (Figure 6.3 A and B), with thickness ranging between 9–12 µm and 8–14 µm, respectively. Furthermore, VSD16 isolate forms several coccoid bacterial aggregates on glass that are denser in the middle, with a thickness of 15 µm (Figure 6.3C). Combining the results of SEM and CLSM images, biofilms produced by VSD9 and VSD10 isolates show a similar structure. However, VSD16 biofilm shows the presence of a massive amount of mucus-like extracellular material masking the cell surface (Figure 6.4). It is possible that this mucous matrix might be formed by extracellular DNA (eDNA) liberated from VSD16 dead cells (visualized with CLSM) or by complexes of eDNA and bacterial proteins, since this matrix was also disrupted by proteinase (Figure 6.2). Biofilms atomic composition is rich in oxygen and carbon (Figure 6.4).
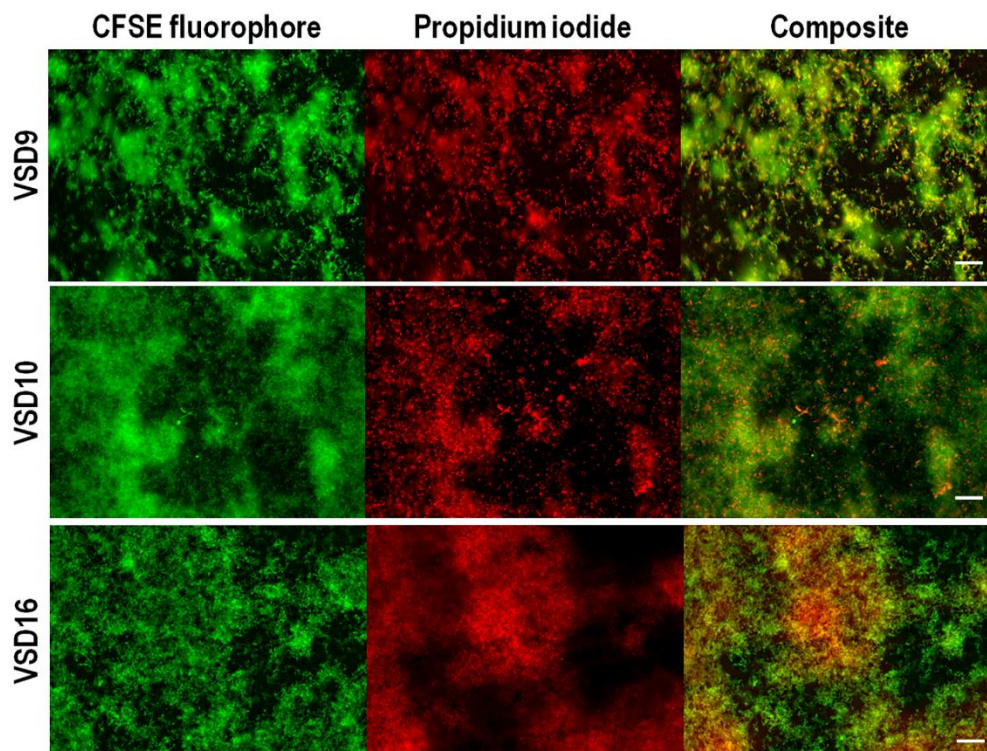
Figure 6.2. LIVE/DEAD fluorescence imaging of **bovine SDSD**. The SDSD isolates were stained with 5(6)-Carboxyfluorescein diacetate N-hydroxysuccinimidyl ester (CFSE) fluorophore and propidium iodide, which promotes intracellular labeling of live (green) or dead cells (red); respectively. The left line images were obtained using a green filter (488 nm) and the middle side images were obtained using a red filter (561 nm). Composite image represents the superposition of images acquired for CFSE fluorophore (live cells) and for propidium iodide (dead cells). scale bars with 20 μm. The amplification used was 400 (For interpretation of the references to colour in this figure legend, the reader is referred to the web version of this article).
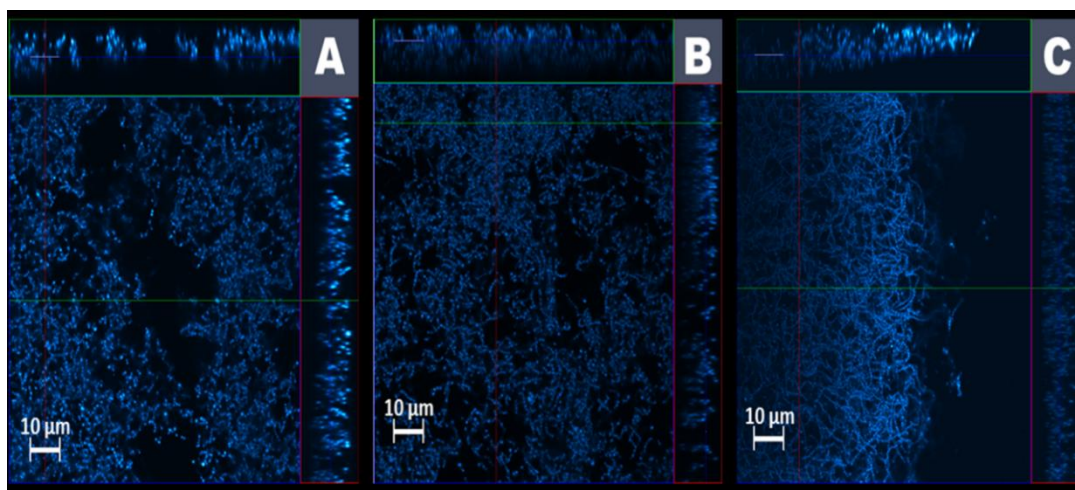
Figure 6.3. Confocal fluorescence microscopy of the biofilms produced by SDSD isolates VSD9 (A), VSD10 (B) and VSD16 (C) on glass. Hoechst 33,258 was used to stain the bacterial nucleic acids (blue). The top and right-side rectangular panels are vertical sections representing the XZ plane and YZ plane, respectively, at the positions indicated by the colored line. The biofilms are 9–12 μm, 8–14 μm, 15 μm thick (i.e. Z-axis) respectively. (For interpretation of the references to colour in this figure legend, the reader is referred to the web version of this article).
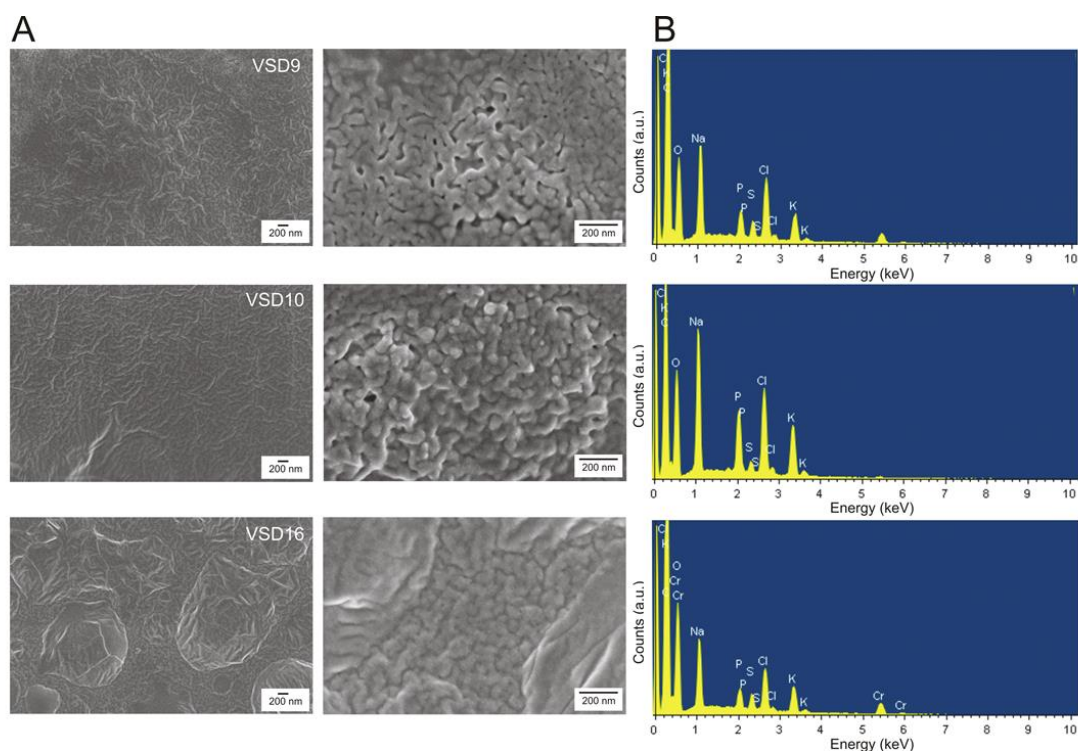
Figure 6.4. (A) Scanning electron microscopy of SDSD isolates VSD9, VSD10 and VSD16. (B) Energy dispersive X-Ray spectroscopy measurements were carried out to compare the elements present at each Biofilm studied.

6.3.4. Inhibition of biofilm formation by Fisetin

The previous demonstration that ellagic acid and fisetin are able to impair biofilm production by Gram-positive bacteria, with a stronger effect for fisetin (Dürig *et al.*, 2010), led us to analyze the effect of this molecule on the biofilm production by SDSD. We found that this compound shows an important inhibitory effect on biofilm developed by VSD1, VSD9 and VSD16 SDSD isolates in a concentration independent manner (Figure 6.5), and that, at the tested concentrations, it is non-toxic for planktonic growth: no difference in the OD value was observed between the growth of control cells (planktonic) and that of the different concentrations of compound. However, macroscopic cell aggregates were formed in the presence of fisetin (32 µg/mL).
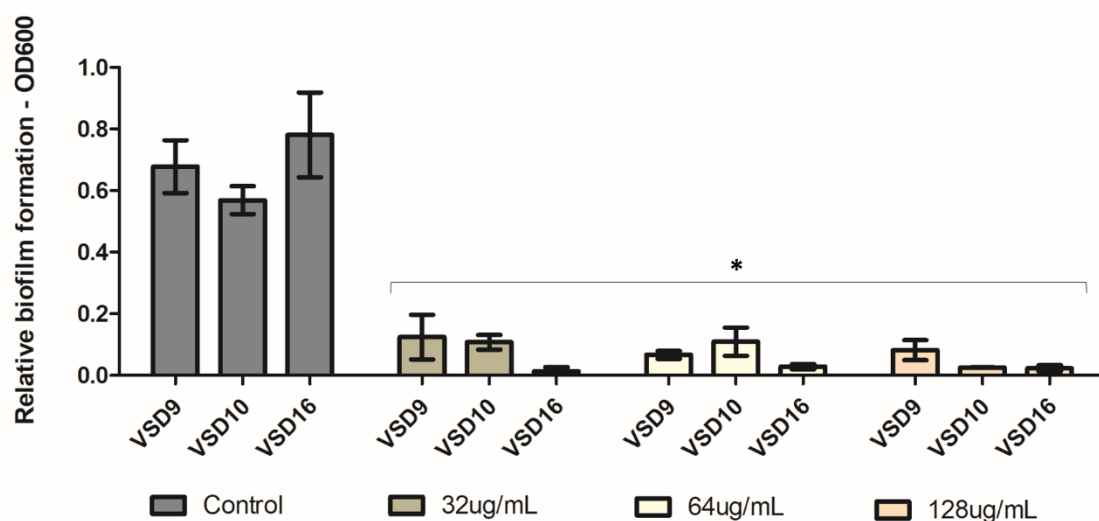
Figure 6.2. Inhibition of biofilm formation/accumulation using fisetin, on glass surface by SDSD isolates VSD9, VSD10 and VSD16. Concentration greater than or equal to 32 μg/mL fisetin resulted in a residual biofilm formation in SDSD compared to the control without Fisetin. Represented values are the mean value with SEM. * p-value < 0.001 for results obtained for the inhibition of biofilm formation by SDSD isolates in the presence of fisetin compared to control (without fisetin).

6.3.5. Detection of *brpA*-like gene in SDSD isolates

Because of the importance of BrpA (LytR) proteins in bacterial biofilm, we assessed the *brpA*-like gene in 20 bovine SDSD isolates and in the two Portuguese SDSE strains (HSM53 and COl 289). The genome sequence of SDSE of Lancefield's group A antigen strain AC-2713 (GenBank access number: NC_019042) was used to design overlapping primers for the 1269 bp *brpA*-like gene. The correct amplification product was detected in all SDSD isolates as well as in both control SDSE strains. RT-PCR allowed to demonstrate that the *brpA*-like gene was transcribed in all the tested SDSD and SDSE isolates. The 16S rRNA gene was used as housekeeping gene.

6.3.6. Reverse transcriptase qPCR

Transcript levels of *brpA*-like were analysed in the biofilms and in the planktonic growth, in the late exponential or stationary phases. This analysis revealed a lower expression of *brpA*-like in biofilm SDSD compared to planktonic in the late exponential phase of growth. The results also showed an increase in the gene expression of VSD9 and VSD16 isolates, during late exponential phase of planktonic growth, when compared to VSD10 isolates. These results are shown in Figure 6.6.
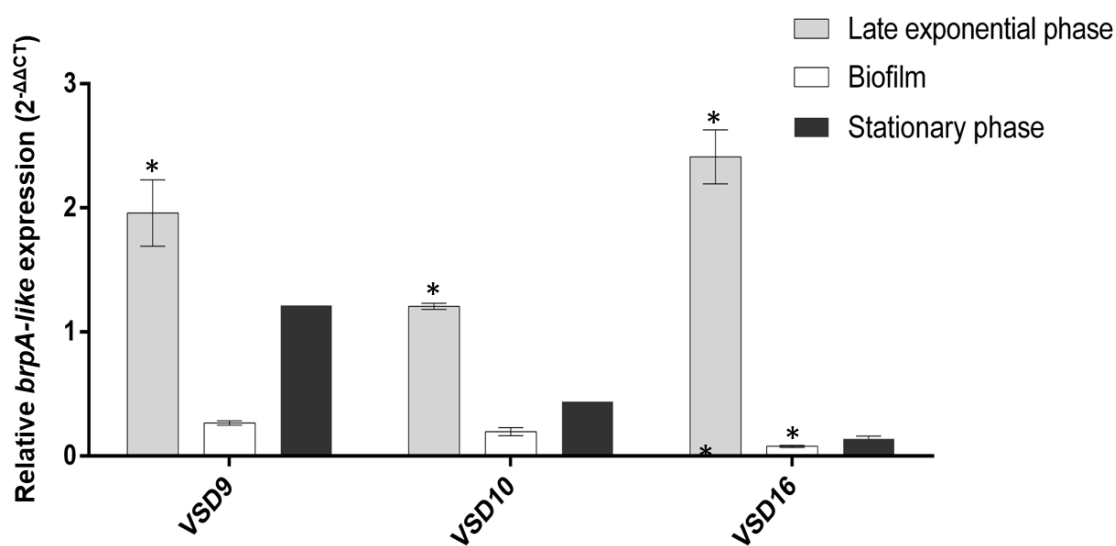
Figure 6.3. Expression levels of brpA-like in SDSD biofilms (white bars), late exponential phase (grey bars) or stationary phase (black) of planktonic growth. The data are expressed as the means with SEM of three biologically independent experiments. *Statistically significant differences ($P < 0.05$) between brpA-like expression in biofilm relative to the late exponential phase of planktonic growth (For interpretation of the references to colour in this figure legend, the reader is referred to the web version of this article).

6.3.7. Primary sequence analysis of BrpA homolog protein

SDSD *brpA*-like *gene* was sequenced by primer walking using specific primers and aligned with the *brpA* (*lytR*) homolog from SDSE to get the complete sequence of this gene. The *brpA*-like gene sequences of SDSD isolates were submitted to GenBank obtaining the following accession numbers: VSD2 (Accession No. KM485638), VSD6 (KM485639), VSD8 (KM485640), VSD9 (KM485641), VSD15 (KM485642), VSD17 (KM485643), VSD19 (KP308400) and GCS-Mo (KM485644). BrpA homolog protein of SDSD is a 45,493 Da protein (422 residues) with a computed pI of 5.1. The calculated instability and aliphatic index suggest that it is thermodynamically stable. According to motif search and cell localization prediction, the BrpA-like protein has an *N*-terminal signal peptide (residues 1–27) for cytoplasm secretion, includes a cell envelope-related transcriptional attenuator domain (residues 81–237), with no transmembrane domain. A highly-disordered region is found in the final *ca* 80 residues of the protein (residues 343–422).

6.3.8. Predicted structure of BrpA homolog protein and putative inhibitors

The three-dimensional structure of BrpA homolog protein of SDSD is essential for understanding its molecular function and the identification of potential lead

molecules for its inhibition. However, a three-dimensional structure of this protein is not yet available, and molecular modeling was used for predicting this structure. The Gbs0355 protein from *Streptococcus agalactiae* (PDB ID: 3OKZ, Northeast Structural Genomics Consortium Target SaR127) has a high sequence identity with BrpA homolog protein (74%) of SDSD and its crystal structure has recently been determined at 2.70 Å resolution. Both Gbs0355 protein and our target protein contain a LytR/CpsA/Psr domain (residues 81–237) and their sequence homology may suggest a common ancestor. Using the ModWeb server (https://modbase.compbio.ucsf.edu/modweb/) (Pieper *et al.*, 2011) and Gbs0355 as a template we predicted the 3-D structure of the 48–342 segment of BrpA homolog protein; the model of the full-length protein could not be attained because the C-terminal region (residues 343 to 422) is highly disordered, with no structural homologs available in the Protein Data Bank (www.rcsb.org). In the obtained model, 99.7% of the residues are in the most favored regions of the Ramachandran plot and the rmsd of the superposition with the template is of 0.287 Å. To identify putative inhibitors of BrpA homolog protein of SDSD, the three-dimensional model was submitted into DrugDiscovery@TACC web portal (https://drugdiscovery.tacc.utexas.edu/), for a virtual screening using AutoDockVina (Trott and Olson, 2010). The snapshot of secondary and three-dimensional model of BrpA protein homolog of SDSD is shown in Figure 6.7.

Considering that ellagic acid and fisetin are known biofilm inhibitors, that our data shows that fisetin strongly impairs SDSD biofilm formation, and that *brpA-like* gene is expressed in SDSD, we became interested in knowing if these two inhibitory substances (ellagic acid and Fisetin) could interact with the BrpA homolog of SDSD and used this information to screen additional biofilm inhibitor candidates.

Out of 194,090 screened compounds from the Zinc Natural compound database (http://zinc.docking.org/) (Irwin and Shoichet, 2005), the top five interacting molecules with BrpA protein homolog of SDSD were chosen and thoroughly analyzed (Table 6.1 and Figure 6.8). Molecular docking results suggest that all five molecules occupy the same binding pocket in SDSD BrpA homolog protein, interacting with the polypeptide chain via hydrogen bonds and hydrophobic contacts. The high docking scores suggest strong binding affinity.
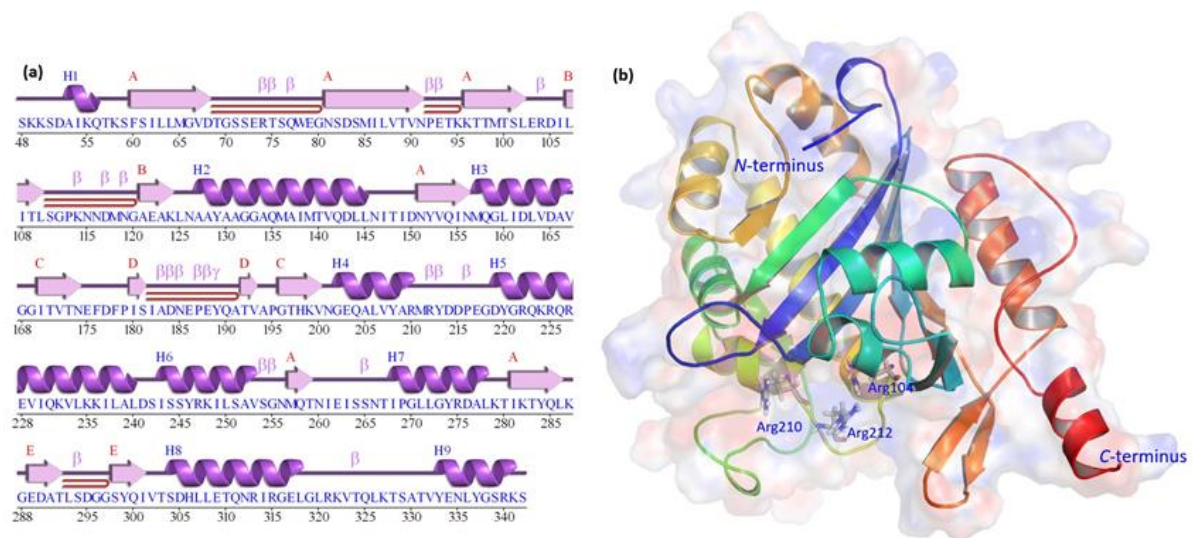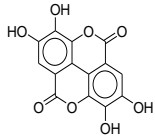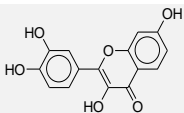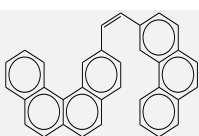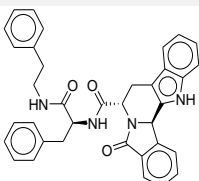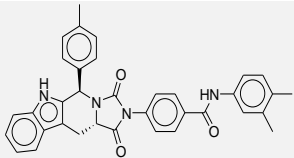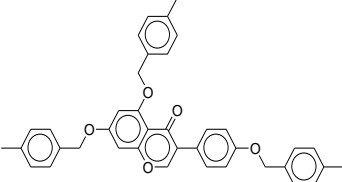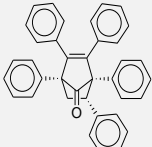
Figure 6.4. Snapshot of (A) secondary structure elements and (B) three-dimensional model of BrpA homolog protein and electrostatic potential. The three-dimensional structure was predicted through homology modeling approach. Crucial substrate binding site residues are shown in sticks.

Table 6.1. Potential inhibitors for biofilm regulatory protein, BrpA protein homolog.

Known Biofilm inhibitors (Dürig et al. 2010)

Zinc Accession Number	Structure	ΔH (kcal/mol)	Ki (nM)
Ellagic acid		-6.8	10400
Fisetin		-7.7	2270

Putative inhibitors obtained from Zinc Database (Irwin and Shoichet 2005)

Zinc Accession Number	Structure	ΔH (kcal/mol)	Ki (nM)
ZINC68569433		-13.7	0.09
ZINC70704696		-13.5	0.13
ZINC70705130		-13.3	0.18
ZINC02666258		-12.9	0.35
ZINC33906294		-12.8	0.41
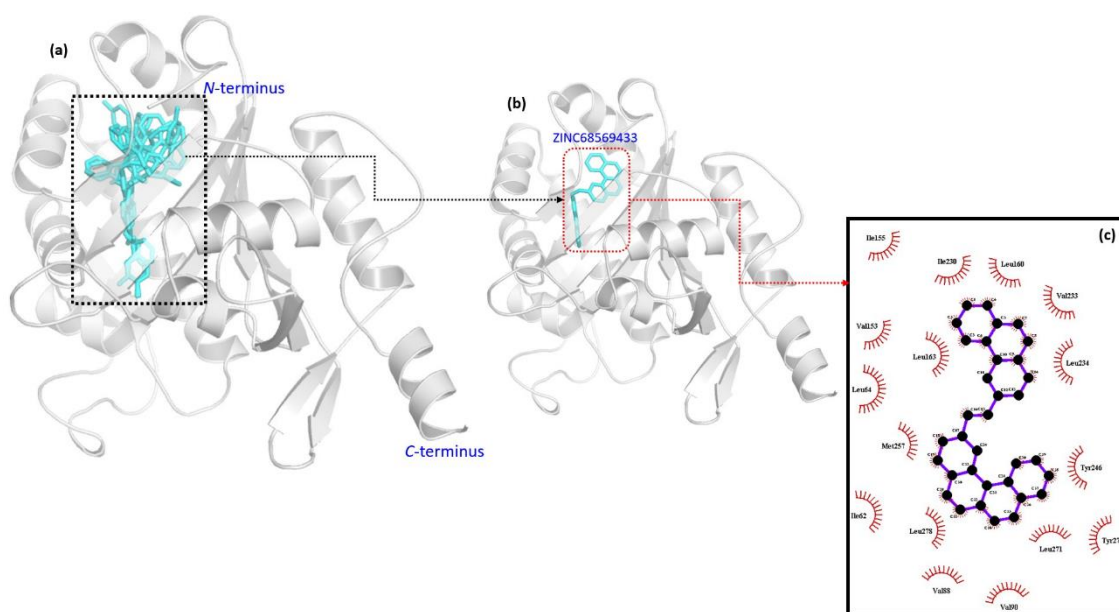
Figure 6.8. (A) Orientation of five putative inhibitors (Source: Zinc database) with BrpA protein homolog (B) Binding conformation of first molecule "ZINC68569433" with BrpA protein homolog (C) Two-dimensional ligand interaction diagram of ZINC68569433 with protein (Source-LigPlot). LigPlot shows the amino acid residues of BrpA protein homolog around the putative inhibitor with hydrophobic contacts.

In comparison with ellagic acid and fisetin (Table 6.1), the proposed five inhibitors show higher binding affinity towards the protein. These highly hydrophobic molecules, rich in aromatic rings, are found in a cleft formed by helices 5 and 7, and, in all five ligand-protein complexes, they are commonly found interacting with Leu64, Leu163, Leu234, Tyr246 amino acid residues. Other hydrophobic residues as Ile62, Leu271 Met257, Ile237, Phe60, Val88, Ile249, Val253, Leu250, and Leu278 are also found to be involved in the same type of interaction, depending on the ligand used for docking. Out of the five molecules, the compound ZINC70704696 is also hydrogen bonded to Tyr246 from an alpha helix at the surface of the protein, putatively stabilizing the ligand in the binding pocket.

6.4.   Discussion

In this study we provide new insights at the molecular level on biofilm development of SDSD. The presented data show for the first time that SDSD isolates accumulate high levels of biofilms on hydrophilic surfaces. The proteinaceous nature of the biofilm matrix was proved by the complete removal of the biologic film after treatment with proteinase. In fact, biofilm production had already been demonstrated in *Streptococcus* spp., including *S. pyogenes* (Young *et al.*, 2016), *S. mutans* (Krzy ciak *et*

al., 2014), *S. agalactiae* (Rosini and Margarit, 2015) and *S. dysgalactiae* subsp. *equisimilis* (Genteluci *et al.*, 2015). Additionally, a hydrophilic biofilm matrix, associated to a fimbriae protein, was recently reported for the SDSD-closely related bacteria, SDSE (Genteluci *et al.*, 2015). The implication of biofilm production in the pathogenesis of different infectious diseases, including bovine mastitis has recurrently been reported (Gomes *et al.*, 2016).

The biofilm development by SDSD isolates was also confirmed by fluorescence microscopy, CLSM and SEM. Under SEM observation, the VSD16 isolate formed cell aggregates in the biofilm growth, while VSD9 and VSD10 developed smooth and filmy layers. In addition, a mucous matrix was visualized for VSD16 suggesting differences in biofilm composition for these isolates. The fact that a higher number of dead cells was visualized in VSD16 biofilm indicate increased eDNA content, which is likely to account for the mucous matrix visualized by SEM in the biofilm formed by this SDSD isolate. The importance of eDNA and bacterial proteins:eDNA complexes as components of the biofilm matrixes is well known (Jakubovics *et al.*, 2013). However, our results showed that DNase treatment (in the concentrations used) was not able to disperse the established biofilms. These findings are in agreement with previous studies in which biofilms containing significant quantities of eDNA could not be dispersed by DNase enzymes (Grande *et al.*, 2011; Shields *et al.*, 2013).

Biofilm formation can be considered as a developmental process, which is characterized by a multiple-step structural changes in biofilm architecture and composition, coordinated by a complex net of regulatory genes and environmental signaling via signal transduction (Donlan, 2001; Donlan and Costerton, 2002). Genes associated with intercellular communication systems, sensing systems, carbohydrate metabolism, and adhesion have been described as important and required for the adaptation of *streptococci* in biofilms (Connolly *et al.*, 2011; Marks *et al.*, 2014a, 2014b; Roberts *et al.*, 2010; Wen and Burne, 2002; Senadheera *et al.*, 2005; Shemesh *et al.*, 2007a, 2007b). Among them *brpA* encoding BrpA regulatory protein has been described as an important regulator of biofilm formation (Bitoun *et al.*, 2012; Chatfield *et al.*, 2005; Wen *et al.*, 2006; Wen and Burne, 2002). Indeed, in *S. mutans*, the *brpA* gene codes for a predicted surface-associated protein with apparent roles in biofilm formation, autolysis, and cell division. Deficiency of BrpA drastically weakens the ability of the deficient mutant to survive to low pH, oxidative challenge and cell envelope stress (Bitoun *et al.*, 2012; Bitoun *et al.*, 2013). *In vitro*, the BrpA-deficient mutant can bind and

establish on a surface, but its ability to accumulate and develop into mature biofilms decreases drastically (Bitoun *et al.*, 2012; Bitoun *et al.*, 2013 Wen *et al.*, 2006).

A *brpA*-like gene was detected and able to be transcribed in all the 20 SDSD isolates. The expression of *brpA*-like gene in SDSD biofilms was compared to late exponential and stationary phase of planktonic growth by reverse transcriptase qPCR. This quantitative analysis revealed lower expression of *brpA*-like in SDSD biofilms compared to late exponential phase of planktonic growth. No significant differences were observed in the expression of *brpA*-like in biofilms compared to stationary phase of planktonic growth. Consistent with the results obtained from biofilm formation on glass, VSD9 and VSD16 isolates showed an increased *brpA*-like expression in the late exponential phase of planktonic growth compared to the VSD10 isolate (Fig. 6.1 A and 6.6). Taken together, our data suggest an important role for the BrpA protein in the initial phase of biofilm formation, with a decreased expression in the mature biofilm. Similar regulation was observed for genes that are involved in the formation of biofilms in *S. pyogenes* (Doern *et al.*, 2009; Reid *et al.*, 2004; Roberts *et al.*, 2010). Due to the inhibition of SDSD biofilm by fisetin, we hypothesized that the inhibitory mechanisms might involve the BrpA homolog. Molecular modeling analysis to predict the 3D structure of BrpA homolog, and a high throughput virtual screening and docking analysis revealed that similarly to fisetin and ellagic acid, the proposed five ligand molecules showed strong binding affinity towards the hydrophobic cleft of the protein.

It is interesting that, in this study, fisetin dramatically inhibited biofilm formation of SDSD isolates, but at the tested concentrations did not affect planktonic growth. Similar results were previously reported for *Staphylococcus aureus* and *Streptococcus dysgalactiae* (Dürig *et al.*, 2010). Taking all together, our data might indicate that inhibition of biofilm formation in SDSD may be mediated by interactions between fisetin and BrpA protein homolog, and this protein might be an important target for the molecular design of antibiofilm drugs. However, further studies should be performed to directly confirm these interactions.

6.5.   Conclusion

The results show for the first time that bovine SDSD can grow forming a biofilm environment, which may be an important factor in the pathogenesis of mastitis. In addition, we show that *brpA*-like gene is present and expressed in SDSD biofilm-producing isolates, and that fisetin dramatically inhibited biofilm formation of SDSD

isolates but at the tested concentrations did not affect planktonic growth. Taken together, our data suggest an important role for the *brpA*-like gene in biofilm formation. Finally, homology modelling and docking analysis selected potential lead inhibitors candidates of BrpA protein homolog. However, further investigations are necessary to better understand the role of BrpA homolog in the regulation of biofilm associated genes.

Author Contributions

CA-B contributed to all-experimental work, performed the statistical analysis and manuscript writing. CA-B and MG contributed to Biofilm formation assay on glass and polystyrene TS-S, NB and JM contributed to sequence analysis of the BrpA homolog protein using Bioinformatics tools and Protein structure prediction and identification of putative inhibitors for BrpA homolog. CA-B, CR-R, EF and DN contributed to analysis of the biofilm structure using fluorescence microscopy, CLSM and SEM. IS-S, BF-C and ARF contributed to the idea or design of the research. The author of this thesis opted for reproduction of the resulting scientific paper, thus apologizing for any repeated content in different contexts of the document.

Chapter 7 - Assessing *in vivo* and *in vitro* biofilm development by *Streptococcus dysgalactiae* subsp. *dysgalactiae* using a murine model of catheter-associated biofilm and human keratinocyte cell

Alves-Barroco, C., Botelho, A.M.N, Américo, M.A, Fracalanzza, S,E., de Matos, A.P.A., Guimaraes, M.A., Ferreira-Carvalho, B.T, Figueiredo, AMS, Fernandes, A.R.

Abstract

In this work, we investigated the capability of bovine SDSD to develop biofilm *in vivo* using a murine animal model and in vitro on HEK cells. Bovine SDSD isolates were selected based on their ability to form weak, moderate, or strong biofilms on glass surfaces. Our results showed that bovine SDSD isolates have an increased ability to form biofilm on catheter surfaces implanted in mice when compared to *in vitro* on abiotic surface. Besides that, *in vitro* scanning electron microscopy demonstrated that SDSD biofilm development is visible after 4 hours of SDSD adhesion to HEK cells. Cell viability tests showed a reduction in the number of HEK cells after the formation of SDSD biofilms.

In addition, an increased biofilm accumulation on glass surfaces was observed after animal passage. In this study, gene expression of *brpA*-like (biofilm regulatory protein) and *fbpA* (fibronectin-binding protein A), *htrA* (serine protease), and *sagA* (streptolysin S precursor) were higher *in vivo* than *in vitro* grown, suggesting a potential role for these virulence genes in the biofilm-development by bovine SDSD.

Taken together, these results demonstrate that SDSD can develop biofilms *in vivo* and on the surface of HEK cells causing important cellular damages. As human SDSD infections are consider zoonotic diseases, our data contribute to a better understanding of the role of biofilm accumulation during SDSD colonization and pathogenesis not only in bovine mastitis; they shed some lights on the mechanisms of prothesis-associated infection and cellulitis caused by SDSD in humans, as well.

7.1. Introduction

It is well known that biofilm is an important mechanism on the pathogenesis of medical device-associated infections, such as orthopedic prostheses (Ronin *et al.*, 2022). Biofilms play an essential role in bacterial pathogenesis, promoting persistent infections and contributing to therapy failure. Biofilm formation involves various phases, including adhesion of the bacterial cells to the biotic surfaces, in which diverse bacterial factors are involved (Kumar *et al.*, 2017; Jamal *et al.*, 2018). The great majority of the studies on bacterial biofilms have been based on *in vitro* growth on abiotic surfaces, which might be relevant for pathogens that grow on pacemakers, catheters, protheses and other implantable medical devices, increasing the risk of infections in hospital environments. Despite that, most bacterial host infections require biofilm formation on biotic surfaces as the initial stage of colonization or infection (Chao *et al.*, 2017). Additionally, host microenvironments, especially plasma proteins, are important for bacterial adherence to biotic or abiotic surfaces and for biofilm development during the process of a natural infection (Speziale *et al.*, 2014). Therefore, *in vivo* models are important to gain a better understanding of the mechanisms involved in the development biofilms and associated diseases.

The ability of bovine SDSD to form biofilms on abiotic surfaces was recently reported (Chapter 6). The biofilm formation by SDSD isolates was also confirmed by confocal laser scanning microscopy, transmission electronic microscopy and scanning electron microscopy (Chapter 6). We also show for the first time that bovine SDSD can adhere and internalize human cells, including human epidermal keratinocytes (HEK) cells. Notably, the adherence and internalization rates of bovine SDSD isolates in HEK are higher than those of human *S. pyogenes* and SDSD DB49998-05 (GCS-Si) isolates (Roma-Rodrigues *et al.* 2016). Besides that, there are histological evidences that bovine SDSD is able to cause invasive infections in a zebrafish model leading to morbidity and mortality (Chapter 4).

Animal models have extensively been used to investigate microbial pathogenesis and host response, allowing the analysis of the host-pathogen interactions. Despite all ethical questions, there is no real alternative to animal models in the study of interactive dynamics. Additionally, animal models have proved to be very useful providing excellent results in studies aimed at the development of new antibacterial agents and alternative therapies (Iii *et al.*, 2003; Proetzel and Wiles 2010; Cusumano *et al.*, 2014).

The ability of bovine SDSD to form biofilms *in vivo* has not yet been reported. Consequently, it is unclear whether the ability to form biofilms facilitates colonization on biotic and abiotic surfaces, bacterial persistence and whether it supports the dissemination of virulent clones.

In the present study, our main goal was to assess SDSD ability to form biofilm *in vivo* using a foreign-body animal model. Additionally, we compare *in vivo* and *in vitro* biofilm developments by bovine SDSD isolates. We also investigated the capability of bovine SDSD isolates to develop biofilm on human keratinocytes cells, since this bacterium can zoonotically infect humans causing, for example, cellulitis (Chennapragada *et al.*, 2018). Finally, the expression profile of genes associated with virulence, including biofilm development and modulation, in other streptococci was analyzed both *in vivo* and *in vitro* to gain some insights on biofilm formation by bovine SDSD*.*

7.2. Materials and methods

The animal experimentation was approved by the ethics committee on the use of animals from Centro de Ciências da Saúde, Universidade Federal do Rio de Janeiro, Brazil (#01200.001568/2013-87- CEAU).

7.2.1. Biofilm formation assay on abiotic surfaces

The ability to form biofilms by 37 SDSD isolates from bovine clinical mastitis obtained between 2011 and 2013 [collection II, (Chapter 2)] was evaluated on polystyrene and glass surface following described protocol in Chapter 6. For a comparative analysis, 18 SDSD isolates from bovine clinical mastitis [collection I, Chapter 6], collected between 2002 and 2003, were included in the study.

7.2.2. SDSD biofilm formation in human keratinocytes cells

This assay was based on previously described protocols (Roma-Rodrigues *et al.*, 2015) with few modifications. Bacteria were grown at 37 °C in Todd Hewitt broth (THB; Oxoid; Basingstoke, UK) supplemented with 0.5% (w/v) yeast extract until the middle exponential growth phase. The infection was started by adding bacterial suspension (containing 10^6 bacterial cells) in Dulbecco's Modified Eagle's Medium supplemented

(DMEM; ThermoFisher Scientific; Waltham, MA, USA) with 10% (v/v) Fetal Bovine Serum (ThermoFisher Scientific) to 10^4 human epithelial keratinocytes (HEK) cells (ATCC-PCS-200-010, ATCC, Manassas, VA, USA). The infected culture was incubated at 37 °C, 5% (v/v) CO_2, and 99% relative humidity. After 2 h and 4 h of incubation, HEK cells were washed with Phosphate Buffer saline (PBS, 137 mM NaCl, 2.7 mM KCl, 10 mM Na_2HPO_4, and 1.8 mM KH_2PO_4, pH 7.4) (Sigma-Aldrich, St. Louis, MO, USA) to remove non-adhered bacteria and then fixed with 2% (v/v) glutaraldehyde (Sigma-Aldrich) in PBS for 2 h at room temperature. The HEK cells were washed with PBS (three times), post-fixed wwith 1.0% (w/v) osmium tetroxide (Sigma-Aldrich) at 4 C for 1 h, and then processed as previously described (García-Pérez *et al.*, 2003). The infected HEK cells were visualized using a scanning electron microscope (JEOL JSM-5400).

Viability of HEK cells was determined using 3-(4,5-dimethylthiazol-2-yl)-5-(3-carboxymethoxyphenyl)-2-(4-sulfophenyl)-2Htetrazolium, inner salt (MTS) assay as previously described (Fernandes *et al.*, 2017). HEK cells were seeded in 96-well plates (ThermoFisher Scientific) and grown at 37 °C, 5% (v/v) CO_2, and 99% relative humidity for 24 h, before incubations in the same conditions for 2 h, 4 h, and 6 h with SDSD cells or bacterial growth supernatant. After the incubation period, the culture medium was removed and, after washing of HEK cells with PBS, replaced by a fresh medium containing 10% MTS reagent (ThermoFisher Scientific). The 96 well plate was incubated at 37 °C, in the same atmosphere, for 60 min. The absorbance (Abs) was measured in a microplate reader at 490 nm (Infinite M200, Tecan, Männedorf, Switzerland). The following equation was applied: cell viability (%) = 100 x [mean Abs of SDSD cells (or mean Abs bacterial growth supernatant)/mean Abs of control group without SDSD cells or bacterial growth supernatant].

7.2.3. *In vitro* biofilm formation on the surface of an intravenous catheter segment

Exponentially growing SDSD isolates in TSB supplemented with 0.5 % (w/v) glucose were harvested by centrifugation and diluted in the fresh broth. A volume of 10 µL [containing 10^4 colony forming units (CFU)] was injected into the lumen of polyurethane catheter with 1 cm segment (C-953-J-UDLM; Cook Inc., Bloomington, IN, USA). Then, the catheter was placed into the well of a 24-well plate and incubated for 72 h. To count the SDSD cells adhered, the catheter was washed with PBS twice to remove non-adherent bacteria and placed in fresh broth. After sonication (15 min; 38.5–

40.5 kHz, in ice), the CFU/mL was determined using THA. Biofilm was assessed by counting the SDSD cells adhering to the catheter.

7.2.4. *In vivo* biofilm formation

The *in vivo* assays using a mouse foreign-body model were performed as described in Genteluci *et al.*, 2015. Briefly, young adult BALB/c mice (age between 8 to 10 weeks) were anesthetized, and a subcutaneous incision was created to introduce an intravenous polyurethane catheter (with 1 cm) with 10 µL volume of bacterial suspension (with 10^6 CFU). The catheter was implanted subcutaneously (at least 1.5 cm from the incision). after 72 hours of infection, the animals were euthanized, and the catheter segments were removed. After that, the catheter segments were washed with 0.15 M NaCl to remove any planktonic bacteria and placed in a tube containing 1 mL saline. After sonication (15 min, 38.5–40.5 kHz, in ice), CFU/mL was determined using THA. Biofilm was assessed by counting the SDSD cells adhering to the catheter.

In order to investigate whether animal passage can increase the ability of SDSD to accumulate biofilms *in vitro,* the cells collected from the catheter implanted in the mice were inoculated in TSB containing 0.5% (w/v) glucose at 37 °C for 18 h. Then, aliquots (with and without animal passage) were obtained to assess biofilm formation on glass surface following the protocol described in Chapter 6.

7.2.5. Reverse transcription quantitative PCR (RT-qPCR)

Expression levels of genes associated with biofilm formation were evaluated *in vivo* and *in vitro*. RNA was extracted using NucleoSpin RNAII kit (Macherey-Nagel, Dueren, Germany) according to the manufacturer's instructions to comparatively evaluate the transcription of the *brpA-like* (biofilm regulatory protein) and *fbpA* (fibronectin-binding protein A), *htrA* (serine protease), and *sagA* (streptolysin S). The cDNA was synthesized from 100 ng of total RNA using the SuperScript first-strand synthesis system (Invitrogen) according to the manufacturer's instructions. The RT-qPCR reaction mixture (20 µL) contained NZY qPCR Green Master Mix (NZYTech, Lisbon, Portugal), 1 µL cDNA, and 0.5 µM of the Forward and Reverse primers described in Table S2, Appendix I. PCR conditions included an initial denaturation at 95 °C for 10 min, followed by 30 cycles of amplification consisting of denaturation at 95 °C for 15 s, and annealing at 58 °C for 30 s and extension at 60 °C for 45 s. All primer pairs were checked for primer-dimer formation using the dissociation curve analysis. The critical

Ct was defined as the cycle in which fluorescence becomes detectable above the background fluorescence. The expression levels were normalized using the 16S rRNA gene as an internal standard. Each assay was performed with at least three independent RNA samples.

7.2.6.   Statistical analysis

GraphPad Prism version 7.0 was used for statistical analysis. All data were expressed as mean ± SEM from at least three independent experiments. The statistical significance was determined for each data set using the student's t-test, and statistical significance was considered when $p < 0.05$. For comparison purposes, biofilm developments between SDSD isolates recovered from catheter implanted in mice (*in vivo*) and in *vitro* were both measured by CFUs. In the case of biofilm developments by bovine SDSD on glass surfaces before and after animal passage, biofilm growth was measured by ODs.

7.3.   Result and discussion

7.3.1. Biofilm formation assay on abiotic surfaces

As a first approach, first approach, the ability of 37 bovine SDSD isolates (collection II) to form biofilms on glass and polystyrene surfaces was evaluated. For a comparative analysis, the results obtained for 18 bovine SDSD isolates (collection I), shown in in Chapter 6, were included in the study. Overall, despite some differences, the results obtained point to a high *in vitro* biofilm-forming ability by most SDSD isolates with isolates from the collection II showing a greater ability to accumulate biofilms than those from the collection I (Figure 7.1).
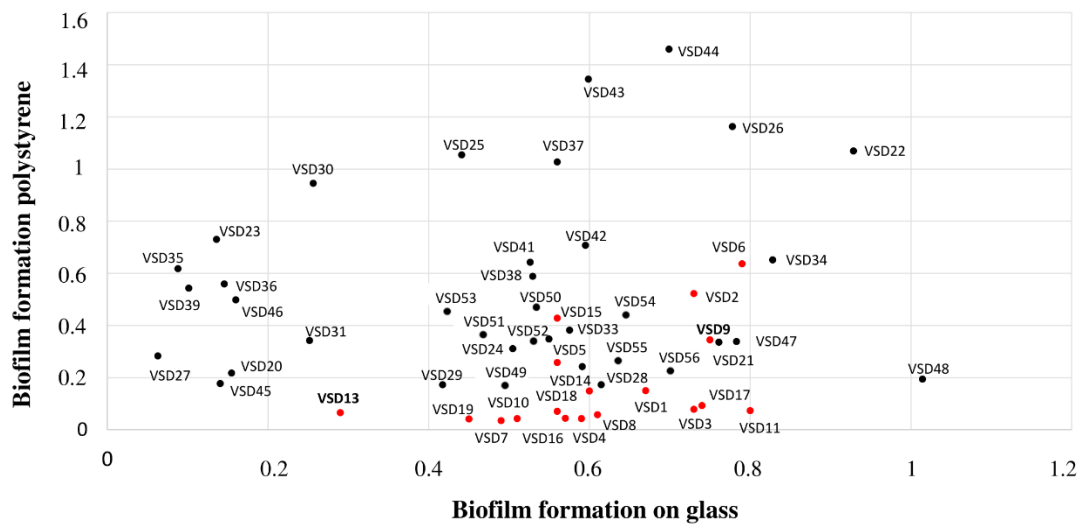
Figure 7.1. Comparison of the *in vitro* ability to form biofilms on abiotic surfaces by bovine SDSD isolates of clinical and subclinical mastitis in Portugal during 2002-03 (collection I, red circles) and 2011-13 (collection II, black circles). Interpretation criteria for biofilm formation on polystyrene surface: i) non-producer OD $\leq$ OD$_{ctrl}$; ii) weak producer OD$_{ctrl}$ < OD $\leq$ 2 OD$_{ctrl}$; iii) moderate producer 2 OD$_{ctrl}$ < OD $\leq$ 4 OD$_{ctrl}$ and iv) strong producer OD > 4 OD$_{ctrl}$. Interpretation criteria for *in vitro* biofilm formation on glass surface: i) non-producer OD$_{600}$ $\leq$ 0.099; ii) weak producer OD$_{600}$ between 0.1–0.299, weak; iii) moderate producer OD$_{600}$ between 0.3–0.599, and iv) strong producer OD$_{600}$>0.600.

7.3.2. SDSD biofilm formation in human keratinocytes cells

HEK cells have an important role in host defense, providing a physical and immunological barrier against pathogenic bacteria. The invasion and/or adherence to HEK cells of Group G streptococci was associated with the severity of skin infections, e.g., necrotizing fasciitis (Siemens *et al.*, 2015). We previously reported for the first time that bovine SDSD isolates are capable to adhere and internalize several human cells, including HEK cells (Alves-Barroco *et al.*, 2018; Roma-Rodrigues *et al.*, 2016). Here, the ability of bovine SDSD to form biofilms on HEK cells was analyzed by scanning electron microscope (Figure 7.2). Our results demonstrated the formation of an extracellular polymeric matrix by growing SDSD biofilms after 2 h of infection of HEK cells (Figure 7.2A). After 4 h of infection, it was possible to visualize a typical biofilm architecture (Figure 7.2B).

Similar results were observed by Matsue and co-workers in investigations with other streptococci. They showed that after 2 h incubation of HEK cells with SDSE, the percentage of adhered bacterial was on average 70%. Furthermore, the adherence of SDSE on HEK cells increased by about 10 times higher than that on polystyrene surfaces (Matsue *et al.*, 2020). Previous studies have also shown the formation of biofilms by *S.*

pyogenes in HEK cells. Visually, *S. pyogenes* biofilms formed on HEK cells were similar to biofilms on abiotic surfaces; however, *S. pyogenes* biofilms on HEK cells were more resistant to antimicrobial therapy (Marks *et al.*, 2014). Marks and co-workers demonstrated that during coculture, the *S. pyogenes* biofilm extended about 20–30 μm above the HEK cells; however, *S. pyogenes* biofilms did not induce the death of HEK cells since the keratinocytes layer remained intact during the experiment (Marks *et al.*, 2014). On the contrary to the observed for *S. pyogenes* (Marks *et al.*, 2014), SDSD biofilm seems to induce a decline in viability of the HEK cells over time (Figure 7.3). After 6 h incubation with SDSD VSD13 biofilm or supernatants from the bacterial growth, the viability of HEK cells was 32% and 86%, respectively. Our results also showed that the formation of biofilms on the HEK cells monolayer exhibited greater cytotoxicity than extracellular products from bacterial growth (Figure 7.3). Our data corroborate with the ability of SDSD to cause skin/soft skin infections, suggesting that it might be an important mechanism in the pathogenesis of human cellulitis caused by SDSD (Koh *et al.* 2009, Park *et al.*, 2012).
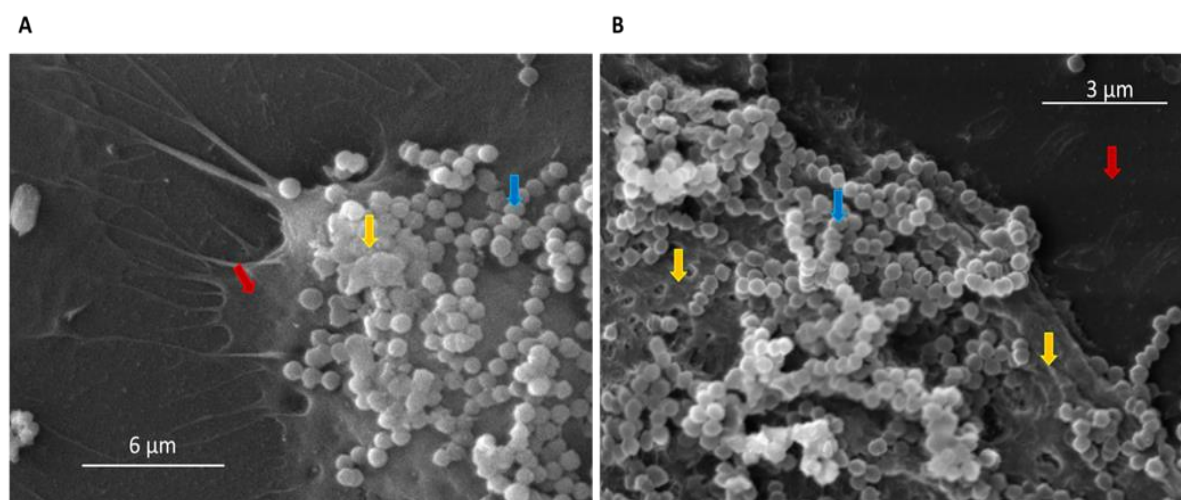
Figure 7.2. Scanning electron microscopy (SEM) of SDSD biofilms formed by VSD13 strain after (A) 2 h and (B) 4 h on human keratinocytes cells. Blue arrow: SDSD VSD13 cells; yellow arrow: Formation of the extracellular polymeric matrix; red arrow: human keratinocytes cells.
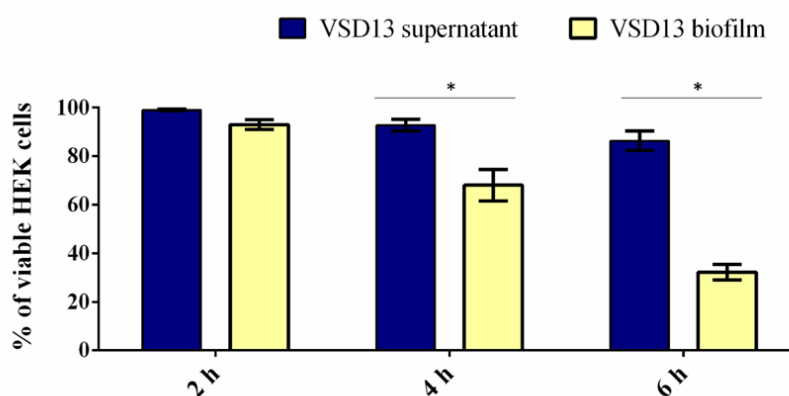
Figure 7.3. Viability of HEK cells exposure to SDSD VSD13 cells or bacterial supernatants for 2 h, 4 h and 6 h. The following equation was applied: cell viability (%) = 100 x [mean Abs SDSD cells (or mean Abs bacterial growth supernatant) /mean Abs control group]. Data are the average of at least three independent (biological) assays with three technical replicates each. Error bars correspondent to standard deviation. Statistically significant differences were observed in the viability of HEK cells exposure to SDSD VSD13 cells and bacterial supernatants at 4 h and 6 h, * $p < 0.05$.

Together, the results suggest an important role for the formation of biofilms by bovine SDSD on human keratinocytes cells, which may contribute to the development of deeper tissue infections and dissemination. In fact, in the last years, the association of SDSD with human infections such as cellulitis has been reported (Chennapragada *et al.*, 2018; Nathan *et al.*, 2021), and one case of cellulitis rapidly evolved into septic shock (Nathan *et al.*, 2021).

7.3.3. *In vivo* biofilm formation

To reduce the number of sacrificed animals and to compare *in vivo* and *in vitro* biofilm formation and accumulation, bovine SDSD isolates were selected based on their *in vitro* ability to form strong (n=2; isolates VSD9 and VSD22; collection I and II, respectively), moderate (n=1; isolate VSD16), or weak (n=2; isolates VSD13 and VSD45; collection I and II, respectively) biofilms on the glass surface. All bovine SDSD isolates tested, including the weak biofilm producers *in vitro*, were able to develop biofilm *in vivo* (Figure 4).

The results showed an important increased ability to develop biofilm on catheter implanted in mice compared with the respective biofilm formed *in vitro*, except for bovine SDSD isolate VSD22, which already produced a very strong biofilm *in vitro*. Overall, the results suggest that the capability of bovine SDSD to develop strong biofilm

in vivo is independent of the ability to form biofilms *in vitro* on the abiotic surface. A possible limitation of this study is the fact that we used a collection of SDSD isolates from 2002 to 2013. However, it is important to emphasize that our results were not influenced by the period of collection of SDSD, being similar for the isolates obtained in 2002-2003 or 2011-2013. Indeed, our data contribute for understanding the pathogenic mechanisms of diseases not only in animals but also in humans, such as cellulitis and prosthetic join infection that happened during these periods (Koh *et al.*, 2009; Park *et al.*, 2012).

The CFU/mL varied from 9.8×10^3 to 4.0×10^7 for VSD9 isolate, from 8.0×10^3 to 7.8×10^6 for VSD13 isolate, from 1.8×10^3 to 3.4×10^6 for VSD16 isolate, and from 7.4×10^4 to 6.4×10^6 in VSD45 isolate. Moreover, an increased ability (approx. 2.2 times) to form biofilm *in vitro* (glass surface) after animal passage was observed for the SDSD isolate VSD45 (weak biofilm producer *in vitro*, Figure 7.5).
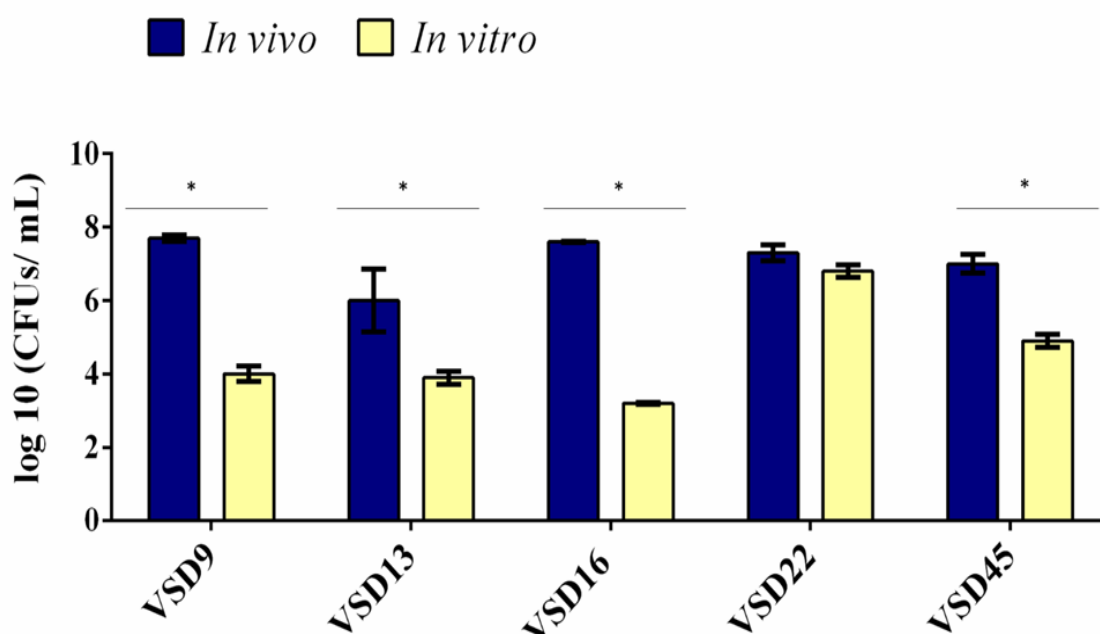
Figure 7.4. Comparison of biofilm development by bovine SDSD isolates recovered from catheter implanted in mice and by the *in vitro* assay. Statistically significant differences were observed the formation of biofilms *in vivo* and *in vitro*, * $p < 0.05$.
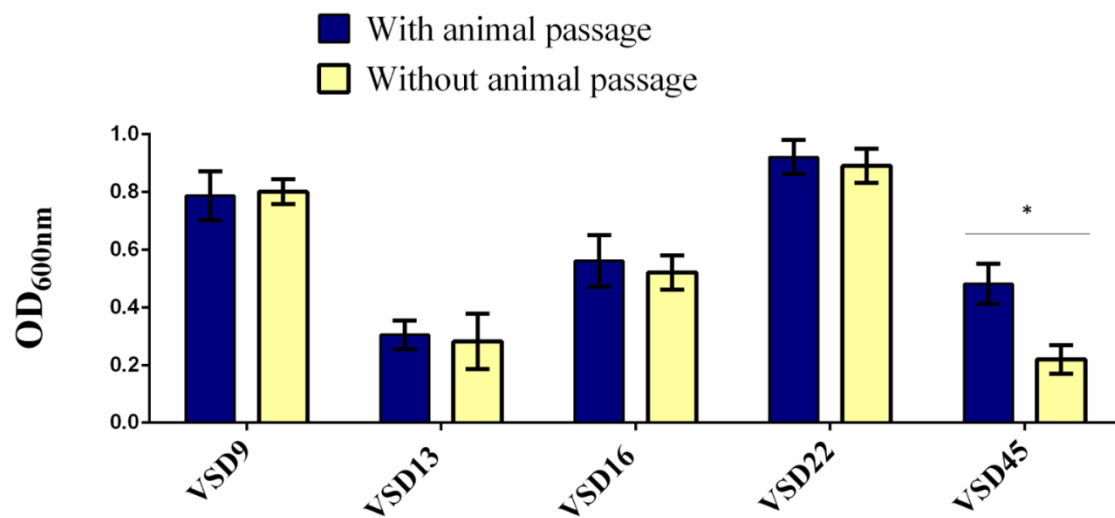
Figure 7.5. Comparison of biofilm development by bovine SDSD isolates recovered from catheter implanted in mice and by the *in vitro* assay. Statistically significant differences were observed in the formation of biofilms after animal passage, * *p* < 0.05.

The foreign-body mouse model used in the present work has also been successfully applied in previous studies with different bacterial species to analyze the ability of bacteria to form biofilms (Ferreira *et al.*, 2012; Marks *et al.*, 2014; Genteluci *et al.*, 2015). Genteluci and co-workers showed that SDSE isolates from humans can form biofilms *in vivo*, regardless of their ability to form biofilms *in vitro*. Marks and co-workers showed that *S. pyogenes* non-biofilm producers on abiotic surfaces produced biofilms on epithelial cells with characteristics similar to an *in vivo* colonization. The *S. pyogenes* biofilm showed a 100-fold higher bacterial burden in nasal-associated lymphoid tissue of mice than in broth-grown bacteria. The study also showed that *S. pyogenes* was naturally transformable when grown in biofilms *in vivo* (Marks *et al.*, 2014).

Taking all these data together, it can be concluded that *in vivo* growth increases the bacterial ability to form biofilms, possibly reflecting an important impact in the course of some streptococci infections, including those associated with bovine SDSD.

7.3.4. Analysis of the expression of genes associated with the formation of biofilms

In vivo colonization by the pyogenic streptococci group requires a series of interactions between the pathogen and host, involving differential gene expression in both pathogen and host (Alves-Barroco *et al.*, 2020). Our data revealed that *in vivo*, a

similar number of sessile cells were recovered from SDSD isolates previous classified as weak and strong biofilm producers *in vitro*. This difference might be explained by changes in gene expression profiles associated with the regulation of biofilm formation (Marks *et al.* 2014). To test this hypothesis, we compared the expression of some biofilm-associated genes in biofilm cells grown *in vivo* and *in vitro* among the SDSD isolates, except VSD22 since no difference was observed between *in vivo* and in *vitro* biofilm formation. Indeed, a remarkably increased expression was observed for the genes *brpA*-like (biofilm regulatory protein) and *fbpA* (fibronectin-binding protein A) in bacterial biofilm collected from catheters recovered from mice model (Figure 7.6A and 7.6B). The *brpA-like* was upregulated ~182, 112, 335, and 144-fold for VSD9, VSD13, VAS16 and VSD45 respectively, while *fbpA* was upregulated ~369, 822, 1419, and 708-fold for VSD9, VSD13, VAS16 and VSD45 respectively. The mRNA expression of *htrA* (serine protease) was more dramatically increased for SDSD VSD9 (796-fold) and VSD13 (1441-fold) isolates, and mRNA expression of *sagA* (streptolysin S percussor) for SDSD VSD13 isolate (~9.8-fold) (Figure 7.6C and 7.6D).

The role of the biofilm regulatory protein A (BrpA) in autolysis and cell division of the *Streptococcus mutans* has been shown. *In vitro*, the BrpA-deficient mutant of *S. mutans* maintained its adherence property, but the ability to form biofilms was considerably affected. Additionally, the deficiency of BrpA impaired cell envelope stress responses and acid and oxidative stress tolerance. (Bitoun *et al.*, 2012, 2014). The biofilm-producing SDSD isolates carry a *brpA*-like gene, which expression level was associated with the ability to form biofilms *in vitro* (Chapter 6). Therefore, our data showing a parallel increase of biofilm accumulation and *brpA*-like gene expression in the *in vivo* model corroborate a role played by this gene in the development of biofilm by SDSD.
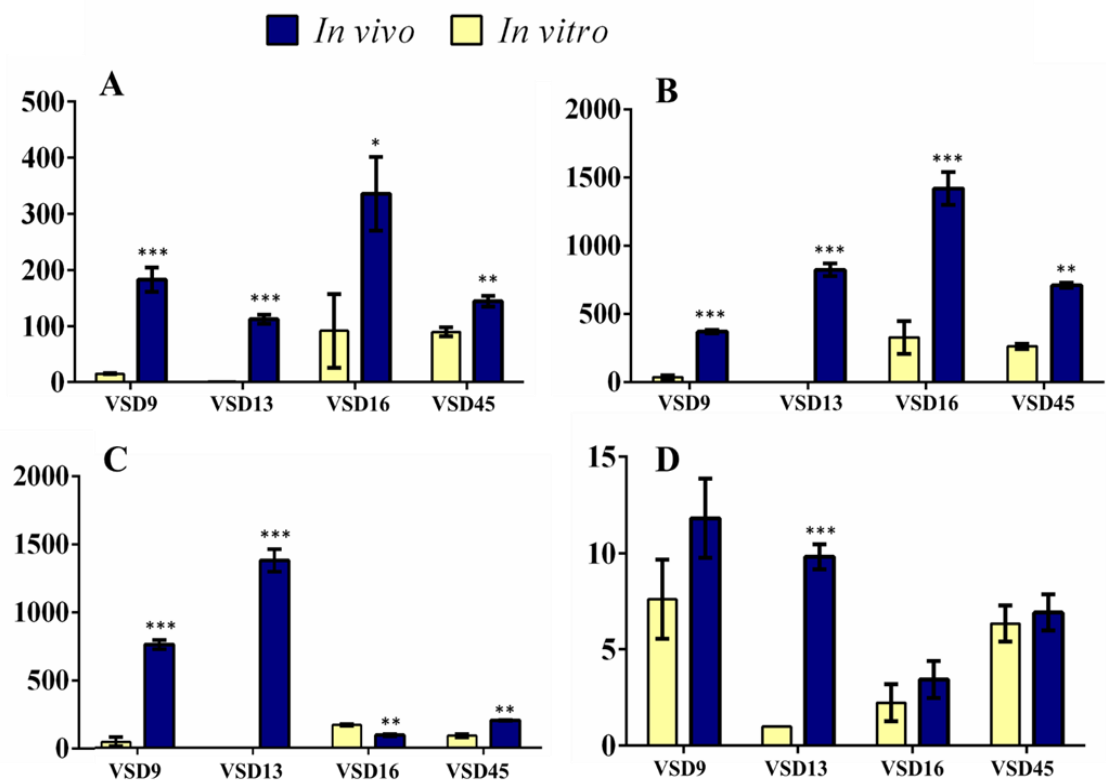
Figure 7.6. Relative expression levels of (A) *brpA*-like (B) *fbpA* (C) *htrA* and (D) *sagA* in sessile cells generated *in vivo* compared with those formed *in vitro*. RT-qPCR was expressed as the mean of three biologically independent experiments. The bar represents the standard deviation. The calibration sample was the cDNA for VSD13 biofilm grown *in vitro*. Statistically significant differences were observed for gene expression in SDSD biofilm grown *in vivo* or *in vitro*: * p < 0.05; ** p < 0.01; *** p < 0.001.

Studies estimated that initial adherence to host cells is mainly mediated by adhesins, such as fibronectin-binding proteins that allow adherence to providing the biofilm formation in host tissues and/or promoting the internalization of bacteria (Cue *et al.*, 2000; Šmitran *et al.*, 2018). Several fibronectin-binding proteins are expressed by *S. dysgalactiae*, with different binding affinities and properties. For some strains, the fibronectin-binding proteins have an affinity to soluble fibronectin, whereas other strains require immobilized fibronectin (Alves-Barroco *et al.*, 2020a). These proteins provide adherence to human cells such as fibroblasts and keratinocytes cells, contributing to biofilm development *in vivo* and consequently to persistent infections (Brandt and Spellerberg, 2009; Collin and Olsén, 2003). In this work, we observed an increased expression of fibronectin-binding protein A (*fbpA*) gene for sessile cells of bovine SDSD grown *in vivo* compared with *in vitro* (Figure 7.6B). These results corroborate studies showing the important role of fibronectin-binding proteins in biofilm formation (Brandt and Spellerberg, 2009, O'Neill *et al.*, 2009).

The high temperature requirement protein A (HtrA, also known as DegP) is a serine protease widely distributed among streptococci (Alves-Barroco *et al.*, 2020). Homologs of the HtrA protein have been identified in several Gram-positive isolates that degrade abnormal proteins in response to adverse environmental conditions (Kim and Kim, 2005). In *Streptococcus mutans*, the deletion of *htrA* gene causes decreased ability to tolerate environmental stresses (Diaz-Torres and Russell, 2001), and in *S. pyogenes*, the expression of virulence determinants was affected (Lyon and Caparon, 2004). In addition to the proteolytic properties, this enzyme is capable to adherer to the extracellular matrix of host tissues (Lyon and Caparon, 2004; Kim and Kim, 2005). Herein, differential expression of the *htrA* gene was observed between *in vitro* and *in vivo* biofilms. Isolates VSD9, VSD13 and VSD45 exhibited an increased *htrA* gene expression *in vivo* (Figure 7.6C). Interestingly, VSD16 isolate exhibited a decreased expression of this gene (Figure 7.6C). Unlike other VSD isolates, such as VSD9 and VSD10, which produce extracellular biofilm matrix mainly composed of protein, VSD16 biofilm shows the presence of a massive amount of mucus-like extracellular material (Chapter 6), suggesting that this mucous matrix might be formed by extracellular DNA (eDNA) or by complexes of eDNA and proteins (Chapter 6). Taken together, these results indicate that the VSD16 isolate may have a different biofilm formation pathway.

The *sagA* gene encodes the mature streptolysin S (SLS) toxin responsible mainly for the β-hemolytic activity among the pyogenic group of streptococci (Datta *et al.*, 2005; Molloy *et al.*, 2011). The operon encoding SLS includes the propeptide structural gene (*sagA*), followed by genes that provide the conversion of SagA into SLS (*sagB* to *D*), leader cleavage (*sagE*) and transport across the membrane (*sagF* to *I*). The *S. pyogenes* SLS causes host soft-tissue damages, impacts phagocytes, and contributes to translocation across the epithelial barrier (Molloy *et al.*, 2011). SLS also promotes programmed cell death and enhances inflammatory in HEK cells (Flaherty *et al.*, 2015). Studies revealed that SLS promotes host-associated biofilm formation (Vajjala *et al.*, 2019), besides inducing mitochondrial damage and macrophage death (Tsao *et al.*, 2019). Datta and co-works reported that all genes of the *sag* operon are required for the functional expression of streptolysin S (Datta *et al.*, 2005). The loss of *Sag*B-I observed in bovine SDSD isolates is associated with loss of β-hemolytic activity (Chapter 2); however, the *sagA* gene has been maintained in the bovine SDSD genome, which possibly indicates an additional function to the product of this gene (Chapter 2). Some studies suggested that SLS also functions as a quorum-sensing molecule, and SagA

mRNA has been implicated in the regulation of several virulence genes, including M proteins (Datta *et al.*, 2005; Molloy *et al.*, 2011). The mechanisms by which SagA mRNA contributes to virulence have been the subject of several investigations. In the present study, a high and significant increase in *sagA* expression was observed *in vivo* for the sessile cells of the VSD13 isolate (Figure 7.6D), suggesting that the regulation of SagA expression may differ in a strain-specific manner.

7.4.   Conclusions

To the best of our knowledge, the present study demonstrates for the first time in literature the ability of bovine SDSD to form biofilm *in vivo* and suggests that the mechanism underlying the biofilm development appears to be multifactorial. Despite that, the increase of *fbpA* transcripts in all sessile cells grown *in vivo* suggest a possible role for fibronectin-binding protein A in biofilm formation/accumulation. Indeed, the number of *brpA*-like gene transcripts was also higher in sessile cells corroborating a role of biofilm regulatory protein A in biofilm modulation of SDSD. In this work, we demonstrated that the capability of bovine SDSD to develop strong biofilm *in vivo* is independent on the ability to form biofilms *in vitro* on the abiotic surface. Additional studies are required toward a better understanding of the mechanisms associated with the regulation of biofilm formation by bovine SDSD isolates and the precise role of biofilm development in SDSD infections.

Chapter 8 - Light triggered enhancement of antibiotic efficacy in biofilm elimination mediated by gold-silver alloy nanoparticles.

Alves-Barroco, C., Rivas-García, L., Fernandes, A. R., and Baptista, P.V.

Abstract

Nanotechnology has proposed new approaches against microbial infections by inhibiting the biofilm formation and/or eradicating the mature biofilm. Among alternative strategies to combat the infections associated with biofilm-forming bacteria, metallic nanoparticles have gained significant attention, particularly gold and silver nanoparticles, which have an important role in the current increase of the use of nanomaterials.

This study provides a proof-of-concept investigation into the use of gold-silver alloy nanoparticles (AuAgNPs) towards eradication of bacterial biofilms. Upon visible light irradiation of AuAgNPs there was considerable disturbance of the biofilms' matrix. The hindering of structural integrity of the biofilm matrix resulted in an increased permeability for entry of antibiotics, which then cause the eradication of biofilm and inhibit subsequent biofilm formation. Additionally, our results reveal an action of AuAgNPs by inhibiting SDSD biofilm formation. Our results also suggest that SDSD biofilm reduction by AuAgNPs may trigger distinct stress pathways that lead to the downregulation of the two genes critical for biofilm production, namely *brpA*-like encoding biofilm regulatory protein and *fbpA* fibronectin-binding protein A.

This study provides useful information to assist the development of nanoparticle-based strategies for the active treatment of biofilm-related infections triggered by photoirradiation in the visible.

8.1. Introduction

Biofilms and their associated infections are a significant medical apprehension, which often climax in life-threatening effects. A biofilm is formed by bacteria and is formed by a mass of microbial cells embedded in matrix of extracellular polymeric substances (EPS) produced by the bacteria cluster (Alves-Barroco *et al.*, 2020a). These biofilms are extremely infectious and seem to be present throughout the environment, and wherever the microbes adsorb on and/or proliferate towards colonization (Marks *et al.*, 2014). The formation of this complex three-dimensional matrix creates a protective environment for pathogens to grow, which is hard to eliminate with standard antibiotics (Høiby *et al.*, 2010). In fact, biofilm-related infections are considered a key factor in the surge of antibiotic resistance, which poses a threat to human health and to bacteria control that impacts several economic sectors, such as agriculture and food processing. whose ability to increase resistance to several antimicrobial agents has been demonstrated to be 10 to 1000 times higher than that of planktonic bacteria (Alves-Barroco *et al.*, 2020a). Several resistance mechanisms have been associated with biofilms, namely by preventing the entrance of polar and charged antibiotics within the biofilm matrix or as the results of the metabolic change of bacterial growth, making these persistent infections hard to treat and eradicate (Baldassarri *et al.*, 2006; Chadha, 2014; Rafii, 2015; Wu *et al.*, 2015; Boonyayatra and Pata, 2016; Hwang-Soo *et al.*, 2016; Singh *et al.*, 2017; Alves-Barroco *et al.*, 2020b). Economic projections estimate that antibiotic resistance could cause circa 10 million deaths worldwide each year by 2050 (overshadowing rates caused by cancer-related deaths), with associated impact to health care systems and reduced economic growth (De Kraker *et al.*, 2016; O'Neill, 2016). A good example of this global impact is bovine mastitis, a multifactorial disease that result from a persistent bacterial infection of the mammary glands that leads to an inflammatory response causing visibly abnormal milk (e.g., color, fibrin clots), triggering economic losses of $1.1 billion in India, $2 billion in United States and $371 million in United Kingdom (Zadoks and Fitzpatrick, 2009; De Vliegher *et al.*, 2012; Kurjogi and Kaliwal, 2014; Gomes *et al.*, 2016; Mushtaq *et al.*, 2018). What is more, mastitis poses a tremendous threat to human health since it may be transmissible to humans and, thus, accountable for zoonoses and food intoxication (McDaniel *et al.*, 2014; Gomes *et al.*, 2016). In recent years, cases of zoonotic infections associated with SDSD have been reported, rendering it as one of the most important pathogens causing bovine mastitis (Koh *et al.*, 2009; Zadoks *et al.*, 2011; Park *et al.*, 2012; Jordal *et al.*, 2015; Chennapragada

et al., 2018; Alves-Barroco *et al.*, 2021). Besides that, multidrug resistant SDSD strains with differential sensitivity to antibiotics (e.g., penicillin, oxacillin, clindamycin, vancomycin, third-generation cephalosporin) were found in human infections, only succumbing to complex antibiotic combinations (Koh *et al.*, 2009; Park *et al.*, 2012; Jordal *et al.*, 2015; Chennapragada *et al.*, 2018).

The biofilm production by SDSD strains constitute a key factor in pathogenesis, such as the capability to adhere and internalize into human and bovine cells and infect other animal hosts (Calvinho *et al.*, 1998; Alves-Barroco *et al.*, 2018, 2019). In addition to forming a barrier against antibiotics, the biofilm also favors horizontal gene transfer, delivering compatible conditions for the uptake of genes such as high cell density, induction of competence cell, and accumulation of exogenous (Savage *et al.*, 2013; Fair and Tor, 2014; Marks *et al.*, 2014; Kragh *et al.*, 2016). Thus, the use excessive of antimicrobials favors the persistence of these antibiotic resistance genes and the emergence of multidrug resistance in populations of the same ecological niches (Alves-Barroco *et al.*, 2020a). To overcome these drug resistant bacterial biofilm communities' alternative strategies have been studied, such as the use of nanoparticles of different materials (Alves-Barroco *et al.*, 2020b). Considerable effort has focused on the development of biocidal strategies capable of mitigating biofilm formation and/or potentiating antibiotic effect against bacteria embedded in biofilms (Baptista *et al.*, 2018). A wide range of NPs such as liposomes, metallic nanoparticles, polymeric nanoparticles, or carbon nanotubes has been proposed tackle these issues, which mostly rely on passive diffusion of nanomaterials, usually at high concentrations that pose toxicity concerns (Baptista *et al.*, 2018; Masri *et al.*, 2019). The antimicrobial activity of NPs against planktonic bacteria and biofilms depends on several factors, such as electrostatic attraction, van der walls forces, hydrophobic interactions, nanoparticle size, and stability (Joshi *et al.*, 2020). The interaction between NPs and bacteria can trigger oxidative stress processes, enzymatic inhibition, cell components damage, and gene expression changes. Several NP-based systems have been applied against bacteria (for more details see (Baptista *et al.*, 2018; Lee *et al.*, 2019; Gómez-Núñez *et al.*, 2020; Joshi *et al.*, 2020)). Metallic NPs (e.g., silver, silica, zinc, and gold) provide for a large surface area that increases the interaction with the bacterial membrane or matrix biofilm structures (Adeyemi and Sulaiman, 2015). Particularly, gold and silver NPs have been extensively studied for their antibacterial and anti-biofilm effects (Joshi *et al.*, 2020). Additionally, some strategies have profited from the high extinction coefficient of these NPs and their

light to heat transfer capability (Petrova *et al.*, 2007); where the generated heat might be applied for biofilm eradication based on heat disturbance of the matrix. Indeed, gold (AuNPs) and silver nanoparticles (AgNPs) have been shown to induce biofilm disturbance upon near-infrared (Petrova *et al.*, 2007; Adeyemi and Sulaiman, 2015; Yuwen *et al.*, 2018; Li *et al.*, 2019; Joshi *et al.*, 2020). What is more, bimetallic NPs improve the original metal catalytic properties with increased stability in the surrounding media and higher activity against bacteria. Gold-silver NPs alloys (AuAgNPs) have shown good bactericide activity against bacterial biofilms (Ramasamy *et al.*, 2016), potentiated when subjected to light irradiation (Kyaw *et al.*, 2017), while keeping toxicity against higher eukaryotes at low impact (Taylor *et al.*, 2015). These data suggest that using AuAgNPs to fight infections associated with biofilms would be more advantageous than the use of AuNPs and AgNPs alone. In this work, the use of AuAgNPs were investigated as the pivotal element towards eradication of bacterial biofilms. Mature SDSD biofilms were exposed to AuAgNPs alone or in combination with ciprofloxacin. The irradiation with visible light of AuAgNPs induces photothermal conversion and impart heat transfer to the biofilm, resulting in the disruption of the dense matrix, allowing the perfusion of the antibiotic, and damaging bacteria cells. Importantly, it is the combination of light stimulation that imparts the enhancement of the bactericidal efficacy of the antibiotic. Still, under these conditions, no harm is done to the mammal cells. These findings will inspire the design of next-generation synergistic strategies to tackle biofilm formation.

8.2. Materials and Methods

8.2.1. Nanoparticle synthesis and characterization

Gold nanoparticles (AuNPs) were synthesized according to Pedrosa and co-workers (Pedrosa *et al.*, 2018) by boiling an aqueous solution of 98.4 mg of $HAuCl_4 3H_2O$ (Sigma Aldrich, St Louis, MO, USA) in 250 ml of milli-Q H_2O and adding 38.8 mM of sodium citrate (Sigma Aldrich, St Louis, MO, USA). The mixture was refluxed with stirring for 30 minutes. Silver nanoparticles (AgNPs) were synthesized according to the method described by La Spina and collaborators with several modifications (La Spina *et al.*, 2020), by boiling an aqueous solution of 45 mg of $AgNO_3$ (Merck, Darmstadt, Germany) in 250 ml of milli-Q H_2O while stirring. Then 38.8 mM of sodium citrate was added, and the mixture refluxed for 15 minutes while stirring.

Gold-silver alloy NPs were synthesized following the protocol proposed by Doria and co-workers (Doria *et al.*, 2010). Briefly, 12.5 mg of $HAuCl_4 3H_2O$ (Sigma Aldrich, St Louis, MO, USA) and 5.4 mg of $AgNO3$ (Merck, Darmstadt, Germany) were dissolved in 250 ml of milli-Q $H2O$ and brought to the boil with stirring Then 34 mM of sodium citrate (Sigma Aldrich, St Louis, MO, USA) was added, and the mixture refluxed for 15 minutes with stirring.

To increase stability in complex growth media, the resulting NPs were conjugated to a thiolated polyethylene glycol (PEG-SH) (Mw 2000; 0.01 mg/mL, Sigma Aldrich, St Louis, MO, USA). Following incubation overnight with 0.028% (w/v) Sodium dodecyl sulphate (SDS), the excess PEG was removed by centrifugation (14000 g for 30 min at 4 C), and the NPs washed three times with milli-Q H_2O. The extension of surface functionalization was assessed by determination of free PEG-SH in the supernatant via the Ellman' 's assay (Supporting Information SI) as described (Moser *et al.*, 2016).

All NPs were characterized for size and morphology TEM and Dynamic Light Scattering (DLS), elemental composition by Inductively Coupled Plasma Atomic Emission Spectroscopy (ICP-AES), and optical profile by Ultraviolet-Visible Spectroscopy (UV-VIS). In all assays, the amount of metal (gold and/or silver) was kept constant (AuAgNPs, AuNPs, and AgNPs). The stability of AuAgNPs in a pH range of 2–10 was assessed by UV-VIS (Shimadzu, Kyoto, Japan) after a 48 h incubation at room temperature. For this, 10% (w/v %) HNO_3 and 10% (w/v %) NaOH were used to adjust the target pH of a 10 nM NPs solution in ultrapure water. As control, solutions of

monometallic NPs (AuNPs and AgNPs) were also prepared. Experiments were performed in triplicate and data presented as the average.

TEM characterization

TEM characterization of NPs was developed in the TEM service of Instituto Superior Técnico (ICEMS/IST), Lisbon, Portugal. Hence, 10 μL of each metallic nanoparticle solution were put on carbon copper grids and washed with milli Q-water two times and air dried. Subsequently, TEM images were acquired employing a transmission electronic microscope (Hitachi, Tokyo, Japan).

DLS characterization

For dynamic light scattering (DLS) analysis, a 2 nM solution of each metallic nanoparticle was prepared previously. Thereafter, the hydrodynamic diameter and Z-potential were determined by DLS resorting to a Nanoparticle Analyzer SZ-100 (Horiba Scientific, Kyoto, Japan) at 25 ℃ with a scattering angle of 90°. Samples were measured three times.

UV-Vis spectra

The spectrum of ultraviolet-visible (UV-Vis) was measured by spectroscopy to characterize the metallic nanoparticles. Thus, 2nM solution of each metallic nanoparticle was prepared previously diluting with milli Q-water. Afterward, UV-Visible absorption spectra were recorded at room temperature on a UV-Vis spectrophotometer (Shimadzu, Kyoto, Japan) in the range 400–800 nm with 1 cm path quartz cuvette. Three measurements of each sample were performed.

8.2.2. Bacterial Strains, Growth Conditions, and Sample Preparation

The bovine SDSD isolates were selected based on the genomic profiles, antibiotic resistance profiles, and the ability to accumulate biofilms on glass and polystyrene surfaces (Chapter 6 and 7). For all biological assays, *Staphylococcus aureus* (ATCC 29213) or *Pseudomonas aeruginosa* (ATCC 10145) (from the American Type Culture Collection (ATCC)) were used as positive biofilm producers, while an isolate of *Streptococcus pyogenes* (GAP58) was used as a stable non-biofilm producer (Chapter 6). Biofilm production was carried out as previously described in the Section 6.2.4 of Chapter 6.

8.2.3. Minimum inhibitory concentration (MIC) and minimal biofilm eradication concentration (MBEC)

Susceptibility tests with antibiotics were carried according to the guidelines from the Clinical and Laboratory Standards Institute (CLSI; http://www.clsi.org/). For the determination of MIC and MBEC values, we used antimicrobials with bactericidal action, namely ciprofloxacin (fluoroquinolones class) and gentamicin (aminoglycosides class), and with bacteriostatic activity, namely tetracycline.

Serial dilutions of the antibiotics stock solutions were carried out to obtain the final concentrations of 64 µg/mL; 32 µg/mL; 16 µg/mL; 8 µg/mL; 4 µg/mL; 2 µg/mL and 1 µg/mL. Briefly, bacterial cells were grown to the mid-exponential phase. Then, aliquots of 100 µl of the bacterial cells were seeded in a 96-well microtiter plate at a density of 1 10^6 ml ^{1}. Subsequently, 10 µl of each solution of the antibiotics prepared by serial dilutions was added to the bacterial cells. *Staphylococcus aureus* ATCC 29213 was used as the positive control. The experiments were carried out in triplicates. The MICs were defined as the lowest drug concentration inhibiting visible growth after overnight incubation at 37 C. To determine the minimal biofilm eradication concentration (MBEC), the biofilms were formed as described above. After the biofilm formation, the culture medium was replaced by fresh culture medium supplemented with serial dilutions of the antibiotics stock solutions were carried out to obtain the final concentrations of 64 µg/mL; 32 µg/mL; 16 µg/mL; 8 µg/mL; 4 µg/mL; 2 µg/mL and 1 µg/mL. The plates were incubated for 18h at 37 C. Subsequently, the wells were washed three times with sterile PBS, then was performed the homogenization of the biofilm to disperse cells in a liquid medium and colony-forming units quantified by serial dilutions in solid medium.

8.2.4. Photoirradiation

Before biofilm irradiation, actinometry was performed to measure the exact amount of energy irradiated into the system. Actinometrical measurements were performed with Aberchrome 540TM, E-form ((E)-a-(2,5-dimethyl-3-furylethylidene) (isopropylidene) succinic anhydride)) (Extrasynthese, France) actinometer as previously described (Rappon and Syvitski, 1996; Mendes *et al.*, 2017). This photochromic dye is often used for actinometry studies in the near-UV and visible regions due to its reversible photocyclization into the deep red cyclized valence isomer 7,7a-dihydro-2,4,7,7,7a-pentamethylbenzo(b)furan-5,6-dicarboxylic anhydride (C-form). When irradiated with UV light E-form turns in C-form, which can, in turn, be reverted to E-form when

irradiated with visible light. For these measurements, a solution of 100 μM of Aberchrome 540 was dissolved in absolute ethanol and irradiated at 342 nm for 1h until a photo-stationary state corresponding to the maximum conversion into the C-form was obtained. The C-form solution was irradiated using a continuous wave (CW) 532 nm green diode-pumped solid-state laser (DPSS) (Changchun New Industries Optoelectronics Tech. Co., LTD, Changchun, China) coupled to an optical fiber. The solution exposed to the green laser undergoes back conversion to the E-form, and the number of converted molecules was quantified by UV-VIS (Shimadzu, Japan). This allows to characterize the exact amount of energy being pumped into the system by the laser, i.e. the amount of photons irradiating the NPs and cells/matrix – providing means to tune the intensity of irradiation to limit damage to healthy cells (NPs have an extinction coefficient circa 10^5 higher than any biomolecule inside cells, which allow these NPs to absorb almost all laser light and spare cells to any deleterious effect).

A thermocouple was inserted into the wells with the solution (water, culture media) before and immediately after visible light irradiation to assess the temperature increase. The thermal efficiency was calculated for the variation of initial and final time point for the pH 7 condition. The Therm (IR) camera allows assessment of temperature variation in realtime.

8.2.5. Cell viability on primary human fibroblasts

Human primary fibroblasts were purchased from ATCC (http://www.atcc.org). The cell line was grown in Dulbecco's modified Eagle's medium (DMEM) (Invitrogen, Grand Island, NY, USA) supplemented with 10% (v/v) fetal bovine serum, incubated at 37 °C in an atmosphere with 5% (v/v) CO_2. Fibroblast viability was determined using MTS assay as previously described (Fernandes *et al.*, 2017). Fibroblasts were seeded in 96-well plates and grown for 24 h prior to incubation for 3 h in fresh diluted medium with AuAgNPs (10 nM) or AgNPs (10 nM) (37 °C in a 99% humidified atmosphere of 5% (v/v) CO_2). The culture medium of fibroblasts cells was replaced with DMEM (without phenol red) for visible light irradiation at 2.02 W cm^{-2} for 60 s. Irradiated and non-irradiated fibroblasts cells were incubated for another 3h at 37 °C in DMEM supplemented with 10 nM of NPs (AuAgNP, or AgNP) and 10 nM of NPs + 10 μg/mL CIP. After the incubation period, the culture medium was removed from each well, washed with PBS, and replaced medium containing 10% MTS reagent. The 96 well plate was incubated for 60 min at 37 °C in a 99% humidified atmosphere of 5% v/v) CO_2 and

the absorbance was measured directly from 96 well plates in a microplate reader at 490 nm (Infinite M200, Tecan, Switzerland). The following equation applied to calculate the cell viability (%) = 100 x (mean Abs of treatment group /mean Abs of control group, without treatment). Concentrations of AuNPs with low toxicity for animal cells tested for this study were previously tested by our research group (Pedrosa *et al.*, 2018).

8.2.6. Biofilm irradiation

Biofilm irradiation was carried out using a modified microdilution assay with a visible light irradiation power = 2.02 W cm^{-2} following challenging with AuAgNPs, AuNPs, or AgNPs in presence or absence of ciprofloxacin see Figure 8.1.

Biofilms were formed as described in the section 6.2.4 of Chapter 6, with some modifications. After 24 h of incubation at 37 °C, the supernatant was carefully removed, and each well was washed twice with sterile saline solution (0.85 % w/v) to remove non-adherent bacteria. Then, biofilms were incubated with fresh culture medium (TSB, pH 7.5) for 3 h at 37 ° C with i) 10 nM AuAgNPs (AgNPs and AuNPs were used as controls) or ii) TSB medium. The culture medium of biofilms was replaced with TSB only for visible light irradiation at 2.02 W cm^{-2} for 60 s. Irradiated and non-irradiated biofilms were incubated for another 3h at 37 °C in TSB supplemented with i) 10 nM of NPs (AuAgNP, AuNP or AgNP); ii) ciprofloxacin (CIP, 10 μg/mL) or iii) 10 mM of NPs + 10 μg/mL CIP. After incubation, the biofilm was detached, and cell titers were determined by serial dilution. The bioassay was performed in triplicate. The following formula calculated the percentage of biofilm reduction: Reduced cell viability (%) = 100 – [((log$_{10}$ CFU/mL control – log$_{10}$ CFU/mL Treat) / log$_{10}$ CFU/mL control)   100], where CFU/mL control corresponds to the number of colonies forming units per ml per milliliter of untreated biofilms, and CFU/mL Treat corresponds to the number of colonies forming units per ml per milliliter of treated biofilms.
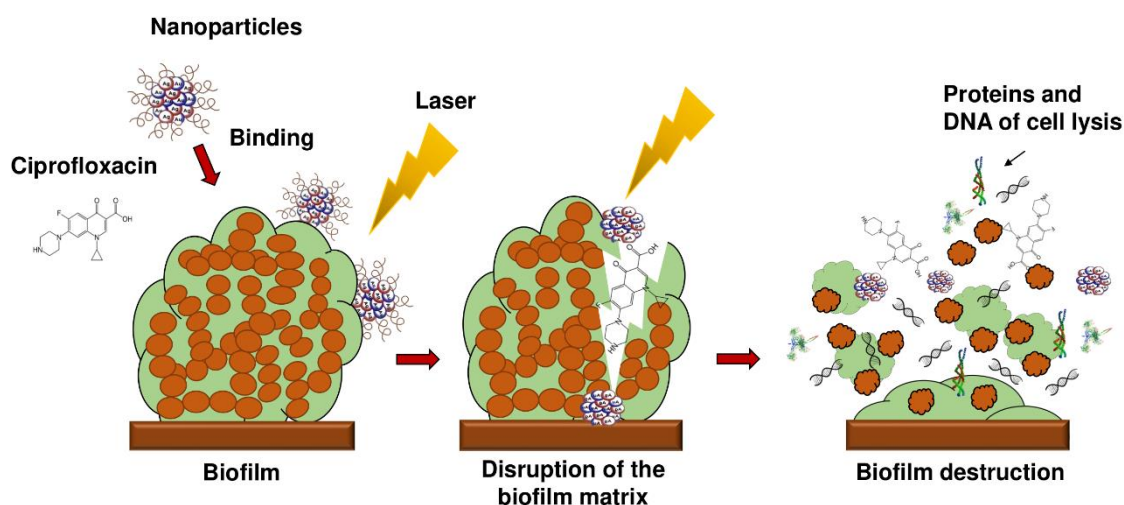
Figure 8.1. Schematic description of experimental setup. From the initial planktonic bacterial growth, biofilms were allowed to form. These were then washed to remove non-adherent bacteria and exposed to AuAgNP When indicated, these were irradiated and further cultured in presence of AuAgNPs and Ciprofloxacin (10 μg/mL).

8.2.7. Inhibition of biofilm formation

The inhibition of biofilm formation by irradiation of AuAgNPs was evaluated on polystyrene surface following an adaptation of a previously described protocol (Sections 6.2.4 of Chapter 6) with minor modifications. Briefly, bacterial cultures grown overnight were diluted with TSB (pH 7.5) supplemented with 0.5% (w/v) glucose (Sigma-Aldrich) to obtain $OD_{570} = 0.6$. These samples were placed in 96 well plates and incubated at 37 °C for 4h. After incubation, culture medium was replaced with TSB (pH 7.5) with 10 nM AuAgNPs without physically disrupting the newly formed biofilm. Samples were subsequently submitted to visible light irradiation (2.02 W cm^{-2}) for 60 s and further incubated at 37 °C for 24 h. Then, the medium was removed, samples were gently washed twice with sterile saline solution to remove the planktonic state/free-floating bacteria and dried for 30 min at room temperature. The biofilms were stained with a 0.1% solution of crystal violet for 20 min. The excess stain was removed by washing with sterile saline solution five times, and stained biofilms were dried at room temperature for one hour. Then, 200 μl of absolute ethanol was added to each stained biofilm sample. The mixture was agitated vigorously for 15 min to extract the stain. The OD of extracted crystal violet was measured at 570 nm. The following formula calculated biofilm inhibition: The percentage of biofilm inhibition = (OD Control – OD Treat) / OD Control 100.

8.2.8. Expression of *brpA-like* and *fbpA* genes

The biofilm formation capability of challenged samples was further assessed by monitoring the expression profile of the two main genes involved in biofilm generation - *brpA-like* and *fbpA* (Chapter 6). Biofilm formation was carried out for total RNA extraction and cDNA synthesis and subjected to challenge with NPs and photoirradiation as described above. Then, the medium was removed, and samples were gently washed twice with sterile saline solution to remove planktonic cells. Total RNA extraction and cDNA synthesis was performed according to Section 4.2.3 of Chapter 4. RT-qPCR was carried out in a total volume of 10 µL containing NZYqPCRGreen Master Mix (NZYTech, Lisbon, Portugal), 1 µL cDNA, and 0.2 µM of forward and reverse primers Primer sequences and amplicons expected sizes are listed in Table S2 (Appendix I). PCR conditions included an initial denaturation at 95 °C for 10 min, followed by 25 cycles of amplification consisting of denaturation at 95 °C for 15 s, annealing at 55 °C for 30 s and an extension at 60 °C for 45 s. The cycle threshold (Ct) was defined as the cycle in which fluorescence becomes detectable (above the background fluorescence). The expression level of each gene was normalized using the housekeeping gene *16S rRNA*.

8.2.9. Sample preparation for TEM analysis

Bacteria were grown in TSB supplemented with 0.5% glucose (pH 7.5) at 37 °C until the mid-exponential phase was reached (OD$_{600}$ of 0.5–0.6). Bacterial cells were washed three times in fresh TSB and finally resuspended TSB with AuAgNP@PEG (10 nM) or TSB alone. Then, the aliquots of cell suspension were irradiated or not with visible light (2.02 W cm^{-2}) for 60 s. Irradiated and non-irradiated cells suspension were incubated for another 3h at 37 °C with TSB supplemented with AuAgNP@PEG (10 nM). Fixation, treatment of samples, and image acquisition were developed in the Electron Microscopy Facility of the Instituto Gulbenkian de Ciência (IGC), Oeiras, Portugal. Briefly, bacterial pellets were fixed for 2 h at room temperature with a solution of 2% formaldehyde, 2.5% glutaraldehyde in 0.1 M HEPES. The samples were washed in 0.1 M HEPES (2 x 5min) and embedded in 2% low melting point agarose. Samples were post-fixed with 1% osmium tetroxide in 0.1 M HEPES for 1 hour on ice, washed with 0.1 M HEPES (2 x 5 min) and dH$_2$O (2 x 5 min). After washing, samples were stained with 1% Tannic Acid for 20 minutes on ice, washed 5 times with dH$_2$O, and stained with

2% Uranyl Acetate for 1 hour at room temperature. Samples were then dehydrated with a graded series of ethanol (30, 50, 75, 90) for 10 min each step and 100% for 10 min 3 times. Samples were infiltrated with 25%, 50%, and 75% resin in ethanol for 1 hour and 30 minutes, and subsequently, samples were infiltrated with 100% Resin overnight. Finally, the samples were embedded with Embed-812 epoxy resin, and the blocks were polymerized at 60 C for at least 24 hours. Thin sections (70 nm) were collected on slot palladium-copper grids, and post-stained with 1% uranyl acetate and Reynolds lead citrate, for 5 minutes each. Grids were examined in a FEI Tecnai G2 Spirit BioTWIN transmission electron microscope (120 keV) equipped with an Olympus-SIS Veleta CCD Camera.

Statistics

GraphPad Prism version 7.0 was used for statistical analysis. Data analyses were performed using the Student's t-test, and statistical significance was considered when $p < 0.05$.

8.3. Results and discussion

8.3.1. Characterization of AuAg-alloy nanoparticles

A solution of spherical AuAgNPs, AuNPs and AgNPs were prepared and conjugated with PEG-SH to achieve 100% coverage for improved stability and biocompatibility. UV-Vis spectra show the characteristic maxima absorbance peaks at 520 nm for AuNPs, 484 nm for AuAgNPs, and 430 nm for AgNPs (Figure 8.2A). The percentage of Au and Ag was determined by ICP-AES showing that the AuAg alloy was constituted by 51.4 ±2.1 % of gold and 48.6 ±2.1% of silver. TEM analysis showed an average diameter of 33(±7) nm, 14(±2) nm, and 37 nm (±12) for AuAgNPs, AuNPs and AgNPs, respectively (Figure 8.2B), corresponding to a hydrodynamic diameter of 19.6 (±1.8) nm, 46.9 (±2.5) nm, and 36.2(±2.9) nm, respectively (Supplementary Table S1, Appendix V). Zeta Potential values were also determined (Supplementary Table S1, Appendix V).

Considering that these nanoparticles must endure extreme salt and pH condition when diffusing into the biofilm matrices (Zhang *et al.*, 2012), where metabolic active bacteria continuously acidify the medium (Alves-Barroco *et al.*, 2020a), the stability of the produced nanoparticles in a pH range of 2 to 10 was assessed through their UV-Vis profile. Despite being protected against aggregation by the PEG coverage of the surface,

AuAgNPs show a tendency to aggregate at pH values lower than 4, while for pH values between 5 and 10 spectra show that the particles remain stable (Figure 5.2C).

The optical profile of these nanoparticles in complex media, whether aggregate or in stable colloidal dispersion, is critical for optimal photothermal conversion. In fact, irradiation at the plasmon peak ensures higher efficiency of light to heat conversion, with minimal energy dispersion due to scattering. Conversely, aggregation of nanoparticles, with concomitant red-shift of the SPR peak and augmented scattering cross-section leads to energy dissipation and, thus, lower photo-thermal conversion efficiencies (Yang *et al.*, 2014; Guo *et al.*, 2017). Thus, since irradiation was set at 532 nm, stability of the nanoparticles against pH induced aggregation and the effect on the heating capability was evaluated. For AuAgNPs, the photothermal effect decreased below pH 5 (Supplementary Table S2, Appendix V). Similarly, acidic pH promoted the aggregation of AgNPs, which lowered their photothermal effect, but at higher pH values, they were stable (Figure 5.2C). Contrary, AuNPs showed good stability for all pH conditions studied, which did not influence their heat capacity (Supplementary Table S2, Appendix V). The stability of alloy nanoparticles upon irradiation (different laser powers) was also assessed by UV-Vis spectra and DLS (Supplementary Figure S1, Appendix V). Data show only but minor variations to the AuAgNPs' profiles, indicating that these nanoparticles are stable after irradiation.
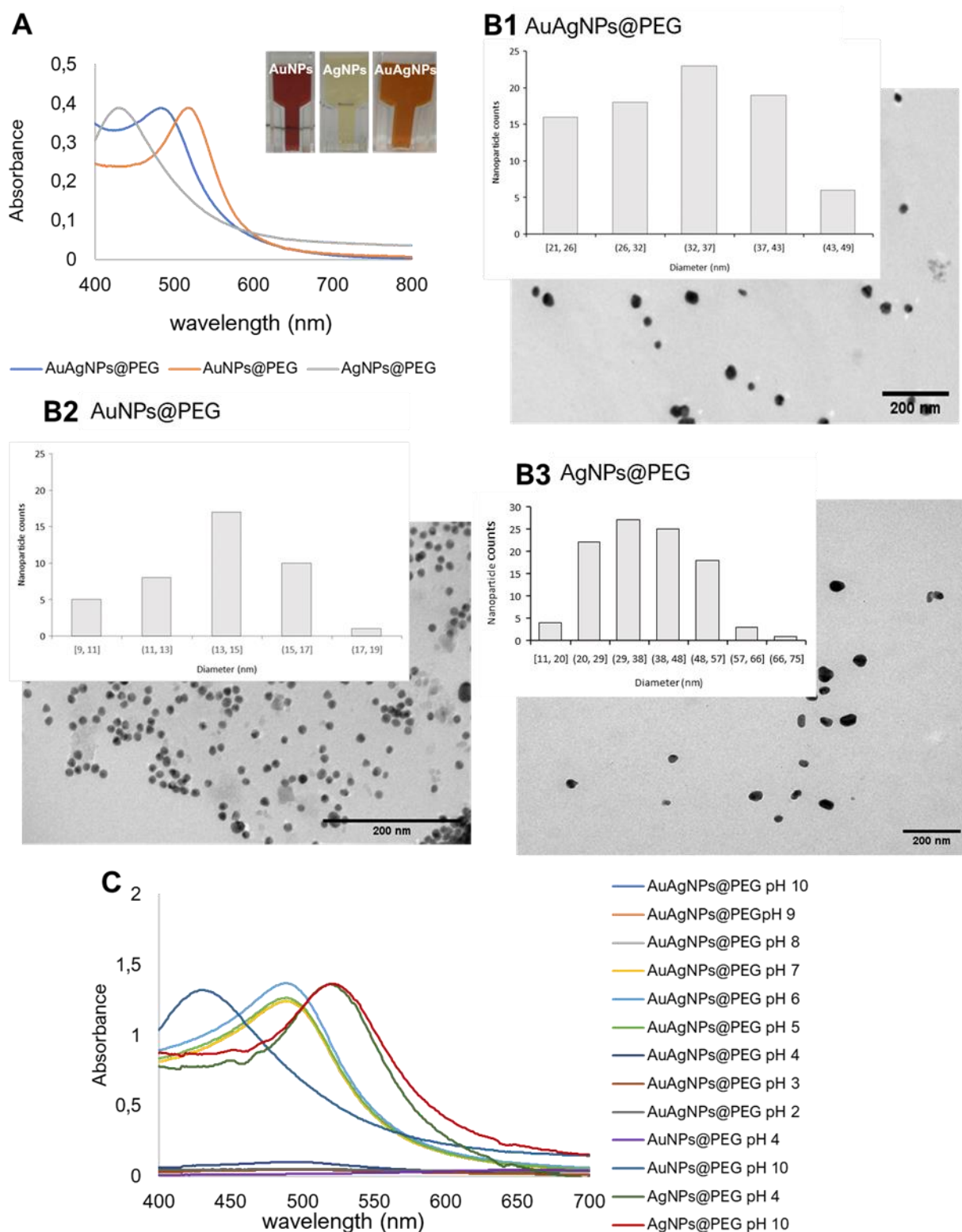
Figure 8.2. A) UV-spectrum of produced nanoparticles. AuNPs solution show an intense red color corresponding to a LSPR peak at 520 nm; AgNPs solution showed the typical faint yellow color corresponding to the LSPR peak at 430 nm; the alloy AuAgNPs resulted orange with an LSPR peak at 484 nm. B1-3) Respective TEM images NPs with indication of the size distribution. C) UV spectra of NPs in different pH solutions correlating to the colloid stability of the different nanoconjugates.

8.3.2. Biological activity of nanoparticles and CIP

To assess the effect of visible light irradiation of AuAgNPs on biofilm disruption, extreme care was taken to use nanoparticle concentrations that would not influence microbial growth. Despite, several reports on the antimicrobial activity of noble metal nanoparticles (Castillo-Martínez *et al.*, 2015; Le Ouay and Stellacci, 2015; Quinteros *et al.*, 2016; Ramasamy *et al.*, 2016; Alhmoud *et al.*, 2017; Wang *et al.*, 2019), the biocidal effect strongly depends on size, functionalization, and concentration of nanomaterial. For our studies, we selected NP concentrations that did not hamper planktonic bacteria growth, thus allowing to clearly highlight the synergistic effect of photoirradiation. Indeed, the effects of NPs alone in reference bacterial strains are negligible - see Supplementary Figure S2, Appendix V.

Although several studies have shown high activity of NPs (AuNPs, AgNPs, and AuAgNPs) against Gram-positive and Gram-negative bacteria in planktonic or sessile growth (Joshi *et al.*, 2020), the possible toxicological implications of these nanomaterials hinder application in the clinical. In fact, most reports tested high concentrations of metallic nanoparticles to eradicate the bacteria in biofilms (Ramasamy *et al.*, 2016; Singh *et al.*, 2018). However, this is often toxic for animal cells, and thus limit human and veterinary clinical applications.

Therefore, we assessed the effect of AuAgNPs and AgNPs and the effect of visible light irradiation of NPs on viability of primary human fibroblasts that, for the tested concentrations, did not show any impact to cell viability (Figure S3, Appendix V). These observations ae in line with data in the literature on the toxicity of noble metal nanoparticles on mammal cells (Asharani *et al.*, 2009; Conde *et al.*, 2014; Taylor *et al.*, 2015; Fernandes *et al.*, 2020; Chang *et al.*, 2021).

Similarly, we assessed the MIC of ciprofloxacin, gentamicin, and tetracycline of bovine SDSD isolates, *Staphylococcus aureus* (ATCC 29213), and *Pseudomonas aeruginosa* (ATCC 10145) (Table 8.1). According to the Clinical and Laboratory Standards Institute (CLSI M31-A3, 2008) criteria, resistance values for interpretation of MIC results were: 4 for ciprofloxacin (CIP), 16 for gentamicin, and 8 for tetracycline. Tetracycline resistance was found in all SDSD isolates/strains. High-level gentamicin resistance was observed for VSD22 and VSD45 (>16), and a high-level erythromycin resistance was shown for VSD9 and VSD13 (>16). According to the CLSI standard, all the studied isolates/strains were ciprofloxacin-susceptible (Table 8.1).

The minimal concentration of antibiotics required to eradication of biofilm cell (MBEC) was also assessed. Our results revealed that, under these criteria, MBEC was not achieved for the tested antibiotics, even at the highest concentrations tested.

The susceptibility of SDSD strains to different antibiotics by disk diffusion method was previously investigated (Chapter 2). Herein, we used antibiotics whose resistance has been associated with the formation of biofilms, such as ciprofloxacin that shows similar bactericidal action on planktonic growths of isolates/strains and loss of bacterial cell activity in biofilms.

Table 8.1. Minimum inhibitory concentration values for ciprofloxacin, gentamicin, and tetracycline

	MIC Values (µg/mL)		
Strains	Ciprofloxacin	Gentamicin	Tetracycline
SDSD VSD9	<1	2	16
SDSD VSD13	<1	2	16
SDSD VSD16	<1	2	64
SDSD VSD22	<1	> 16	32
SDSD VSD45	<1	> 16	64
S. aureus ATCC 29213	<1	2	4
P. aeruginosa ATCC 10145	<1	2	4

8.3.3. Photoirradiation effects of AuAgNPs in mature biofilms

The *in vitro* therapeutic potential of photoirradiation in the visible (2.02 W cm^{-2} for 60 s) of NPs (AgNPs, AuNPs, and AuAgNPs) alone or in combination with ciprofloxacin was evaluated in mature biofilms of *Staphylococcus aureus* ATCC 29213 and *Pseudomonas aeruginosa* ATCC 10145 (Figure 8.3 and Supplementary Figure S2, Appendix V). No statistically significant differences were observed for AuAgNPs, AgNPs, and AuNPs when used as a single strategy or in combination with ciprofloxacin and/or photoirradiation in the eradication of mature biofilms from *S. aureus* ATCC 29213 and *P. aeruginosa* ATCC 10145 (Figure 8.3 and Supplementary Figure S2, Appendix V).

Data show that AuAgNPs alone have little to no effect on SDSD biofilm stability and bacteria viability (Figure 8.3 – condition i)). Results show a reduction of viability of mature biofilms produced by SDSD (less than 5% reduction) upon exposure to AuAgNPs similar to that of control strains (*S. aureus* ATCC 29213 and *P. aeruginosa*

ATCC 10145). Interestingly, CIP (Figure 3 condition ii)) showed different degrees of antibacterial activity for SDSD isolates with 5% reduction of VSD9 viability to 22.5% reduction in VSD13, but still higher than values for *S. aureus* ATCC 29213 (0.57%) and for *P. aeruginosa* ATCC 1014 (4.95%). Combinations of AuAgNPs and CIP (Figure 8.3 condition iii)) leads to higher inhibitory activity than AuAgNPs alone (Figure 8.3 condition i). Data for control strains also show that no relevant effect is observed for CIP alone or in combination with AuAgNP.

Interestingly, the higher synergistic interaction was observed against VSD16 (100%), which exhibits a matrix richer in extracellular DNA (Chapter 6). It is known that regardless of the bacterial species, all biofilms share common properties; thus, biofilms interact specifically (e.g., ligand-receptor) or not specifically (e.g., electrostatic interactions) with biotic and abiotic surfaces. However, the composition of biofilm matrices can vary dramatically from strain to strain.

We have previously shown that the extracellular matrix of SDSD biofilms is rich in proteins and a mucus-like extracellular component associated to extracellular DNA (eDNA), whose proportion in VSD16 biofilm showed a massive amount of the latter (Chapter 6). AuNPs and AgNPs coated by molecules with positive electrostatic charges play the primary role in the interaction to eDNA with a polyanionic nature. The eDNA also interacts with NPs via Van der Waals forces or hydrophobic forces, preventing the aggregation of NPs in the solution. Some authors attributed the biofilm inhibition to the interactions of Au^+ and Ag^+ with eDNA, and these interactions are believed to play a predominant role in inhibiting eDNA function (Jiang and Ran, 2018; Radzig *et al.*, 2019).

Silver and gold are well-known to promote bactericidal activity against Gram-negative and Gram-positive, although the mechanisms are not yet fully elucidated. Some authors have suggested that the bactericidal activity is mediated by the production of reactive oxide species (ROS) like superoxide or hydrogen peroxide by silver ions that interact and inactivate some cellular components (e.g., proteins, lipids, and nucleic acids) and affect the electron transport chain causing cell death (Costa *et al.*, 2010; Le Ouay and Stellacci, 2015; Quinteros *et al.*, 2016). Another hypothesis relates to the fact that increasing levels of oxygen decrease the bacteria's resistance to different antibiotics classes, since some antibiotics, such as ciprofloxacin (and aminoglycosides in general) are not active in anaerobic conditions, thus affecting only the outer part of the biofilm (Borriello *et al.*, 2004). To our knowledge, this study reports for the first-time ciprofloxacin resistance associated with biofilm formation by SDSD strains. Taken

together, our data suggest that AuAgNPs could interact with the biofilm matrix increasing the permeability and diffusion of the antibiotic into the biofilm, thus capable to kill the bacteria, since the VSD16 strain is sensitive to ciprofloxacin in its planktonic form.

Our data show that photoirradiation of AuAgNPs in combination with ciprofloxacin leads to extensive biofilm degradation and loss of bacterial cells' viability, reaching eradication values of 100% for some strains – Figure 8.3 condition vii). No statistical differences are observed in the number of viable cells after irradiation compared to non-irradiated biofilms (Figure 8.3 – condition iv)).

We focused on light irradiation combination with metal nanoparticles since no mechanism of resistance has yet been identified. The photothermal conversion mediated by metal nanoparticles (Kim *et al.*, 2019; Yang *et al.*, 2020) triggers a local surge in temperature (Supporting Table S2, Appendix V) that impacts bacteria cells' viability and the stability of the extracellular matrix, decreasing its thickness (Jo and Kim, 2013; Wang *et al.*, 2019; Beckwith *et al.*, 2020; Pinel *et al.*, 2021). Previous studies have shown that the structure and the integrity of bacterial biofilms could be disrupted at higher temperatures (Ibelli *et al.*, 2018), thus decreasing the barrier limiting antimicrobial diffusion to different layers of the biofilm. In fact, some studies have demonstrated the possibility to use near-infrared irradiation to induce nanoparticle heat transfer (Castillo-Martínez *et al.*, 2015; Alhmoud *et al.*, 2017; Ding *et al.*, 2017; Astuti *et al.*, 2019; Li *et al.*, 2019). Our data suggest that the nanomaterial could interact with the biofilm matrix increasing the permeability and diffusion of the antibiotic into the biofilm, then becoming capable to kill the bacteria, since the VSD16 strain is sensitive to CIP in its planktonic form. Previous studies reveal that in immature biofilms, the number and dimensions of pores are larger, which facilitates diffusion of nanoparticles (Peulen and Wilkinson, 2011). Also, NPs deposition inside the biofilms depends on the biofilm surface's electrostatic interaction, so does adhesion of bacteria, and, thus, metal NPs might contribute to a change to the environment inhibiting bacterial adhesion and consequently the formation of new biofilms.

Here, we use visible light irradiation (2.02 W cm^{-2} for 60 s) of the AuAgNPs (10 nM) to induce antibiofilm activity against *S. aureus* ATCC 29213, *P. aeruginosa* ATCC 10145, and SDSD strains.
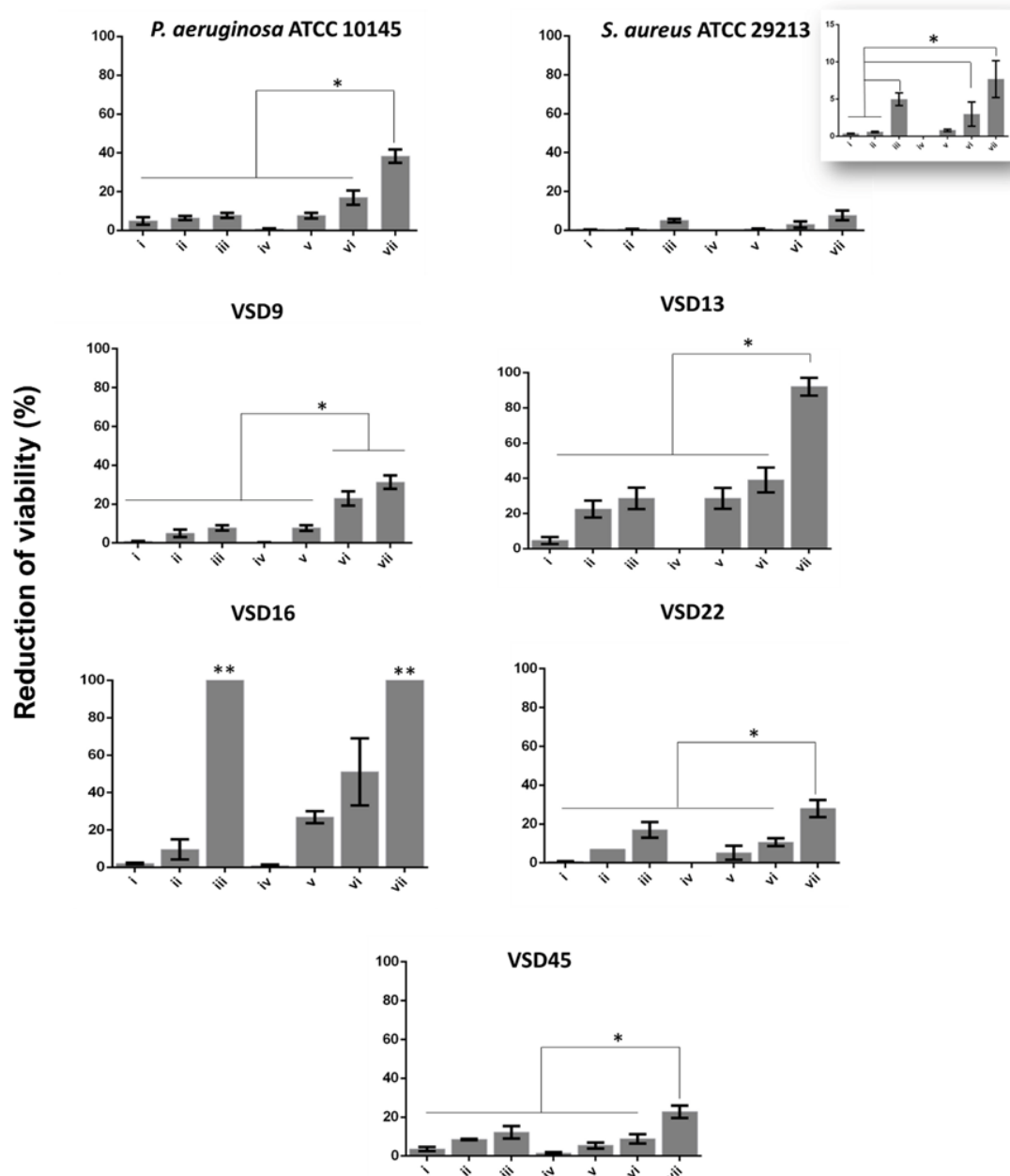
Figure 8.3. Biofilm destruction (%). (i) AuAgNPs; (ii) ciprofloxacin (CIP); (iii) AuAgNPs + CIP; (iv) visible light irradiation (VLI); (v) AuAgNPs + VLI; (vi) VLI + CIP; (vii) AuAgNPs + VLI + CIP. Nanoparticles were at 10 nM and VLI at 2.02 W cm^{-2}. Data represented as the mean ± standard deviation (SD) of three independent measurements. The following formula calculated the percentage of biofilm reduction: Reduced cell viability (%) = 100 − [((log$_{10}$ CFU/mL control − log$_{10}$ CFU/mL Treat) / log$_{10}$ CFU/mL control)   100], where CFU/mL control corresponds to the number of colonies forming units per ml per milliliter of untreated biofilms, and CFU/mL Treat corresponds to the number of colonies forming units per ml per milliliter of treated biofilms. *$p < .05$, Significant differences regarding each condition as a single strategy or when compared to treatment with two conditions simultaneously. **$p < .05$ Significant differences AuAgNPs + CIP or AuAgNPs + VLI + CIP when compared to treatment with other conditions.

8.3.4. Effect of photoirradiation of AuAgNPs on *de novo* biofilm formation

One critical aspect when dealing with infectious biofilms is their capability to be formed, even upon disinfection and cleaning of surfaces and tissues. So, the effect of photoirradiation of AuAgNPs on *de novo* biofilm formation was assessed – Figure 8.4.

Treatment with AuAgNPs immediately upon seeding on surfaces showed to be an obstacle (inhibition of 89–91%) for biofilm growth and development. What is more, the alloy nanoparticles showed to have a statistically more pronounced effect against biofilm formation when compared to the single metal counterparts – Figure 8.4. More significant biofilm formation inhibition was observed for VSD13 (weak biofilm producer) and VSD16 (moderate biofilm producer) than for VSD22 (strong biofilm producer) (Chapter 6 and 7). Together, these results seem to indicate that challenge with AuAg-alloy NPs yield less robust biofilm.
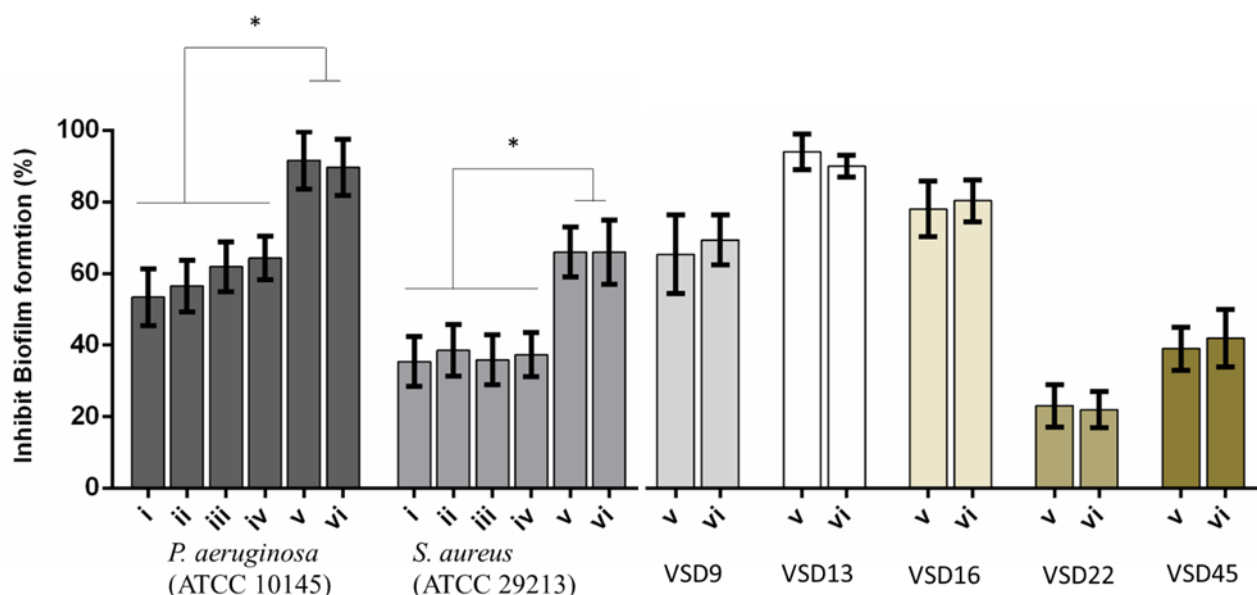
Figure 8.4. Percent inhibition of biofilm formation of (i) AuNPs; (ii) AuNPs + visible light irradiation (VLI); (iii) AgNPs; (iv) AgNPs + VLI; (v) alloy AuAgNPs; (vi) alloy AuAgNPs + VLI. To assess biofilm formation, the absorbance was measured at 570 nm. All nanoparticles were at 10 nM and VLI at 2.02 W cm^{-2}. Statistically significant differences * $p < 0.05$.

Interestingly, there was no observable difference for irradiated vs. non-irradiated samples. This observation corroborates the idea that photoconversion within the biofilm is critical for the matrix stability and support. When irradiation occurs prior to biofilm establishment, since no organized extracellular matrix is present, the effect is solely attributed to the impact of the nanomaterial on bacterial cells' viability (Yuwen *et al.*, 2018; Kirui *et al.*, 2019; Ortiz-Benítez *et al.*, 2019).

This hypothesis seems to be further supported on data from gene expression analysis on the effects of AuAgNPs upon critical genes involved in biofilm formation, *brpA*-like, which encodes a biofilm regulatory protein that is an important regulator of biofilm formation, and *fbpA*, a fibronectin-binding protein A pivotal for the adherence process. The expression of these genes was evaluated in VSD9 and VSD45 challenged with AuAgNPs with and without photoirradiation. – Figure 8.5. Challenging bacteria with AuAgNPs triggered downregulation of both genes, which is more pronounced for non-irradiated samples (*brpA-like* downregulated ~0.45 and 0.32-fold for AuAgNPs alone and AuAgNPs + irradiation, respectively; *fbpA* gene downregulated ~0.2–0.4-fold for AuAgNPs alone and ~0.025–0.075-fold for AuAgNPs + irradiation. These data are in line with the observed decrease in biofilm formation that show that the alloy nanoparticles have a more pronounced effect in decreasing the capability of bacteria cells to produce viable biofilms, probably mediated by impacting gene expression. These results agree with previous studies that report that NPs can modulate bacterial properties since the adhesion to different surfaces requires regulated events in response through crucial regulatory genes (Singh *et al.*, 2018). Data indicates that SDSD biofilm reduction by AuAgNPs may trigger distinct stress pathways that lead to downregulation of these two genes critical for biofilm production, resulting in less robust biofilm. Still, further studies are required to assess the true potential of AuAgNPs in the regulation of genes associated with the formation of biofilms.
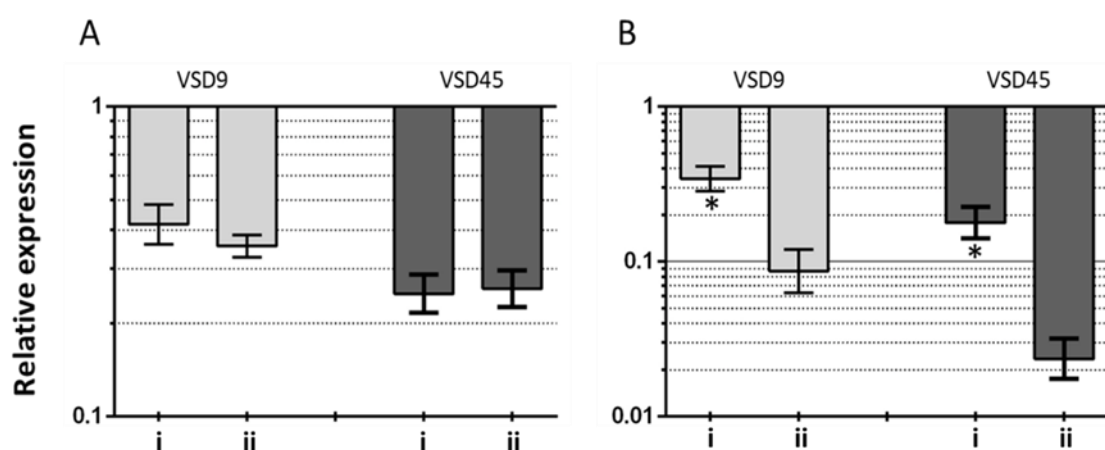
Figure 8.5. Transcriptional profiling of (A) *brpA*-like (encoding biofilm regulatory protein) and (B) *fbpA* (fibronectin-binding protein A) in the SDSD strains AuAgNPs combined with visible light irradiation (VLI) relative to the untreated. 16S rRNA gene was used as the internal control for normalization. Relative expression was calculated by the 2-ΔΔCt method. (i) AuAgNP and (ii) AuAgNP and VLI. Nanoparticles were at 10 nM and VLI at 2.02 W cm^{-2}. Statistically significant differences * $p < 0.05$.

8.3.5. TEM microphotographs of SDSD exposed to AuAgNPs and photoirradiation

To assess the localization and eventual interaction between NPs and bacteria, SDSD VSD22 cells treated with AuAgNPs with and without photoirradiation were examined by TEM. Overall, TEM images show that the AuAgNPs were not internalized by the SDSD VSD22 cells but seem to be adhering to the outer structures and components, such as cell envelope. This is agreement with previous studies that show that nanoparticles of 30 nm in diameter and larger do not penetrate bacteria cells due to the dimensions of pores within the bacterial cell wall (sized between 4 and 16 nm) (Turner *et al.*, 2013; Pajerski *et al.*, 2019). Also, it has been demonstrated that noble metal NPs interact with various proteins outside the bacteria cells which might modify their structural features, thus hampering the function in biofilms assembly (Joshi *et al.*, 2020). Even though some alteration to the structure of the SDSD VSD22 cells after treatment were observed (Figure 6), these did not affect the growth of this strain. Untreated cells exhibited a uniform cytoplasm, while aggregation of the cytoplasmic components was observed among treated cells (see Figure 6C) (Espana-Sanchez *et al.*, 2017). It has been suggested that these cytoplasmic alterations might be associated to some degree of damage to the cell membrane (Dakal *et al.*, 2016; Wang *et al.*, 2016).

TEM microphotographs show that exposure to AuAgNPs followed by photoirradiation triggered some alterations to the cell walls. The SDSD VSD22 untreated cells exhibit a well-defined wall with a continuous cell envelope (Figure 8.6A), whereas challenged cells exhibit less defined cell envelope with wrinkling of the cell wall (Figure 8.6D and 8.6E). This alteration could be partially justified by the decreased expression of the *brpA* gene since BrpA proteins have an important role in cell-wall biogenesis and structure (Bitoun *et al.*, 2012). The observed structural features also support the observed decrease in biofilm formation, suggesting an important role in the ability of bacterial biofilm production.
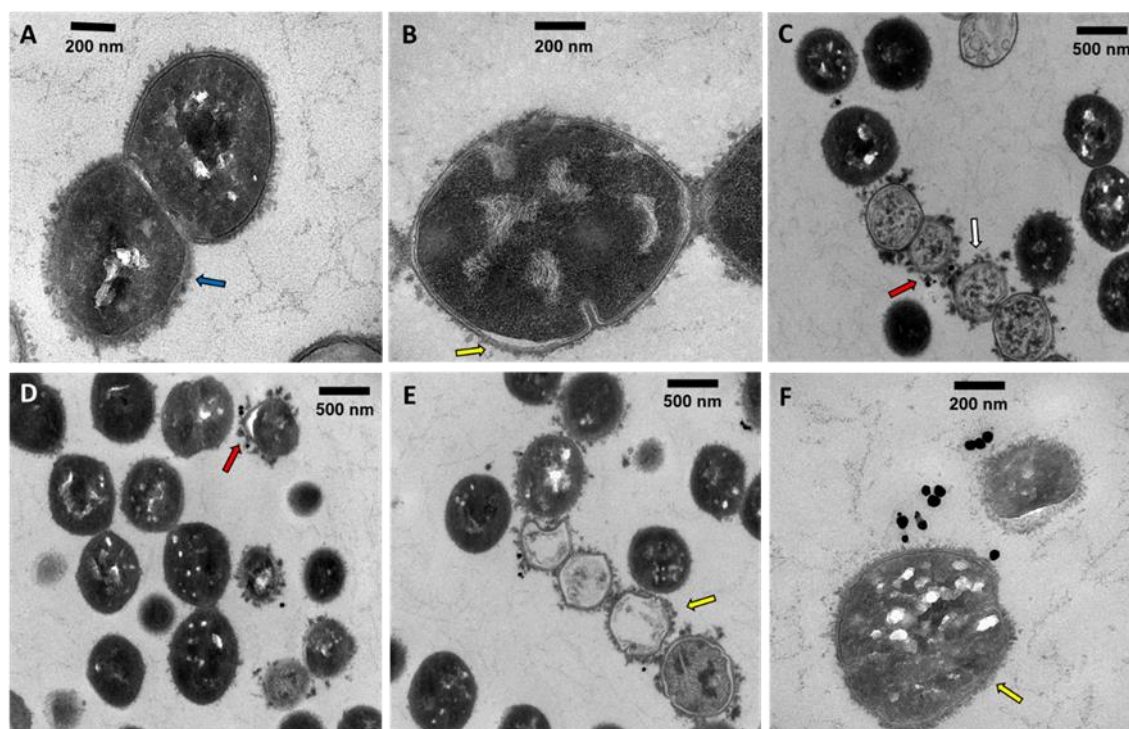
Figure 8.6. TEM microphotographs of SDSD VSD22 cells (A) untreated; (B and C) treated with AuAgNPs (10 nM) combined with visible light irradiation at 2.02 W cm^{-2} for 60s; (D to F) treated with AuAgNPs alone. Blue arrow shows glycocalyx from untreated cells; Yellow arrow shows cell envelope not defined with wrinkling of the cell wall; Red arrows show nanoparticles adhered to the cell envelope; White arrow shows aggregation of the cytoplasmic components.

8.4. Conclusion

In this study, we evaluated the impact of AuAg-alloy nanoparticles in the biofilm forming capability of bacterial strains that could be potentiated by light irradiation. Under the tested condition (10 nM), these AuAg-alloy nanoparticles had only but negligible effect on the planktonic growth of the bacterial strains. However, an increase in the reduction to the number of viable cells of SDSD was observed when biofilms were treated with gold-silver-alloy nanoparticles (10 nM) + ciprofloxacin (10 µg/mL) + visible light irradiation (2.02 W cm^{-2}). Notably, the higher synergistic interaction was observed against VSD16 (100%), which exhibits a matrix richer in extracellular DNA, which may be more sensitive to thermo-denaturation and, thus, disruption of its structural features. We also evaluated the effects of AuAgNPs alone or with irradiation on the expression of two genes involved in biofilm formation by bovines SDSD, *brpA*-like and *fbpA* fibronectin-binding protein A, revealing that both genes were downregulated upon insult resulting in less robust biofilm. Our findings suggest that a combination of AuAg-alloy NPs and photoirradiation provides disturbance of the biofilms' matrix, increasing the permeability and entry of antibiotic into the biofilm. Besides, we demonstrated that

AuAgNPs were also found to be effective for biofilms inhibition. Our results suggest that AuAgNPs activity downregulate genes critical for SDSD biofilm production, namely *brpA*-like encoding biofilm regulatory protein and *fbpA* fibronectin-binding protein A

Chapter 9 - General Discussion and Future Perspectives

The phylogenetic relationship based on the core genome suggests that *S. dysgalactiae* strains do not cluster by subspecies as it was suggested by Vieira *et al.*, 1998. The phylogenetic analysis and ANI pairwise comparison showed that human and animal isolates are segregated into two clearly distinct groups, supporting the classification proposed by Vandamme *et al.*, 1996. According to the proposal of Vandamme and co-workers, all SD isolates from the animal source must be classified as SDSD. Thus, the existence of an SDSD group that causes human-animal cluster infections may be due to opportunistic infections, and the exact incidence of SDSD human infections may be underestimated due to failures in identification based on the hemolytic patterns (Chapter 2 and 3). Yet, more detailed research into the isolation of human SD is needed to assess whether it is a carrier phenomenon or whether the species can be permanently integrated into the human microbiome, making it ready to cause opportunistic infections.

The differences between the typical bovine SDSD and the other *S. dysgalactiae* isolates are reinforced by characteristics of the accessory genome, such as the differential presence of the lactose, fructose, and sorbitol/glucitol utilization operon and absence of Streptolysin S operon among bovine SDSD (Chapter 3). Features of the accessory genome provide further support for the phylogenetic relationships observed, suggesting a signature of host adaptation and host-specific SDSD population in bovines (Chapter 3).

The number and diversity of prophages regions in the *S. dysgalactiae* genome suggest that horizontal transfer influences genomic features, contributing to genetic repertoire and adaptation to changing environments. Different prophage regions were observed in the *S. dysgalactiae* genomes. Despite the different origins of isolates (bovine or human), or subspecies (SDSD and SDSE) most prophages are related. Among the regions of intact prophages, the most prevalent correspond to the regions of prophages initially identified in *S. pyogenes*, which demonstrates phage HGT involving these species (Chapter 3). The results demonstrate that bovine SDSD isolates carry *speK, speC, speL, speM, spd1*, and *sdn* virulence genes of *S. pyogenes* prophages, and that these genes are maintained over time and seem to be exclusively a property of bovine SDSD (Chapter 2 and 3).

This work reports for the first time the ability of bovine SDSD to adhere to and internalize human cells, namely, keratinocytes, Detroit 562, a cell line derived from the

metastatic site of pharynx carcinoma, primary Bronchial/Tracheal Epithelial Cells (BTEC) and A549, a cell line derived from a human adenocarcinoma of the alveolar basal epithelial cells. The results indicate that there is no correlation between presence and expression of *S. pyogenes* phage-encoded virulence genes in the bovine SDSD isolates and the ability to interact with human cell lines, suggesting that other mechanisms may be responsible for this characteristic (Chapter 4).

Adherence and invasion of bovine SDSD isolates in epithelial cells have been previously documented to occur in mammary cell lines and fish epithelial cell lines cultured *in vitro* (Calvinho *et al.*, 1998; Calvinho and Oliver, 1998). According to Calvinho and Oliver (1998), the involvement of host kinases, intact microfilaments and *de novo* eukaryotic protein synthesis are required for the internalization process: a process that appeared to occur by a receptor mediated endocytosis mechanism. In this thesis, evidence was presented for the internalization and cytotoxicity induction by bovine SDSD in human keratinocytes cells (Chapter 5 and 7). The findings of TEM and SEM hereby described show that bovine SDSD infection of keratinocytes cells caused ultrastructural changes resembling those changes following macropinocytosis. The data from this study reveal that bovine SDSD infection induces considerable metabolic stress in keratinocytes as directly measured by mitochondrial membrane potential changes, and consequently cell death (Chapter 5 and 7). Proteomic analysis data allowed us to postulate that the interaction of bovine SDSD with human keratinocytes cells triggers similar responses as the *S. pyogenes* invasive strain. Our data showed that the interaction between human keratinocytes cells and SDSD VSD13 isolate affects the cell's metabolic pathways, proteins involved in stress response, protein folding, and the regulation of cell growth, proliferation, and glycolysis (Chapter 5).

Additionally, results indicate that bovine SDSD can cause invasive infections producing zebrafish morbidity and mortality. The infectious potential of these isolates showed to be isolate-specific and appeared to be independent of the presence of *S. pyogenes* phage-encoded virulence genes (Chapter 4). Results of the present study revealed that the immune system of fish was activated in all cases, with emphasis of massive inflammatory response. The dissemination of infection was piecemeal in the abdominal cavity, from the interorgan space to the surface of visceral organs. However, the kidney was the most rapidly and most severely affected organ in all cases. This led to seemingly little compromised hepatic function under the present circumstances of assessment, where other main organs exhibited early failure due to infection, with

emphasis on kidney, leading to death (Chapter 4). The current results are accordant with recent studies with the adult model to address *Mycobacterium* inoculation (Oksanen *et al.*, 2013) with respect to efficiency as a model but the present work revealed that bovine SDSD infects primarily B-cell forming tissue, thus hindering adaptive immune responses. These observations may indicate that bovine SDSD strains may have a broader spectrum of hosts than anticipated.

This thesis shows for the first time that bovine SDSD can grow forming a biofilm *in vitro* and *in vivo* using a murine animal model (Chapter 6 and 7), which may be an important pathogenic factor since biofilm-producing ability can make them highly difficult to eradicate (Savage *et al.*, 2013; Kragh *et al.*, 2016; Emamalipour *et al.*, 2020). To our knowledge, this study reports for the first-time ciprofloxacin and gentamicin resistance associated with biofilm formation by SDSD strains. The increasing recognition of the impact of infections associated with *Streptococcus* spp., particularly when adopting the biofilm phenotype, which causes recurrent infections, therapeutic failure and morbidity, motivated scientists to find new solutions for this old problem. Therefore, to overcome the resistance of biofilm, alternative strategies and antibiofilm agents have been studied (Alves-Barroco *et al.* 2020b). In this study, the impact of AuAg-alloy NPs in the bovine SDSD biofilm-forming capability that could be potentiated by light irradiation was evaluated (Chapter 8). The findings suggest that a combination of AuAg-alloy NPs and photoirradiation provides disturbance of the biofilms' matrix, increasing the permeability and entry of antibiotic into the biofilm. Besides, the results demonstrated that AuAgNPs were also found to be effective for bovine SDSD biofilms inhibition (Chapter 8). The most significant concern safety of alternative therapies is the gap of understanding of interaction with the human host. Thus, evaluate the impacts of alternative therapies on the host is essential for future widespread application. Future studies must investigate *in vivo* efficacy of combination therapy to assess their potential, impact of the host, and evolution of bacterial resistance.

In addition, the data from the present study showed that the fisetin dramatically inhibited biofilm formation of SDSD isolates (Chapter 6). Similar results were previously reported for *Staphylococcus aureus* (Dürig *et al.*, 2010). Taking all together, these data might indicate that inhibition of biofilm formation in SDSD may be mediated by interactions between fisetin and BrpA protein homolog. Structural and functional data on these and similar proteins will be an asset for the development of new antimicrobials with high specificity toward SDSD infection, decreasing biofilm formation, and then

affecting bacteria viability and decreasing antibiotic tolerance. Finally, homology modelling and docking analysis selected potential lead inhibitors candidates of BrpA protein homolog.

Ongoing transcriptome analysis to comparisons of gene expression within biofilm and planktonic cell populations of the bovine SDSD isolates to better understand the role of biofilm associated genes. In the future, it would be of utmost interest to monitor infections of the human and bovine SDSD isolates to investigate changes in transcriptome/proteome from different organs or tissues of the animal models' before and after infection. The comparation between the responses of infection with SDSD strains isolated from bovine mastitis with strains isolated from humans will allow to discriminate pathogen-specific responses and identify important differentially expressed immune-related genes and signaling pathways. Altogether, that will provide useful insights on the mechanisms of animal defense against infection associated with SDSD. Ultimately, unraveling the mechanisms associated with pathogenicity and defining the molecular mechanisms of host specificity provides new fundamental knowledge and can provide potential targets for the design of new strategies therapeutics for the control of SDSD diseases.

References

Abdelsalam, M., Asheg, A., and Eissa, A. E. (2013). *Streptococcus dysgalactiae*: An emerging pathogen of fishes and mammals. *Int. J. Vet. Sci. Med.* 1, 1–6. doi:10.1016/j.ijvsm.2013.04.002.

Abdelsalam, M., Fujino, M., Eissa, A. E., Chen, S. C., and Warda, M. (2015). Expression, genetic localization and phylogenic analysis of NAPlr in piscine *Streptococcus dysgalactiae* subspecies *dysgalactiae* isolates and their patterns of adherence. *J. Adv. Res.* doi: 10.1016/j.jare.2014.05.005.

Adeyemi, O. S., and Sulaiman, F.A. (2015). Evaluation of metal nanoparticles for drug delivery systems. *J. Biomed. Res.* 29, 145–149. doi:10.7555/JBR.28.20130096.

Akiyama, H., Morizane, S., Yamasaki, O., Oono, T., and Iwatsuki, K. (2003). Assessment of Streptococcus pyogenes microcolony formation in infected skin by confocal laser scanning microscopy. *J. Dermatol. Sci.*, 32(3), 193–199. doi: org/10.1016/s0923-1811(03)00096-3.

Al Safadi, R., Amor, S., Hery-Arnaud, G., Spellberg, B., Lanotte, P., Mereghetti, L., Gannier, F., Quentin, R., and Rosenau, A. (2010). Enhanced expression of *lmb* gene encoding laminin-binding protein in *Streptococcus agalactiae* strains harboring IS1548 in scpB-lmb intergenic region. *PloS one, 5*(5), e10794.

Aldini, G., Yeum, K.-J. and Niki, E. (2011). *Biomarkers for Antioxidant Defense and Oxidative Damage.* doi: 10.1002/9780813814438.

Alhmoud, H., Cifuentes-Rius, A., Delalat, B., Lancaster, D. G., and Voelcker, N. H. (2017). Gold-decorated porous silicon nanopillars for targeted hyperthermal treatment of bacterial infections. ACS *Appl. Mater. Interfaces* 9, 33707–33716. doi:10.1021/acsami.7b13278.

Almeida, A., Alves-Barroco, C., Sauvage, E., Bexiga, R., Albuquerque, P., Tavares, F., Santos-Sanches, I., and Glaser, P. (2016). Persistence of a dominant bovine lineage of group B Streptococcus reveals genomic signatures of host adaptation. *Environ. Microbiol.*, 18(11), 4216–4229. doi: org/10.1111/1462-2920.13550.

Almeida, R., and Oliver, S. P. (1995). Invasion of bovine mammary epithelial cells by *Streptococcus dysgalactiae*. J. Dairy Sci. 78, 1310–7. doi:10.3168/jds.S0022-0302(95)76752-2.

Alves-Barroco, C., Caço, J., Roma-Rodrigues, C., Fernandes, A. R., Bexiga, R., Oliveira, M., Chambel, L., Tenreiro, R., Mato, R., and Santos-Sanches, I. (2021). New insights on *Streptococcus dysgalactiae* subsp. *dysgalactiae* isolates. *Front. Microbiol.* 2021. 12, 1–16. doi:10.3389/fmicb.2021.686413.

Alves-Barroco, C., Paquete-Ferreira, J., Santos-Silva, T., and Fernandes, A. R. (2020a). Singularities of pyogenic streptococcal biofilms – from formation to health implication. *Front. Microbiol.* 11, 1–22. doi:10.3389/fmicb.2020.584947.

Alves-Barroco, C., Rivas-García, L., Fernandes, A. R., and Baptista, P. V. (2020b). Tackling multidrug resistance in streptococci – from novel biotherapeutic strategies to nanomedicines. *Front. Microbiol.* 11, 1–21. doi:10.3389/fmicb.2020.579916.

Alves-Barroco, C., Roma-Rodrigues, C., Balasubramanian, N., Guimarães, M. A., Ferreira-Carvalho, B. T., Muthukumaran, J., Nunes, D., Fortunato, E., Martins, R., Santos-Silva, T., Figueiredo, A., Fernandes, A. R., and Santos-Sanches, I. (2019). Biofilm development and computational screening for new putative inhibitors of a homolog of the regulatory protein BrpA in *Streptococcus dysgalactiae* subsp. *dysgalactiae. Int. J. Med. Microbiol*, 309(3-4), 169–181. doi: org/10.1016/j.ijmm.2019.02.001.

Alves-Barroco, C., Roma-Rodrigues, C., Raposo, L. R., Brás, C., Diniz, M., Caço, J., Costa, P. M., Santos-Sanches, I., and Fernandes, A. R. (2018). *Streptococcus dysgalactiae* subsp. *dysgalactiae* isolated from milk of the bovine udder as emerging pathogens: *In vitro* and *in vivo* infection of human cells and zebrafish as biological models. *MicrobiologyOpen,* 8(1), e00623. doi: org/10.1002/mbo3.623.

Amendoeira, A., García, L. R., Fernandes, A. R., and Baptista, P. V. (2019). Light irradiation of gold nanoparticles toward advanced cancer therapeutics. *Adv. Ther.,* 1900153. doi:10.1002/adtp.201900153.

Aminov, R. I., Garrigues-Jeanjean, N., and Mackie, R. I. (2001). Molecular ecology of tetracycline resistance: development and validation of primers for detection of tetracycline resistance genes encoding ribosomal protection proteins. *Appl Environ Microbiol,* 67(1), 22–32. doi: org/10.1128/AEM.67.1.22-32.2001.

Anbalagan, S., and Chaussee, M. S. (2013). Transcriptional Regulation of a Bacteriophage Encoded Extracellular DNase (Spd-3) by Rgg in *Streptococcus pyogenes*. *PLoSOne,* 8. doi:10.1371/journal.pone.0061312.

Arndt, D., Grant, J. R., Marcu, A., Sajed, T., Pon, A., Liang, Y., *et al.* (2016). PHASTER: a better, faster version of the PHAST phage search tool. *Nucleic Acids Res.* 44, W16–W21. doi:10.1093/nar/gkw387.

AshaRani, P. V., Low Kah Mun, G., Hande, M. P., and Valiyaveettil, S. (2009)Cytotoxicity and genotoxicity of silver nanoparticles in human cells. *ACS nano.* 3(2), 279–290. doi.org/10.1021/nn800596w.

Astuti, S. D., Puspita, P. S., Putra, A. P., Zaidan, A. H., Fahmi, M. Z., Syahrom, A., and Suhariningsih. (2019). The antifungal agent of silver nanoparticles activated by diode laser as light source to reduce *C. albicans* biofilms: an *in vitro* study. *Lasers in medical science.* 34(5), 929–937. doi.org/10.1007/s10103-018-2677-4,

Aziz, R. K., Bartels, D., Best, A. A., DeJongh, M., Disz, T., Edwards, R. A., Formsma, K., Gerdes, S., Glass, E. M., Kubal, M., Meyer, F., Olsen, G. J., Olson, R., Osterman, A. L., Overbeek, R. A., McNeil, L. K., Paarmann, D., Paczian, T., Parrello, B., Pusch, G. D., *et al.,* (2008). The RAST Server: rapid annotations using subsystems technology. *BMC Genom.,* 9, 75. doi: org/10.1186/1471-2164-9-75.

Baiano, J. C., and Barnes, A. C. (2009). Towards control of *Streptococcus iniae*. *Emerg Infect Dis,* 15(12), 1891–1896. doi: org/10.3201/eid1512.090232.

Baldassarri, L., Creti, R., Recchia, S., Imperi, M., Facinelli, B., Giovanetti, E., Pataracchia, M., Alfarone, G., and Orefici, G. (2006). Therapeutic failures of antibiotics used to treat macrolide-susceptible *Streptococcus pyogenes* infections may be due to biofilm formation. *J. Clin. Microbiol.,* 44(8), 2721–2727. doi: org/10.1128/JCM.00512-06.

Balsalobre, L., Ferrándiz, M. J., Liñares, J., Tubau, F., and De la Campa, A. G. (2003). Viridans group streptococci are donors in horizontal transfer of topoisomerase IV genes to *Streptococcus pneumoniae*. *Antimicrob. Agents Chemother.* 47, 2072–2081. doi:10.1128/AAC.47.7.2072-2081.2003

Banks, D. J., Lei, B., and Musser, J. M. (2003). Prophage Induction and Expression of Prophage-Encoded Virulence Factors in Group A Streptococcus Serotype M3 Strain Prophage Induction and Expression of Prophage-Encoded Virulence Factors in Group A Streptococcus Serotype M3 Strain MGAS315. doi:10.1128/IAI.71.12.7079.

Baptista, P. V., McCusker, M. P., Carvalho, A., Ferreira, D. A., Mohan, N. M., Martins, M., and Fernandes, A. R. (2018). Nano-Strategies to Fight Multidrug Resistant Bacteria-"A Battle of the Titans". *Front. Microbiol.* 9, 1441. doi: org/10.3389/fmicb.2018.01441.

Barnett, T. C., Cole, J. N., Rivera-Hernandez, T., Henningham, A., Paton, J. C., Nizet, V., and Walker, M. J. (2015). Streptococcal toxins: role in pathogenesis and disease. *Cell. Microbiol., 17*(12), 1721–1741. doi: org/10.1111/cmi.12531.

Barrangou, R., and Marraffini, L. (2014). CRISPR-Cas systems: Prokaryotes upgrade to adaptive immunity. *Mol. Cell.* 54, 234–44. doi:10.1016/j.molcel.2014.03.011.

Basaranoglu, S. T., Ozsurekci, Y., Aykac, K., Aycan, A. E., Bıcakcigil, A., Altun, B., Sancak, B., Cengiz, A. B., Kara, A., and Ceyhan, M. (2019). *Streptococcus mitis/oralis* Causing Blood Stream Infections in Pediatric Patients. *Japanese journal of infectious diseases,* 72(1), 1–6. doi: org/10.7883/yoken.JJID.2018.074.

Beckwith, J. K., VanEpps, J. S., and Solomon, M. J. (2020). Differential Effects of Heated Perfusate on Morphology, Viability, and Dissemination of *Staphylococcus epidermidis* Biofilms. *Applied and Environ. Microbiol.* 86(20), e01193-20. doi.org/10.1128/AEM.01193-20.

Beres, S. B., and Musser, J. M. (2007). Contribution of exogenous genetic elements to the group A *Streptococcus* metagenome. *PLoS One* 2. doi:10.1371/journal.pone.0000800.

Berluttil, F., Catizone, A., Riccp, G., Frioni, A., Natalizi, T., and Valenti, P. (2010). *Streptococcus mutans* and *Streptococcus sobrinus* are able to adhere and invade human gingival fibroblast cell line. *Int J Immunopathol Pharmacol.* 23, 1253–1260. doi: org/10.1177/039463201002300430.

Berman, H. M., Westbrook, J., Feng, Z., Gilliland, G., Bhat, T. N., Weissig, H., Shindyalov, I. N., and Bourne, P. E. (2000). The Protein Data Bank. *Nucleic Acids Res.,* 28(1), 235–242. doi: org/10.1093/nar/28.1.235.

Bhaya, D., Davison, M., and Barrangou, R. (2011). CRISPR-Cas systems in bacteria and archaea: versatile small RNAs for adaptive defense and regulation. *Annu. Rev. Genet.,* 45, 273–297. doi: org/10.1146/annurev-genet-110410-132430.

Bitoun, J. P., Liao, S., Yao, X., Ahn, S. J., Isoda, R., Nguyen, A. H., Brady, L. J., Burne, R. A., Abranches, J., and Wen, Z. T. (2012). BrpA is involved in regulation of cell envelope stress responses in *Streptococcus mutans. Applied and Environ. Microbiol.,* 78(8), 2914–2922. doi: org/10.1128/AEM.07823-11.

Bitoun, J.P., Liao, S., Xie, G.G., Beatty, W.L., Wen, Z.T. (2014). Deficiency of BrpB causes major defects in cell division, stress responses and biofilm formation by *Streptococcus mutans. Microbiol* (United Kingdom). 160:67-78. doi:10.1099/mic.0.072884-0.

Bjarnsholt, T., Ciofu, O., Molin, S., Givskov, M., and Høiby, N. (2013). Applying insights from biofilm biology to drug development-can a new approach be developed? *Nat. Rev. DrugDiscov.* 12, 791–808. doi: 10.1038/nrd4000.

Black, A. T., Gray, J. P., Shakarjian, M. P., Laskin, D. L., Diane, E., and Laskin, J. D. (2009). Increased oxidative stress and antioxidant expression in mouse keratinocytes following exposure to paraquat. *Toxicol Appl Pharmacol.* 231, 384–392. doi:10.1016/j.taap.2008.05.014.
Bondy-Denomy, J., Pawluk, A., Maxwell, K. L., and Davidson, A. R. (2013). Bacteriophage genes that inactivate the CRISPR/Cas bacterial immune system. *Nature,* 493(7432), 429–432. doi: org/10.1038/nature11723.

Bonofiglio, L., Gagetti, P., García Gabarrot, G., Kaufman, S., Mollerach, M., Toresani, I., *et al.* (2018). Susceptibility to β-lactams in β-hemolytic streptococci. *Rev. Argent. Microbiol.* 50, 431–

435. doi:10.1016/j.ram.2017.11.002.

Boonyayatra, S., and Pata, P. (2016). Antimicrobial resistance of biofilm-forming *Streptococcus agalactiae* isolated from bovine mastitis. *J. Vet. Sci. Technol.* 7. doi:10.4172/2157-7579.1000374.

Borriello, G., Werner, E., Roe, F., Kim, A. M., Ehrlich, G. D., and Stewart, P. S. (2004). Oxygen limitation contributes to antibiotic tolerance of Pseudomonas aeruginosa in biofilms. Antimicrobial agents and chemotherapy, 48(7), 2659–2664. doi: org/10.1128/AAC.48.7.2659-2664.2004 Del Pozo, J. L. (2018).

Borst, L. B., Patterson, S. K., Lanka, S., Suyemoto, M. M., and Maddox, C. W. (2013). Zebrafish (Danio rerio) as a screen for attenuation of Lancefield group C streptococci and a model for streptococcal pathogenesis. *Vet. Pathol.*, 50(3), 457–467. doi: org/10.1177/0300985811424731.

Botrel, M. A., Haenni, M., Morignat, E., Sulpice, P., Madec, J. Y., and Calavas, D. (2010). Distribution and antimicrobial resistance of clinical and subclinical mastitis pathogens in dairy cows in Rhône-Alpes, France. *Foodborne Pathog Dis*, 7(5), 479–487. doi: org/10.1089/fpd.2009.0425.

Bozdogan, B., Berrezouga, L., Kuo, M. S., Yurek, D. A., Farley, K. A., Stockman, B. J., and Leclercq, R. (1999). A new resistance gene, linB, conferring resistance to lincosamides by nucleotidylation in *Enterococcus faecium* HM1025. *Antimicrob. Agents Chemother.*, 43(4), 925–929. doi: org/10.1128/AAC.43.4.925.

Brandt, C. M., and Spellerberg, B. (2009). Human infections due to *Streptococcus dysgalactiae* subspecies *equisimilis*. *Clin Infect Dis* 49(5), 766–772. doi: org/10.1086/605085.

Brenciani, A., Bacciaglia, A., Vecchi, M., Vitali, L. A., Varaldo, P. E., and Giovanetti, E. (2007). Genetic elements carrying *erm(B)* in *Streptococcus pyogenes* and association with *tet(M)* tetracycline resistance gene. *Antimicrob Agents Chemother.*, 51(4), 1209–1216. doi: org/10.1128/AAC.01484-06.

Brenciani, A., Bacciaglia, A., Vignaroli, C., Pugnaloni, A., Varaldo, P. E., and Giovanetti, E. (2010). Φ m46.1, the main *Streptococcus pyogenes* element carrying *mef(A)* and *tet(O)* genes. *Antimicrob Agents Chemother.*, 54(1), 221–229. doi: 10.1128/AAC.00499-09.

Brenciani, A., Ojo, K. K., Monachetti, A., Menzo, S., Roberts, M. C., Varaldo, P. E., *et al.* (2004). Distribution and molecular analysis of mef(A)-containing elements in tetracycline-susceptible and -resistant *Streptococcus pyogenes* clinical isolates with efflux-mediated erythromycin resistance. *J. Antimicrob. Chemother.* 54, 991–998. doi: 10.1093/jac/dkh481.

Brenciani, A., Tiberi, E., Bacciaglia, A., Petrelli, D., Varaldo, P. E., and Giovanetti, E. (2011). Two distinct genetic elements are responsible for *erm*(TR)-mediated erythromycin resistance in tetracycline-susceptible and tetracycline-resistant strains of *Streptococcus pyogenes*. *Antimicrob. Agents Chemother.* 55, 2106– 2112. doi: 10.1128/AAC.01378-10.

Brigante, G., Luzzaro, F., Bettaccini, A., Lombardi, G., Meacci, F., Pini, B., Stefani, S., and Toniolo, A. (2006). Use of the Phoenix automated system for identification *of Streptococcus* and *Enterococcus* spp. *J. Clin. Microbiol.*, 44(9), 3263–3267. doi: org/10.1128/JCM.00299-06.

Brochet, M., Rusniok, C., Couvé, E., Dramsi, S., Poyart, C., Trieu-Cuot, P., Kunst, F., and Glaser, P. (2008). Shaping a bacterial genome by large chromosomal replacements, the evolutionary history of *Streptococcus agalactiae*. *Proc Natl Acad Sci USA.*, 105(41), 15961–15966. doi: org/10.1073/pnas.0803654105.

Broudy, T. B., Pancholi, V., and Fischetti, V. (2001). Induction of lysogenic bacteriophage and phage-associated toxin from group a streptococci during coculture with human pharyngeal cells. *Infect. Immun.* 69, 1440–3. doi:10.1128/IAI.69.3.1440-1443.2001.

Broudy, T. B., Pancholi, V., and Fischetti, V. A. (2002). The *In vitro* Interaction of *Streptococcus pyogenes* with human pharyngeal cells induces a phage-encoded extracellular DNase. *Infect Immun.* 70, 2805–2811. doi:10.1128/IAI.70.6.2805.

Bruun, T., Kittang, B. R., de Hoog, B. J., Aardal, S., Flaatten, H. K., Langeland, N., Mylvaganam, H., Vindenes, H. A., and Skrede, S. (2013). Necrotizing soft tissue infections caused by *Streptococcus pyogenes* and *Streptococcus dysgalactiae* subsp. *equisimilis* of groups C and G in western Norway. *Clin. Microbiol. Infect.*19(12), E545–E550. doi: org/10.1111/1469-0691.12276.

Burrell, H. E., Wlodarski, B., Foster, B. J., Buckley, K. A., Sharpe, G. R., Quayle, J. M., Simpson, A. W., and Gallagher, J. A. (2005). Human keratinocytes release ATP and utilize three mechanisms for nucleotide interconversion at the cell surface. *J. Biol. Chem.,* 280(33), 29667–29676. doi: org/10.1074/jbc.M505381200.

Reygaert, W. (2018). An overview of the antimicrobial resistance mechanisms of bacteria. *AIMS Microbiol.* 4, 482–501. doi:10.3934/microbiol.2018.3.482.

Calvinho, L., Almeida, R., and Oliver, S. (1998). Potential virulence factors of Streptococcus dysgalactiae associated with bovine mastitis. *Vet. Microbiol.* 61, 93–110. doi:10.1016/S0378-1135(98)00172-2.

Calvinho, L., and Oliver, S. (1998a). Characterization of mechanisms involved in uptake of Streptococcus dysgalactiae by bovine mammary epithelial cells. *Vet. Microbiol.* 63, 261–274. doi:10.1016/S0378-1135(98)00239-9.

Calvinho, L., and Oliver, S. (1998b). Invasion and persistence of streptococcus dysgalactiae within bovine mammary epithelial cells. *J. Dairy Sci.* 81, 678–686. doi:10.3168/jds.S0022-0302(98)75623-1.

Camacho, C., Coulouris, G., Avagyan, V., Ma, N., Papadopoulos, J., Bealer, K., and Madden, T. L. (2009). BLAST+: architecture and applications. *BMC bioinformatics,* 10, 421. doi: org/10.1186/1471-2105-10-421.

Canaparo, R., Foglietta, F., Giuntini, F., Pepa, C. Della, Dosio, F., and Serpe, L. (2019). Recent developments in antibacterial therapy: Focus on stimuli-responsive drug-delivery systems and therapeutic nanoparticles. *Molecules.* 24. doi:10.3390/molecules24101991.

Canchaya, C., Proux, C., Fournous, G., Bruttin, A., and Brüssow, H. (2003). Prophage Genomics. *Microbiol. Mol. Biol. Rev.* 67, 238–276. doi:10.1128/mmbr.67.2.238-276.2003.

Cantas, L., Sørby, J. R., Aleström, P., and Sørum, H. (2012). Culturable gut microbiota diversity in zebrafish. *Zebrafish,* 9(1), 26–37. doi: org/10.1089/zeb.2011.0712.

Canton J. (2018). Macropinocytosis: New insights into its underappreciated role in innate immune cell surveillance. *Front. Immunol.,* 9, 2286. doi: org/10.3389/fimmu.2018.02286.

Cao, K., Li, N., Wang, H., Cao, X., He, J., Zhang, B., He, Q. Y., Zhang, G., and Sun, X. (2018). Two zinc-binding domains in the transporter AdcA from *Streptococcus pyogenes* facilitate high-affinity binding and fast transport of zinc. *J. Biol. Chem.,* 293(16), 6075–6089. doi: org/10.1074/jbc.M117.818997.

Castilho, I. G., Dantas, S., Langoni, H., Araújo, J. P., Jr, Fernandes, A., Jr, Alvarenga, F., Maia, L., Cagnini, D. Q., and Rall, V. (2017). Host-pathogen interactions in bovine mammary epithelial

cells and HeLa cells by *Staphylococcus aureus* isolated from subclinical bovine mastitis. *J. Dairy Sci.*, 100(8), 6414–6421. doi: org/10.3168/jds.2017-12700.

Castillo-Martínez, J. C., Martínez-Castañón, G. A., Martínez-Gutierrez, F., Zavala-Alonso, N. V., Patiño-Marín, N., Niño-Martinez, N., Zaragoza-Magaña, V. and Cabral-Romero, C. (2015). Antibacterial and antibiofilm activities of the photothermal therapy using gold nanorods against seven different bacterial strains. *J. Nanomater.* 2015, 1–7. doi:10.1155/2015/783671.

Cattoir, V. (2016). Mechanisms of Antibiotic Resistance. In J. J. Ferretti (Eds.) *et. al., Streptococcus pyogenes*: Basic Biology to Clinical Manifestations. University of Oklahoma Health Sciences Center. https://pubmed.ncbi.nlm.nih.gov/26866217/

Cervinkova, D., Vlkova, H., Borodacova, I., Makovcova, J., Babak, V., Lorencova, A., Vrtkova, I., Marosevic, D., and Jaglic, Z. (2013). Prevalence of mastitis pathogens in milk from clinically healthy cows. *Vet. Med.* (Praha). 58, 567–575. https://www.agriculturejournals.cz/publicFiles/107534.pdf.

Chadha, T. (2014), Bacterial Biofilms: Survival mechanisms and antibiotic resistance. *J. Bacteriol. Parasitol.* 05, 5–8. doi:10.4172/2155-9597.1000190.

Chang, C. H., Lee, Y. H., Liao, Z. H., Chen, M. H. C., Peng, F. C., and Lin, J. J. (2021). Composition of nanoclay supported silver nanoparticles in furtherance of mitigating cytotoxicity and genotoxicity. *PLoSOne.* 2021. 16, 1–15. doi:10.1371/journal.pone.0247531.

Chang, Y. Y., Enninga, J., & Stévenin, V. (2021). New methods to decrypt emerging macropinosome functions during the host-pathogen crosstalk. *Cell. Microbiol., 23*(7), e13342. doi: org/10.1111/cmi.13342.

Chanter, N., Collin, N., Holmes, N., Binns, M., and Mumford, J. (1997). Characterization of the Lancefield group C streptococcus 16S-23S RNA gene intergenic spacer and its potential for identification and sub-specific typing. *Epidemiol. Infect.,* 118(2), 125–135. doi.org/10.1017/s0950268896007285.

Chatfield, C.H., Koo, H., Quivey, R.G. (2005). The putative autolysin regulator LytR in *Streptococcus mutans* plays a role in cell division and is growth-phase regulated. *Microbiology.* 151(2): 625-631. doi:10.1099/mic.0.27604-0.

Chen, L., and Wen, Y. M. (2011). The role of bacterial biofilm in persistent infections and control strategies. *Int J Oral Sci.,* 3(2), 66–73. doi: org/10.4248/IJOS11022.

Chennapragada, S. S., Ramphul, K., Barnett, B. J., Mejias, S. G., and Lohana, P. (2018). A Rare Case of *Streptococcus dysgalactiae* subsp. *dysgalactiae* human zoonotic infection. *Cureus,* 10(7), e2901. doi: org/10.7759/cureus.2901.

Christ, E. A., Meals, E., and English, B. K. (1997). Streptococcal pyrogenic exotoxins A (SpeA) and C (SpeC) stimulate the production of inducible nitric oxide synthase (iNOS) protein in RAW 264.7 macrophages. *Shock (Augusta, Ga.),* 8(6), 450–453.

Ciric, L., Jasni, A., Vries, L. E. De, Agersø, Y., Mullany, P., and Roberts, A. P. (2011). The Tn 916 /Tn 1545 Family of Conjugative Transposons. 1–17. https://www.ncbi.nlm.nih.gov/books/NBK63531/

Collin, M., and Olsén, A. (2003). Extracellular enzymes with immunomodulating activities: variations on a theme in *Streptococcus pyogenes. Infect Immun,* 71(6), 2983–2992. doi: org/10.1128/IAI.71.6.2983-2992.2003.

Conde, J., Larguinho, M., Cordeiro, A., Raposo, L. R., Costa, P. M., Santos, S. (2014). Gold-nanobeacons for gene therapy: Evaluation of genotoxicity, cell toxicity and proteome profiling analysis. *Nanotoxicology*. 8, 521–532. doi:10.3109/17435390.2013.802821.

Connolly, K. L., Roberts, A. L., Holder, R. C., and Reid, S. D. (2011). Dispersal of Group A streptococcal biofilms by the cysteine protease SpeB leads to increased disease severity in a murine model. *PloSOne*, 6(4), e18984. doi: org/10.1371/journal.pone.0018984.

Costa, C. S., Ronconi, J. V. V., Daufenbach, J. F., Gonçalves, C. L., Rezin, G. T., Streck, E. L., *et al.* (2010). In vitro effects of silver nanoparticles on the mitochondrial respiratory chain. *Mol. Cell. Biochem*. 342, 51–56. doi:10.1007/s11010-010-0467-9.

Costa, P.M. (2018). The handbook of histopathological practices in aquatic environments: guide to histology for environmental toxicology. Academic Press, Cambridge, MA, USA, 292 pp. 2018. (ISBN: 978-0-12-812032-3, doi: 10.1016/B978-0-12-812032-3.00006-X).

Courtney, H. S., Ofek, I., Penfound, T., Nizet, V., Pence, M. A., Kreikemeyer, B., Podbielski, A., Hasty, D. L., and Dale, J. B. (2009). Relationship between expression of the family of M proteins and lipoteichoic acid to hydrophobicity and biofilm formation in *Streptococcus pyogenes*. *PloSOne*, 4(1), e4166. doi: org/10.1371/journal.pone.0004166.

Crang, R.F.E. and Klomparens, K.L. (1998). Artifacts in Biological Electron Microscopy. *Science*. Vol. 242, (4876), 309. doi: 10.1126/science.242.4876.309.

Cui, Y., Zhao, Y., Tian, Y., Zhang, W., Lü, X., and Jiang, X. (2012). The molecular mechanism of action of bactericidal gold nanoparticles on *Escherichia coli*. *Biomaterials*. 33, 2327–2333. doi:10.1016/j.biomaterials.2011.11.057.

Cunha, V. Da, Davies, M. R., Douarre, P., and Rosinski-, I. (2015). Europe PMC Funders Group *Streptococcus agalactiae* clones infecting humans were selected and fixed through the extensive use of tetracycline. *Nat Commun*. 337549, 1–23. doi:10.1038/ncomms5544.

Dakal, T. C., Kumar, A., Majumdar, R. S., and Yadav, V. (2016). Mechanistic basis of antimicrobial actions of silver nanoparticles. *Front. Microbiol*. 7. doi:10.3389/fmicb.2016.01831.

Darenberg, J., Luca-Harari, B., Jasir, A., Sandgren, A., Pettersson, H., Schalén, C., Norgren, M., Romanus, V., Norrby-Teglund, A., and Normark, B. H. (2007). Molecular and clinical characteristics of invasive group A streptococcal infection in Sweden. *Clin Infect Dis.,* 45(4), 450–458. doi: org/10.1086/519936.

Datta, V., Myskowski, S. M., Kwinn, L. A., Chiem, D. N., Varki, N., Kansal, R. G., Kotb, M., and Nizet, V. (2005). Mutational analysis of the group A streptococcal operon encoding streptolysin S and its virulence role in invasive infection. *Mol. Microbiol., 56*(3), 681–695. doi: org/10.1111/j.1365-2958.2005.04583.x.

Davies, M. R., McIntyre, L., Mutreja, A., Lacey, J. A., Lees, J. A., Towers, R. J., *et al.* (2019). Atlas of group A streptococcal vaccine candidates compiled using large-scale comparative genomics. *Nat. Genet*. 51, 1035–1043. doi:10.1038/s41588-019-0417-8.

Davies, M. R., McMillan, D. J., Beiko, R. G., Barroso, V., Geffers, R., Sriprakash, K. S., and Chhatwal, G. S. (2007). Virulence profiling of *Streptococcus dysgalactiae* subspecies *equisimilis* isolated from infected humans reveals 2 distinct genetic lineages that do not segregate with their phenotypes or propensity to cause diseases. *Clinical infectious diseases.,* 44(11), 1442–1454. doi: org/10.1086/516780.

Davies, M. R., McMillan, D. J., Van Domselaar, G. H., Jones, M. K., and Sriprakash, K. S. (2007). Phage 3396 from a *Streptococcus dysgalactiae* subspecies *equisimilis* pathovar may have its

origins in *Streptococcus pyogenes. J. Bacteriol.* 189, 2646–2652. doi:10.1128/JB.01590-06.

De Kraker, M. E. A., Stewardson, A. J., and Harbarth, S. (2016). Will 10 Million People Die a Year due to Antimicrobial Resistance by 2050? *PLoSMed.* 13, 1–6. doi: 10.1371/journal.pmed.1002184.

De la Casa-Esperón E. (2012). Horizontal transfer and the evolution of host-pathogen interactions. *Int. J. Evol. Biol.*, 2012, 679045. doi: org/10.1155/2012/679045.

De Vliegher, S., Fox, L. K., Piepers, S., McDougall, S., and Barkema, H. W. (2012). Invited review: Mastitis in dairy heifers: nature of the disease, potential impact, prevention, and control. *J. Dairy Sci.* 95, 1025–40. doi:10.3168/jds.2010-4074.

Del Grosso, M., Camilli, R., Barbabella, G., Northwood, J. B., Farrell, D. J., and Pantosti, A. (2011). Genetic resistance elements carrying mef subclasses other than mef(A) in *Streptococcus pyogenes. Antimicrob. Agents Chemother.* 55, 3226–3230. doi: 10.1128/AAC.01713-10.

Del Pozo, J.L. (2018). "Biofilm-Related Disease." *Expert Rev Anti Infect Ther.* 16(1): 51–65. doi: org/10.1080/14787210.2018.1417036.

Di Luca, M. C., D'Ercole, S., Petrelli, D., Prenna, M., Ripa, S., and Vitali, L. A. (2010). Lysogenic transfer of mef(A) and tet(O) genes carried by m46.1 among group A streptococci. *Antimicrob. Agents Chemother.* 54, 4464–4466. doi:10.1128/AAC.01318-09.

Ding, X., Yuan, P., Gao, N., Zhu, H., Yang, Y.Y., and Xu, Q.H. (2017). Au-Ag core-shell nanoparticles for simultaneous bacterial imaging and synergistic antibacterial activity. *Nanomedicine.* 13(1), 297–305. doi.org/10.1016/j.nano.2016.09.003.

Diniz, M. S., Salgado, R., Pereira, V. J., Carvalho, G., Oehmen, A., Reis, M. A., and Noronha, J. P. (2015). Ecotoxicity of ketoprofen, diclofenac, atenolol and their photolysis byproducts in zebrafish (*Danio rerio*). *Sci. Total Environ*, 505, 282-289. doi: org/10.1016/j.scitotenv.2014.09.103.

Dinkla, K., Rohde, M., Jansen, W. T., Kaplan, E. L., Chhatwal, G. S., and Talay, S. R. (2003). Rheumatic fever-associated *Streptococcus pyogenes* isolates aggregate collagen. *J Clin Invest*, 111(12), 1905–1912. doi: org/10.1172/JCI17247.

Doern, C. D., Roberts, A. L., Hong, W., Nelson, J., Lukomski, S., Swords, W. E., and Reid, S. D. (2009). Biofilm formation by group A Streptococcus: a role for the streptococcal regulator of virulence (Srv) and streptococcal cysteine protease (SpeB). *Microbiology*, 155(Pt1), 46–52. doi: org/10.1099/mic.0.021048-0.

Dogan, B., Schukken, Y. H., Santisteban, C., and Boor, K. J. (2005). Distribution of serotypes and antimicrobial resistance genes among *Streptococcus agalactiae* isolates from bovine and human hosts. *J. Clin. Microbiol.* 43, 5899–5906. doi:10.1128/JCM.43.12.5899-5906.2005.

Döhrmann, S., Anik, S., Olson, J., Anderson, E. L., Etesami, N., No, H., Snipper, J., Nizet, V., and Okumura, C. Y. (2014). Role for streptococcal collagen-like protein 1 in M1T1 group A *Streptococcus* resistance to neutrophil extracellular traps. *Infect. Immun.*, 82 (10), 4011–4020. doi: org/10.1128/IAI.01921-14.

Donlan R. M. (2001). Biofilm formation: a clinically relevant microbiological process. *Clinical infectious diseases*, 33 (8), 1387–1392. doi: org/10.1086/322972.

Donlan R. M. (2002). Biofilms: microbial life on surfaces. *Emerg Infect Dis*, 8(9), 881–890. doi: org/10.3201/eid0809.020063.

Donlan, R. M., and Costerton, J. W. (2002). Biofilms: survival mechanisms of clinically relevant microorganisms. *Clin Microbiol Rev*, 15(2), 167–193. doi: org/10.1128/CMR.15.2.167-193.2002.

Doria, G., Larguinho, M., Dias, J.T., Pereira, E., Franco, R., and Baptista, P.V. (2010). Gold-silver-alloy nanoprobes for one-pot multiplex DNA detection. *Nanotechnology*. 21. doi:10.1088/0957-4484/21/25/255101.

Dos Santos, M. M., Queiroz, M. J., and Baptista, P. V. (2012). Enhancement of antibiotic effect via gold:silver-alloy nanoparticles. *J. Nanoparticle Res*. 14, 859–867. doi:10.1007/s11051-012-0859-8.

Doumith, M., Mushtaq, S., Martin, V., Chaudhry, A., Adkin, R., Coelho, J., Chalker, V., MacGowan, A., Woodford, N., Livermore, D. M., and BSAC Resistance Surveillance Standing Committee (2017). Genomic sequences of *Streptococcus agalactiae* with high-level gentamicin resistance, collected in the BSAC bacteraemia surveillance. *J Antimicrob Chemother*, 72(10), 2704–2707. doi: org/10.1093/jac/dkx207.

Dürig, A., Kouskoumvekaki, I., Vejborg, R. M., and Klemm, P. (2010). Chemoinformatics-assisted development of new anti-biofilm compounds. *Appl. Microbiol. Biotechnol.*, 87(1), 309–317. doi: org/10.1007/s00253-010-2471-0.

Dutta, D., and Donaldson, J. G. (2012). Search for inhibitors of endocytosis. *Cell. Logist.* 2, 203–208. doi:10.4161/cl.23967.

Dy, R. L., Przybilski, R., Semeijn, K., Salmond, G. P. C., and Fineran, P. C. (2014). A widespread bacteriophage abortive infection system functions through a Type IV toxin-antitoxin mechanism. *Nucleic Acids Res*. 42, 4590–4605. doi:10.1093/nar/gkt1419.

Dziduszko, A., and Ozbun, M. A. (2013). Annexin A2 and S100A10 regulate human papillomavirus type 16 entry and intracellular trafficking in human keratinocytes. *J. Virol.*, 87(13), 7502–7515. doi: org/10.1128/JVI.00519-13.

Dziduszko, A., and Ozbun, M. A. (2013). Annexin A2 and S100A10 regulate human papillomavirus type 16 entry and intracellular trafficking in human keratinocytes. *J. Virol.*, *87*(13), 7502–7515. doi: org/10.1128/JVI.00519-13.

Eberhardt, A., Hoyland, C. N., Vollmer, D., Bisle, S., Cleverley, R. M., Johnsborg, O., Håvarstein, L. S., Lewis, R. J., and Vollmer, W. (2012). Attachment of capsular polysaccharide to the cell wall in *Streptococcus pneumoniae*. *Microbial drug resistance*, 18(3), 240–255. doi: org/10.1089/mdr.2011.0232.

Efstratiou, A. (1997). Pyogenic streptococci of Lancefield groups C and G as pathogens in man. *Soc. Appl. Bacteriol. Symp. Ser.* 26:72S-79S. doi: 10.1046/j.1365-2672.83.s1.8.x.

Efstratiou, A., Colman, G., Hahn, G., Timoney, J. F., Boeufgras, J. M., and Monget, D. (1994). Biochemical differences among human and animal streptococci of Lancefield group C or group G. *Journal of medical microbiology*, *41*(2), 145–148. doi: org/10.1099/00222615-41-2-145.

Emaneini, M., Mirsalehian, A., Beigvierdi, R., Fooladi, A. A., Asadi, F., Jabalameli, F., and Taherikalani, M. (2014). High incidence of macrolide and tetracycline resistance among *Streptococcus agalactiae* strains isolated from clinical samples in Tehran, Iran. *Maedica*, 9(2), 157–161. https://pubmed.ncbi.nlm.nih.gov/25705271/

Enault, F., Briet, A., Bouteille, L., Roux, S., Sullivan, M. B., and Petit, M. A. (2017). Phages rarely encode antibiotic resistance genes: A cautionary tale for virome analyses. *ISME J*. 11, 237–247. doi:10.1038/ismej.2016.90.

Eraso, J. M., Kachroo, P., Olsen, R. J., Beres, S. B., Zhu, L., Badu, T., Shannon, S., Cantu, C. C., Saavedra, M. O., Kubiak, S. L., Porter, A. R., DeLeo, F. R., and Musser, J. M. (2020). Genetic heterogeneity of the Spy1336/R28-Spy1337 virulence axis in *Streptococcus pyogenes* and effect on gene transcript levels and pathogenesis. *PloSOne*, 15(3), e0229064. doi:

org/10.1371/journal.pone.0229064.

Fair, R. J., and Tor, Y. (2014). Antibiotics and bacterial resistance in the 21st century. *Perspect. Medicinal Chem.* 6, 25–64. doi.org/10.4137/PMC.S14459.

Fernandes, A. R., Mendonça-Martins, I., Santos, M., Raposo, L. R., Mendes, R., Marques, J., Romão, C. C., Romão, M. J., Santos-Silva, T., and Baptista, P. V. (2020). Improving the Anti-inflammatory Response via Gold Nanoparticle Vectorization of CO-Releasing Molecules. *ACS Biomater. Sci. Eng.* 6, 1090–1101. doi:10.1021/acsbiomaterials.9b01936.

Fernandes, A.R., Jesus, J., Martins, P., Figueiredo, S., Rosa, D., Martins, L.M., Corvo, M.L., Carvalheiro, M. C., Costa, P. M., and Baptista, P.V. (2017). Multifunctional gold-nanoparticles: A nanovectorization tool for the targeted delivery of novel chemotherapeutic agents. *Journal of controlled release: official journal of the Controlled Release Society*, *245*, 52–61. doi:org/10.1016/j.jconrel.2016.11.021.

Fernandez, A., Lechardeur, D., Derré-Bobillot, A., Couvé, E., Gaudu, P., and Gruss, A. (2010). Two coregulated efflux transporters modulate intracellular heme and protoporphyrin ix availability in *Streptococcus agalactiae*. *PLoS Pathog.* 6, 1–14. doi:10.1371/journal.ppat.1000860.

Ferreira, F. A., Souza, R. R., Bonelli, R. R., Américo, M. A., Fracalanzza, S. E., and Figueiredo, A. M. (2012). Comparison of *in vitro* and *in vivo* systems to study ica-independent *Staphylococcus aureus* biofilms. *J.Microbiol. Methods*, 88(3), 393–398. doi: org/10.1016/j.mimet.2012.01.007.
Fiedler, T., Köller, T., and Kreikemeyer, B. (2015). *Streptococcus pyogenes* biofilms- formation, biology, and clinical relevance. *Front. Cell. Infect. Microbiol*, 5:15. doi: 10.3389/fcimb.2015.00015

Fiedler, T., Riani, C., Koczan, D., Standar, K., Kreikemeyer, B., and Podbielski, A. (2013). Protective mechanisms of respiratory tract Streptococci against *Streptococcus pyogenes* biofilm formation and epithelial cell infection. *Appl. Environ. Microbiol.* 79, 1265–1276. doi: 10.1128/AEM.03350-12.

Fisher A.B. (2011). Peroxiredoxin 6: a bifunctional enzyme with glutathione peroxidase and phospholipase A$_2$ activities. *Antioxidants and redox signaling*, *15*(3), 831–844. doi: org/10.1089/ars.2010.3412.

Flemming, H. C., and Wingender, J. (2010). The biofilm matrix. Nature reviews. Microbiology, 8(9), 623–633. doi: org/10.1038/nrmicro2415.

Frost, H. R., Sanderson-Smith, M., Walker, M., Botteaux, A., and Smeesters, P. R. (2018). Group A streptococcal M-like proteins: From pathogenesis to vaccine potential. *FEMS microbiology reviews*, *42*(2), 193–204. doi: org/10.1093/femsre/fux057.

Fuursted, K., Stegger, M., Hoffmann, S., Lambertsen, L., Andersen, P. S., Deleuran, M., and Thomsen, M. K. (2016). Description and characterization of a penicillin-resistant *Streptococcus dysgalactiae* subsp. *equisimilis* clone isolated from blood in three epidemiologically linked patients. *The Journal of antimicrobial chemotherapy*, *71*(12), 3376–3380. doi: org/10.1093/jac/dkw320.

Galante, J., Ho, A. C., Tingey, S., and Charalambous, B. M. (2015). Quorum sensing and biofilms in the pathogen, *Streptococcus pneumoniae*. *Current pharmaceutical design*, *21*(1), 25–30. doi: org/10.2174/1381612820666140905113336.

Galimand, M., Lambert, T., Gerbaud, G., and Courvalin, P. (1999). High-level aminoglycoside resistance in the beta-hemolytic group G *Streptococcus* isolate BM2721. *Antimicrob. Agents Chemother.* 43, 3008–3010. doi:10.1128/aac.43.12.3008.

Gao, J., Yu, F. Q., Luo, L. P., He, J. Z., Hou, R. G., Zhang, H. Q., *et al.* (2012). Antibiotic resistance of *Streptococcus agalactiae* from cows with mastitis. *Vet. J.* 194, 423–424. doi:10.1016/j.tvjl.2012.04.020.

Gao, K., Guan, X., Zeng, L., Qian, J., Zhu, S., Deng, Q., *et al.* (2018). An increasing trend of neonatal invasive multidrug-resistant group B streptococcus infections in Southern China, 2011–2017. Infect. Drug Resist. 11, 2561–2569. doi:10.2147/IDR.S178717.

Gardy, J. L., Spencer, C., Wang, K., Ester, M., Tusnády, G. E., Simon, I., Hua, S., deFays, K., Lambert, C., Nakai, K., and Brinkman, F. S. (2003). PSORT-B: Improving protein subcellular localization prediction for Gram-negative bacteria. *Nucleic Acids Res., 31*(13), 3613–3617. doi: org/10.1093/nar/gkg602.

Garnett, J. A., and Matthews, S. (2012). Interactions in bacterial biofilm development: a structural perspective. *Curr. Protein Pept. Sci.*, 13(8), 739–755. doi: org/10.2174/138920312804871166.

Garnett, J. A., Martínez-Santos, V. I., Saldaña, Z., Pape, T., Hawthorne, W., Chan, J., Simpson, P. J., Cota, E., Puente, J. L., Girón, J. A., and Matthews, S. (2012). Structural insights into the biogenesis and biofilm formation by the *Escherichia coli* common pilus. *Proc Natl Acad Sci USA.*, 109(10), 3950–3955. doi: org/10.1073/pnas.1106733109.

Garrett, T. R., Bhakoo, M., and Zhang, Z. (2008). Bacterial adhesion and biofilms on surfaces. *Prog. Nat. Sci.*, 18(9), 1049-1056. doi: org/10.1016/j.pnsc.2008.04.001.

Gasteiger, E., Hoogland. C., Gattiker, A. (2005). Protein Identification and Analysis Tools on the ExPASy Server. Proteomics Protoc Handb. 571-607. doi:10.1385/1-59259-890-0:571.

Genteluci, G. L., Silva, L. G., Souza, M. C., Glatthardt, T., de Mattos, M. C., Ejzemberg, R., Alviano, C. S., Figueiredo, A. M., and Ferreira-Carvalho, B. T. (2015). Assessment and characterization of biofilm formation among human isolates of *Streptococcus dysgalactiae* subsp. *equisimilis. IJMM*, 305(8), 937–947. doi: org/10.1016/j.ijmm.2015.10.004.

Ghinet, M. G., Asli, A., Brouillette, E., Ster, C., Brzezinski, R., Lacasse, P., Jacques, M., and Malouin, F. (2017). Antibiofilm and antibacterial effects of specific chitosan molecules on *Staphylococcus aureus* isolates associated with bovine mastitis. *PloSOne*, 12(5), e0176988. doi: org/10.1371/journal.pone.0176988.

Ghosh, C., Sarkar, P., Issa, R., and Haldar, J. (2019). Alternatives to conventional antibiotics in the era of antimicrobial resistance. *Trends in microbiol*, 27(4), 323–338. doi: org/10.1016/j.tim.2018.12.010.

Giovanetti, E., Brenciani, A., Lupidi, R., Roberts, M. C., and Varaldo, P. E. (2003). Presence of the tet(O) gene in erythromycin- and tetracycline-resistant strains of Streptococcus pyogenes and linkage with either the *mef*(A) or the *erm*(A) gene. *Antimicrob. Agents Chemother.* 47, 2844–2849. doi:10.1128/AAC.47.9.2844-2849.2003.

Giovanetti, E., Brenciani, A., Morroni, G., Tiberi, E., Pasquaroli, S., Mingoia, M., and Varaldo, P. E. (2015). Transduction of the *Streptococcus pyogenes* bacteriophage m46.1, carrying resistance genes *mef(A)* and *tet(O)*, to other *Streptococcus* species. *Front. Microbiol.*, 5, 746. doi: org/10.3389/fmicb.2014.00746.

Giuliano, S., Rubini, G., Conte, A., Goldoni, P., Falcone, M., Vena, A., Venditti, M., and Morelli, S. (2012). *Streptococcus anginosus* group disseminated infection: case report and review of literature. *Le infezioni in medicina, 20*(3), 145–154.

Gomes, F., Saavedra, M. J., and Henriques, M. (2016). Bovine mastitis disease/pathogenicity: evidence of the potential role of microbial biofilms. *Pathog. Dis.*, 74(3), ftw006. doi:

org/10.1093/femspd/ftw006.

Gomes, L. C., and Mergulhão, F. J. (2017). SEM Analysis of Surface Impact on Biofilm Antibiotic Treatment. *Scanning, 2017*, 2960194. doi: org/10.1155/2017/2960194.

Gómez-Núñez, M.F., Castillo-López, M., Sevilla-Castillo, F., Roque-Reyes, O.J., Romero-Lechuga, F., Medina-Santos, D.I., Martínez-Daniel, R., and Peón, A.N. (2020). Nanoparticle-Based Devices in the Control of Antibiotic Resistant Bacteria. *Front. Microbiol.* 11, 1–15. doi:10.3389/fmicb.2020.563821.

Graham, S. W., Olmstead, R. G., and Barrett, S. C. (2002). Rooting phylogenetic trees with distant outgroups: a case study from the commelinoid monocots. *Mol. Biol. Evol., 19*(10), 1769–1781. doi: org/10.1093/oxfordjournals.molbev.a003999.

Grande, R., Di Giulio, M., Bessa, L. J., Di Campli, E., Baffoni, M., Guarnieri, S., and Cellini, L. (2011). Extracellular DNA in Helicobacter pylori biofilm: a backstairs rumour. *J. Appl. Microbiol.,* 110(2), 490–498. doi: org/10.1111/j.1365-2672.2010.04911.x.

Green, N. M., Beres, S. B., Graviss, E. A., Allison, J. E., McGeer, A. J., Vuopio-Varkila, J., LeFebvre, R. B., and Musser, J. M. (2005). Genetic diversity among type emm28 group A Streptococcus strains causing invasive infections and pharyngitis. *J. Clin. Microbiol.,* 43(8), 4083–4091. doi: org/10.1128/JCM.43.8.4083-4091.2005.

Grissa, I., Vergnaud, G., and Pourcel, C. (2007). CRISPRFinder: a web tool to identify clustered regularly interspaced short palindromic repeats. *Nucleic Acids Res.,* 35, W52–W57. doi: org/10.1093/nar/gkm360.

Grohmann, E., Muth, G., and Espinosa, M. (2003). Conjugative plasmid transfer in gram-positive bacteria. *Microbiol Mol Biol Rev:* 67(2), 277–301. doi: org/10.1128/mmbr.67.2.277-301.2003.

Guo, A., Fu, Y., Wang, G., and Wang, X. (2017). Diameter effect of gold nanoparticles on photothermal conversion for solar steam generation. *RSC Adv.* 7, 4815–4824. doi:10.1039/C6RA26979F.

Gupta, P., Sarkar, S., Das, B., Bhattacharjee, S., and Tribedi, P. (2016). Biofilm, pathogenesis and prevention--a journey to break the wall: a review. *Arch. Microbiol.,* 198(1), 1–15. doi: org/10.1007/s00203-015-1148-6.

Hadjirin, N. F., Harrison, E. M., Holmes, M. A., and Paterson, G. K. (2014). Conjugative transfer frequencies of *mef*(A)-containing Tn1207.3 to macrolide- susceptible *Streptococcus pyogenes* belonging to different emm types. *Lett. Appl. Microbiol.* 58, 299–302. doi: 10.1111/lam.12213.

Haenni, M., Saras, E., Bertin, S., Leblond, P., Madec, J. Y., and Payot, S. (2010). Diversity and mobility of integrative and conjugative elements in bovine isolates of *Streptococcus agalactiae, S. dysgalactiae* subsp. *dysgalactiae,* and *S. uberis. Appl Environ Microbiol,* 76(24), 7957–7965. doi: org/10.1128/AEM.00805-10.

Hagiya, H., Okita, S., Kuroe, Y., Nojima, H., Otani, S., Sugiyama, J., Naito, H., Kawanishi, S., Hagioka, S., and Morimoto, N. (2013). A fatal case of streptococcal toxic shock syndrome due to Streptococcus dysgalactiae subsp. equisimilis possibly caused by an intramuscular injection. *Internal medicine,* 52(3), 397–402. doi: org/10.2169/internalmedicine.52.8846.

Hall-Stoodley, L., Costerton, J. W., and Stoodley, P. (2004). Bacterial biofilms: from the natural environment to infectious diseases. *Nat. Rev. Microbiology,* 2(2), 95–108. doi: org/10.1038/nrmicro821.

Hampton, M. B., and O'Connor, K. M. (2016). Peroxiredoxins and the Regulation of Cell Death. *Molecules and cells, 39*(1), 72–76. doi: org/10.14348/molcells.2016.2351.

Hardie, M., and Whiley, R. A. (1997). Classification and overview of the genera streptococcus and enterococcus ü. J. *Appl. Microbiol. Symp. Suppl.* 83, 1–11. doi:10.1046/j.1365-2672.83.s1.1.x.

Hendriksen, R. S., Mevius, D. J., Schroeter, A., Teale, C., Meunier, D., Butaye, P., Franco, A., Utinane, A., Amado, A., Moreno, M., Greko, C., Stärk, K., Berghold, C., Myllyniemi, A. L., Wasyl, D., Sunde, M., and Aarestrup, F. M. (2008). Prevalence of antimicrobial resistance among bacterial pathogens isolated from cattle in different European countries: 2002-2004. *Acta Vet. Scand.*, 50(1), 28. doi: org/10.1186/1751-0147-50-28.

Henriques-Normark, B., and Tuomanen, E. I. (2013). The pneumococcus: Epidemiology, microbiology, and pathogenesis. *Cold Spring Harb. Perspect. Med.* 3, 1–15. doi:10.1101/cshperspect.a010215.

Hille, F., Richter, H., Wong, S. P., Bratovi , M., Ressel, S., and Charpentier, E. (2018). The biology of CRISPR-Cas: backward and forward. *Cell,* 172(6), 1239–1259. doi: org/10.1016/j.cell.2017.11.032.

Holden, M. T., Heather, Z., Paillot, R., Steward, K. F., Webb, K., Ainslie, F., Jourdan, T., Bason, N. C., Holroyd, N. E., Mungall, K., Quail, M. A., Sanders, M., Simmonds, M., Willey, D., Brooks, K., Aanensen, D. M., Spratt, B. G., Jolley, K. A., Maiden, M. C., Kehoe, M., … Waller, A. S. (2009). Genomic evidence for the evolution of *Streptococcus equi*: host restriction, increased virulence, and genetic exchange with human pathogens. *PLoS pathog., 5*(3), e1000346. doi: org/10.1371/journal.ppat.1000346.

Hooper, D. C., and Jacoby, G. A. (2016). Topoisomerase inhibitors: fluoroquinolone mechanisms of action and resistance. *Cold Spring Harb Perspect Biol,* 6(9), a025320. doi: org/10.1101/cshperspect.a025320.

Horiuk, Y., Kukhtyn, M., Kovalenko, V., Kornienko, L., Horiuk, V. and Liniichuk, N. (2019). Biofilm formation in bovine mastitis pathogens and the effect on them of antimicrobial drugs. *IJM&P.* 10(7):897. doi: 10.14807/ijmp.v10i7.1012.

Hsu, H. H., Hoffmann, S., Di Marco, G. S., Endlich, N., Peter-Katalini , J., Weide, T., and Pavenstädt, H. (2011). Downregulation of the antioxidant protein peroxiredoxin 2 contributes to angiotensin II-mediated podocyte apoptosis. *Kidney Int.,* 80(9), 959–969. doi: org/10.1038/ki.2011.250.

Hu, T., Cui, Y., and Qu, X. (2020). Characterization and comparison of CRISPR Loci in *Streptococcus thermophilus. Arch. Microbiol.,* 202(4), 695–710. doi: org/10.1007/s00203-019-01780-3.

Hwang-Soo, J., Chih-Iung, F., and Michael, O. (2016). Bacterial strategies of resistance to antimicrobial peptides. *Philos. Trans. R. Soc. B Biol. Sci.* 371, 20150292. doi:10.1098/rstb.2015.0292.

Ibelli, T., Templeton, S., and Levi-Polyachenko, N. (2018). Progress on utilizing hyperthermia for mitigating bacterial infections. *Int. J. Hyperth.* 34(2), 144–156. doi.org/10.1080/02656736.2017.1369173

Irwin, J. J., and Shoichet, B. K. (2005). ZINC--a free database of commercially available compounds for virtual screening. *J Chem Inf Model,* 45(1), 177–182. doi: org/10.1021/ci049714+.

Isaacs, D., and Dobson, S. R. M. (2016). Severe Group A Streptococcal Infections. *Curr. Opin. Infect. Dis.* 2, 453–456. doi:10.1097/00001432-198906000-00022.

Jakubovics, N. S., Shields, R. C., Rajarajan, N., and Burgess, J. G. (2013). Life after death: the critical role of extracellular DNA in microbial biofilms. *Lett. Appl. Microbiol.*, *57*(6), 467–475. doi: org/10.1111/lam.12134.

Jalava, J., Vaara, M., and Huovinen, P. (2004). Mutation at the position 2058 of the 23S rRNA as a cause ofmacrolide resistance in *Streptococcus pyogenes*. *Ann. Clin. Microbiol. Antimicrob.* 3:5. doi: 10.1186/1476-0711-3-5.

Jamal, M., Ahmad, W., Andleeb, S., Jalil, F., Imran, M., Nawaz, M. A., Hussain, T., Ali, M., Rafiq, M., and Kamil, M. A. (2018). Bacterial biofilm and associated infections. *JCMA*, 81(1), 7–11. doi: org/10.1016/j.jcma.2017.07.012.

Jasir, A., Tanna, A., Efstratiou, A., and Schalén, C. (2001). Unusual occurrence of M type 77, antibiotic-resistant group A streptococci in southern Sweden. *J. Clin. Microbiol.*, 39(2), 586–590. doi: org/10.1128/JCM.39.2.586-590.2001.

Jefferson K. K. (2004). What drives bacteria to produce a biofilm? *FEMS Microbiol. Lett.*, 236(2), 163–173. doi: org/10.1016/j.femsle.2004.06.005.

Jensen, A., and Kilian, M. (2012). Delineation of *Streptococcus dysgalactiae*, its subspecies, and its clinical and phylogenetic relationship to *Streptococcus pyogenes*. *J. Clin. Microbiol.*, 50(1), 113–126. doi: org/10.1128/JCM.05900-11.

Jiang, W.Y., and Ran, S.Y. (2018). Two-stage DNA compaction induced by silver ions suggests a cooperative binding mechanism. *J. Chem. Phys.* 148. doi:10.1063/1.5025348.

Jo, W., and Kim, M.J. (2013). Influence of the photothermal effect of a gold nanorod cluster on biofilm disinfection. *Nanotechnology.* 24. doi:10.1088/0957-4484/24/19/195104.

Johansson, L. H., & Borg, L. A. (1988). A spectrophotometric method for determination of catalase activity in small tissue samples. *Analytical biochemistry*, *174*(1), 331–336. doi: org/10.1016/0003-2697(88)90554-4.

John P. Dekker, A. F. L. (2016). An Update on the *Streptococcus bovis* Group: Classification, Identification, and Disease Associations. 54, 1694–1699. doi:10.1128/JCM.02977-15.

Jordal, S., Glambek, M., Oppegaard, O., and Kittang, B. R. (2015). New tricks from an old cow: infective endocarditis caused by *Streptococcus dysgalactiae* subsp. *dysgalactiae*. *J. Clin. Microbiol.*, *53*(2), 731–734. doi: org/10.1128/JCM.02437-14.

Joshi, A.S., Singh, P., and Mijakovic, I. (2020). Interactions of gold and silver nanoparticles with bacterial biofilms: Molecular interactions behind inhibition and resistance. *Int. J. Mol. Sci.* 21, 1–24. doi:10.3390/ijms21207658.

Joubert, L., Dagieu, J. B., Fernandez, A., Aurélie, D. B., Elise, B. D., Fleurot, I., *et al.* (2017). Visualization of the role of host heme on the virulence of the heme auxotroph *Streptococcus agalactiae*. *Sci. Rep.* 7, 1–13. doi:10.1038/srep40435.

Junckerstorff, R. K., Robinson, J. O., and Murray, R. J. (2014). International Journal of Infectious Diseases Invasive *Streptococcus anginosus* group infection — does the species predict the outcome? *Int. J. Infect. Dis.* 18, 38–40. doi:10.1016/j.ijid.2013.09.003.

Kaczorek, E., Małaczewska, J., Wójcik, R., and Siwicki, A. K. (2017). Biofilm production and other virulence factors in *Streptococcus* spp. isolated from clinical cases of bovine mastitis in Poland. BMC veterinary research, 13(1), 398. doi: org/10.1186/s12917-017-1322-y.

Kalia, A., and Bessen, D. E. (2004). Natural selection and evolution of streptococcal virulence genes involved in tissue-specific adaptations. *J. Bacteriol.* 186, 110–121. doi:10.1128/JB.186.1.110-121.2004.

Kawai, Y., Marles-Wright, J., Cleverley, R. M., Emmins, R., Ishikawa, S., Kuwano, M., Heinz, N., Bui, N. K., Hoyland, C. N., Ogasawara, N., Lewis, R. J., Vollmer, W., Daniel, R. A., and Errington, J. (2011). A widespread family of bacterial cell wall assembly proteins. *The EMBO journal*, 30(24), 4931–4941. doi: org/10.1038/emboj.2011.358.

Khan, A., Farooq, U., Ahmad, T., Sarwar, R., Shafiq, J., Raza, Y., *et al.* (2019). Rifampicin conjugated silver nanoparticles: A new arena for development of antibiofilm potential against methicillin resistant *Staphylococcus aureus* and *Klebsiella pneumonia*. *Int. J. Nanomedicine* 14, 3983–3993. doi:10.2147/IJN.S198194.

Khatoon, Z., Mctiernan, C. D., Suuronen, E. J., and Mah, T. (2018). Bacterial biofilm formation on implantable devices and approaches to its treatment and prevention. *Heliyon*, e01067. doi:10.1016/j.heliyon.2018.e01067.

Kim, M., Lee, J.H., and Nam, J.M. (2019). Plasmonic Photothermal Nanoparticles for Biomedical Applications. *Adv. Sci.* 6. doi:10.1002/advs.201900471.

Kimura, K., Nagano, N., Nagano, Y., Suzuki, S., Wachino, J., Shibayama, K., and Arakawa, Y. (2013). High frequency of fluoroquinolone- and macrolide-resistant streptococci among clinically isolated group B streptococci with reduced penicillin susceptibility. *J Antimicrob Chemother*, 68(3), 539–542. doi: org/10.1093/jac/dks423.

Kirui, D. K., Weber, G., Talackine, J., and Millenbaugh, N.J. (2019). Targeted laser therapy synergistically enhances efficacy of antibiotics against multidrug resistant *Staphylococcus aureus* and *Pseudomonas aeruginosa* biofilms. *Nanomedicine Biol. Med.* 20, 102018. doi:10.1016/j.nano.2019.102018.

Klaas, I.C. and Zadoks, R.N. (2018). An update on environmental mastitis: challenging perceptions. *Transbound Emerg Dis*, 65(S1), 166-185. doi:10.1111/tbed.12704.

Kline, J. B., Xu, S., Bisno, A. L., and Collins, C. M. (1996). Identification of a fibronectin-binding protein (GfbA) in pathogenic group G streptococci. *Infect. Immun.*, 64(6), 2122–2129. doi: org/10.1128/iai.64.6.2122-2129.1996.

Koh, T. H., Binte Abdul Rahman, N., and Sessions, O. M. (2020). Comparative genomic analysis of *Streptococcus dysgalactiae* subspecies *dysgalactiae*, an occasional cause of zoonotic infection. *Pathology* 52, 262–266. doi:10.1016/j.pathol.2019.09.016.

Koh, T. H., Sng, L. H., Yuen, S. M., Thomas, C. K., Tan, P. L., Tan, S. H., and Wong, N. S. (2009). Streptococcal cellulitis following preparation of fresh raw seafood. *Zoonoses Public Health*, 56(4), 206–208. doi: org/10.1111/j.1863-2378.2008.01213.x.

Koivusalo, M., Welch, C., Hayashi, H., Scott, C. C., Kim, M., Alexander, T., Touret, N., Hahn, K. M., and Grinstein, S. (2010). Amiloride inhibits macropinocytosis by lowering submembranous pH and preventing Rac1 and Cdc42 signaling. *J. Cell Biol*, 188(4), 547–563. doi:org/10.1083/jcb.200908086.

Kojima, A., Nakano, K., Wada, K., Takahashi, H., Katayama, K., Yoneda, M., *et al.* (2012). Infection of specific strains of *Streptococcus mutans*, oral bacteria, confers a risk of ulcerative colitis. *Sci. Rep.* 2, 1–11. doi:10.1038/srep00332.

Kokare, C.R., Chakraborty, S., Khopade, A.N., and Mahadik, K.R. (2009). Biofilm: Importance and applications. *Indian Journal of Biotechnology*. 8, 159–168. http://nopr.niscair.res.in/handle/123456789/3883.

Konto-Ghiorghi, Y., Mairey, E., Mallet, A., Duménil, G., Caliot, E., Trieu-Cuot, P., and Dramsi, S. (2009). Dual role for pilus in adherence to epithelial cells and biofilm formation in *Streptococcus agalactiae*. *PLoS pathog.*, 5(5), e1000422. doi: org/10.1371/journal.ppat.1000422.

Kosecka-Strojek, M., Wolska, M., abicka, D., Sadowy, E., and Mi dzobrodzki, J. (2020). Identification of clinically relevant streptococcus and enterococcus species based on biochemical methods and 16s rRNA, SODA, TUF, RPOB, and RECA gene sequencing. *Pathogens* 9, 1–21. doi:10.3390/pathogens9110939.

Kostakioti, M., Hadjifrangiskou, M., and Hultgren, S. J. (2013). Bacterial biofilms: development, dispersal, and therapeutic strategies in the dawn of the postantibiotic era. *Cold Spring Harb Perspect Med*, 3(4), a010306. doi: org/10.1101/cshperspect.a010306.

Kragh, K. N., Hutchison, J. B., Melaugh, G., Rodesney, C., Roberts, A. E., Irie, Y., Jensen, P. Ø., Diggle, S. P., Allen, R. J., Gordon, V., and Bjarnsholt, T. (2016). Role of Multicellular Aggregates in Biofilm Formation. *mBio.* 7(2), e00237. doi.org/10.1128/mBio.00237-16.

Krantz, A. M., Ratnaraj, F., Velagapudi, M., Krishnan, M., Gujjula, N. R., Foral, P. A., *et al.* (2017). Streptococcus Gordonii Empyema: A Case Report and Review of Empyema. *Cureus* 9. doi:10.7759/cureus.1159.

Kristich, C. J., Rice, L. B., Arias, C. A. (2014). "Enterococcal infection treatment and antibiotic resistance", in Enterococci: from commensals to leading causes of drug resistant infection, ed Massachusetts Eye and Ear Infirmary (Boston, MA),123–185. https://www.ncbi.nlm.nih.gov/books/NBK190424/

Krzy ciak, W., Jurczak, A., Ko cielniak, D., Bystrowska, B., and Skalniak, A. (2014). The virulence of Streptococcus mutans and the ability to form biofilms. *European J. Clin. Microbiol. and infectious disease.* 33(4), 499–515. doi: org/10.1007/s10096-013-1993-7.

Kumar, A., Alam, A., Rani, M., Ehtesham, N. Z., and Hasnain, S. E. (2017). Biofilms: survival and defense strategy for pathogens. *Int. J. Med. Microbiol.* 307, 481–489. doi:10.1016/j.ijmm.2017.09.016.

Kumar, S., Stecher, G., Li, M., Knyaz, C., and Tamura, K. (2018). MEGA X: molecular evolutionary genetics analysis across computing platforms. *Mol. Biol. Evol.*, 35(6), 1547–1549. doi: org/10.1093/molbev/msy096.

Kurjogi, M. M., and Kaliwal, B. B. (2014). Epidemiology of bovine mastitis in cows of dharwad district. *Int. Sch. Res. Not.*, 1–9. doi:10.1155/2014/968076.

Kvist, M., Hancock, V., and Klemm, P. (2008). Inactivation of efflux pumps abolishes bacterial biofilm formation. *Applied and Environ. Microbiol.*, 74(23), 7376–7382. doi: org/10.1128/AEM.01310-08.

Kyaw, K., Ichimaru, H., Kawagoe, T., Terakawa, M., Miyazawa, Y., Mizoguchi, D., D., Tsushida, M., and Niidome, T. (2017). Effects of pulsed laser irradiation on gold-coated silver nanoplates and their antibacterial activity. *Nanoscale* 9, 16101–16105. doi:10.1039/c7nr06513b.

La Spina, R., Mehn, D., Fumagalli, F., Holland, M., Reniero, F., Rossi, F., and Gilliland, D. (2020). Synthesis of citrate-stabilized silver nanoparticles modified by thermal and pH preconditioned tannic acid. *Nanomaterials.* 10, 1–16. doi:10.3390/nano10102031.

Labrie, S. J., Samson, J. E., and Moineau, S. (2010). Bacteriophage resistance mechanisms. *Nat. Publ. Gr.* 8, 317–327. doi:10.1038/nrmicro2315.

Lacasta, D., Ferrer, L. M., Ramos, J. J., Loste, A., and Bueso, J. P. (2008). Digestive pathway of infection in *Streptococcus dysgalactiae* polyarthritis in lambs. *Small Rumin. Res.* 78, 202–205. doi:10.1016/j.smallrumres.2008.06.001.

Lai, L., Dai, J., Tang, H., Zhang, S., Wu, C., Qiu, W., Lu, C., Yao, H., Fan, H., and Wu, Z. (2017). *Streptococcus suis* serotype 9 strain GZ0565 contains a type VII secretion system putative substrate EsxA that contributes to bacterial virulence and a *vanZ*-like gene that confers resistance to teicoplanin and dalbavancin in *Streptococcus agalactiae. Vet Microbiol,* 205, 26–33. doi: org/10.1016/j.vetmic.2017.04.030.

Lal, D., Verma, M., and Lal, R. (2011). Exploring internal features of 16S rRNA gene for identification of clinically relevant species of the genus *Streptococcus. Ann. Clin. Microbiol. Antimicrob.* 10, 28. doi:10.1186/1476-0711-10-28.

Lancefield R. C. (1933). A serological differentiation of human and other groups of hemolytic streptococci. *J. Exp. Med.,* 57(4), 571–595. doi: org/10.1084/jem.57.4.571.

Landsberger, M., Gandon, S., Meaden, S., Rollie, C., Chevallereau, A., Chabas, H., Buckling, A., Westra, E. R., and van Houte, S. (2018). Anti-CRISPR Phages cooperate to overcome CRISPR-Cas immunity. *Cell,* 174(4), 908–916.e12. doi: org/10.1016/j.cell.2018.05.058.

Lansdown, A. B. G. (2006). Silver in health care: Antimicrobial effects and safety in use. *Curr. Probl. Dermatol.* 33, 17–34. doi:10.1159/000093928.

Laskowski, R. A., and Swindells, M. B. (2011). LigPlot+: multiple ligand-protein interaction diagrams for drug discovery. *J Chem Inf Model,* 51(10), 2778–2786. doi: org/10.1021/ci200227u.

Le Ouay, B., and Stellacci, F. (2015). Antibacterial activity of silver nanoparticles: A surface science insight. *Nano Today.* 10, 339–354. doi:10.1016/j.nantod.2015.04.002.

Le Rhun, A., Escalera-Maurer, A., Bratovi, M., and Charpentier, E. (2019). CRISPR-Cas in *Streptococcus pyogenes. RNA Biol.,* 16(4), 380–389. doi: org/10.1080/15476286.2019.1582974.

Lécuyer, F., Bourassa, J. S., Gélinas, M., Charron-Lamoureux, V., Burrus, V., and Beauregard, P. B. (2018). Biofilm formation drives transfer of the conjugative element ICE*Bs1* in *Bacillus subtilis. mSphere.* 3(5), e00473-18. doi.org/10.1128/mSphere.00473-18.

Lee, B., Park, J., Ryu, M., Kim, S., Joo, M., Yeom, J. H., *et al.* (2017). Antimicrobial peptide-loaded gold nanoparticle-DNA aptamer conjugates as highly effective antibacterial therapeutics against *Vibrio vulnificus. Sci. Rep.* 7. doi:10.1038/s41598-017-14127-z.

Lee, N. Y., Ko, W. C., and Hsueh, P. R. (2019). Nanoparticles in the treatment of infections caused by multidrug-resistant organisms. *Front. Pharmacol.* 10, 1–10. doi:10.3389/fphar.2019.01153.

Lee, S. F., Delaney, G. D., and Elkhateeb, M. (2004). A two-component covRS regulatory system regulates expression of fructosyltransferase and a novel extracellular carbohydrate in *Streptococcus mutans. Infect. Immun.,* 72(7), 3968–3973. doi: org/10.1128/IAI.72.7.3968-3973.2004.

Lefébure, T., Richards, V. P., Lang, P., Pavinski-Bitar, P., and Stanhope, M. J. (2012). Gene repertoire evolution of *Streptococcus pyogenes* inferred from phylogenomic analysis with *Streptococcus canis* and *Streptococcus dysgalactiae. PloS one,* 7(5), e37607. doi: org/10.1371/journal.pone.0037607.

Lehtinen, S., Blanquart, F., Lipsitch, M., and Fraser, C. (2019). On the evolutionary ecology of multidrug resistance in bacteria. *PLoS Pathog.* 15, 1–22. doi:10.1371/journal.ppat.1007763.

Lembke, C., Podbielski, A., Hidalgo-Grass, C., Jonas, L., Hanski, E., and Kreikemeyer, B. (2006). Characterization of biofilm formation by clinically relevant serotypes of group A streptococci. *Applied and Environ. Microbiol.*, 72(4), 2864–2875. doi: org/10.1128/AEM.72.4.2864-2875.2006.

Li, W., Geng, X., Liu, D., and Li, Z. (2019). Near-infrared light-enhanced protease-conjugated gold nanorods as a photothermal antimicrobial agent for elimination of exotoxin and biofilms. *Int. J. Nanomedicine,* 14, 8047–8058. doi:10.2147/IJN.S212750.

Li, Y., and Burne, R. A. (2001). Regulation of the gtfBC and ftf genes of Streptococcus mutans in biofilms in response to pH and carbohydrate. *Microbiology,* 147(Pt 10), 2841–2848. doi: org/10.1099/00221287-147-10-2841.

Lier, C., Baticle, E., Horvath, P., Haguenoer, E., Valentin, A. S., Glaser, P., Mereghetti, L., and Lanotte, P. (2015). Analysis of the type II-A CRISPR-Cas system of *Streptococcus agalactiae* reveals distinctive features according to genetic lineages. *Front. Genet.,* 6, 214. doi: org/10.3389/fgene.2015.00214.

Lima, B. P., Kho, K., Nairn, B. L., Davies, J. R., Svensäter, G., Chen, R., Steffes, A., Vreeman, G. W., Meredith, T. C., and Herzberg, M. C. (2019). *Streptococcus gordonii* Type I Lipoteichoic Acid Contributes to Surface Protein Biogenesis. *mSphere, 4*(6), e00814-19. doi: org/10.1128/mSphere.00814-19.

Lima, E., Guerra, R., Lara, V., and Guzmán, A. (2013). Gold nanoparticles as efficient antimicrobial agents for *Escherichia coli* and *Salmonella* typhi. *Chem. Cent. J.* 7, 11. doi:10.1186/1752-153X-7-11.

Lima-Mendez, G., Van Helden, J., Toussaint, A., and Leplae, R. (2008). Prophinder: a computational tool for prophage prediction in prokaryotic genomes. *Bioinformatics,* 24(6), 863–865. doi: org/10.1093/bioinformatics/btn043.

Lin, H. P., Singla, B., Ghoshal, P., Faulkner, J. L., Cherian-Shaw, M., O'Connor, P. M., She, J. X., Belin de Chantemele, E. J., and Csányi, G. (2018). Identification of novel macropinocytosis inhibitors using a rational screen of Food and Drug Administration-approved drugs. *Br. J. Pharmacol.*, 175(18), 3640–3655. doi:org/10.1111/bph.14429.

Lindgren, P. E., Signäs, C., Rantamäki, L., and Lindberg, M. (1994). A fibronectin-binding protein from Streptococcus equisimilis: characterization of the gene and identification of the binding domain. *Vet. Microbiol.*, 41(3), 235–247. doi: org/10.1016/0378-1135(94)90104-x.

Lone, A. G., Atci, E., Renslow, R., Beyenal, H., Noh, S., Fransson, B., Abu-Lail, N., Park, J. J., Gang, D. R., and Call, D. R. (2015). Colonization of epidermal tissue by *Staphylococcus aureus* produces localized hypoxia and stimulates secretion of antioxidant and caspase-14 proteins. *Infect. Immun., 83*(8), 3026–3034. doi:org/10.1128/IAI.00175-15

Lopetuso, L. R., Giorgio, M. E., Saviano, A., Scaldaferri, F., Gasbarrini, A., and Cammarota, G. (2019). Bacteriocins and bacteriophages: therapeutic weapons for gastrointestinal diseases? *Int J Mol Sci.*, 20(1), 183. doi: org/10.3390/ijms20010183.

Lopez-Sanchez, M. J., Sauvage, E., Da Cunha, V., Clermont, D., Ratsima Hariniaina, E., Gonzalez-Zorn, B., Poyart, C., Rosinski-Chupin, I., and Glaser, P. (2012). The highly dynamic CRISPR1 system of *Streptococcus agalactiae* controls the diversity of its mobilome. *Mol. Microbiol.*, 85(6), 1057–1071. doi: org/10.1111/j.1365-2958.2012.08172.x.

Lovell, S. C., Davis, I. W., Arendall, W. B., 3rd, de Bakker, P. I., Word, J. M., Prisant, M. G., Richardson, J. S., and Richardson, D. C. (2003). Structure validation by Calpha geometry: phi,psi and Cbeta deviation. *Proteins, 50*(3), 437–450. doi: org/10.1002/prot.10286.

Lu, T. K., and Collins, J. J. (2007). Dispersing biofilms with engineered enzymatic bacteriophage. *Proc. Natl. Acad. Sci.* 104, 11197–11202. doi:10.1073/pnas.0704624104.

Lukomski, S., Bachert, B. A., Squeglia, F., and Berisio, R. (2017). Collagen-like proteins of pathogenic streptococci. *Mol. Microbiol., 103*(6), 919–930. doi: org/10.1111/mmi.13604.

Lundberg, A., Nyman, A., Unnerstad, H., and Waller, K. (2014). Prevalence of bacterial genotypes and outcome of bovine clinical mastitis due to *Streptococcus dysgalactiae* and *Streptococcus uberis. Acta Vet. Scand.* 56, 80. doi:10.1186/s13028-014-0080-0.

Macheboeuf, P., Buffalo, C., Fu, C. Y., Zinkernagel, A. S., Cole, J. N., Johnson, J. E., Nizet, V., and Ghosh, P. (2011). Streptococcal M1 protein constructs a pathological host fibrinogen network. *Nature,* 472(7341), 64–68. doi: org/10.1038/nature09967.

Macià, M. D., Rojo-Molinero, E., and Oliver, A. (2014). Antimicrobial susceptibility testing in biofilm-growing bacteria. *Clin. Microbiol. Infect.* 20, 981–990. doi: 10.1111/1469-0691.12651.

Maciejewska, B., Olszak, T., and Drulis-Kawa, Z. (2018). Applications of bacteriophages versus phage enzymes to combat and cure bacterial infections: an ambitious and also a realistic application? *Appl. Microbiol. Biotechnol.* 102, 2563–2581. doi:10.1007/s00253-018-8811-1.

Makarova, K. S., Wolf, Y. I., Alkhnbashi, O. S., Costa, F., Shah, S. A., Saunders, S. J., Barrangou, R., Brouns, S. J., Charpentier, E., Haft, D. H., Horvath, P., Moineau, S., Mojica, F. J., Terns, R. M., Terns, M. P., White, M. F., Yakunin, A. F., Garrett, R. A., van der Oost, J., Backofen, R., … Koonin, E. V. (2015). An updated evolutionary classification of CRISPR-Cas systems. *Nat. Rev.Microbiology,* 13(11), 722–736. doi: org/10.1038/nrmicro3569.

Makarova, K. S., Wolf, Y. I., and Koonin, E. V. (2018). Classification and nomenclature of CRISPR-Cas systems: Where from here?. *The CRISPR journal,* 1(5), 325–336. doi: org/10.1089/crispr.2018.0033.

Malbruny, B., Nagai, K., Coquemont, M., Bozdogan, B., Andrasevic, A. T., Hupkova, H., Leclercq, R., and Appelbaum, P. C. (2002). Resistance to macrolides in clinical isolates of *Streptococcus pyogenes* due to ribosomal mutations. *J. Antimicrob. Chemother.,* 49(6), 935–939. doi: org/10.1093/jac/dkf038.

Malbruny, B., Werno, A. M., Anderson, T. P., Murdoch, D. R., and Leclercq, R. (2004). A new phenotype of resistance to lincosamide and streptogramin A-type antibiotics in *Streptococcus agalactiae* in New Zealand. *J Antimicrob Chemother,* 54(6), 1040–1044. doi: org/10.1093/jac/dkh493.

Marcelino, V. R., Clausen, P., Buchmann, J. P., Wille, M., Iredell, J. R., Meyer, W., Lund, O., Sorrell, T. C., and Holmes, E. C. (2020). CCMetagen: comprehensive and accurate identification of eukaryotes and prokaryotes in metagenomic data. *Genome Biol.,* 21(1), 103. doi: org/10.1186/s13059-020-02014-2

Marks, L. R., Mashburn-Warren, L., Federle, M. J., and Hakansson, A. P. (2014a). *Streptococcus pyogenes* biofilm growth *in vitro* and *in vivo* and its role in colonization, virulence, and genetic exchange. *Int J Infect Dis,* 210(1), 25–34. doi: org/10.1093/infdis/jiu058.

Marks, L. R., Reddinger, R. M., and Hakansson, A. P. (2014b). Biofilm formation enhances fomite survival of *Streptococcus pneumoniae* and *Streptococcus pyogenes. Infect. Immun.,* 82(3), 1141–1146. doi: org/10.1128/IAI.01310-13.

Martin, D. P., Varsani, A., Roumagnac, P., Botha, G., Maslamoney, S., Schwab, T., Kelz, Z., Kumar, V., and Murrell, B. (2020). RDP5: a computer program for analyzing recombination in,

and removing signals of recombination from, nucleotide sequence datasets. *Virus evolution, 7*(1), veaa087. doi: org/10.1093/ve/veaa087.

Martinez-Garriga, B., Vinuesa, T., Hernandez-Borrell, J., and Viñas, M. (2007). The contribution of efflux pumps to quinolone resistance in *Streptococcus pneumoniae* clinical isolates. *Int. J. Med. Microbiol.* 297, 187–195. doi:10.1016/j.ijmm.2007.01.004.

Masri, A., Anwar, A., Khan, N. A., and Siddiqui, R. (2019). The use of nanomedicine for targeted therapy against bacterial infections. *Antibiotics*. 8, 260. doi:10.3390/antibiotics8040260.

Matsumoto, M., Hoe, N. P., Liu, M., Beres, S. B., Sylva, G. L., Brandt, C. M., Haase, G., and Musser, J. M. (2003). Intrahost sequence variation in the streptococcal inhibitor of complement gene in patients with human pharyngitis. *J Infect Dis*, 187(4), 604–612. doi: org/10.1086/367993.

May, R. C., and Machesky, L. M. (2001). Phagocytosis and the actin cytoskeleton. *J. Cell Sci.*, 114(Pt 6), 1061–1077.

McDaniel, C. J., Cardwell, D. M., Moeller, R. B., and Gray, G. C. (2014). Humans and cattle: A review of bovine zoonoses. *Vector-Borne Zoonotic Dis.* 14, 1–19. doi:10.1089/vbz.2012.1164.

McMillan, D. J., Bessen, D. E., Pinho, M., Ford, C., Hall, G. S., Melo-Cristino, J., and Ramirez, M. (2010). Population genetics of *Streptococcus dysgalactiae* subspecies *equisimilis* reveals widely dispersed clones and extensive recombination. *PloSOne*, 5(7), e11741. doi: org/10.1371/journal.pone.0011741.

McNamara, K., and Tofail, S. A. M. (2017). Nanoparticles in biomedical applications. *Adv. Phys. X* 2, 54–88. doi:10.1080/23746149.2016.1254570.

McNeilly, C. L., and McMillan, D. J. (2014). Horizontal gene transfer and recombination in *Streptococcus dysgalactiae* subsp. *equisimilis*. *Front. Microbiol.* 5, 676. doi: org/10.3389/fmicb.2014.00676.

McShan, W.M., Nguyen, S.V. (2016). The Bacteriophages of *Streptococcus pyogenes*. [Updated 2016 Mar 25]. In: Ferretti JJ, Stevens DL, Fischetti VA, editors. Streptococcus pyogenes: Basic Biology to Clinical Manifestations [Internet]. Oklahoma City (OK): University of Oklahoma Health Sciences Center, Available from: https://www.ncbi.nlm.nih.gov/books/NBK333409/

Melchior, M. B., Vaarkamp, H., and Fink-Gremmels, J. (2006). Biofilms: a role in recurrent mastitis infections? *Vet. J.*, 171(3), 398–407. doi: org/10.1016/j.tvjl.2005.01.006.

Mendes, R., Pedrosa, P., Lima, J. C., Fernandes, A. R., and Baptista, P. V. (2017). Photothermal enhancement of chemotherapy in breast cancer by visible irradiation of Gold Nanoparticles. *Sci. Rep.* 2017. 1–9. doi:10.1038/s41598-017-11491-8.

Miaczynska, M., and Stenmark, H. (2008). Mechanisms and functions of endocytosis. *J. Cell Biol.* 180, 7–11. doi:10.1083/jcb.200711073.

Mihara, M., & Uchiyama, M. (1978). Determination of malonaldehyde precursor in tissues by thiobarbituric acid test. *Anal. Biochem.*, 86(1), 271–278. doi: org/10.1016/0003-2697(78)90342-1.

Miller, J. D., and Neely, M. N. (2005). Large-scale screen highlights the importance of capsule for virulence in the zoonotic pathogen *Streptococcus iniae*. *Infect. Immun.*, 73(2), 921–934. doi: org/10.1128/IAI.73.2.921-934.2005.

Mingoia, M., Morici, E., Brenciani, A., Giovanetti, E., and Varaldo, P. E. (2015). Genetic basis of the association of resistance genes *mef*(I) (macrolides) and *catQ* (chloramphenicol) in streptococci. *Front. Microbiol.* 6, 1–5. doi:10.3389/fmicb.2014.00747.

Mioni, M., Castro, F., Moreno, L. Z., Apolinário, C. M., Belaz, L. D., Peres, M. G., Ribeiro, B., Castro, M., Ferreira, A. M., Cortez, A., Moreno, A. M., Heinemann, M. B., and Megid, J. (2018). Septicemia due to *Streptococcus dysgalactiae* subspecies *dysgalactiae* in vampire bats (*Desmodus rotundus*). *Scientific reports*, *8*(1), 9772. doi: org/10.1038/s41598-018-28061-1.

Molinari, G., Rohde, M., Guzmán, C., and Chhatwal, G.S. (2000). Two distinct pathways for the invasion of *Streptococcus pyogenes* in non-phagocytic cells. *Cell. Microbiol.* 2, 145–154. doi:10.1046/j.1462-5822.2000.00040.x.

Molloy, E.M., Cotter, P.D., Hill, C., Mitchell, D.A., and Ross, R.P. (2011). Streptolysin S-like virulence factors: The continuing sagA. *Nat. Rev. Microbiol.* 9, 670–681. doi:10.1038/nrmicro2624.

Moroi, H., Kimura, K., Kotani, T., Tsuda, H., Banno, H., Jin, W., Wachino, J. I., Yamada, K., Mitsui, T., Yamashita, M., Kikkawa, F., and Arakawa, Y. (2019). Isolation of group B Streptococcus with reduced β-lactam susceptibility from pregnant women. *Emerg. Microbes Infect.*, 8(1), 2–7. doi: org/10.1080/22221751.2018.1557987.

Moser, M., Schneider, R., Behnke, T., Schneider, T., Falkenhagen, J., and Resch-Genger, U. (2016). Ellman's and aldrithiol assay as versatile and complementary tools for the quantification of thiol groups and ligands on nanomaterials. *Anal. Chem.* 88(17), 8624–8631. doi.org/10.1021/acs.analchem.6b01798.

Moulin, P., Patron, K., Cano, C., Zorgani, M. A., Camiade, E., Borezée-Durant, E., Rosenau, A., Mereghetti, L., and Hiron, A. (2016). The Adc/Lmb system mediates zinc acquisition in *Streptococcus agalactiae* and contributes to bacterial growth and survival. *J. Bacteriol.*, 198(24), 3265–3277. doi: org/10.1128/JB.00614-16.

Munita, J. M., Arias, C. A., Unit, A. R., and Santiago, A. De (2016). HHS public access mechanisms of antibiotic resistance. *HHS Public Access* 4, 1–37. doi:10.1128/microbiolspec.VMBF-0016-2015.

Mushtaq, S., Shah, A. M., Shah, A., Lone, S. A., Hussain, A., Hassan, Q. P., and Ali, M. N. (2018). Bovine mastitis: An appraisal of its alternative herbal cure. *Microb. Pathog.*, 114, 357–361. doi: org/10.1016/j.micpath.2017.12.024.

Musser, J. M., Beres, S. B., Zhu, L., Olsen, R. J., Vuopio, J., Hyyryläinen, H. L., Gröndahl-Yli-Hannuksela, K., Kristinsson, K. G., Darenberg, J., Henriques-Normark, B., Hoffmann, S., Caugant, D. A., Smith, A. J., Lindsay, D., Boragine, D. M., and Palzkill, T. (2020). Reduced *In vitro* Susceptibility of *Streptococcus pyogenes* to β-Lactam Antibiotics Associated with Mutations in the pbp2x Gene Is Geographically Widespread. *Clin Microbiol Infect*, 58(4), e01993-19. doi: org/10.1128/JCM.01993-19

Narayana, S.V.V.S and Srihari, S.V.V. (2019). A review on surface modifications and coatings on implants to prevent biofilm. *Regen. Eng. Transl. Med.* 6, 330–346. doi: org/10.1007/s40883-019-00116-3.

Nathan, B., Pillai, V., Ayyan, S. M., Ss, A., & Prakash Raju, K. (2021). *Streptococcus dysgalactiae* subspecies *dysgalactiae* infection presenting with septic shock. *Cureus*, 13(1), e12465. doi: org/10.7759/cureus.12465.

Ng LK, Martin, I., Alfa, M., and Mulvey, M. (2001). Multiplex PCR for the detection of tetracycline resistant genes. *Mol. Cell. Probes.*, 15(4), 209–215. doi: org/10.1006/mcpr.2001.0363.

Nguyen, F., Starosta, A. L., Arenz, S., Sohmen, D., Dönhöfer, A., and Wilson, D. N. (2014). Tetracycline antibiotics and resistance mechanisms. *Biol. Chem.* 395, 559–575. doi:10.1515/hsz-2013-0292.

Nguyen, L. T., Schmidt, H. A., Von Haeseler, A., and Minh, B. Q. (2015). IQ-TREE: A fast and effective stochastic algorithm for estimating maximum-likelihood phylogenies. *Mol. Biol. Evol.* 32, 268–274. doi:10.1093/molbev/msu300.

Nikaido, H. (2009). Multidrug resistance in bacteria. *Annu. Rev. Biochem.,* 119–146. doi:10.1146/annurev.biochem.78.082907.145923.

Nobbs, A. H., Jenkinson, H. F., and Everett, D. B. (2015). Generic determinants of *Streptococcus* colonization and infection. *Infect. Genet. Evol.* 33, 361–370. doi:10.1016/j.meegid.2014.09.018.

Noguchi, S., Yatera, K., Kawanami, T., Yamasaki, K., Naito, K., Akata, K., Shimabukuro, I., Ishimoto, H., Yoshii, C., and Mukae, H. (2015). The clinical features of respiratory infections caused by the *Streptococcus anginosus* group. *BMC Pulm. Med., 15,* 133. doi: org/10.1186/s12890-015-0128-6.

Novoa, B., and Figueras, A. (2012). Zebrafish: model for the study of inflammation and the innate immune response to infectious diseases. *Adv. Exp. Med. Biol.,* 946, 253–275. doi: org/10.1007/978-1-4614-0106-3_15.

Nozawa, T., Furukawa, N., Aikawa, C., Watanabe, T., Haobam, B., Kurokawa, K., Maruyama, F., and Nakagawa, I. (2011). CRISPR inhibition of prophage acquisition in *Streptococcus pyogenes. PloSOne,* 6(5), e19543. doi: org/10.1371/journal.pone.0019543.

O'Neill (2016). Book review: Tackling drug-resistant infections globally. *Arch. Pharm. Pract.* 7, 110. doi:10.4103/2045-080x.186181.

Oh, S. I., Kim, J. W., Kim, J., So, B., Kim, B., and Kim, H. Y. (2020). Molecular subtyping and antimicrobial susceptibility of *Streptococcus dysgalactiae* subspecies *equisimilis* isolates from clinically diseased pigs. *J. Vet. Sci.* 21, 1–11. doi:10.4142/JVS.2020.21.E57.

Oliveira, H., Roma-Rodrigues, C., Santos, A., Veigas, B., Brás, N., Faria, A., Calhau, C., de Freitas, V., Baptista, P. V., Mateus, N., Fernandes, A. R., and Fernandes, I. (2019). GLUT1 and GLUT3 involvement in anthocyanin gastric transport Nanobased targeted approach. *Sci. Rep.,* 9(1), 789. doi:org/10.1038/s41598-018-37283-2.

Oliver-Kozup, H. A., Elliott, M., Bachert, B. A., Martin, K. H., Reid, S. D., Schwegler-Berry, D. E., Green, B. J., and Lukomski, S. (2011). The streptococcal collagen-like protein-1 (Scl1) is a significant determinant for biofilm formation by group A *Streptococcus. BMC microbiology,* 11, 262. doi: org/10.1186/1471-2180-11-262.

Olsen, I. (2015). Biofilm-specific antibiotic tolerance and resistance. *Eur J Clin Microbiol Infect Dis.* 34(5): 877-886. doi:10.1007/s10096-015-2323-z.

O'Neill, E., Humphreys, H., and O'Gara, J. P. (2009). Carriage of both the *fnbA* and f*nbB* genes and growth at 37 degrees C promote FnBP-mediated biofilm development in meticillin-resistant *Staphylococcus aureus* clinical isolates. *J. Med. Microbiol.,* 58(Pt 4), 399–402. doi: org/10.1099/jmm.0.005504-0.

O'Neill, L. A., and Pearce, E. J. (2016). Immunometabolism governs dendritic cell and macrophage function. The Journal of experimental medicine, 213(1), 15–23. doi:org/10.1084/jem.20151570.

Oppegaard, O., Mylvaganam, H., Skrede, S., and Kittang, B. R. (2018). Exploring the arthritogenicity of *Streptococcus dysgalactiae* subspecies *equisimilis. BMC microbiology, 18*(1), 17. doi: org/10.1186/s12866-018-1160-5.

Orscheln, R. C., Johnson, D. R., Olson, S. M., Presti, R. M., Martin, J. M., Kaplan, E. L., and Storch, G. A. (2005). Intrinsic reduced susceptibility of serotype 6 *Streptococcus pyogenes* to fluoroquinolone antibiotics. *J. Infect. Dis.*, 191(8), 1272–1279. doi: org/10.1086/428856.

Ortiz-Benítez, E. A., Velázquez-Guadarrama, N., Durán Figueroa, N. V., Quezada, H., and De Jesús Olivares-Trejo, J. 2019. Antibacterial mechanism of gold nanoparticles on: *Streptococcus pneumoniae. Metallomics*. 11, 1265–1276. doi:10.1039/c9mt00084d.

Osei Sekyere, J., and Mensah, E. (2019). Molecular epidemiology and mechanisms of antibiotic resistance in *Enterococcus* spp., *Staphylococcus* spp., and *Streptococcus* spp. in Africa: a systematic review from a One Health perspective. *Ann. N. Y. Acad. Sci.* doi:10.1111/nyas.14254.

O'Shaughnessy, R., and Brown, S. J. (2015). Insight from the air-skin interface. *J Invest Dermatol*, 135(2), 331–333. doi:org/10.1038/jid.2014.457.

Ozer, E. A., Allen, J. P., and Hauser, A. R. (2014). Characterization of the core and accessory genomes of Pseudomonas aeruginosa using bioinformatic tools Spine and AGEnt. *BMC Genomics* 15, 1–17. doi:10.1186/1471-2164-15-737.

Pajerski, W., Ochonska, D., Brzychczy-Wloch, M., Indyka, P., Jarosz, M., Golda-Cepa, M., Sojka, Z. and Kotarba, A. (2019). Attachment efficiency of gold nanoparticles by Gram-positive and Gram-negative bacterial strains governed by surface charges. *J. Nanoparticle Res.* 21. doi:10.1007/s11051-019-4617-z.

Panchaud, A., Guy, L., Collyn, F., Haenni, M., Nakata, M., Podbielski, A., *et al.* (2009). M-protein and other intrinsic virulence factors of *Streptococcus pyogenes* are encoded on an ancient pathogenicity island. *BMC Genomics*. 10, 198. doi:10.1186/1471-2164-10-198.

Pang, M., Sun, L., He, T., Bao, H., Zhang, L., Zhou, Y., Zhang, H., Wei, R., Liu, Y., and Wang, R. (2017). Molecular and virulence characterization of highly prevalent Streptococcus agalactiae circulated in bovine dairy herds. *Veterinary research*, 48(1), 65. doi: org/10.1186/s13567-017-0461-2.

Park, C., Nichols, M., and Schrag, S. J. (2014). Two cases of invasive vancomycin-resistant group B streptococcus infection. *N. Engl. J. Med.* 370, 885–6. doi:10.1056/NEJMc1308504.

Park, J., Lee, J., and Choi, C. (2011). Mitochondrial network determines intracellular ROS dynamics and sensitivity to oxidative stress through switching inter-mitochondrial messengers. *PLoSOne* 6. doi:10.1371/journal.pone.0023211.

Park, M. J., Eun, I. S., Jung, C. Y., Ko, Y. C., Kim, Y. J., Kim, C. K., and Kang, E. J. (2012). *Streptococcus dysgalactiae* subspecies *dysgalactiae* infection after total knee arthroplasty: a case report. *Knee Surg Relat Res*, 24(2), 120–123. doi: org/10.5792/ksrr.2012.24.2.120.

Parnasa, R., Nagar, E., Sendersky, E., Reich, Ziv., Simkovsky, R., Golden, S., Schwarz, R. (2016). "Small secreted proteins enable biofilm development in the *Cyanobacterium Synechococcus elongatus.*" Scientific Reports. 1–10. http://dx.doi.org/10.1038/srep32209.

Patras, K. A., Derieux, J., Al-Bassam, M. M., Adiletta, N., Vrbanac, A., Lapek, J. D., Zengler, K., Gonzalez, D. J., and Nizet, V. (2018). Group B Streptococcus biofilm regulatory protein a contributes to bacterial physiology and innate immune resistance. *J. Infect. Dis.*, 218(10), 1641–1652. doi: org/10.1093/infdis/jiy341.

Patterson, H., Saralahti, A., Parikka, M., Dramsi, S., Trieu-Cuot, P., Poyart, C., Rounioja, S., and Rämet, M. (2012). Adult zebrafish model of bacterial meningitis in *Streptococcus agalactiae* infection. *Dev. Comp. Immunol.*, 38(3), 447–455. doi: org/10.1016/j.dci.2012.07.007.

Pedrosa, P., Mendes, R., Cabral, R., Martins, L. M. D. R. S., Baptista, P. V., and Fernandes, A. R. (2018). Combination of chemotherapy and Au-nanoparticle photothermy in the visible light to tackle doxorubicin resistance in cancer cells. *Sci. Rep.* 8, 1–8. doi:10.1038/s41598-018-29870-0.

Pelling, H., Nzakizwanayo, J., Milo, S., Denham, E.L., MacFarlane, W.M., Bock, L.J., Sutton, J.M. and Jones, B.V. (2019). Bacterial biofilm formation on indwelling urethral catheters. Letters in *Applied Microbiology*. 68 (4), 277-293. doi: org/10.1111/lam.13144.

Peters, J. (2017). Staphylococcal and streptococcal infections key points. *Medicine*. 45, 727–734. doi:10.1016/j.mpmed.2017.09.010.

Petrova, H., Hu, M., and Hartland, G. V. (2007). Photothermal properties of gold nanoparticles. *Zeitschrift fur Phys. Chemie,* 221, 361–376. doi:10.1524/zpch.2007.221.3.361.

Peule, T.O., and Wilkinson, K.J. (2011). Diffusion of nanoparticles in a biofilm. *Environ Sci Technol.* 45(8): 3367-3373. doi:10.1021/es103450g.

Peyssonnaux, C., Boutin, A. T., Zinkernagel, A. S., Datta, V., Nizet, V., and Johnson, R. S. (2008). Critical role of HIF-1alpha in keratinocyte defense against bacterial infection. *J. Invest. Dermatol.,* 128(8), 1964–1968. doi:org/10.1038/jid.2008.27.

Pham, T. D. M., Ziora, Z. M., and Blaskovich, M. A. T. (2019). Quinolone antibiotics. *Medchemcomm* 10, 1719–1739. doi:10.1039/c9md00120d.

Phelps, H. A., Runft, D. L., and Neely, M. N. (2009). Adult zebrafish model of streptococcal infection. *Current protocols in microbiology,* Chapter 9, Unit–9D.1. doi: org/10.1002/9780471729259.mc09d01s13.

Pieper, U., Webb, B. M., Dong, G. Q., Schneidman-Duhovny, D., Fan, H., Kim, S. J., Khuri, N., Spill, Y. G., Weinkam, P., Hammel, M., Tainer, J. A., Nilges, M., and Sali, A. (2014). ModBase, a database of annotated comparative protein structure models and associated resources. *Nucleic Acids Res. Spec. Publ.,* 42(Database issue), D336–D346. doi: org/10.1093/nar/gkt1144.

Pillai, D. R., Shahinas, D., Buzina, A., Pollock, R. A., Lau, R., Khairnar, K., Wong, A., Farrell, D. J., Green, K., McGeer, A., and Low, D. E. (2009). Genome-wide dissection of globally emergent multi-drug resistant serotype 19A *Streptococcus pneumoniae. BMC genomics, 10,* 642. doi: org/10.1186/1471-2164-10-642.

Pinel, I., Biškauskaitė, R., Palová, E., Vrouwenvelder, H., and van Loosdrecht, M. (2021). Assessment of the impact of temperature on biofilm composition with a laboratory heat exchanger module. *Microorganisms.* 9. doi:10.3390/microorganisms9061185.

Pinho, M. D., Erol, E., Ribeiro-Gonçalves, B., Mendes, C. I., Carriço, J. A., Matos, S. C., Preziuso, S., Luebke-Becker, A., Wieler, L. H., Melo-Cristino, J., and Ramirez, M. (2016). Beta-hemolytic *Streptococcus dysgalactiae* strains isolated from horses are a genetically distinct population within the *Streptococcus dysgalactiae* taxon. *Sci. Rep.,* 6, 31736. doi: org/10.1038/srep31736.

Pires, R., Rolo, D., Gama-Norton, L., Morais, A., Lito, L., Salgado, M. J., Johansson, C., Möllerberg, G., Henriques-Normark, B., Gonçalo-Marques, J., and Santos-Sanches, I. (2005). Group A Streptococci from carriage and disease in Portugal: evolution of antimicrobial resistance and T antigenic types during 2000-2002. *Microb. Drug Resist.,* 11(4), 360–370. doi: org/10.1089/mdr.2005.11.360.

Pires, R., Rolo, D., Morais, A., Brito-Avô, A., Johansson, C., Henriques-Normark, B., Gonçalo-Marques, J., and Santos-Sanches, I. (2012). Description of macrolide-resistant and potential virulent clones of Streptococcus pyogenes causing asymptomatic colonization during 2000-2006 in the Lisbon area. *Eur. J. Clin. Microbiol. Infect. Dis.,* 31(5), 849–857. doi:org/10.1007/s10096-

011-1384-x.

Pirovich, D. B., Da'dara, A. A., and Skelly, P. J. (2021). Multifunctional Fructose 1,6-Bisphosphate Aldolase as a Therapeutic Target. Frontiers in molecular biosciences, 8, 719678. doi:org/10.3389/fmolb.2021.719678.

Pletz, M. W., McGee, L., Van Beneden, C. A., Petit, S., Bardsley, M., Barlow, M., and Klugman, K. P. (2006). Fluoroquinolone resistance in invasive *Streptococcus pyogenes* isolates due to spontaneous mutation and horizontal gene transfer. *Antimicrob Agents Chemother,* 50(3), 943–948. doi: org/10.1128/AAC.50.3.943-948.2006.

Pluk, H., Stokes, D. J., Lich, B., Wieringa, B., and Fransen, J. (2009). Advantages of indium-tin oxide-coated glass slides in correlative scanning electron microscopy applications of uncoated cultured cells. *J. Microsc., 233*(3), 353–363. doi: org/10.1111/j.1365-2818.2009.03140.x.

Pooja, S., Pushpanathan, M., Gunasekaran, P., and Rajendhran, J. (2015). Endocytosis-mediated invasion and pathogenicity of *Streptococcus agalactiae* in rat cardiomyocyte (H9C2). *PLoSOne* 10, 1–16. doi:10.1371/journal.pone.0139733.

Porcellato, D., Smistad, M., Skeie, S. B., Jørgensen, H. J., Austbø, L., and Oppegaard, O. (2021). Whole genome sequencing reveals possible host species adaptation of *Streptococcus dysgalactiae. Sci. Rep.* 11, 1–13. doi:10.1038/s41598-021-96710-z.

Proft T and Fraser JD. (2016). Streptococcal Superantigens: Biological properties and potential role in disease. Feb 10. In: Ferretti JJ, Stevens DL, Fischetti VA, editors. *Streptococcus pyogenes*: Basic Biology to Clinical Manifestations [Internet]. Oklahoma City (OK): University of Oklahoma Health Sciences Center, Available from: https://www.ncbi.nlm.nih.gov/books/NBK333435/

Prudhomme, M., Turlan, C., Claverys, J. P., and Chandler, M. (2002). Diversity of Tn4001 transposition products: the flanking IS256 elements can form tandem dimers and IS circles. *J. Bacteriol.* 184, 433–443. doi:10.1128/JB.184.2.433-443.2002.

Quinteros, M. A., Cano Aristizábal, V., Dalmasso, P. R., Paraje, M. G., and Páez, P. L. (2016). Oxidative stress generation of silver nanoparticles in three bacterial genera and its relationship with the antimicrobial activity. *Toxicol. Vitr.* 36, 216–223. doi:10.1016/j.tiv.2016.08.007.

Radzig, M., Koksharova, O., Khmel, I., Ivanov, V., Yorov, K., Kiwi, J., Rtimi, S., Tastekova, E., Aybush, A., and Nadtochenko, V. (2019). Femtosecond Spectroscopy of Au Hot-Electron Injection into TiO_2: Evidence for Au/TiO_2 Plasmon Photocatalysis by Bactericidal Au Ions and Related Phenomena. *Nanomaterials. 9*(2), 217. doi.org/10.3390/nano9020217

Rafii, F. (2015). Antimicrobial resistance in clinically important biofilms. *World J. Pharmacol.* 4, 31. doi:10.5497/wjp.v4.i1.31.

Rajagopal, L. (2009). Understanding the regulation of Group B Streptococcal virulence factors. *Future Microbiol.* 4, 201–221. doi:10.2217/17460913.4.2.201.

Ramasamy, M., Lee, J. H., and Lee, J. (2016). Potent antimicrobial and antibiofilm activities of bacteriogenically synthesized gold-silver nanoparticles against pathogenic bacteria and their physiochemical characterizations. *J. Biomater. Appl.* 31, 366–378. doi:10.1177/0885328216646910.

Rappon, M. and Syvitski, R. T. (1996). Kinetics of photobleaching of aberchrome 540 in various solvents: solvent effects. *J. Photochem. Photobiol. A Chem.* 94, 243–247. doi:10.1016/1010-6030(95)04216-4.

Rath, D., Amlinger, L., Rath, A., and Lundgren, M. (2015). The CRISPR-Cas immune system: biology, mechanisms and applications. *Biochimie,* 117, 119–128. doi: org/10.1016/j.biochi.2015.03.025.

Rato, M. G., Bexiga, R., Florindo, C., Cavaco, L. M., Vilela, C. L., and Santos-Sanches, I. (2013). Antimicrobial resistance and molecular epidemiology of streptococci from bovine mastitis. *Vet Microbiol*, 161(3-4), 286–294. doi: org/10.1016/j.vetmic.2012.07.043.

Rato, M. G., Bexiga, R., Nunes, S. F., Cavaco, L. M., Vilela, C. L., and Santos-Sanches, I. (2008). Molecular epidemiology and population structure of bovine *Streptococcus uberis*. *J. Dairy Sci.*, 91(12), 4542–4551. doi: org/10.3168/jds.2007-0907.

Rato, M. G., Bexiga, R., Nunes, S. F., Vilela, C. L., and Santos-Sanches, I. (2010). Human group A streptococci virulence genes in bovine group C streptococci. *Emerg Infect Dis*, 16(1), 116–119. doi: org/10.3201/eid1601.090632.

Rato, M. G., Nerlich, A., Bergmann, R., Bexiga, R., Nunes, S. F., Vilela, C. L., Santos-Sanches, I., and Chhatwal, G. S. (2011). Virulence gene pool detected in bovine group C *Streptococcus dysgalactiae* subsp. *dysgalactiae* isolates by use of a group A *S. pyogenes* virulence microarray. *J. Clin. Microbiol.*, 49(7), 2470–2479. doi: org/10.1128/JCM.00008-11.

Regnier, E., Grange, P. A., Ollagnier, G., Crickx, E., Elie, L., Chouzenoux, S., Weill, B., Plainvert, C., Poyart, C., Batteux, F., and Dupin, N. (2016). Superoxide anions produced by Streptococcus pyogenes group A-stimulated keratinocytes are responsible for cellular necrosis and bacterial growth inhibition. *J Innate Immu*, 22(2), 113–123. doi: org/10.1177/1753425915619476

Reid, S. D., Hong, W., Dew, K. E., Winn, D. R., Pang, B., Watt, J., Glover, D. T., Hollingshead, S. K., and Swords, W. E. (2009). *Streptococcus pneumoniae* forms surface-attached communities in the middle ear of experimentally infected chinchillas. *The Journal of infectious diseases*, 199(6), 786–794. doi: org/10.1086/597042.

Reid, S. D., Montgomery, A. G., and Musser, J. M. (2004). Identification of *srv,* a PrfA-like regulator of group A streptococcus that influences virulence. *Infect. Immun.*, 72(3), 1799–1803. doi: org/10.1128/IAI.72.3.1799-1803.2004.

Reinoso, J. (2017). Bovine mastitis caused by *Streptococcus uberis*: virulence factors and biofilm. *Microb Biochem Technol,* 9:5 doi: 10.4172/1948-5948.100037.

Remmington, A., and Turner, C.E. (2018). The DNases of pathogenic Lancefield streptococci. *Microbiology* 164, 242–250. doi: 10.1099/mic.0.000612

Reygaert, W. (2018). An overview of the antimicrobial resistance mechanisms of bacteria. *AIMS Microbiol.* 4, 482–501. doi:10.3934/microbiol.2018.3.482.

Rhee S.G. (2016). Overview on Peroxiredoxin. *Mol. Cells.*, 39(1), 1–5. doi: org/10.14348/molcells.2016.2368.

Ribet, D., and Cossart, P. (2015). How bacterial pathogens colonize their hosts and invade deeper tissues. *Microbes Infect.,* 17(3), 173–183. doi: org/10.1016/j.micinf.2015.01.004.

Richards, V. P., Choi, S. C., Pavinski Bitar, P. D., Gurjar, A. A., and Stanhope, M. J. (2013). Transcriptomic and genomic evidence for *Streptococcus agalactiae* adaptation to the bovine environment. *BMC genomics*, 14, 920. Doi: org/10.1186/1471-2164-14-920.

Richards, V. P., Lang, P., Bitar, P. D., Lefébure, T., Schukken, Y. H., Zadoks, R. N., and Stanhope, M. J. (2011). Comparative genomics and the role of lateral gene transfer in the evolution of bovine adapted *Streptococcus agalactiae. Infect. Genet. Evol.* 11, 1263–1275. doi:10.1016/j.meegid.2011.04.019.

Richards, V. P., Palmer, S. R., Pavinski Bitar, P. D., Qin, X., Weinstock, G. M., Highlander, S. K., Town, C. D., Burne, R. A., and Stanhope, M. J. (2014). Phylogenomics and the dynamic genome

evolution of the genus *Streptococcus*. *Genome Biol. Evol.*, 6(4), 741–753. doi: org/10.1093/gbe/evu048.

Richards, V. P., Zadoks, R. N., Pavinski Bitar, P. D., Lefébure, T., Lang, P., Werner, B., Tikofsky, L., Moroni, P., and Stanhope, M. J. (2012). Genome characterization and population genetic structure of the zoonotic pathogen, *Streptococcus canis*. *BMC Microbiol*, 12, 293. doi: org/10.1186/1471-2180-12-293.

Roberts, A. L., Connolly, K. L., Doern, C. D., Holder, R. C., and Reid, S. D. (2010). Loss of the group A Streptococcus regulator Srv decreases biofilm formation *in vivo* in an otitis media model of infection. *Infect. Immun.*, 78(11), 4800–4808. doi: org/10.1128/IAI.00255-10.

Rohde, M., Cleary, P.P. (2016). Adhesion and invasion of *Streptococcus pyogenes* into host cells and clinical relevance of intracellular streptococci. 10. In: Ferretti, J.J., Stevens, D.L., Fischetti, V.A. editors. *Streptococcus pyogenes*: Basic Biology to Clinical Manifestations [Internet]. Oklahoma City (OK): University of Oklahoma Health Sciences Center. Available from: https://www.ncbi.nlm.nih.gov/books/NBK333420/

Rohde, M., Graham, R. M., Branitzki-Heinemann, K., Borchers, P., Preuss, C., Schleicher, I., Zähner, D., Talay, S. R., Fulde, M., Dinkla, K., and Chhatwal, G. S. (2011). Differences in the aromatic domain of homologous streptococcal fibronectin-binding proteins trigger different cell invasion mechanisms and survival rates. *Cell. Microbiol.*, 13(3), 450–468. doi: org/10.1111/j.1462-5822.2010.01547.x.

Rohde, M., Müller, E., Chhatwal, G. S., & Talay, S. R. (2003). Host cell caveolae act as an entry-port for group A streptococci. *Cell. Microbiol.*, 5(5), 323–342. doi: org/10.1046/j.1462-5822.2003.00279.x

Rollefson, J. B., Stephen, C. S., Tien, M., and Bond, D. R. (2011). Identification of an extracellular polysaccharide network essential for cytochrome anchoring and biofilm formation in *Geobacter sulfurreducens*. *J. Bacteriol.*, 193(5), 1023–1033. doi: org/10.1128/JB.01092-10.

Roma-Rodrigues, C., Alves-Barroco, C., Raposo, L. R., Costa, M. N., Fortunato, E., Baptista, P. V., Fernandes, A. R., and Santos-Sanches, I. (2016). Infection of human keratinocytes by *Streptococcus dysgalactiae* subspecies *dysgalactiae* isolated from milk of the bovine udder. *Microbes Infect.*, 18(4), 290–293 doi:org/10.1016/j.micinf.2015.11.005.

Rosini, R., and Margarit, I. (2015). Biofilm formation by *Streptococcus agalactiae*: influence of environmental conditions and implicated virulence factors. *Front. Cell. Infect. Microbiol.* 5, 2013–2016. doi:10.3389/fcimb.2015.00006.

Rother, K. (2005). Introduction to PyMOL. *Methods Mol Biol Clift Nj.* 635(8):0-32. doi:10.1213/ANE.0b013e3181e9c3f3.

Rutherford, S. J., Jeckel, S., and Ridler, A. (2015). Characteristics of sheep flocks affected by *Streptococcus dysgalactiae* arthritis. *Vet. Rec.* 176, 435. doi:10.1136/vr.102781.

Sachi, S., Ferdous, J., Sikder, M. H., and Azizul Karim Hussani, S. M. (2019). Antibiotic residues in milk: Past, present, and future. *J. Adv. Vet. Anim. Res.*, 6(3), 315–332. DOI: org/10.5455/javar.2019.f350.

Sandvig, K., Kavaliauskiene, S., and Skotland, T. (2018). Clathrin-independent endocytosis: an increasing degree of complexity. *Histochem. Cell Biol.*, 150(2), 107–118. doi: org/10.1007/s00418-018-1678-5.

Santoro, F., Vianna, M. E., and Roberts, A. P. (2014). Variation on a theme, an overview of the Tn916/Tn1545 family of mobile genetic elements in the oral and nasopharyngeal streptococci.

Front. Microbiol., 5, 535. doi: org/10.3389/fmicb.2014.00535.

Saralahti, A., and Rämet, M. (2015). Zebrafish and Streptococcal Infections. *Scand. J. Immunol.,* 82(3), 174–183. doi: org/10.1111/sji.12320.

Savage, V. J., Chopra, I., and O'Neill, A. J. (2013). *Staphylococcus aureus* biofilms promote horizontal transfer of antibiotic resistance. *Antimicrob. Agents Chemother.,* 57(4), 1968–1970. doi: org/10.1128/AAC.02008-12.

Schaefer, K., Matano, L. M., Qiao, Y., Kahne, D., and Walker, S. (2017). *In vitro* reconstitution demonstrates the cell wall ligase activity of LCP proteins. *Nat. Chem. Biol., 13*(4), 396–401. doi: org/10.1038/nchembio.2302.

Schmidt, H., and Hensel, M. (2004). Pathogenicity islands in bacterial pathogenesis. *Clin Microbiol Rev, 17*(1), 14–56. doi: org/10.1128/CMR.17.1.14-56.2004.

Schmitz, F. J., Beyer, A., Charpentier, E., Normark, B. H., Schade, M., Fluit, A. C., Hafner, D., and Novak, R. (2003). Toxin-gene profile heterogeneity among endemic invasive European group A streptococcal isolates. *J. Infect. Dis.* 188(10), 1578–1586. doi: org/10.1086/379230Sorek, R., Lawrence, C. M., and Wiedenheft, B. (2013). CRISPR-mediated adaptive immune systems in bacteria and archaea. *Annu. Rev. Biochem.,* 82, 237–266. doi: org/10.1146/annurev-biochem-072911-172315.

Schwarz, S., Kehrenberg, C., Doublet, B., and Cloeckaert, A. (2004). Molecular basis of bacterial resistance to chloramphenicol and florfenicol. *FEMS Microbiol. Rev.* 28, 519–542. doi:10.1016/j.femsre.2004.04.001.

Seifert, K. N., McArthur, W. P., Bleiweis, A. S., and Brady, L. J. (2003). Characterization of group B streptococcal glyceraldehyde-3-phosphate dehydrogenase: surface localization, enzymatic activity, and protein-protein interactions. *Can. J. Microbiol.,* 49(5), 350–356. doi: org/10.1139/w03-042.

Senadheera, M. D., Guggenheim, B., Spatafora, G. A., Huang, Y. C., Choi, J., Hung, D. C., Treglown, J. S., Goodman, S. D., Ellen, R. P., and Cvitkovitch, D. G. (2005). A VicRK signal transduction system in *Streptococcus mutans* affects gtfBCD, gbpB, and ftf expression, biofilm formation, and genetic competence development. *J. Bacteriol. Res.,* 187(12), 4064–4076. doi: org/10.1128/JB.187.12.4064-4076.2005.

Seppälä, H., Skurnik, M., Soini, H., Roberts, M. C., and Huovinen, P. (1998). A novel erythromycin resistance methylase gene (ermTR) in *Streptococcus pyogenes. Antimicrob. Agents Chemother., 42*(2), 257–262. doi: org/10.1128/AAC.42.2.257.

Sequeira, D., Baptista, P. V., Valente, R., Piedade, M., Garcia, M. H., Morais, T. S., & Fernandes, A. R. (2021). Cu(I) complexes as new antiproliferative agents against sensitive and doxorubicin resistant colorectal cancer cells: synthesis, characterization, and mechanisms of action. *Dalton transactions*, 50(5), 1845–1865. doi.org/10.1039/d0dt03566a.

Serbanescu, M. A., Cordova, M., Krastel, K., Flick, R., Beloglazova, N., Latos, A., Yakunin, A. F., Senadheera, D. B., and Cvitkovitch, D. G. (2015). Role of the *Streptococcus mutans* CRISPR-Cas systems in immunity and cell physiology. *J. Bacteriol.,* 197(4), 749–761. doi: org/10.1128/JB.02333-14.

Shalova, I. N., Lim, J. Y., Chittezhath, M., Zinkernagel, A. S., Beasley, F., Hernández-Jiménez, E., Toledano, V., Cubillos-Zapata, C., Rapisarda, A., Chen, J., Duan, K., Yang, H., Poidinger, M., Melillo, G., Nizet, V., Arnalich, F., López-Collazo, E., and Biswas, S. K. (2015). Human monocytes undergo functional re-programming during sepsis mediated by hypoxia-inducible factor-1 . *Immunity,* 42(3), 484–498. doi:org/10.1016/j.immuni.2015.02.001

Sharma, D., Misba, L., and Khan, A. U. (2019). Antibiotics versus biofilm: an emerging battleground in microbial communities. *Antimicrob. Resist. Infect.* 8:76. doi: 10.1186/s13756-019-0533-3.

Sharma, K., and Pagedar Singh, A. (2018). Antibiofilm effect of DNase against single and mixed species biofilm. *Foods* 7:42. doi: 10.3390/foods7030042.

Sharmila, V., Joseph, N. M., Babu, T. A., Chaturvedula, L., and Sistla, S. (2011). Genital tract group B streptococcal colonization in pregnant women: A south Indian perspective. *J. Infect. Dev. Ctries.* 5, 592–595. doi:10.3855/jidc.1551.

Shelburne, S. A., Sahasrabhojane, P., Saldana, M., Yao, H., Su, X., Horstmann, N., Thompson, E., and Flores, A. R. (2014). *Streptococcus mitis* strains causing severe clinical disease in cancer patients. *Emerg Infect Dis*, 20(5), 762–771. doi: org/10.3201/eid2005.130953.

Shemesh, M., Tam, A., and Steinberg, D. (2007a). Differential gene expression profiling of Streptococcus mutans cultured under biofilm and planktonic conditions. *Microbiology*, 153(Pt 5), 1307–1317. doi: org/10.1099/mic.0.2006/002030-0.

Shemesh, M., Tam, A., and Steinberg, D. (2007b). Expression of biofilm-associated genes of Streptococcus mutans in response to glucose and sucrose. *J. Med. Microbiol.*, 56(Pt 11), 1528–1535. doi: org/10.1099/jmm.0.47146-0.

Shewmaker, P. L., Gertz, R. E., Jr, Kim, C. Y., de Fijter, S., DiOrio, M., Moore, M. R., and Beall, B. W. (2010). *Streptococcus salivarius* meningitis case strain traced to oral flora of anesthesiologist. *J. Clin. Microbiol.*, 48(7), 2589–2591. doi: org/10.1128/JCM.00426-10.

Shields, R. C., Mokhtar, N., Ford, M., Hall, M. J., Burgess, J. G., ElBadawey, M. R., and Jakubovics, N. S. (2013). Efficacy of a marine bacterial nuclease against biofilm forming microorganisms isolated from chronic rhinosinusitis. *PloSOne*, 8(2), e55339. doi: org/10.1371/journal.pone.0055339.

Shiraishi, T., Yokota, S., Fukiya, S., and Yokota, A. (2016). Structural diversity and biological significance of lipoteichoic acid in Gram-positive bacteria: focusing on beneficial probiotic lactic acid bacteria. *Biosci Microbiota Food Health*, 35(4), 147–161. doi: org/10.12938/bmfh.2016-006.

Sieber, J., Wieder, N., Ostrosky-Frid, M., Dvela-Levitt, M., Aygün, O., Udeshi, N. D., Carr, S. A., and Greka, A. (2017). Lysine trimethylation regulates 78-kDa glucose-regulated protein proteostasis during endoplasmic reticulum stress. *J. Biol. Chem.*, 292(46), 18878–18885. doi: org/10.1074/jbc.M117.797084.

Silva, L. G., Genteluci, G. L., de Mattos, M. C., Glatthardt, T., Sà Figueiredo, A. M., and Ferreira-Carvalho, B. T. (2015). Group C *Streptococcus dysgalactiae* subsp. *equisimilis* in south-east Brazil: genetic diversity, resistance profile and the first report of human and equine isolates belonging to the same multilocus sequence typing lineage. *J. Med. Microbiol.* 64, 551–558. doi: 10.1099/jmm.0.000052.

Silva, V. O., Soares, L. O., Silva Júnior, A., Mantovani, H. C., Chang, Y. F., and Moreira, M. A. (2014). Biofilm formation on biotic and abiotic surfaces in the presence of antimicrobials by Escherichia coli Isolates from cases of bovine mastitis. *Applied and Environ. Microbiol.*, 80(19), 6136–6145. doi: org/10.1128/AEM.01953-14.

Singh, P., Pandit, S., Beshay, M., Mokkapati, V., Garnaes, J., Olsson, M. E., Sultan, A., Mackevica, A., Mateiu, R. V., Lütken, H., Daugaard, A. E., Baun, A., and Mijakovic, I. (2018). Anti-biofilm effects of gold and silver nanoparticles synthesized by the Rhodiola rosea rhizome extracts. *Artif. Cells, Nanomedicine Biotechnol.* 46, S886–S899. doi:10.1080/21691401.2018.1518909.

Singh, S., Singh, S. K., Chowdhury, I., and Singh, R. (2017). Understanding the Mechanism of Bacterial Biofilms Resistance to Antimicrobial Agents. *Open Microbiol. J.* 11, 53–62. doi:10.2174/1874285801711010053.

Sivandzade, F., Bhalerao, A., and Cucullo, L. (2019). Analysis of the Mitochondrial Membrane Potential Using the Cationic JC-1 Dye as a Sensitive Fluorescent Probe. *Bio-protocol, 9*(1), e3128. doi: org/10.21769/BioProtoc.3128.

Skerman, V., McGowan, V., and Sneath, P. (1980). *Approved Lists of Bacterial Names* (Amended). ASM Press. https://pubmed.ncbi.nlm.nih.gov/20806452/

Smistad, M., Tollersrud, T. S., Austbø, L., Porcellato, D., Wolff, C., Asal, B., Phythian, C. J., Oppegaard, O., and Jørgensen, H. J. (2021). Molecular detection and genotype characterization of *Streptococcus dysgalactiae* from sheep flocks with outbreaks of infectious arthritis. *Vet. Microbiol.*, 262, 109221. doi: org/10.1016/j.vetmic.2021.109221.

Sorek, R., Lawrence, C. M., and Wiedenheft, B. (2013). CRISPR-mediated adaptive immune systems in bacteria and archaea. *Annu. Rev. Biochem.* 82, 237–66. doi:10.1146/annurev-biochem-072911-172315.

Sousa De Almeida, M., Susnik, E., Drasler, B., Taladriz-Blanco, P., Petri-Fink, A., and Rothen-Rutishauser, B. (2021). Understanding nanoparticle endocytosis to improve targeting strategies in nanomedicine. *Chem. Soc. Rev.* 50, 5397–5434. doi:10.1039/d0cs01127d.

Srinivasan, V., Metcalf, B. J., Knipe, K. M., Ouattara, M., McGee, L., Shewmaker, P. L., Glennen, A., Nichols, M., Harris, C., Brimmage, M., Ostrowsky, B., Park, C. J., Schrag, S. J., Frace, M. A., Sammons, S. A., and Beall, B. (2014). vanG element insertions within a conserved chromosomal site conferring vancomycin resistance to *Streptococcus agalactiae* and *Streptococcus anginosus. mBio, 5*(4), e01386-14. doi: org/10.1128/mBio.01386-14.

Stepanovi, S., Vukovi, D., Hola, V., Di Bonaventura, G., Djuki, S., Cirkovi, I., and Ruzicka, F. (2007). Quantification of biofilm in microtiter plates: overview of testing conditions and practical recommendations for assessment of biofilm production by staphylococci. *APMIS: acta pathologica, microbiologica, et immunologica Scandinavica, 115*(8), 891–899. doi: org/10.1111/j.1600-0463.2007.apm_630.x.

Stewart, P. S., and Bjarnsholt, T. (2020). Risk factors for chronic biofilm-related infection associated with implanted medical devices. *Clin. Microbiol. Infect.*, 26(8), 1034–1038. DOI: org/10.1016/j.cmi.2020.02.027.

Stone, E., Campbell, K., Grant, I., and McAuliffe, O. (2019). Understanding and Exploiting Phage-Host Interactions. *Viruses*, 11(6), 567. doi: org/10.3390/v11060567.

Sun, Y., Oberley, L. W., & Li, Y. (1988). A simple method for clinical assay of superoxide dismutase. *Clinical chemistry*, 34(3), 497–500. doi: org/10.1093/clinchem/34.3.497.

Sutherland, I. W. (2001). The biofilm matrix - An immobilized but dynamic microbial environment. *Trends Microbiol.* 9, 222–227. doi:10.1016/S0966-842X(01)02012-1.

Suzuki, H., Lefébure, T., Hubisz, M. J., Pavinski Bitar, P., Lang, P., Siepel, A., and Stanhope, M. J. (2011). Comparative genomic analysis of the *Streptococcus dysgalactiae* species group: gene content, molecular adaptation, and promoter evolution. *Genome Biol. Evol.*, 3, 168–185. doi: org/10.1093/gbe/evr006.

Swanson, J. A., and King, J. S. (2019). The breadth of macropinocytosis research. *Philosophical transactions of the Royal Society of London. Series B, Biological sciences*, *374*(1765), 20180146. doi:org/10.1098/rstb.2018.0146.

Swidsinski, A., Göktas, O., Bessler, C., Loening-Baucke, V., Hale, L. P., Andree, H., Weizenegger, M., Hölzl, M., Scherer, H., and Lochs, H. (2007). Spatial organization of microbiota in quiescent adenoiditis and tonsillitis. *J. Clin. Pathol.*, 60(3), 253–260. doi: org/10.1136/jcp.2006.037309.

Takahashi, T., Kaneko, M., Mori, Y., Tsuji, M., Kikuchi, N., and Hiramune, T. (1997). Phylogenetic analysis of *Staphylococcus* based on the 16S rDNA sequence and assignment of clinical isolates from animals. *J. Vet. Med. Sci.*, 59(9), 775–783. doi: org/10.1292/jvms.59.775.

Tao, C. (2018). Antimicrobial activity and toxicity of gold nanoparticles: research progress, challenges and prospects. *Lett. Appl. Microbiol.* 67, 537–543. doi:10.1111/lam.13082.

Tapia, J. C., Kasthuri, N., Hayworth, K. J., Schalek, R., Lichtman, J. W., Smith, S. J., and Buchanan, J. (2012). High-contrast en bloc staining of neuronal tissue for field emission scanning electron microscopy. *Nature protocols*, 7(2), 193–206. doi: org/10.1038/nprot.2011.439

Taylor, U., Tiedemann, D., Rehbock, C., Kues, W. A., Barcikowski, S., and Rath, D. (2012). Influence of gold, silver and gold-silver alloy nanoparticles on germ cell function and embryo development. *Beilstein J. Nanotechnol.* 2015. 6, 651–664. doi:10.3762/bjnano.6.66.

Tejchman, K., Kotfis, K., and Sie ko, J. (2021). Biomarkers and mechanisms of oxidative stress—last 20 years of research with an emphasis on kidney damage and renal transplantation. *Int. J. Mol. Sci.* 22. doi:10.3390/ijms22158010.

Toledo-Arana, A., Merino, N., Vergara-Irigaray, M., Débarbouillé, M., Penadés, J. R., and Lasa, I. (2005). *Staphylococcus aureus* develops an alternative, ica-independent biofilm in the absence of the arlRS two-component system. *J. Bacteriol. Res.*, 187(15), 5318–5329. doi: org/10.1128/JB.187.15.5318-5329.2005.

Tomazi, T., de Souza Filho, A. F., Heinemann, M. B., and Dos Santos, M. V. (2018). Molecular characterization and antimicrobial susceptibility pattern of *Streptococcus agalactiae* isolated from clinical mastitis in dairy cattle. *PloSOne*, *13*(6), e0199561. doi: org/10.1371/journal.pone.0199561.

Tran, M. P., Caldwell-McMillan, M., Khalife, W., and Young, V. B. (2008). *Streptococcus intermedius* causing infective endocarditis and abscesses: A report of three cases and review of the literature. *BMC Infect. Dis.* 8, 1–6. doi:10.1186/1471-2334-8-154.

Trappetti, C., Ogunniyi, A. D., Oggioni, M. R., and Paton, J. C. (2011). Extracellular matrix formation enhances the ability of Streptococcus pneumoniae to cause invasive disease. *PloSOne*, 6(5), e19844. doi: org/10.1371/journal.pone.0019844.

Trieu-Cuot, P., de Cespédès, G., Bentorcha, F., Delbos, F., Gaspar, E., and Horaud, T. (1993). Study of heterogeneity of chloramphenicol acetyltransferase (CAT) genes in streptococci and enterococci by polymerase chain reaction: characterization of a new CAT determinant. *Antimicrob. Agents Chemother.*, 37(12), 2593–2598. doi: org/10.1128/aac.37.12.2593.

Trott, O., and Olson, A. J. (2010). AutoDock Vina: improving the speed and accuracy of docking with a new scoring function, efficient optimization, and multithreading. *J. Comput. Chem.*, 31(2), 455–461. doi: org/10.1002/jcc.21334.

Tsao, N., Kuo, C. F., Cheng, M. H., Lin, W. C., Lin, C. F., and Lin, Y. S. (2019). Streptolysin S induces mitochondrial damage and macrophage death through inhibiting degradation of glycogen synthase kinase-3β in *Streptococcus pyogenes* infection. *Sci. Rep.* 9, 1–13. doi:10.1038/s41598-019-41853-3.

Tsirigos, K. D., Peters, C., Shu, N., Käll, L., and Elofsson, A. (2015). The TOPCONS web server for consensus prediction of membrane protein topology and signal peptides. *Nucleic Acids Res., 43*(W1), W401–W407. doi: org/10.1093/nar/gkv485.

Turner, R. D., Hurd, A. F., Cadby, A., Hobbs, J. K., and Foster, S. J. (2013). Cell wall elongation mode in Gram-negative bacteria is determined by peptidoglycan architecture. *Nat. Commun.* 4, 1496–1498. doi:10.1038/ncomms2503.

Vakirlis, N., Carvunis, A. R., and McLysaght, A. (2020). Synteny-based analyses indicate that sequence divergence is not the main source of orphan genes. *Elife* 9, 1–23. doi:10.7554/eLife.53500.

Valentin-Weigand, P., Jungnitz, H., Zock, A., Rohde, M., and Chhatwal, G. S. (1997). Characterization of group B streptococcal invasion in HEp-2 epithelial cells. *FEMS Microbiol. Lett.*, 147(1), 69–74. doi: org/10.1111/j.1574-6968.1997.tb10222.x.

Vandamme, P., Pot, B., Falsen, E., Kersters, K., and Devriese, L. A. (1996). Taxonomic study of lancefield streptococcal groups C, G, and L (*Streptococcus dysgalactiae*) and proposal of *S. dysgalactiae* subsp. *equisimilis. Int. J. Syst. Evol. Microbiol.*, 46(3), 774–781. doi: org/10.1099/00207713-46-3-774.

Vannice, K. S., Ricaldi, J., Nanduri, S., Fang, F. C., Lynch, J. B., Bryson-Cahn, C., Wright, T., Duchin, J., Kay, M., Chochua, S., Van Beneden, C. A., and Beall, B. (2020). *Streptococcus pyogenes* pbp2x mutation confers reduced susceptibility to β-lactam antibiotics. *Clin. Infect. Dis.*, 71(1), 201–204. doi: org/10.1093/cid/ciz1000.

Vasi, J., Frykberg, L., Carlsson, L. E., Lindberg, M., and Guss, B. (2000). M-like proteins of *Streptococcus dysgalactiae. Infect. Immun.* 68, 294–302. doi:10.1128/IAI.68.1.294-302.2000.

Vasudevan, R. (2014). Biofilms: microbial cities of scientific significance. *J. Microbiol. Exp.* 1, 84–98. DOI:10.15406/jmen.2014.01.00014.

Vélez, J. R., Cameron, M., Rodríguez-Lecompte, J. C., Xia, F., Heider, L. C., Saab, M., McClure, J. T., and Sánchez, J. (2017). Whole-genome sequence analysis of antimicrobial resistance genes in *Streptococcus uberis* and *Streptococcus dysgalactiae* isolates from canadian dairy herds. *Front. vet. sci.*, 4, 63. doi: org/10.3389/fvets.2017.00063.

Vieira, V. V., Teixeira, L. M., Zahner, V., Momen, H., Facklam, R. R., Steigerwalt, A. G., Brenner, D. J., and Castro, A. C. (1998). Genetic relationships among the different phenotypes of *Streptococcus dysgalactiae* strains. *Int. J. Syst. Evol. Microbiol.*, 48 *Pt 4*, 1231–1243. doi: org/10.1099/00207713-48-4-1231.

Wallis, J. K., Krömker, V., and Paduch, J. H. (2018). Biofilm formation and adhesion to bovine udder epithelium of potentially probiotic lactic acid bacteria. *AIMS Microbiol.* 4, 209–224. doi: 10.3934/microbiol.2018.2.209.

Wang, Y., Jin, Y., Chen, W., Wang, J., Chen, H., Sun, L. (2019). Construction of nanomaterials with targeting phototherapy properties to inhibit resistant bacteria and biofilm infections. *Chem. Eng. J.* 358, 74–90. doi:10.1016/j.cej.2018.10.002.

Wang, Y., Wan, J., Miron, R. J., Zhao, Y., and Zhang, Y. (2016). Antibacterial properties and mechanisms of gold-silver nanocages. *Nanoscale.* 8, 11143–11152. doi:10.1039/c6nr01114d.

Watanabe, S., Kirikae, T., and Miyoshi-Akiyama, T. (2013). Complete genome sequence of *Streptococcus dysgalactiae* subsp. *equisimilis* 167 carrying lancefield group C antigen and

comparative genomics of *S. dysgalactiae* subsp. *equisimilis* strains. *Genome Biol. Evol.* 5, 1644–1651. doi:10.1093/gbe/evt117.

Watanabe, S., Kirikae, T., and Miyoshi-Akiyama, T. (2013). Complete genome sequence of *Streptococcus dysgalactiae subsp. equisimilis* 167 carrying lancefield group C antigen and comparative genomics of *S. dysgalactiae subsp. equisimilis* strains. *Genome Biol. Evol.* 5, 1644–1651. doi:10.1093/gbe/evt117.

Weckel, A., Ahamada, D., Bellais, S., Méhats, C., Plainvert, C., Longo, M., Poyart, C., and Fouet, A. (2018). The N-terminal domain of the R28 protein promotes *emm28* group A *Streptococcus* adhesion to host cells via direct binding to three integrins. *J. Biol. Chem.*, 293(41), 16006–16018. doi: org/10.1074/jbc.RA118.004134.

Wen, Z. T., and Burne, R. A. (2002). Functional genomics approach to identifying genes required for biofilm development by *Streptococcus mutans*. *Applied and Environ. Microbiol.*, 68(3), 1196–1203. doi: org/10.1128/AEM.68.3.1196-1203.2002.

Wen, Z. T., Baker, H. V., and Burne, R. A. (2006). Influence of BrpA on critical virulence attributes of *Streptococcus mutans*. *J. Bacteriol. Res.*, 188(8), 2983–2992. doi: org/10.1128/JB.188.8.2983-2992.2006.

Whiley, R.A., and Hardie, J.M. (2009). Volume 3: The Firmicutes - Genus I Streptococcus. In Bergey's Manual of Systematic Bacteriology, P. Vos, G. Garrity, D. Jones, N.R. Krieg, W. Ludwig, F. Rainey, K.-H. Schleifer, and W.B. Whitman, eds. (New York, NY: Springer New York), pp. 655–711.

Wickersham, M., Wachtel, S., Wong Fok Lung, T., Soong, G., Jacquet, R., Richardson, A., Parker, D., and Prince, A. (2017). Metabolic Stress Drives Keratinocyte Defenses against *Staphylococcus aureus* Infection. *Cell reports*, 18(11), 2742–2751. doi: org/10.1016/j.celrep.2017.02.055.

Wong, S. S., and Yuen, K. Y. (2012). *Streptococcus pyogenes* and re-emergence of scarlet fever as a public health problem. *Emerg Microbes Infect*, 1(7), e2. doi: org/10.1038/emi.2012.9.

Woodford N. (2005). Biological counterstrike: antibiotic resistance mechanisms of Gram-positive cocci. *Clin. Microbiol. Infect.*, 11 Suppl 3, 2–21. doi: org/10.1111/j.1469-0691.2005.01140.x.

Wu, H., Moser, C., Wang, H. Z., Høiby, N., and Song, Z. J. (2015). Strategies for combating bacterial biofilm infections. *Int. J. Oral Sci.* 7, 1–7. doi:10.1038/ijos.2014.65.

Wu, Z., Wu, C., Shao, J., Zhu, Z., Wang, W., Zhang, W., Tang, M., Pei, N., Fan, H., Li, J., Yao, H., Gu, H., Xu, X., and Lu, C. (2014). The *Streptococcus suis* transcriptional landscape reveals adaptation mechanisms in pig blood and cerebrospinal fluid. *RNA (New York)*, 20(6), 882–898. doi: org/10.1261/rna.041822.113.

Yamada, S., Shibasaki, M., Murase, K., Watanabe, T., Aikawa, C., Nozawa, T., and Nakagawa, I. (2019). Phylogenetic relationship of prophages is affected by CRISPR selection in Group A *Streptococcus*. *BMC Microbiol*, 19(1), 24. doi: org/10.1186/s12866-019-1393-y.

Yang, L., Yan, Z., Yang, L., Yang, J., Jin, M., Xing, X., Zhouab, G. and Shui, L. (2020). Photothermal conversion of SiO2@Au nanoparticles mediated by surface morphology of gold cluster layer. *RSC Adv.* 2020. 10, 33119–33128. doi:10.1039/d0ra06278b.

Yang, Y., Hu, Y., Du, H., and Wang, H. (2014). Intracellular gold nanoparticle aggregation and their potential applications in photodynamic therapy. *Chem. Commun.* 50, 7287–7290. doi:10.1039/c4cc02376e.

Young, C., Holder, R. C., and Reid, S. D. (2016). "*Streptococcus pyogenes* Biofilm", in in *Streptococcus pyogenes*: basic biology to clinical manifestitations. ed Univ. Oklahoma Heal. *Sci. Cent.*, OK, 1–26. https://pubmed.ncbi.nlm.nih.gov/26866208/

Yun, S. J., Seo, J. J., Chae, J. Y., and Lee, S. C. (2005). Peroxiredoxin I and II are up-regulated during differentiation of epidermal keratinocytes. *Archives of dermatological research*, 296(12), 555–559. doi: org/10.1007/s00403-005-0561-0.

Yuwen, L., Sun, Y., Tan, G., Xiu, W., Zhang, Y., Weng, L., (2018). MoS2@polydopamine-Ag nanosheets with enhanced antibacterial activity for effective treatment of: *Staphylococcus aureus* biofilms and wound infection. *Nanoscale.* 10, 16711–16720. doi:10.1039/c8nr04111c.

Zadoks, R. N., Middleton, J. R., McDougall, S., Katholm, J., and Schukken, Y. H. (2011). Molecular epidemiology of mastitis pathogens of dairy cattle and comparative relevance to humans. *J Mammary Gland Biol Neoplasia*, *16*(4), 357–372. doi: org/10.1007/s10911-011-9236-y.

Zadoks, R., and Fitzpatrick, J. (2009). Changing trends in mastitis. *Ir. Vet. J.* 62, S59. doi:10.1186/2046-0481-62-S4-S59.

Zhang, X., Servos, M. R., and Liu, J. (2012). Ultrahigh nanoparticle stability against salt, pH, and solvent with retained surface accessibility via depletion stabilization. *J. Am. Chem. Soc.* 134, 9910–9913. doi:10.1021/ja303787e.

Zhu, B., Macleod, L. C., Kitten, T., and Xu, P. (2018). *Streptococcus sanguinis* biofilm formation and interaction with oral pathogens. *Future Microbiol.* 13, 915–932. doi:10.

Appendix I

Table S1. *Streptococcus* genomes used in Chapter 2 - New Insights on *Streptococcus dysgalactiae* subsp. *dysgalactiae* Isolates

Strain	Accession number	Total length (mb)	Protein count	GC%
SDSD ATCC 27957	NZ_CM001076.1	2.14184	3972	39.4
SDSD DB31752-13	NZ_CP033164.1	2.31957	2026	39.3
SDSD DB49998-05	NZ_CP033163.1	2.17141	1850	39.4
SDSD DB60705-15	NZ_CP033165.1	2.19066	1944	39.4
SDSD DB53993-17	INSDC: REFX00000000.1	2.17042	1966	39.6
SDSD Kdys0611	NZ_ AP018726.1	2.22482	1961	39.9
SDSD NCTC13731	NZ_UHFH00000000.1	2.1517	1920	39.2
SDSD NCTC4669	NZ_LR134094.1	2.20189	1987	39.2
SDSD NCTC4670	NZ_UHFG00000000.1	2.25218	2032	39.3
SDSD STREP97-15	NZ_CP033166.1	2.43257	2211	39.5
SDSE NCTC11554	NZ_LR594047.1	2.23328	2062	39.5
SDSE NCTC5370	NZ_LS483318.1	2.07995	1898	39.5
SDSE NCTC5371	NZ_LS483367.1	2.10376	1858	39.6
SDSE NCTC6179	NZ_LS483361.1	2.2552	2033	39.8
SDSE NCTC6181	NZ_LR134316.1	2.2699	2049	39.7
SDSE NCTC7136	NZ_LS483413.1	2.24923	2084	39.4
SDSE NCTC9413	NZ_LR594045.1	2.24174	2019	39.5
SDSE NCTC9414	NZ_LS483363.1	2.16967	2026	39.5
SDSE 167	NZ_AP012976.1	2.0764	1647	39.6
SDSE AC-2713	NZ_HE858529.1	2.17944	1941	39.5
SDSE ATCC 12394	NZ_CP002215.1	2.15949	1893	39.5
SDSE GGS 124	NZ_AP010935.1	2.10634	1931	39.6
SDSE RE378	NZ_AP011114.1	2.15115	1866	39.5
SD NCTC6403	NZ_LR594046.1	2.2005	1965	39.5
SD NCTC13759	INSDC: UHFJ00000000.1	2.15094	1929	38.3
SD FDAARGOS 654	NZ_CP044102.1	2.25353	2045	39.1
SD SCDR-SD1	NZ_CP033391.1	2.17914	1725	41
S. canis B700072	NZ_LR590625.1	2.10661	1867	39.7
S. canis NCTC12191	NZ_LR134293.1	2.08474	1855	39.9
S. canis HL_100	NZ_CP046521.1	2.17824	1952	39.7
S. pyogenes emm64.3	NZ_CP035435.1	1.77977	1693	38.6
S. pyogenes emm70	NZ_CP035448.1	1.82647	1707	38.5
S. pyogenes emm97.1	NZ_CP035447.1	1.81209	1677	38.4
S. pyogenes FDAARGOS_668	NZ_CP044093.1	1.84135	1737	38.4
S. pyogenes HKU360	NZ_CP009612.1	1.94454	1832	38.5
S. pyogenes JS12	NZ_CP021640.1	1.81028	1632	38.5
S. pyogenes NCTC10085	NZ_LS483401.1	1.79527	1679	38.6
S. pyogenes NCTC12052	NZ_LS483352.1	1.85773	1791	38.5
S. pyogenes NCTC12696	NZ_LS483332.1	1.84505	1777	38.5
S. pyogenes NCTC13736	NZ_LS483414.1	1.91321	1814	38.6
S. pyogenes NCTC13738	NZ_LS483382.1	1.84734	1746	38.6
S. pyogenes NCTC8322	NZ_LS483520.1	1.82959	1746	38.5
S. pyogenes SP1336	NZ_CP031738.1	1.87883	1736	38.5

Table S2. Primer sequences, amplicon expected sizes PCR conditions for amplification of all the genetic determinants.

Primer name	Sequence (5'-3')	Product	Reference
Pyrogenic exotoxins:			
speA (for.)	ATGGAAAACAATAAAAAAGTATTG	755	Matsumoto
speA (rev.)	TTACTTGGTTGTTAGGTAGACTTC		*et al.*, 2003
speB (for.)	TTCTAGGATACTCTACCAGC	300	Jasir *et al.*,
speB (rev.)	ATTTGAGCAGTTGCAGTAGC		2001
speC (for.)	GCAGGGTAAATTTTTCAACGACACACA	407	Rato *et al.*,
speC (rev.)	TGTGCCAATTTCGATTCTGCCGC		2011
speF (for.)	TACTTGGATCAAGACG	782	Schmitz *et*
speF (rev.)	GTAATTAATGGTGTAGCC		*al.*, 2003
speG (for.)	TGTATCTTTAGGGATTACTGATCAG	389	Rato *et al.*,
speG (rev.)	CTCGACCTAAAAGCTTATCATCCTT		2011
speH (for.)	AGATTGGATATCACAGG	416	Pires *et al.*,
speH (rev.)	CTATTCTCTCGTTATTGG		2009
speK (for.)	TACAAATGATGTTAGAAATCCAAGGAACATATATGCT	656	Rato *et al.*,
speK (rev.)	CAAAGTGACTTACTTTACTCATATCAATCGTTTC		2011
speL (for.)	CTGTTAGGATGGTTTCTGCGGAAGAG	605	Rato *et al.*,
speL (rev.)	AGCACCTTCCTCTTTCTCGCCT		2011
speM (for.)	CCAATATGAAGATAACAAAGAAAATTGGCACCC	600	Rato *et al.*,
speM (rev.)	CAAAGTGACTTACTTTACTCATATCAATCG		2011
spegg (for.)	GCTTATGATGTTACTCCACTTGA	420	Rato *et al.*,
spegg (rev.)	ATAACGCGATTCCGAATCATAGA		2011
Mitogenic exotoxin Z:			
smeZ (for.)	CAGATATAGTAATTGATTTTA	399	Darenberg
smeZ (rev.)	AGCTAGAACCAGAAGAATAT		*et al.*, 2007
DNAse1:			
spd1 (for.)	CCCTTCAGGATTGCTGTCAT	400	Green *et al.*,
spd1 (rev.)	ACTGTTGACGCAGCTAGGG		2005
Streptodornase			
sdn (for.)	ACCCCATCGGAAGATAAAGC	489	Matsumoto
sdn (rev.)	AACGTTCAACAGGCGCTTAC		*et al.*, 2003
Streptolysin S			
sagA (for.)	TACTTCAAATATTTTAGCTACT	487	Abdelsalam
sagA (rev.)	GATGATACCCCGATAAGGATAA		*et al.*, 2010
sagB (for.)	ACAATCGTCCCCCCCTAA	519	This study
sagB (rev.)	GGAGAGTAATCGGGTATA		
sagE (for.)	TGGGAAAGGAAGTAGTGG	304	
sagE (rev.)	AGCTAGAAGCAAAGGATAGA		
sagH (for.)	GCAACAACACACAACGAA	411	
sagH (rev.)	TGCCCACCAAAAATAAGG		
sagI (for.)	GCTCAGCTAAAACAAACGAA	763	
sagI (rev.)	AAGAAGGGGTAATGGACAA		
Macrolide Resistance			
mefA (for)	GACCAAAAGCCACAATTGTGGA	1432	Pires *et al.*,
mefA (rev.)	CCTCCTGTCTATAATCGCATG		2005
ermA (for.)	CCCGAAAAATACGCAAAATTTCAT	590	Pires *et al.*,
ermA (rev.)	CCCTGTTTACCCATTTATAAACG		2005
ermB (for.)	GGAGTGATACATGAACAAAAATA	531	Pires *et al.*,
ermB (rev.)	TTCCTTTTAGTAACGTGTAACTTT		2005
Tetracycline Resistance			
tetM (for.)	TGGAATTGATTTATCAACGG	1080	Pires *et al.*,
tetM (rev.)	TTCCAACCATACAATCCTTG		2005
tetO (for.)	AACTTAGGCATTCTGGCTCAC	515	

tetO (rev.)	TCCCACTGTTCCATATCGTCA		Ng *et al.*, 2001
tetT (for.)	AAGGTTTATTATATAAAAGTG	169	Aminov *et al.*, 2001
tetT (rev.)	AGGTGTATCTATGATATTTAC		
tetW (for.)	GAGAGCCTGCTATATGCCAGC	168	Aminov *et al.*, 2001
tetW (rev.)	GGGCGTATCCACAATGTTAAC		
tetQ (for.)	TTATACTTCCTCCGGCATCG	904	Ng *et al.*, 2001
tetQ (rev.)	ATCGGTTCGAGAATGTCCAC		
tetS (for.)	GAAAGCTTACTATACAGTAGC	169	Aminov *et al.*, 2001
tetS (rev.)	AGGAGTATCTACAATATTTAC		
tetL (for.)	TCGTTAGCGTGCTGTCATTC	267	Ng *et al.*, 2001
tetL (rev.)	GTATCCCACCAATGTAGCCG		
tetK (for.)	TCGATAGGAACAGCAGTA	169	Ng *et al.*, 2001
tetK (rev.)	CAGCAGATCCTACTCCTT		
<u>Lincosamide Resistance</u>			
linB (for.)	CCTACCTATTGTTTGTGGAA	925	Bozdogan *et al.*, 1999
linB (rev.)	ATAACGTTACTCTCCTATTC		
<u>Type II CRISPR/Cas</u>			
cas9 (for.)	GAAATACAGACCGCCACA	873	
cas9 (rev.)	CATCGTAGCGCTTAATCA		
cas1 (for.)	ACCCACTCGAAATTATCCT	557	
cas1 (rev.)	CCAGACACAACCACTTCA		
cas4 (for.)	CTTTTGGTCTCACGTGCT	435	This study
cas4 (rev.)	TTTTTTACTCAACCTGGGCT		
csn2 (for.)	TAAGAGGCGGTACAATTC	499	
csn2 (rev.)	CTAGCCACTTCATCCTTT		
CRISPR Sdys (for.)	TAGAAAGAATGGGAAGGCA	variable	
CRISPR Sdys (rev.)	AATACAGGGGCTTTTCAAGA		
<u>Biofilm regulatory protein</u>			
brpA-like P1 F	TAA ATC AAA AGA TGG AGA TG	512	
brpA-like P1 R	GTG ATA TTC AAA AGG TCC TG		
brpA-like P2 F	TGA AGC TAA GTT GAA TGC TGC	534	This study
brpA-like P2 R	GAA CCA CCA TCA GAC AAG GT		
brpA-like P3 F	ATT AGG TTA TCG GGA TGC CCT C	544	
brpA-like P3 R	AGA ATG CTA AGC TGG TTG TTT		
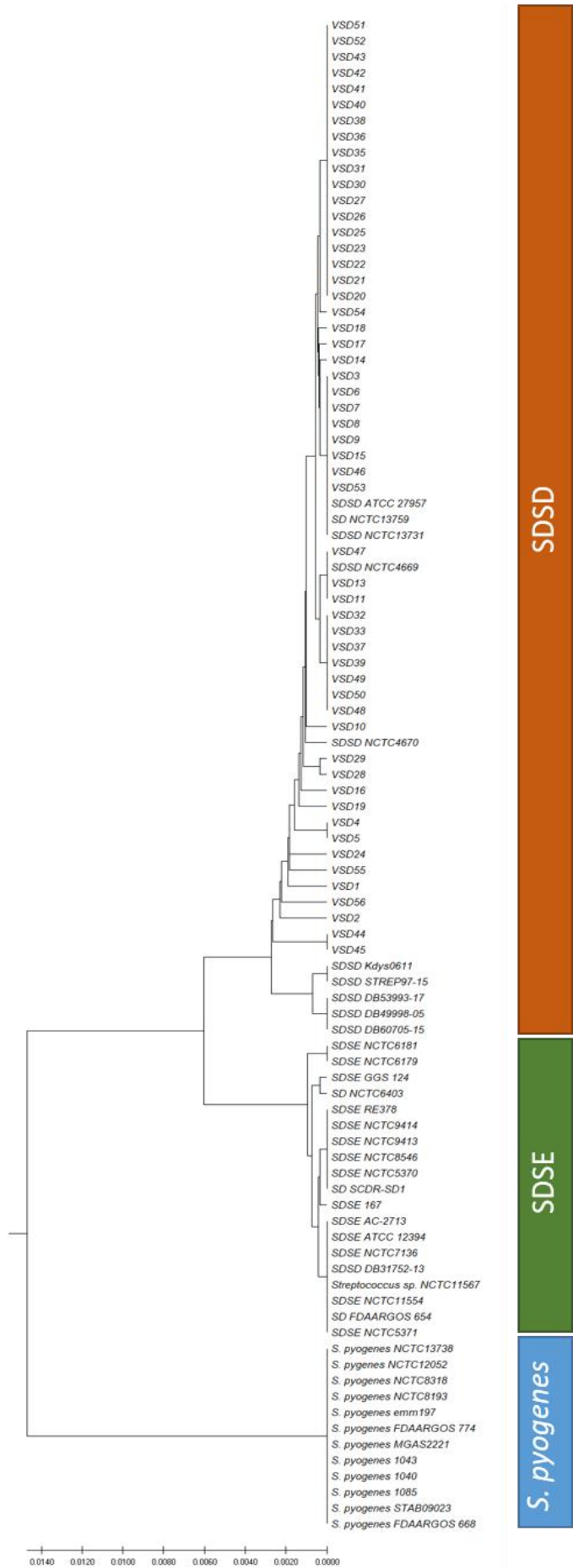
Figure S1. UPGMA dendrogram generated by multiple alignment of rRNA 16S sequence of: i) bovine *Streptococcus dysgalactiae* subspecies *dysgalactiae* isolates (SDSD, n= 36), VSD1 to VSD11 and VSD13 to VSD19 from collection I (2002-2003) and VSD20 to VSD55 from collection II (2011-2013); ii) SDSD sequences deposited in the GenBank database (n= 12); iii) *Streptococcus dysgalactiae* subspecies *equisimilis* isolates (SDSE, n= 16) and iv) *Streptococcus pyogenes* (*S. pyogenes*, n= 12) available at the National Centre for Biotechnology Information. GenBank accession numbers is shown in table 1. The DNA sequence was analyzed by CLC Bio Main Workbench 20.1 alignment program editor (QIAGEN, Netherlands). The optimal tree with the sum of branch length = 0.06766642 is shown. The tree is drawn to scale, with branch lengths in the same units as those of the evolutionary distances used to infer the phylogenetic tree. The evolutionary distances were computed using the Kimura 2-parameter method and are in the units of the number of base substitutions per site. This analysis involved 94 nucleotide sequences. All ambiguous positions were removed for each sequence pair (pairwise deletion option). There were a total of 1432 positions in the final dataset. Evolutionary analyses were conducted in MEGA X software (Kumar et al. 2018). Sequence analysis of the rRNA 16S from bovine SDSD strains showed between 99.2% and 100 % nucleotide identity to SDSD ATCC 2795, SDSD NCTC4670, SDSD NCTC13731 and SDSD NCTC4669 strains deposited in the National Center for Biotechnology Information Nucleotide database.
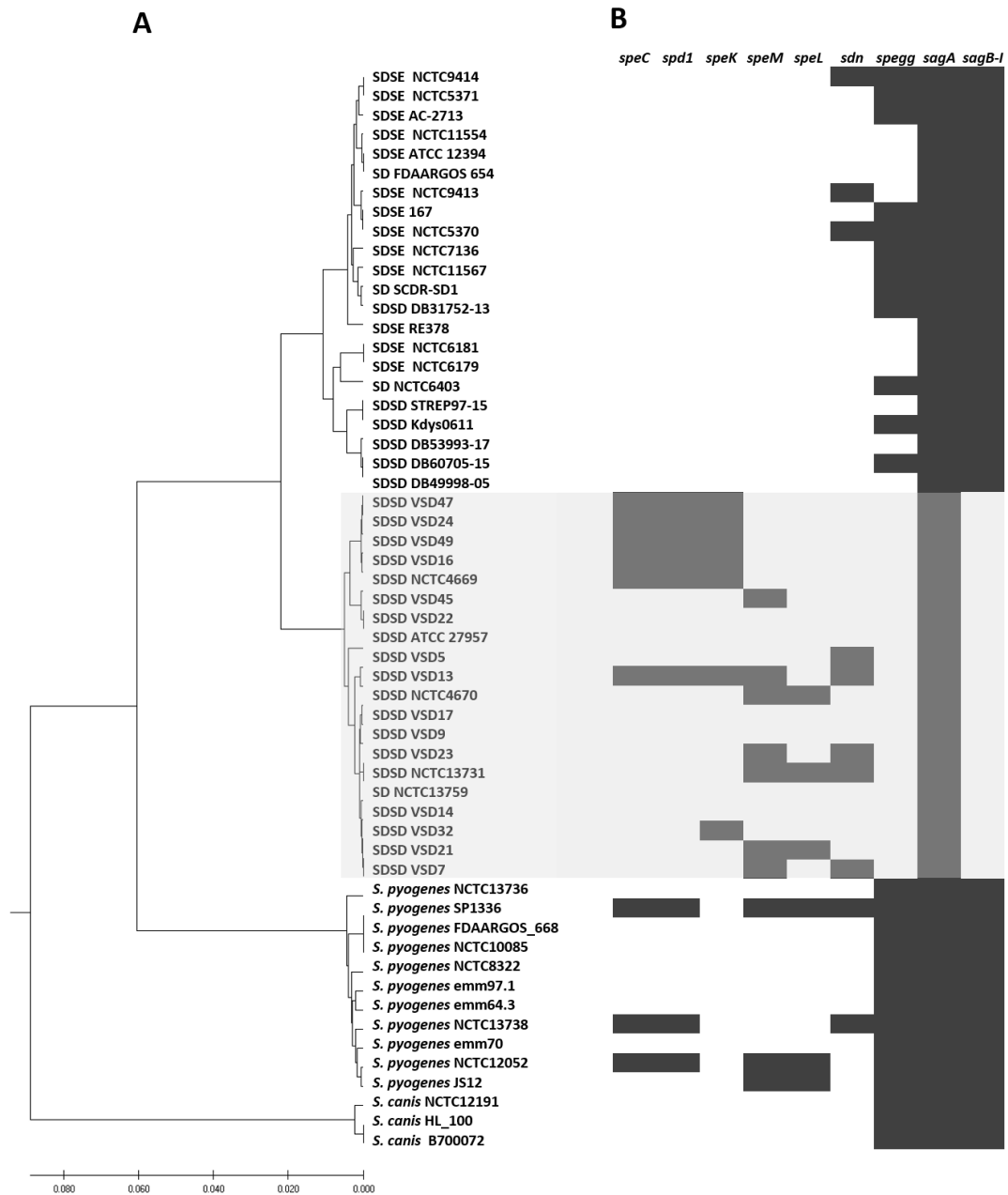
Figure S2. Molecular marker hierarchical clustering dendrogram compared to virulence genes profiles. (A) Hierarchical clustering dendrogram generated by multiple alignment of concatenated sequences of seven housekeeping genes (*gki, gtr, murI, mutS, recP, xpt,* and *atoB*). Cluster analysis of similarity matrices was calculated with the unweighted pairgroup method with arithmetic means. The distances were computed using the Kimura 2-parameter method and are in the units of the number of base substitutions per site. All ambiguous positions were removed for each sequence pair (pairwise deletion option). Evolutionary analyses were conducted in MEGA X. (B) Graphic representation of the virulence gene profile. *S. pyogenes* virulence genes encoding phage: *speC, speK, speL, speM, spegg* - superantigens; *spd1* - DNase; *sdn* streptodornase. *sagA* to *sagI* – Streptolysin (SLS) operon is organized into nine genes *sagA* to *sagI*. SagBCD is responsible for the conversion of SagA into SLS. The role of the remaining Sag proteins is not yet clear. SagF is membrane-associated and SagE is a peptidase responsible for leader cleavage. SagG, SagH, and SagI are thought to be membrane proteins that form an (ABC)-type transporter.

Appendix II

Nucleotide sequence accession numbers

Sequence data have been deposited in GenBank (http://www.ncbi.nlm.nih.gov/genbank/) under the following accession numbers:

Accession numbers of the acetoacetyl-coathioloase – *atoB* gene

Strain	Accession numbers	Collection date	Isolation source	Country
VSD3	MW828881	2002-03	Bovine Mastitis	Portugal
VSD5	MW828882	2002-03	Bovine Mastitis	Portugal
VSD7	MW828883	2002-03	Bovine Mastitis	Portugal
VSD9	MW828884	2002-03	Bovine Mastitis	Portugal
VSD13	MW828885	2002-03	Bovine Mastitis	Portugal
VSD14	MW828886	2002-03	Bovine Mastitis	Portugal
VSD16	MW828887	2002-03	Bovine Mastitis	Portugal
VSD17	MW828888	2002-03	Bovine Mastitis	Portugal
VSD21	MW828889	2011-13	Bovine Mastitis	Portugal
VSD22	MW828890	2011-13	Bovine Mastitis	Portugal
VSD23	MW828891	2011-13	Bovine Mastitis	Portugal
VSD24	MW828892	2011-13	Bovine Mastitis	Portugal
VSD32	MW828893	2011-13	Bovine Mastitis	Portugal
VSD45	MW828894	2011-13	Bovine Mastitis	Portugal
VSD47	MW828895	2011-13	Bovine Mastitis	Portugal
VSD49	MW828896	2011-13	Bovine Mastitis	Portugal

Accession numbers of the glucose kinase – *gki* gene

Strain	Accession numbers	Collection date	Isolation source	Country
VSD3	MW828897	2002-03	Bovine Mastitis	Portugal
VSD5	MW828898	2002-03	Bovine Mastitis	Portugal
VSD7	MW828899	2002-03	Bovine Mastitis	Portugal
VSD9	MW828900	2002-03	Bovine Mastitis	Portugal
VSD13	MW828901	2002-03	Bovine Mastitis	Portugal
VSD14	MW828902	2002-03	Bovine Mastitis	Portugal
VSD16	MW828903	2002-03	Bovine Mastitis	Portugal
VSD17	MW828904	2002-03	Bovine Mastitis	Portugal
VSD21	MW828905	2011-13	Bovine Mastitis	Portugal
VSD22	MW828906	2011-13	Bovine Mastitis	Portugal
VSD23	MW828907	2011-13	Bovine Mastitis	Portugal
VSD24	MW828908	2011-13	Bovine Mastitis	Portugal
VSD32	MW828909	2011-13	Bovine Mastitis	Portugal
VSD45	MW828910	2011-13	Bovine Mastitis	Portugal
VSD47	MW828911	2011-13	Bovine Mastitis	Portugal
VSD49	MW828912	2011-13	Bovine Mastitis	Portugal

Accession numbers of the glutamine transport protein – *gtr* gene

Strain	Accession numbers	Collection date	Isolation source	Country
VSD3	MW828913	2002-03	Bovine Mastitis	Portugal
VSD5	MW828914	2002-03	Bovine Mastitis	Portugal
VSD7	MW828915	2002-03	Bovine Mastitis	Portugal
VSD9	MW828916	2002-03	Bovine Mastitis	Portugal
VSD13	MW828917	2002-03	Bovine Mastitis	Portugal
VSD14	MW828918	2002-03	Bovine Mastitis	Portugal
VSD16	MW828919	2002-03	Bovine Mastitis	Portugal
VSD17	MW828920	2002-03	Bovine Mastitis	Portugal
VSD21	MW828921	2011-13	Bovine Mastitis	Portugal
VSD22	MW828922	2011-13	Bovine Mastitis	Portugal
VSD23	MW828923	2011-13	Bovine Mastitis	Portugal
VSD24	MW828924	2011-13	Bovine Mastitis	Portugal
VSD32	MW828925	2011-13	Bovine Mastitis	Portugal
VSD45	MW828926	2011-13	Bovine Mastitis	Portugal
VSD47	MW828927	2011-13	Bovine Mastitis	Portugal
VSD49	MW828928	2011-13	Bovine Mastitis	Portugal

Accession numbers of the glutamate racemase protein – *murI* gene

Strain	Accession numbers	Collection date	Isolation source	Country
VSD3	MW828929	2002-03	Bovine Mastitis	Portugal
VSD5	MW828930	2002-03	Bovine Mastitis	Portugal
VSD7	MW828931	2002-03	Bovine Mastitis	Portugal
VSD9	MW828932	2002-03	Bovine Mastitis	Portugal
VSD13	MW828933	2002-03	Bovine Mastitis	Portugal
VSD14	MW828934	2002-03	Bovine Mastitis	Portugal
VSD16	MW828935	2002-03	Bovine Mastitis	Portugal
VSD17	MW828936	2002-03	Bovine Mastitis	Portugal
VSD21	MW828937	2011-13	Bovine Mastitis	Portugal
VSD22	MW828938	2011-13	Bovine Mastitis	Portugal
VSD23	MW828939	2011-13	Bovine Mastitis	Portugal
VSD24	MW828940	2011-13	Bovine Mastitis	Portugal
VSD32	MW828941	2011-13	Bovine Mastitis	Portugal
VSD45	MW828942	2011-13	Bovine Mastitis	Portugal
VSD47	MW828943	2011-13	Bovine Mastitis	Portugal
VSD49	MW828944	2011-13	Bovine Mastitis	Portugal

Accession numbers of the DNA mismatch repair protein – *mutS* gene

Strain	Accession numbers	Collection date	Isolation source	Country
VSD3	MW828945	2002-03	Bovine Mastitis	Portugal
VSD5	MW828946	2002-03	Bovine Mastitis	Portugal
VSD7	MW828947	2002-03	Bovine Mastitis	Portugal
VSD9	MW828948	2002-03	Bovine Mastitis	Portugal
VSD13	MW828949	2002-03	Bovine Mastitis	Portugal
VSD14	MW828950	2002-03	Bovine Mastitis	Portugal
VSD16	MW828951	2002-03	Bovine Mastitis	Portugal
VSD17	MW828952	2002-03	Bovine Mastitis	Portugal
VSD21	MW828953	2011-13	Bovine Mastitis	Portugal
VSD22	MW828954	2011-13	Bovine Mastitis	Portugal
VSD23	MW828955	2011-13	Bovine Mastitis	Portugal
VSD24	MW828956	2011-13	Bovine Mastitis	Portugal
VSD32	MW828957	2011-13	Bovine Mastitis	Portugal
VSD45	MW828958	2011-13	Bovine Mastitis	Portugal
VSD47	MW828959	2011-13	Bovine Mastitis	Portugal
VSD49	MW828960	2011-13	Bovine Mastitis	Portugal

Accession numbers of the xanthine phosphoribosyl transferase – *xpt* gene

Strain	Accession numbers	Collection date	Isolation source	Country
VSD3	MW828961	2002-03	Bovine Mastitis	Portugal
VSD5	MW828962	2002-03	Bovine Mastitis	Portugal
VSD7	MW828963	2002-03	Bovine Mastitis	Portugal
VSD9	MW828964	2002-03	Bovine Mastitis	Portugal
VSD13	MW828965	2002-03	Bovine Mastitis	Portugal
VSD14	MW828966	2002-03	Bovine Mastitis	Portugal
VSD16	MW828967	2002-03	Bovine Mastitis	Portugal
VSD17	MW828968	2002-03	Bovine Mastitis	Portugal
VSD21	MW828969	2011-13	Bovine Mastitis	Portugal
VSD22	MW828970	2011-13	Bovine Mastitis	Portugal
VSD23	MW828971	2011-13	Bovine Mastitis	Portugal
VSD24	MW828972	2011-13	Bovine Mastitis	Portugal
VSD32	MW828973	2011-13	Bovine Mastitis	Portugal
VSD45	MW828974	2011-13	Bovine Mastitis	Portugal
VSD47	MW828975	2011-13	Bovine Mastitis	Portugal
VSD49	MW828976	2011-13	Bovine Mastitis	Portugal

Accession numbers of the transketolase protein – *recP* gene

Strain	Accession numbers	Collection date	Isolation_source	Country
VSD3	MW837790	2002-03	Bovine Mastitis	Portugal
VSD5	MW837791	2002-03	Bovine Mastitis	Portugal
VSD7	MW837792	2002-03	Bovine Mastitis	Portugal
VSD9	MW837793	2002-03	Bovine Mastitis	Portugal
VSD13	MW837794	2002-03	Bovine Mastitis	Portugal
VSD14	MW837795	2002-03	Bovine Mastitis	Portugal
VSD16	MW837796	2002-03	Bovine Mastitis	Portugal
VSD17	MW837797	2002-03	Bovine Mastitis	Portugal
VSD21	MW837798	2011-13	Bovine Mastitis	Portugal
VSD22	MW837799	2011-13	Bovine Mastitis	Portugal
VSD23	MW837800	2011-13	Bovine Mastitis	Portugal
VSD24	MW837801	2011-13	Bovine Mastitis	Portugal
VSD32	MW837802	2011-13	Bovine Mastitis	Portugal
VSD45	MW837803	2011-13	Bovine Mastitis	Portugal
VSD47	MW837804	2011-13	Bovine Mastitis	Portugal
VSD49	MW837805	2011-13	Bovine Mastitis	Portugal

Accession numbers of the *sagA* gene (streptolysin S)

Strain	Accession numbers	Collection date	Isolation source	Country
VSD16	MW837806	2002-03	Bovine Mastitis	Portugal
VSD24	MW837807	2011-13	Bovine Mastitis	Portugal

Appendix III

Table S1. List of genomes included in Chapter 3

Strain	Species	Host	Origin/year	Size(Mb)	GC%	CDS
SDSD ATCC 27957	*S. dysgalactiae*	Bovine		2.14184	39.4	4214
SDSD DB3175213	*S. dysgalactiae*	Homo sapiens blood	Singapore	2.31957	39.3	2028
SDSD DB4999805	*S. dysgalactiae*	Homo sapiens Septsemia	Singapore	2.17141	39.4	1856
SDSD DB5399317	*S. dysgalactiae*	Homo sapiens blood	Singapore	2.17042	39.6	1966
SDSD DB6070515	*S. dysgalactiae*	Homo sapiens Septsemia	Singapore	2.19066	39.7	1952
SDSD FDAARGOS1157	*S. dysgalactiae*	Bovine	United Kingdom (1970)	2.15118	39.3	1934
SDSD Kdys0611	*S. dysgalactiae*	Fish	Japan 2006	2.22482	39.9	1963
SDSD NCTC13731	*S. dysgalactiae*	Bovine		2.1517	39.3	1926
SDSD NCTC4669	*S. dysgalactiae*	Bovine	United Kingdom (1935)	2.20189	39.2	1982
SDSD NCTC4670	*S. dysgalactiae*	Bovine	United Kingdom (1935)	2.25218	39.2	2031
SDSD NCTC4671	*S. dysgalactiae*	Bovine	United Kingdom (1935)	2.123	39.3	1889
SDSD STREP9715	*S. dysgalactiae*	Fish	Singapore (2015)	2.43257	39.5	2230
SDSD VSD9*	*S. dysgalactiae*	Bovine	Portugal (2002-2003)	2083252	39,3	2154
SDSD VSD16*	*S. dysgalactiae*	Bovine	Portugal (2002-2003)	2061227	39,3	2176
SDSD VSD22*	*S. dysgalactiae*	Bovine	Portugal (2012-2013)	2053505	39,3	2067
SDSD VSD45*	*S. dysgalactiae*	Bovine	Portugal (2012-2013)	2029374	39,2	2095
SDSE 118	*S. dysgalactiae*	Homo sapiens blood	Norway	2.18122	39.1	2051
SDSE 140	*S. dysgalactiae*	Homo sapiens blood	Norway	2.10765	39.3	1941
SDSE 155	*S. dysgalactiae*	Homo sapiens blood		2.11607	39.1	1943
SDSE 159	*S. dysgalactiae*	Homo sapiens	Japan 2001	2.11152	39.4	1910
SDSE 167A	*S. dysgalactiae*	Homo sapiens blood	Norway	2.12096	39.4	1964
SDSE 196	*S. dysgalactiae*	Homo sapiens	Norway	2.11407	39.2	1970
SDSE 207	*S. dysgalactiae*	Homo sapiens blood	Norway	2.09135	39.3	1899
SDSE 222	*S. dysgalactiae*	Homo sapiens blood	Norway	2.17245	39.2	2003
SDSE 230	*S. dysgalactiae*	Homo sapiens blood	Norway	2.09284	39.2	1917
SDSE 257	*S. dysgalactiae*	Homo sapiens blood	Norway	2.11673	39.2	1979
SDSE 299	*S. dysgalactiae*	Homo sapiens blood	Norway	2.05634	39.3	1878
SDSE 302SDYS	*S. dysgalactiae*	Homo sapiens	USA	2.025	39.3	1872
SDSE 305	*S. dysgalactiae*	Homo sapiens blood	Norway	2.02648	39.5	1873
SDSE 309	*S. dysgalactiae*	Homo sapiens blood	Norway	2.19236	38.9	2006
SDSE 322	*S. dysgalactiae*	Homo sapiens blood	Norway	2.25884	39.4	2143
SDSE 324	*S. dysgalactiae*	Homo sapiens blood		2.16662	39.2	2012
SDSE 333	*S. dysgalactiae*	Homo sapiens blood	Norway	2.13359	39.3	1950
SDSE 348	*S. dysgalactiae*	Homo sapiens blood	Norway	2.1104	39.2	1957
SDSE 355	*S. dysgalactiae*	Homo sapiens		2.0992	39.3	1926
SDSE 357	*S. dysgalactiae*	Homo sapiens blood	Norway	2.05522	39.4	1870
SDSE 359	*S. dysgalactiae*	Homo sapiens blood	Norway	2.07254	39.3	1888
SDSE 89	*S. dysgalactiae*	Homo sapiens	Japan 1998	2.15861	39.4	1950
SDSE AC2713	*S. dysgalactiae*	Homo sapiens	United Kingdom	2.17944	39.5	1939
SDSE AKSDE4288	*S. dysgalactiae*	Homo sapiens blood	USA	2.21755	39.2	2027
SDSE ASDSE96	*S. dysgalactiae*	Homo sapiens	India	2.21031	39.3	2039
SDSE ASDSE99	*S. dysgalactiae*	Homo sapiens		2.24066	39.2	2079
SDSE ATCC 12394	*S. dysgalactiae*	Homo sapiens		2.15949	39.5	2056
SDSE FDAARGOS1017	*S. dysgalactiae*	Homo sapiens	Germany	2.17433	39.6	1976
SDSE FDAARGOS1087	*S. dysgalactiae*	Homo sapiens	Germany	2.13831	39.5	1908
SDSE FDAARGOS654	*S. dysgalactiae*	Homo sapiens	USA	2.25353	39.1	2046
SDSE GCH3	*S. dysgalactiae*	Homo sapiens	South Korea	2.03728	39.3	1833
SDSE GGS124	*S. dysgalactiae*	Homo sapiens		2.10634	39.6	1938
SDSE INFECT2086	*S. dysgalactiae*	Homo sapiens	Denmark	2.12592	39.3	1948
SDSE INFECT5029	*S. dysgalactiae*	Homo sapiens	Sweden	2.24159	39.2	2072
SDSE INFECT5041	*S. dysgalactiae*	Homo sapiens blood	Sweden	2.11301	39.4	1977
SDSE INFECT6037	*S. dysgalactiae*	Homo sapiens blood	Norway	2.1273	39.2	1966
SDSE INFECT6056	*S. dysgalactiae*	Homo sapiens blood	Norway	2.08107	39.3	1903

SDSE INFECT6065	*S. dysgalactiae*	Homo sapiens blood	Norway	2.02648	39.5	1863
SDSE KNZ01A	*S. dysgalactiae*	Homo sapiens joint fluid	Japan	2.07792	39.4	1901
SDSE KNZ03	*S. dysgalactiae*	Homo sapiens blood	Japan	2.15532	39.1	2017
SDSE KNZ04	*S. dysgalactiae*	Homo sapiens blood	Japan	2.16398	39.3	2006
SDSE KNZ06	*S. dysgalactiae*	Homo sapiens blood	Japan	2.1095	39.2	1933
SDSE KNZ07	*S. dysgalactiae*	Homo sapiens blood	Japan	2.04527	39.4	1864
SDSE KNZ10	*S. dysgalactiae*	Homo sapiens	Japan	2.05551	39.4	1886
SDSE KNZ12	*S. dysgalactiae*	Homo sapiens blood	Japan	2.09356	39.4	1920
SDSE KNZ15	*S. dysgalactiae*	Homo sapiens blood	Japan	2.09114	39.4	1942
SDSE KNZ16	*S. dysgalactiae*	Homo sapiens	Japan	2.16448	39.3	2029
SDSE NCTC10238	*S. dysgalactiae*	Dog		2.39676	39.1	2248
SDSE NCTC11554	*S. dysgalactiae*	Homo sapiens		2.23328	39.5	2047
SDSE NCTC11555	*S. dysgalactiae*	Homo sapiens	United Kingdom	2.27719	39.3	2086
SDSE NCTC11556	*S. dysgalactiae*	Homo sapiens blood	United Kingdom	2.19365	39.5	1981
SDSE NCTC11557	*S. dysgalactiae*	Homo sapiens Ucer	United Kingdom	2.43084	39.1	2273
SDSE NCTC11564	*S. dysgalactiae*	hospital environment	United Kingdom	2.43501	39.3	2210
SDSE NCTC13762	*S. dysgalactiae*	Homo sapiens		2.2852	39.5	2181
SDSE NCTC5370	*S. dysgalactiae*	Homo sapiens	1900/1938	2.07995	39.6	1888
SDSE NCTC6179	*S. dysgalactiae*	Horse (Mare) Genital Tract		2.2552	39.8	2024
SDSE NCTC6181	*S. dysgalactiae*	Horse (Mare) Genital Tract	United Kingdom	2.2699	39.7	2045
SDSE NCTC6403	*S. dysgalactiae*	Pig	United Kingdom	2.2005	39.6	1967
SDSE NCTC6407	*S. dysgalactiae*	Dog	United Kingdom 1963	2.23559	39.7	2031
SDSE NCTC7982	*S. dysgalactiae*	Dog Septsemia		2.27715	39.7	2030
SDSE NCTC8543	*S. dysgalactiae*	Homo sapiens		2.17382	39.7	1978
SDSE NCTC8547	*S. dysgalactiae*	Homo sapiens		2.63296	39.4	2792
SDSE NCTC9413	*S. dysgalactiae*	Homo sapiens		2.24174	39.5	2002
SDSE NCTC9414	*S. dysgalactiae*	Homo sapiens	1900/1953	2.16967	39.5	2011
SDSE S5005	*S. dysgalactiae*	Homo sapiens	Sweden	2.16453	39.2	2011
SDSE S6006	*S. dysgalactiae*	Homo sapiens		2.20336	39.2	2041
SDSE S6007	*S. dysgalactiae*	Homo sapiens		2.14566	39.5	1963
SDSE S6017	*S. dysgalactiae*	Homo sapiens		2.3024	39.5	2176
SDSE S6020	*S. dysgalactiae*	Homo sapiens		2.20356	39.3	2041
SDSE SCDRSD1	*S. dysgalactiae*	Homo sapiens	Saudi Arabia	2.17914	41	1729
SDSE SK1249	*S. dysgalactiae*	Homo sapiens		2.16037	39.5	2310
SDSE SK1250	*S. dysgalactiae*	Homo sapiens		2.12251	39.6	2104
SDSE SS1575	*S. dysgalactiae*	Homo sapiens impetigo	Trinidad and Tobago	2.02181	39.5	1890
SDSE T642	*S. dysgalactiae*	Homo sapiens	Norway	2.09561	39.2	1903
SDSE TPCHA19	*S. dysgalactiae*	Homo sapiens bacteremia	Japan 2001	2.10252	39.5	1902
SDSE TPCHA74	*S. dysgalactiae*	Homo sapiens bacteremia	Japan 2017	2.18263	39.5	1994
SDSE TPCHA88	*S. dysgalactiae*	Homo sapiens bacteremia	Japan 2018	2.18092	39.5	1992
SDSE UT4031	*S. dysgalactiae*	Homo sapiens bacteremia	Argentin	2.11784	39.5	1938
SDSE UT4231	*S. dysgalactiae*	Homo sapiens blood	USA	2.17431	39.2	2036
SDSE UT4234	*S. dysgalactiae*	Homo sapiens blood		2.21493	39.2	2040
SDSE UT4241	*S. dysgalactiae*	Homo sapiens blood	USA	2.05604	39.5	1911
SDSE UT4242AB	*S. dysgalactiae*	Homo sapiens blood	USA	2.11738	39.4	1969
SDSE UT4255	*S. dysgalactiae*	Homo sapiens Septsemia		2.26866	39.1	2051
SDSE UT4277	*S. dysgalactiae*	Homo sapiens blood	USA	2.11287	39.5	1956
SDSE UT4966RC	*S. dysgalactiae*	Homo sapiens Pharyngitis		2.11709	39.5	1932
SDSE UT5345	*S. dysgalactiae*	Homo sapiens	USA	2.20776	39.3	2057
SDSE UT5354	*S. dysgalactiae*	Homo sapiens blood		2.07269	39.2	1847
SDSE UTSS1069	*S. dysgalactiae*	Homo sapiens Upper respiratory tract	USA	2.01559	39.5	1743
SDSE UTSS957	*S. dysgalactiae*	Homo sapiens		2.03871	39.3	1897
SDSE WCHSDSE1	*S. dysgalactiae*	Homo sapiens Pharyngitis	China	2.08601	39.4	2000
SP 1336	*S. pyogenes*	Homo sapiens		1.88	38.50	1726
SP FDAARGOS668	*S. pyogenes*	Homo sapiens		1.84	38.48	1694
SP NCTC10085	*S. pyogenes*	Homo sapiens		1.80	38.60	1634
SP NCTC13736	*S. pyogenes*	Homo sapiens		1.91	38.60	1778
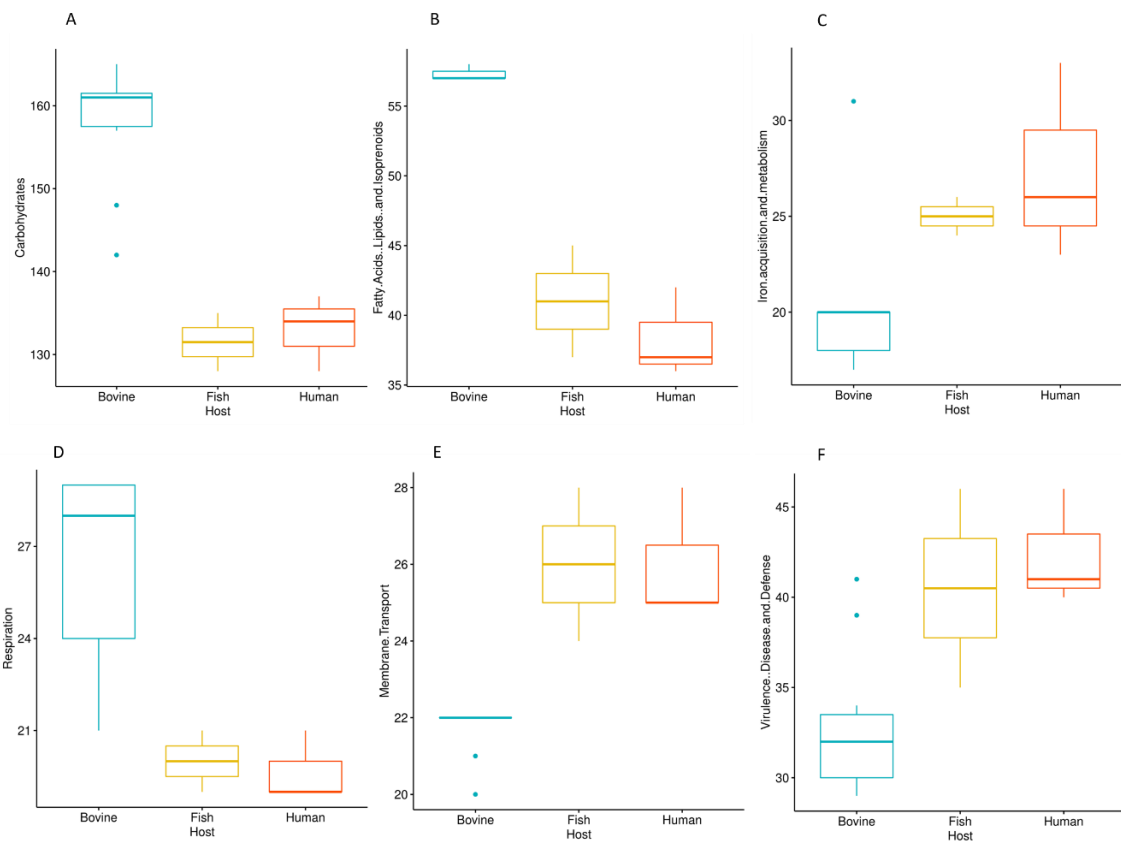
Figure S1. Box-plot of the Kruskal-Wallis test for (A) **Carbohydrates**; (B) Fatty Acids, Lipids and Isoprenoids; (C) Iron acquisition and metabolism; (D) **Membrane Transport**; (E) Respiration and (F) Virulence and Defense sistems.
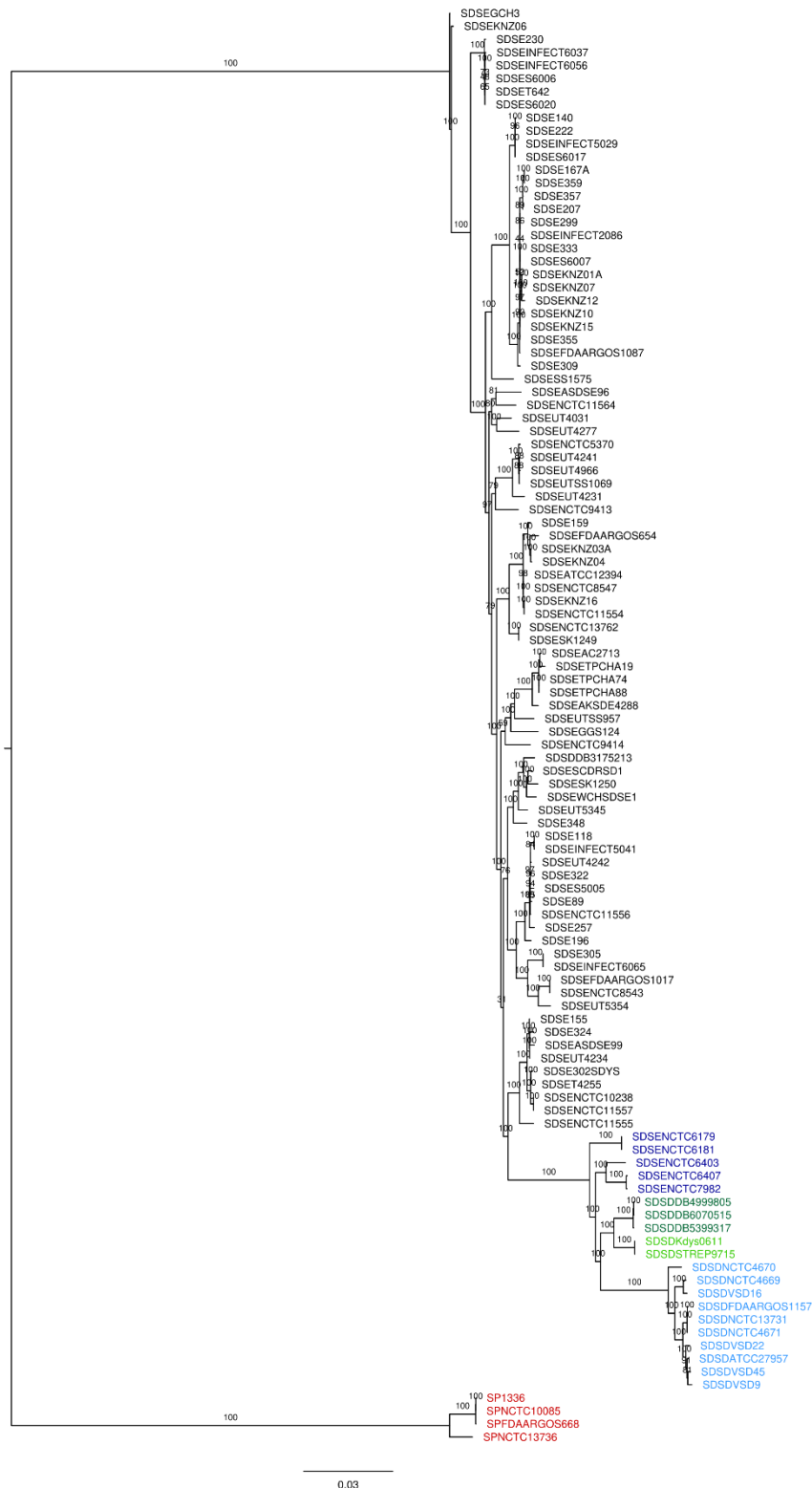
Figure S2. The evolutionary history inferred using the Maximum Likelihood analysis of the alignment of 431 single-copy core protein-coding sequences shared by 106 *S. dysgalactiae* and 4 *S. pyogenes* genomes. Bootstrap support values were calculated from 1000 replicates. Black – human SDSE; Dark blue – non-human SDSE, Light blue – SDSD bovine; Light Green – Fish SDSD, Dark Green – Human SDSD; Red – *S. pyogenes.*

Figure S3. Sequences from VSD22, VSD45, and NCTC4670 SDSD isolates produced significant results against chain M of 2XNX PDB structure that corresponds to bc1 fragment of streptococcal M1 protein, while sequences from FDAARGOS1157 and NCTC4671 strains had significant results against chains B and D, respectively of 2OTO structure PDB matching the N-terminal fragment M1 protein.
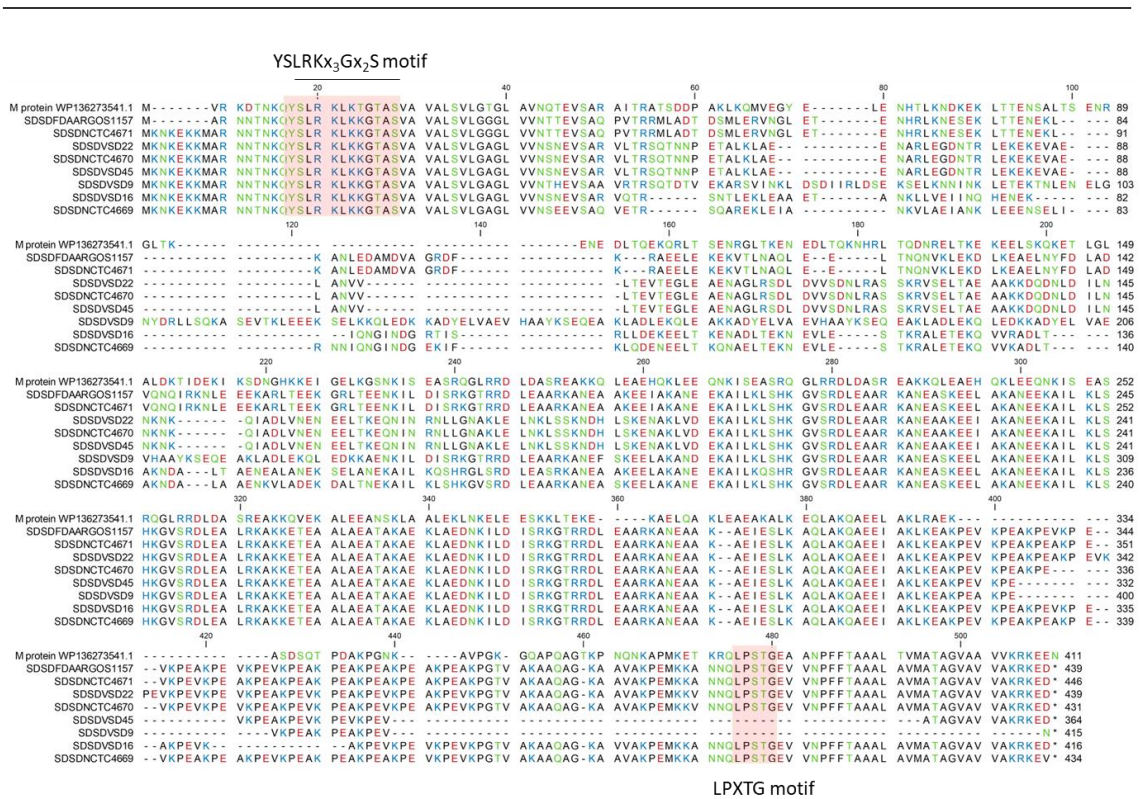
Figure S4. Sequence alignment of the M protein of the *S. pyogenes* (NCBI Reference Sequence: WP136273541.1) and bovines SDSD sequences. These sequences include an signal sequence in the N-terminal region that directs the protein for secretion. The YSLRKx$_3$Gx$_2$S motif contained in the signal sequence conserved among SD and *S. pyogenes* isolates is shown. In the C-terminal region LP$_X$TG, the motif was lost in VSD9 and VSD45 bovine isolates.
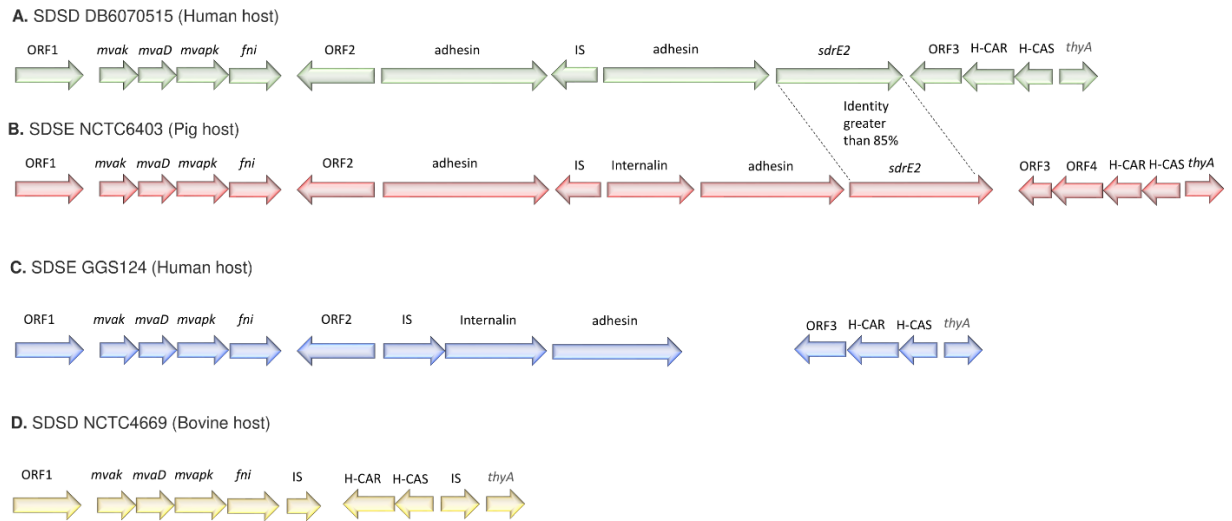
Figure S5. Structure of the genomic regions flanking the *sdrE_2* gene in (A) SDSD DB4999805 and (B) SDSE NCTC6403 isolates. The *sdrE_2* gene shares an identity greater than 85% among animal SDSE and human SDSD isolates but absent in the other SD isolates. The homologous genomic region of (C) SDSE GGS124 and (D) SDSD NCTC4669 isolates is also shown. The SdrE2 belongs to MSCRAMM family SdrC/SdrD. ORF 1 - ABC transporter ATP-binding; ORF2, ORF3 and ORF4 - putative transcriptional regulator; Adhesin - LPXTG cell wall anchor domain-containing protein; *mvaK* - mevalonate kinase; *mvaD* - diphosphomevalonate decarboxylase; *mvapK* - phosphomevalonate kinase; *fni* - isopentenyl pyrophosphate isomerase; IS – transposase; Internalin; H-CAR - HMG-CoA reductase; H-CAS - HMG-CoA synthase; *thyA* - thymidylate synthase.
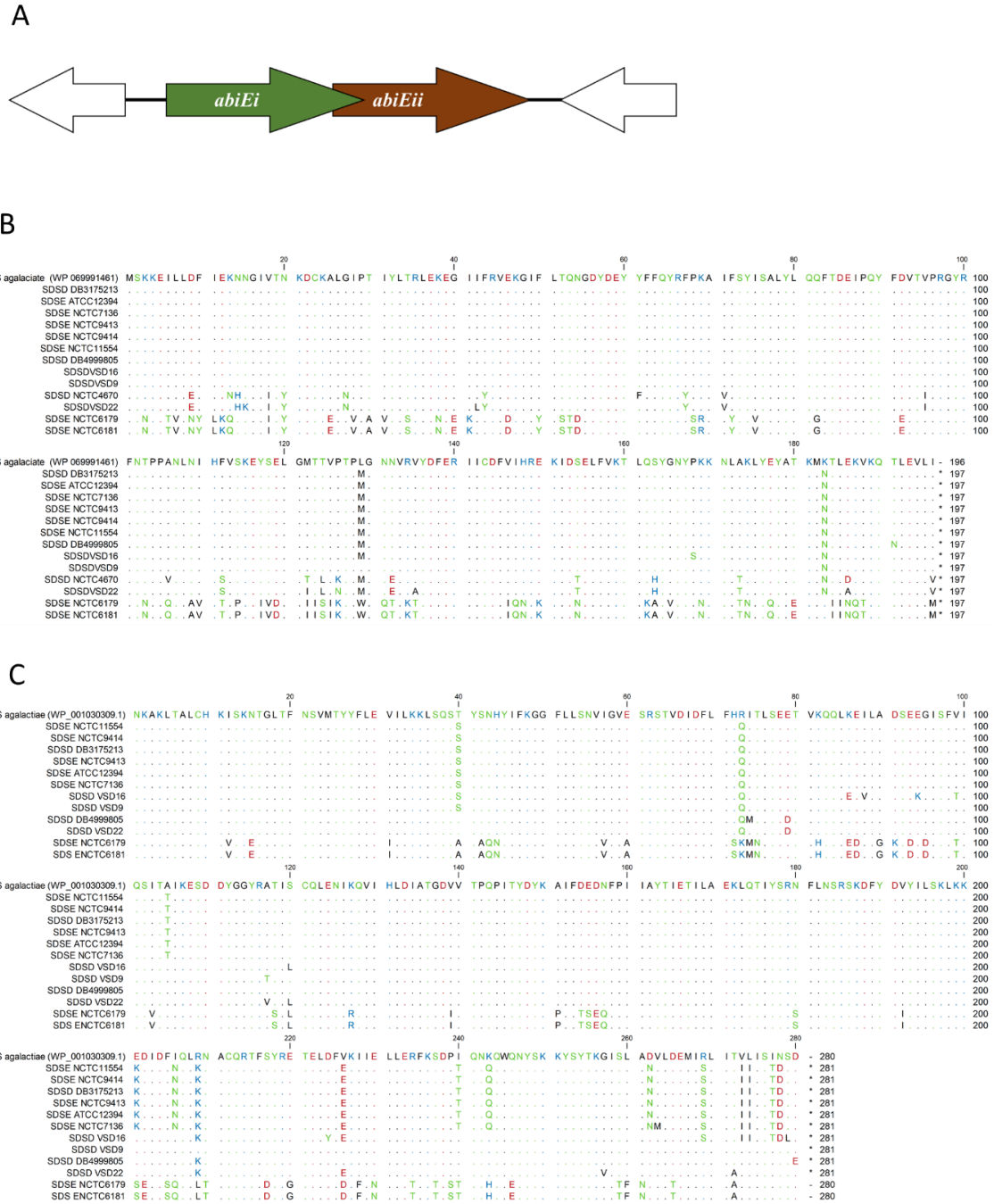
Figure S6. (A) Schematic diagram of the genetic organization of *abiE* in the *S. agalactiae* V/R 2603 genome (not to scale). Alignment of AbiEi **(B)** and AbiEii **(C)** peptides. AbiE is organized in bicistronic operon, encoding the AbiEi antitoxin and AbiEii antagonistic toxin. Both proteins share high amino acid identity (>87%) with *S. agalactiae* sequences. The high homology of AbiEi (96%) was observed between VSD22 and SDSD NCTC4670 strain. The NCTC4670 strain seems to have lost AbiEii at some point during evolutionary process. Deduced amino acid sequences from this bovine allele were compared with similar sequences from the NCBI database and were analyzed with the CLC-Genomic Workbench sequence alignment tool.

Table S2. Virulence, carbohydrate metabolism, antimicrobial and metal resistance profiles of the 106 *S. dysgalactiae* isolates.

Isolates	1 2 3 4 5 6 7 8 9 10 11 12 13 14 15 16 17 18 19 20 21 22 23 24 25 26 27 28 29 30 31 32 33 34 35 36 37 38 39 40 41 42 43 44 45 46 47 48 49 50 51 52 53 54 55 56 57 58 59 60 61 62
SDSDATCC27957	
SDSDDB3175213	
SDSDDB4999805	
SDSDDB5399317	
SDSDDB6070515	
SDSDFDAARGOS1157	
SDSDKdys0611	
SDSDNCTC13731	
SDSDNCTC4669	
SDSDNCTC4670	
SDSDNCTC4671	
SDSDSTREP9715	
SDSDVSD16	
SDSDVSD22	
SDSDVSD45	
SDSDVSD9	
SDSE118	
SDSE140	
SDSE155	
SDSE159	
SDSE167A	
SDSE196	
SDSE207	
SDSE222	
SDSE230	
SDSE257	
SDSE299	
SDSE302SDYS	
SDSE305	
SDSE309	
SDSE322	
SDSE324	
SDSE333	
SDSE348	
SDSE355	
SDSE357	
SDSE359	
SDSE89	
SDSEAC2713	
SDSEAKSDE4288	
SDSEASDSE96	
SDSEASDSE99	
SDSEATCC12394	
SDSEFDAARGOS1017	
SDSEFDAARGOS1087	
SDSEFDAARGOS654	
SDSEGCH3	
SDSEGGS124	
SDSEINFECT2086	
SDSEINFECT5029	
SDSEINFECT5041	
SDSEINFECT6037	
SDSEINFECT6056	
SDSEINFECT6065	
SDSEKNZ01A	
SDSEKNZ03A	
SDSEKNZ04	
SDSEKNZ06	
SDSEKNZ07	
SDSEKNZ10	
SDSEKNZ12	
SDSEKNZ15	
SDSEKNZ16	
SDSENCTC10238	
SDSENCTC11554	
SDSENCTC11555	
SDSENCTC11556	
SDSENCTC11557	
SDSENCTC11564	
SDSENCTC13762	
SDSENCTC5370	
SDSENCTC6179	
SDSENCTC6181	
SDSENCTC6403	
SDSENCTC6407	
SDSENCTC7982	
SDSENCTC8543	
SDSENCTC8547	
SDSENCTC9413	
SDSENCTC9414	
SDSES5005	
SDSES6006	
SDSES6007	
SDSES6017	
SDSES6020	
SDSESCDRSD1	
SDSESK1249	
SDSESK1250	
SDSESS1575	
SDSET642	
SDSETPCHA19	
SDSETPCHA74	
SDSETPCHA88	
SDSEUT4031	
SDSEUT4231	
SDSEUT4234	
SDSEUT4241	
SDSEUT4242	
SDSEUT4255	
SDSEUT4277	
SDSEUT4966	
SDSEUT5345	
SDSEUT5354	
SDSEUTSS1069	
SDSEUTSS957	
SDSEWCHSDSE1	

Black: gene/operon present; blank: gene/operon absent. 1 to 5 - Superantigens (speC - ID:HQ696925, speG - ID: AJ489606.1, speK - ID: HQ724300, speL - ID: HQ724303, speM - ID: HQ724305); 6 to 14 - Streptolysin S operon (IDs: QGH01767.1 to QGH01774.1); 15 - Streptolysin O (ID: VTS45764.1); 16 to 21 – adhesins (ID: WP043040055, WP200894311, VTT00995.1, WP153228040, VDZ40360.1, VDZ40918.1); 22 - Aglutinin receptor (ID: EFY03268.1); 23 and 24 – Collagenases (WP003049992.1 and WP115247118.1); 25 - M protein-like (bovine SDSD); 26 – cpsZ gene (ID: VDZ39525.1); 27 – C5a peptidase (vpr ID: VDZ40442.1); 28 - Teichoic acids export (ID: WP003049800.1); 29 - Heme efflux system ATPase HrtAB (ID: BBE40302.1 and BBE40301.1); 30 - M protein trans-acting positive regulator Mga (ID. VDZ39523.1); 31 - Accessory SecA2/SecY2 system (ID: VDZ39462.1 to VDZ39469.1); 32 - Lac1 operon (ID: QQT03641.1 to QQT03643.1); 33 – Fructose operon (ID: VED65115.1 to VED65117.1); 34 to 36 – lacR (ID: VED65119.1); lacA-G (ID: VED65120.1 to VED65126.1) and lacX (ID: VED65127.1) of Lac2 operon; 37 - Glucitol_sorbitol operon (ID: QQT03173.1 to QQT03168.1); 38 to 42 - System toxin-antitoxin (DinJ like, RelB, RelE-like and Doc-like); 43 and 44 - abiE operon; 45 – abiSDi; 46 and 47 - β-lactamase A (ID: WP226316797.1) and C (ID: WP226316205.1); 48 and 49 - Erythromycin resistance genes (ermB ID: QBP04659.1 and mefA ID: QGG98635.1); 50 - lincosamide ucleotidyltransferase (lnuD, ID: QGH01410.1); 51 - tetracycline-resistant ribosomal protection protein (tetO, ID: WP063856404.1); 52 - PatB (ID: TVV92928); 53 and 54 - Multidrug ABC transporter (ID: VDZ41307.1 and VDZ41306.1; ID: QQT04365.1 and QQT04366.1); 55 - vanZ gene (Glycopeptide antibiotics resistance protein (ID: WP003049062.1); 56 - Multidrug resistance efflux pump (Bcr, ID: VDZ39913.1); 57 - Arsenical resistance (ID: MCC9751410.1); 58 - Inorganic ion transport and metabolism (Fe/Co/Zn/Cd) transporter (ID: WP003050997.1), 59 - Mercuric resistance operon regulatory protein MerR (ID. QUW40391.1); 60 - Cadmium and Zinc resistance (ID: WP014612225.1); 61 - Tellurite resistance protein (ID: VDZ39471.1); 62 - Nisin resistance (ID: WP003057518.1).
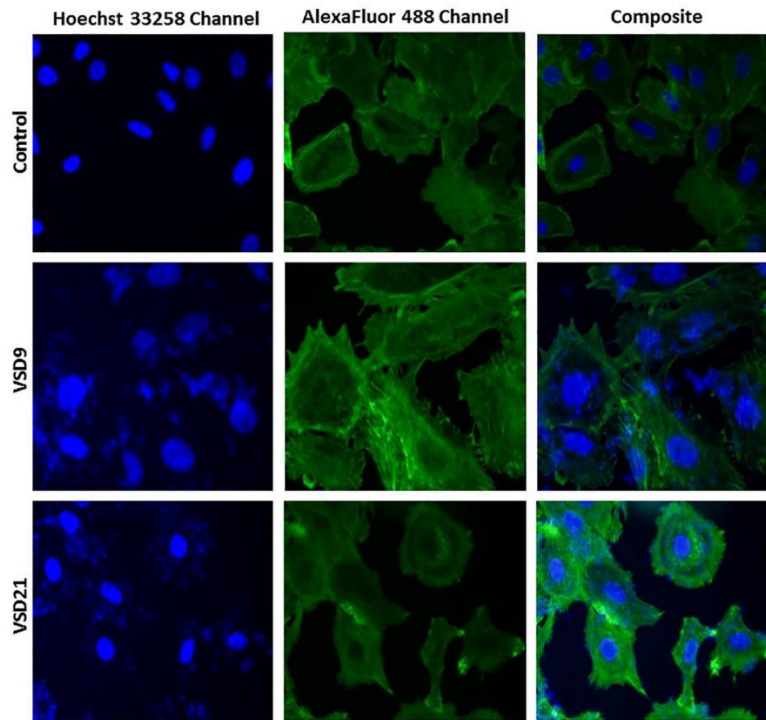
250

Appendix IV

Figure S1. Representative images of A549 cells incubated for 2 hours at 37°C with *S. dysgalactiae* subspecies *dysgalactiae* isolates VSD9 and VSD21. Bacterial cells were stained with Hoechst 33258 before infection. A549 cells are stained after infection with AlexaFluor 488 phalloidin. It is possible to observe interaction of bacterial cells with the A459 cells, either in the cell surface or within the eukaryotic cells.
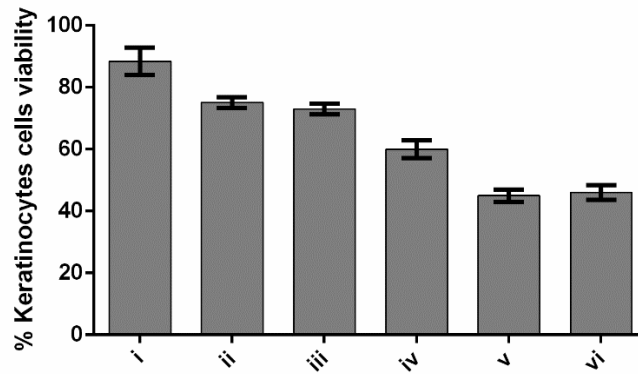
Figure S2. MTS assay of human primary keratinocytes previous 6h exposure to with different combination sets of the four inhibitors endocytic inhibitors previously used, namely, **i)** filipin (5 µM); **ii)** chlorpromazine (30 µM); **iii)** chlorpromazine (30 µM) + filipin (5 µM); **iv)** amiloride (12,5 µM); **v)** wortmannin (0,3 µM) and **vi)** amiloride (12,5 µM) + wortmannin (0,3 µM). The following equation applied to calculate the cell viability (%) = 100 x (mean Abs of treatment group /mean Abs of control group, without treatment). Data are the average of at least three independent assays and error bars correspondent to standard deviation.

Appendix V

Table S1. Characterization of gold, silver and alloy nanoparticles by Dynamic Light Scattering and Zeta Potential

	DLS		Zeta	
	Average (nm)	St Dev	Average (mV)	St Dev
AuNPs	16.8	1.7	-57.2	2.1
AuNPs@PEG	19.6	1.8	-79.0	2.7
AgNPs	24.1	2.7	-53.5	3.4
AgNPs@PEG	36.2	2.9	-65.5	2.6
AuAgNPs	36.9	3.0	-21.8	2.6
AuAgNPs@PEG	46.9	2.5	-47.2	2.7

Table S2. Heat capacity of AuAgNPs@PEG and AuNPs@PEG produced by irradiation at 532 nm (respect pH 7 solution). Heat capacity of AuAgNPs@PEG decreased for upon pH 4. Heat capacity of AuNPs@PEG remained unalterable at all pH situation studied.

	Reduction of heat induction* (% respect pH 7 solution)	
pH	AuAgNPs@PEG	AuNPs@PEG
10	88	97
9	87	
8	88	
6	85	
5	61	
4	20	99
3	16	98
2	18	98

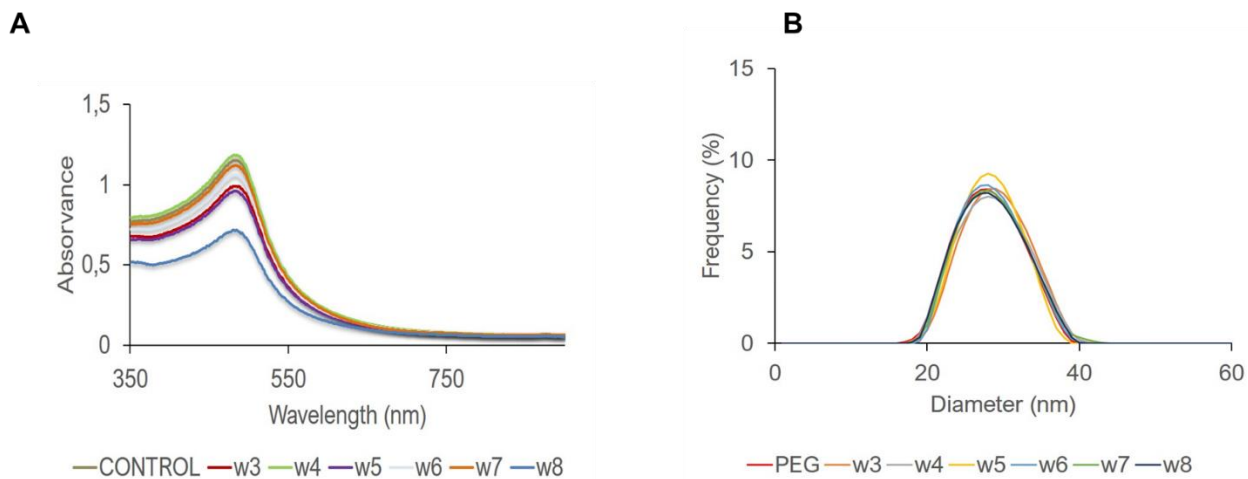$$*\text{Reduction heat induction}(\%) = \frac{\Delta \text{tempeture pH X}}{\Delta \text{ temperature pH 7}} x100$$

Figure S1. A) Visible spectrum of AuAgNPs@PEG after irradiation using different laser powers (w4-8) **B)** Size distribution determined by DLS of AuAgNPs@PEG after irradiation using different laser powers (w4-w8).
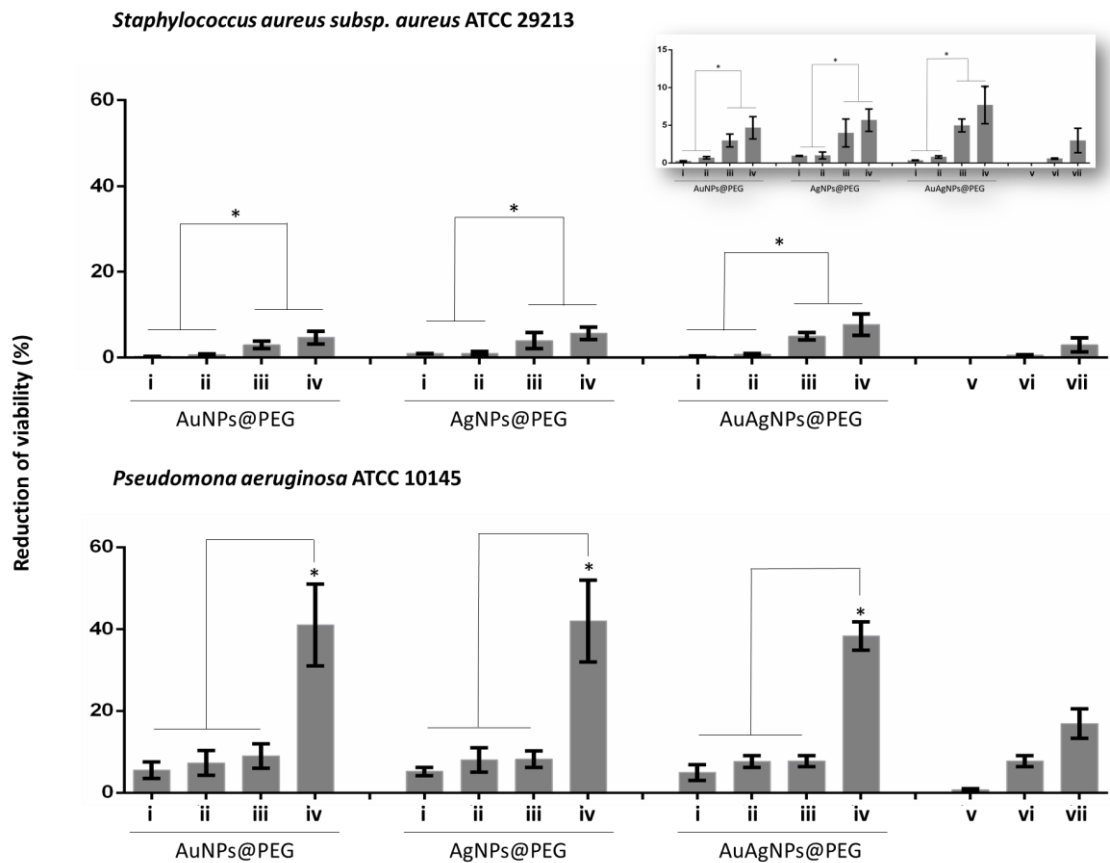
Figure S2. Biofilm destruction (%): **(i)** NPs@PEG: Nanoparticles; **(ii)** NPs@PEG + visible light irradiation (VLI); **(iii)** NPs@PEG + ciprofloxacin (CIP); **(iv)** NPs@PEG + VLI + CIP; **(v)** VLI; **(vi)** CIP; **(vii)** VLI + CIP. Nanoparticles were at 10 nM, ciprofloxacin at 10 μg/mL and VLI at 2.02 W cm^{-2}. Data represented as the mean ± standard deviation (SD) of three independent measurements. The following formula calculated the percentage of biofilm reduction: Reduced cell viability (%) = 100 − [((log$_{10}$ CFU/mL control − log$_{10}$ CFU/mL Treat) / log$_{10}$ CFU/mL control) 100], where CFU/mL control corresponds to the number of colonies forming units per ml per milliliter of untreated biofilms, and CFU/mL Treat corresponds to the number of colonies forming units per ml per milliliter of treated biofilms. *p < .05, Significant differences.
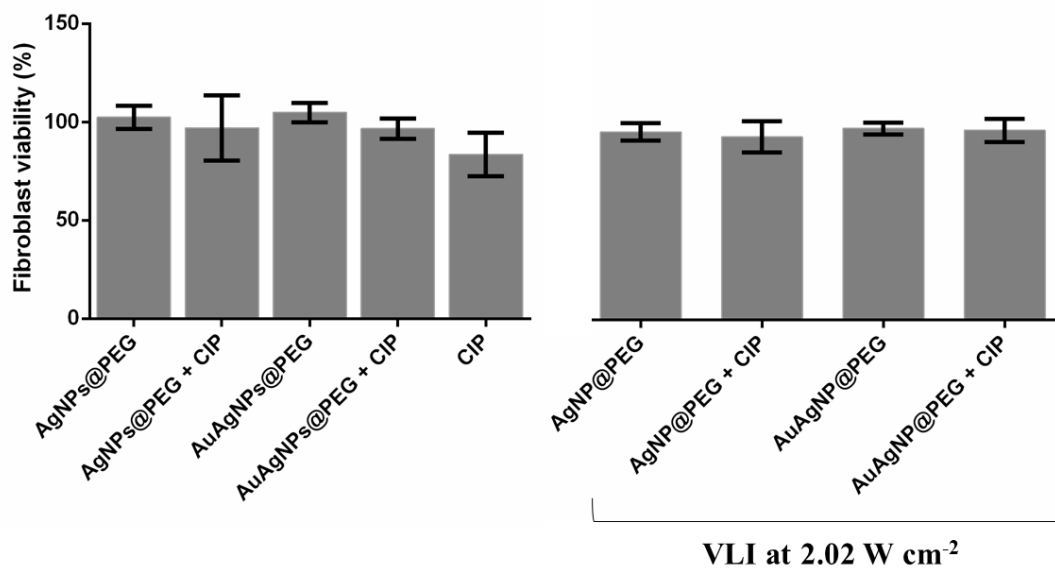
Figure S3. MTS assay of human primary fibroblasts previous 6h exposure to AuAg@PEG (10 nM), Ag@PEG (10 nM), CIP - ciprofloxacin (10 μg/mL), AuAg@PEG + CIP or Ag@PEG + CIP. VLI - visible light irradiation at 2.02 W cm^{-2}. The following equation applied to calculate the cell viability (%) = 100 x (mean Abs of treatment group /mean Abs of control group, without treatment). Data are the average of at least three independent assays and error bars correspondent to standard deviation.

Unraveling the host specificity within
Streptococcus dysgalactiae subsp. dysgalactiae

CINTHIA ALVES BARROCO

2022